Experimental and Computational Investigation of Building Integrated PV Thermal Air System Combined with Thermal Storage

BY

YETAO XIANG

BEng

Thesis submitted to the University of Nottingham for the degree of Doctor of Philosophy

February 2017

ABSTRACT

Issues from global warming with increased CO_2 emissions have been to a main concern over world. As an example in the UK, the energy demand in the domestic sector has risen by 17% in 2010 compared with that of 1970. Applying renewable energy is widely agreed to be the most effective and promising way to solve the problem where solar energy and photovoltaic technology have been greatly developing from the last century.

Photovoltaic combines with Phase Change Material (PV/PCM) system is a hybrid solar system which uses phase change material to reduce the PV temperature and to store energy for other applications. This thesis aims to investigate the performance of a designed building integrated photovoltaic thermal system (BIPVT) with PCM as thermal storage for building applications. The research objectives are to increase the building integrated photovoltaic (BIPV) efficiency by incorporating PCM while utilising the stored heat in PCM for controlling indoor conditions and reduce the total building energy consumption.

The research starts with solar energy convection technologies including solar thermal and solar photovoltaic. Then a combined technology named photovoltaic thermal system (PVT) was introduced and discussed. Research work on a different type of PVT using water and air as thermal energy medium was further reviewed and discussed. An analytical approach investigation was presented on a PVT system and the results were used to design the experiment work on PV/PCM configuration. Experiments have been carried out on a prototype PV/PCM air system using monocrystalline photovoltaic modules.

Transient simulations of the system performance have also been performed using a commercial computational fluid dynamics (CFD) package based on the finite volume method. The results from simulation were validated by comparing with experimental results. The results indicated that PCM is effective in limiting temperature rise in PV device and the heat from PCM can enhance night ventilation and decrease the building energy consumption to achieve indoor thermal comfort for certain periods of time. An entire building energy simulation with designed PV/PCM air system was also carried out under real weather condition of Nottingham, UK and Shanghai, China. The result also shows a market potential of PV/PCM system and a payback time of 11 years in the UK condition if using electrical heater.

PUBLISHED PAPERS AS A RESULTS OF THE PhD RESEARCH

Xiang Y.T. and Gan G.G. *Optimization of building integrated photovoltaic thermal air system combined with thermal storage* International Journal of Low carbon Technologies 2015 10: 146-156.

Xiang Y.T. and Gan G.G. *Experimental and numerical investigations of a building integrated photovoltaic thermal air system with PCM* SET2014 - 13 International Conference on Sustainable Energy Technologies, Geneva, Switzerland

ACKNOWLEDGEMENTS

I would like to take this opportunity to express my special thanks to my principle supervisors Dr Guohui Gan for all valuable and productive academic suggestions during the planning and development of this research work. I would also like to my very great appreciation to my second supervisor Dr Jie Zhu for his advice and help on my PhD research.

I would like to extend my thanks to all technicians in the Department of Architecture and Built Environment especially for David Oliver, David Taylor, and Robert Clarke.

I would also like to thank all my friends for their continued support. I also want to express my appreciation for my girlfriend Nikki Chen who accompanied with me during my entire PhD time and the long months of thesis writing.

Finally, I would especially like to thank my parents for their encouragement and support during my study, and for giving me the courage and confidence to overcome the problems I encountered and carry on with my research.

TABLE OF CONTENTS

ABSTRACT i
PUBLISHED PAPERS AS A RESULTS OF THE PhD RESEARCH iii
ACKNOWLEDGEMENTS iv
TABLE OF CONTENTS v
LIST OF FIGURES ix
LIST OF TABLES xiii
NOMENCLATURE xiv
Chapter 1 Introduction 1
1.1 Background 1
1.2 Research aims and objectives 5
1.3 Research methods 7
1.3.1 Experimental method 7
1.3.2 Modelling method 7
1.4 Thesis structure 7
Chapter 2 Literature review 10
2.1 Introduction of review 10
2.2 Solar energy and technologies employed in the conversion of solar energy 12
2.2.1 Solar thermal technology 13
2.2.2 Solar cell 15
2.3 PV Thermal system (PVT) 18
2.3.1 PVT water system 19
2.3.2 PVT air system 21
2.3.3 Building integrated photovoltaic (BIPV) thermal collector 24
2.4 Thermal energy storage systems 29
2.4.1 Sensible thermal energy storage 30
2.4.2 Latent heat storage 31
2.4.3 Thermal energy storage through chemical reactions 34
2.5 PV/ PCM systems 35
2.6 Techniques employed to improve thermal performance 41

2.7 Opportunities for further work 44
2.8 Summary 45
Chapter 3 Methodology 47
3.1 Introduction 47
3.2 Stage 1 Analytical model 48
3.3 Stage 2 Experimental study 59
3.3.1 Solar cell selection 59
3.3.2 PCM selection 61
3.3.3 Experiment construction 63
3.3.4 Measurement equipment and uncertainty analysis 67
3.4 Stage 3 CFD simulation and system optimisation 71
3.4.1 Phase change simulation 71
3.4.2 Natural convection model 73
3.4.3 Balance equations 75
3.5 Stage 4 Building energy simulation with PVT/PCM system 78
3.5.1 Phase change model 80
3.5.2 PV performance model with electric storage system 81
3.5.3 HVAC model 83
3.5.4 Economic analysis 84
3.6 Summary 85
Chapter 4 Results of analytical investigations 86
4.1 Results for natural convection 87
4.1.1 Effects of incident radiation 87
4.1.2 Effects of air gap size 90
4.1.3 Effect of PV panel length and total area 94
4.2 Results for forced convection 96
4.2.1 Effect of air velocity (Fan speed) 96
4.2.2 Effects of gap spacing 98
4.2.3 Effects of inlet air temperature 100
4.3 Summary of analytical results 102

Chapter 5 Experimental design and results of a PV/PCM system 104
5.1 Introduction 104
5.2 Experimental design and procedure 105
5.3 Experiment results for Case 1 106
5.3.1 Thermal energy storage 106
5.3.2 Energy release process 114
5.4 Experimental results for different cases and their comparison 117
5.4.1 Results of Case 1, 2, and 4, reflecting the variations in the PCM thickness 118
5.4.2 Results of Case 1, 3, and 5, reflecting the variations in the air gap size 120
5.4.3 Results of Case 1 and 6, comparing the system with vertical fins 122
5.5 Summary 125
Chapter 6 CFD simulation work on the PV/PCM system 127
6.1 Introduction 127
6.2 Fluent code 128
6.2.1 Physical model description 128
6.2.2 Boundary and initial conditions 130
6.2.3 Time step and grid independence study 132
6.3 Validation of the CFD model 136
6.4 Simulation results 139
6.4.1 Case 1 139
6.4.2 Case 2 143
6.4.3 Case 3 144
6.5 Summary 148
Chapter 7 Investigation of the PVT/PCM system performance 150
7.1 Introduction 150
7.2 Effects of solar isolation 150
7.3 PCM thickness 153
7.4 Air duct depth 157
7.5 Effects of the PV angle 162

7.6 Effects of forced ventilation 166
7.6.1 Melting process 167
7.6.2 Solidification 171
7.7 Effect of fins 173
7.8 Summary 178
Chapter 8 Building simulation for a typical house equipped with the PVT/PCM system 180
8.1 Introduction 180
8.2 Model configuration 180
8.3 Three cases and their descriptions 184
8.4 Building energy performance simulation results 185
8.4.1 Comparison of Case 1a and 1b for two different locations without an active thermal control system 186
8.4.2 Case 1a and Case 1c, Model 1 for two different locations, with forced ventilation 194
8.5 Economic considerations of the designed PVT with the PCM system 197
8.5.1 Cost of the BIPVT/PCM wall 198
8.5.2 Three cases for economic analysis 199
8.5.3 Economic analysis results 201
8.6 Summary 202
Chapter 9 Conclusion and Further work 205
9.1 Summary of the thesis 205
9.2 Conclusions and contributions of this research 208
9.3 Recommendations for Future work 211
Reference 213
Appendix 224

LIST OF FIGURES

Figure 1.1 Final energy consumption by sector, UK, 1970 to 2013 (Source: DECC, ECUK Table 1.05) 2
Figure 2.1 Simple solar hot water system (from internet) 14
Figure 2.2 Schematic diagram of Trombe wall (solar energy house, 2003).... 15
Figure 2.3 Various collector concepts: (A) sheet-and-tube PVT, (B) channel PVT, (C) free flow PVT, (D) two-absorber PVT (insulated type) (Zondag et al., 2003) 19
Figure 2.4 Cross-section of PVT experimental models: (a) PV/Water, (b) PV/Water + Glazing, (c) PV/Air, and (d) PV/ Air + Glazing 23
Figure 2.5 Schematic diagram of BIPVT system on wall and roof 25
Figure 2.6 The CIS Tower in Manchester, England 26
Figure 2.7 Projet BIPV, Gare de Perpignan, Southern France 26
Figure 2.8 BIPV solar façade on a municipal building located in Madrid (Spain) 27
Figure 2.9 Diagram of the designed PV/PCM system (Huang, 2000) 36
Figure 2.10 System configuration of PV/PCM 37
Figure 2.11 Hybrid thermal energy storage system (HTESS) 42
Figure 3.1 One dimensional heat transfer model (Duffie and Beckman, 2006). 49
Figure 3.2 Validation with total energy efficiency 58
Figure 3.3 Schematic diagram of the experimental system 63
Figure 3.4 Photograph of the test unit with the artificial light source 64
Figure 3.5 Photograph of the PCM container 65
Figure 3.6 Photograph of the test unit back side with the air duct inlet and outlet 65
Figure 3.7 PCM container with vertical fins 66
Figure 3.8 The calibration curve of thermocouples by using digital thermometer as a reference 67
Figure 3.9 Possible observed point location 68
Figure 3.10 Data logger connection from the side of the test unit 69
Figure 3.11 Measuring points for mean air velocity 70
Figure 3.12 Temperature Enthalpy of PCM Data 81
Figure 3.13 Layout of a HVAC system with a PV/T as preheater 84
Figure 4.1 Variation of mass flow rate with irradiance 88
Figure 4.2 Temperature variation for different system components as a function of irradiance 89
Figure 4.3 Variations in thermal and electrical efficiency with irradiance 90
Figure 4.4 Temperature variation as a function of gap spacing 91
Figure 4.5 Boundary layer in the air duct 91
Figure 4.6 Variation in thermal and electrical efficiency with gap spacing 93
Figure 4.7 Variation in thermal and electrical efficiency as a function of PV panel length 93
Figure 4.8 Convective heat transfer coefficient between the PV and the back wall 95

Figure 4.9 Variation in temperatures with air velocity 97
Figure 4.10 Variation in thermal and electrical efficiency with air velocity ... 98
Figure 4.11 Variation in power with air velocity 98
Figure 4.12 Variation in temperatures with gap spacing 99
Figure 4.13 Variation in thermal and electrical efficiency with gap spacing 100
Figure 4.14 Variation in temperatures with the changes in inlet air temperature 101
Figure 4.15 Variation in thermal and electrical efficiency as a function of inlet air temperature 101
Figure 5.1 Intensity measurement positions 106
Figure 5.2 Temperature of the three points at the centre of PCM 107
Figure 5.3 Temperature of three points located at different heights inside the PCM 108
Figure 5.4 A comparison of the mean PV temperature with and without a PCM unit 110
Figure 5.5 Mean airflow rate at the air outlet 111
Figure 5.6 Electrical efficiency increase due to the PCM unit 112
Figure 5.7 Thermal efficiency of the PVT and the PV/PCM system 114
Figure 5.8 The temperature of the three points in the solidification phase ... 115
Figure 5.9 Airflow rate at the outlet in the solidification phase 115
Figure 5.10 Temperature difference between the air inlet and the outlet 116
Figure 5.11 Mean PV temperature of three cases with different PCM thickness 118
Figure 5.12 Electrical efficiency increase due to the PCM unit compared to the reference system without the PCM 119
Figure 5.13 Temperature of the point at the centre of the PCM container for three different air gaps sizes 121
Figure 5.14 Mean airflow rate at the air outlet 122
Figure 5.15 Mean PV temperature of the systems with and without fins 123
Figure 5.16 Temperature difference between the air inlet and outlet for Case 1 and Case 6 124
Figure 5.17 Air velocity at the air outlet for Case 1 and Case 6 125
Figure 6.1 Schematic view of the 2D version of the simulation model 129
Figure 6.2 3D version of the simulation model 129
Figure 6.3 Boundary condition positions 131
Figure 6.4 Point 1, Point 2, and Point 3 from left to right 133
Figure 6.5 Temperature at different points for three different mesh sizes 133
Figure 6.6 Mean velocity at the air outlet for three different mesh sizes 134
Figure 6.7 Temperature at Point 2 for different time steps 135
Figure 6.8 Velocity at Point 2 for different time steps 135
Figure 6.9 Predicted and experimental transient temperatures at three points inside the PCM 136
Figure 6.10 Predicted and experimental transient temperatures at three points inside the air duct 137
Figure 6.11 Transient velocity of three points in the air duct 138
Figure 6.12 Temperature distribution in the PCM for Case 1 140

Figure 6.13 Temperature in the air duct for Case 1 141
Figure 6.14 Velocity and temperature distribution contours in the air duct at time 3,000 s (left) and 10,000 s (right) 141
Figure 6.15 Temperature distribution in the PCM in the solidifying process 142
Figure 6.16 The temperature variations of the PV surface and rear temperature with time 143
Figure 6.17 Velocity at two points in the air duct 144
Figure 6.18 Schematic diagram of the PV/PCM system with fins inside the PCM 144
Figure 6.19 Temperature at three observed points in the PCM for Case 3 ... 145
Figure 6.20 Temperature distribution at the top side of model in Case 3 at time 10,000 s 146
Figure 6.21 Velocity distribution in the air duct in Case 3 at time 10,000 s . 146
Figure 6.22 Temperature distribution in the PCM in the solidification process for Case 3 147
Figure 7.1 Temperature at Point 1 for three different heat fluxes 151
Figure 7.2 Mean velocity of three different heat fluxes at the air outlet 152
Figure 7.3 Temperature of Point 1 in the PCMs of different thickness..... 154
Figure 7.4 Temperature of Point 1 in the PCMs of different thickness..... 154
Figure 7.5 Liquid fraction 1 for PCMs of different thickness 156
Figure 7.6 Rayleigh number for the back of the PCM container wall..... 156
Figure 7.7 Temperature of two points inside the PCM 158
Figure 7.8 Mean temperature of the PCM back surface for different duct sizes 158
Figure 7.9 Mean velocity at the air outlet for three different duct sizes..... 160
Figure 7.10 Mass flow rate at the air outlet for three different duct sizes..... 161
Figure 7.11 Velocity vector distribution in the air duct for the 150 mm case at 20,000 s 161
Figure 7.12 Mean PV temperature for two PV angle cases..... 163
Figure 7.13 Liquid distribution for two cases at time 90min 163
Figure 7.14 Liquid distribution for two cases at time 180min 164
Figure 7.15 Liquid faction of three PVs positioned at different solar angles 165
Figure 7.16 Rayleigh number for two different solar angles at the same intensity..... 166
Figure 7.17 Temperature at Point 1 and Point 2 for two forced ventilation cases and free convection 168
Figure 7.18 Liquid fraction for two forced ventilation cases and free convection..... 169
Figure 7.19 Thermal efficiency for two forced ventilation cases and free convection..... 170
Figure 7.20 Mean PV temperature for two forced ventilation cases and free convection..... 171
Figure 7.21 Liquid fraction for two forced ventilation cases and natural convection..... 172
Figure 7.22 Heat transfer rate from the air outlet for two forced ventilation cases and natural convection in the solidification process 172

Figure 7.23 Top view of a PCM container with vertical fins 174
Figure 7.24 Simulated 3D model with vertical fins at both sides..... 175
Figure 7.25 Temperature for PCM with and without fins 176
Figure 7.26 Liquid fraction for the system with and without vertical fins 176
Figure 7.27 Liquid fraction for three cases..... 177
Figure 7.28 Heat transfer rate for three cases in the solidification process ... 178
Figure 8.1 Base case, 3D view of the building model with a door facing south 181
Figure 8.2 Base case, 3D view of the building model, the north wall view .. 181
Figure 8.3 Model 1 PVT wall as a part of the south wall..... 182
Figure 8.4 Designed PVT wall with different openings..... 183
Figure 8.5 A special wall designed to simulate the PV façade..... 184
Figure 8.6 Model 2 PVT roof mounted as part of south roof..... 184
Figure 8.7 Room temperature during a week in January for location Nottingham, UK 186
Figure 8.8 Room temperature during a week in July..... 187
Figure 8.9 PV cell temperature in a week in January for Nottingham, UK .. 188
Figure 8.10 PV cell temperature in a week in January..... 189
Figure 8.11 Hourly room temperature in a week in January for Shanghai, China, weather conditions 189
Figure 8.12 Hourly room temperature in a week in July..... 190
Figure 8.13 Hourly PV cell temperature in a week in January for Shanghai weather conditions..... 191
Figure 8.14 Hourly PV cell temperature in a week in July for Shanghai..... 191
Figure 8.15 Temperature of the PV cell with two different PCMs in seven days in July 192
Figure 8.16 Room temperature difference with two different PCMs on two days in June..... 193
Figure 8.17 Yearly room temperature difference due to fan system in Fan Sch1 in Nottingham 195
Figure 8.18 Yearly room temperature difference due to fan system in Fan Sch1 in Shanghai 195
Figure 8.19 Yearly Room temperature difference due to fan system in Fan Sch1 in Shanghai at 0.3 m^3/s flow rate..... 196
Figure 8.20 Heating and cooling load for the model houses in the UK 200

LIST OF TABLES

Table 1 Comparison of organic and inorganic materials for heat storage 32
Table 2 Specifications of the photovoltaic panel 60
Table 3 Thermal and physical properties of the selected PCM 62
Table 4 Location of possible observed points 69
Table 5 PV cell specifications 82
Table 6 Reference parameters used in the analytical method 86
Table 7 Configuration of six test units 105
Table 8 Intensity on measured points 106
Table 9 Configuration of six test units 117
Table 100 Yearly heating savings and electricity output for all cases 202
Table 111 Initial costs and payback for all cases 202

NOMENCLATURE

A effective air collector's area (m^2)

A_{musH} mushy zone constant

C linear-anisotropic phase function coefficient

C_p specific heat capacity (J/kg K)

D spacing between PV and back wall (m)

D_H hydraulic diameter (m)

F_R overall collector heat removal efficiency factor

f friction factor

F' collector factor

F_j force vector

g gravitational acceleration (N/kg)

G incident radiation on the collector surface (W/m^2)

H head loss (m)

h_c convective heat transfer coefficient between PV and back wall

h_w convective heat transfer coefficient of wind

$h_{r,p-w}$ radiative heat transfer coefficient between PV and back wall

i thickness of back wall (m)

k conductivity of back wall (W/mK)

K loss coefficient

L length of the collector (m)

$\dot{m}$ mass flow rate (kg/s)

N number of glass cover

Nu Nusselt number

S spacing between PV and cover (m)

T_a ambient air temperature (K)

T_i air gap inlet temperature (K)

To air gap outlet temperature (K)

T_p mean temperature of PV plate (K)

T_c mean temperature of glass cover (K)

T_f mean air temperature (K)

Ts equivalent sky temperature (K)

T_w mean temperature of back wall (K)

T_{ref} reference temperature (K)

Ra Rayleigh number

P total pressure (Pa)

P static pressure (Pa)

Q_u useful energy gain (J)

U_L coefficient of heat loss (W/m^2K)

U'_L the actual overall heat loss coefficient

U_t coefficient of heat loss from top (W/m^2K)

U_b coefficient of heat loss from top (W/m^2K)

v system flow velocity (m/s)

v_w wind speed (m/s)

W width of PV (m)

Greek

α absorption coefficient

σ Stefan-Boltzmann constant

β collector tilt angle

ε_c the emittance of front cover

ε_p the emittance of PV

ε_w the emittance of back wall (insulation)

$\bar{\tau}$ stress tensor

ρ density (kg/m3)

η_e electrical efficiency of PV

η collector efficiency

λ conductivity

τα effective transmittance absorptance product

Chapter 1 Introduction

1.1 Background

At present, fossil fuel is still a dominant type of energy used in the world. Around 85% of the UK's energy needs are met by fossil fuels, which are expected to remain the predominant source of energy for decades to come (ECUK, 2014). The main concern associated with fossil fuel consumption stems from the greenhouse gases emitted as its by-product, along with the anticipated shortage of its natural sources in the near future. While many greenhouse gases exist, most scientists focus on CO_2, as it is purported to be the leading source of global warming, which has resulted in an increase in the average temperature by about 0.2 ºC during the last century (IPCC Fourth Assessment Report, 2007). According to estimation from International Energy Agency (IEA, 2005), the traditional sources of fossil fuels will be exhausted by 2050 if the upward consumption trend continues to increase. Consequently, fuel prices will dramatically increase, resulting in a possible international economic crisis. Therefore, reducing the fossil fuels dependence is necessary. Utilisation of renewable energy is widely agreed to be the most effective and promising way to solve this problem (IEA, 2014). It is also noteworthy that, according to the government data from the Department of Energy and Climate Change of UK (DECC, 2014) on the energy consumption by sector in the UK from 1970 to 2013 (Figure 1.1), the domestic sector contributes about 30% to the total energy consumption in the country and this percentage is expected to increase further (ECUK, 2014). Reduction in greenhouse gas emissions can be achieved by

developing low carbon buildings that reduce heating and cooling demand, as well as supply electricity with photovoltaic and heating through the use of sustainable energy.

Sustainable energy has been widely agreed and proved as one of the promising energy sources, with the potential to mitigate the dependency on fossil fuels (Sopian et al., 2009; IEA 2011; World Energy Council, 2013). For example, solar energy is a renewable energy that, owing to its abundance, can meet a significant proportional of the world's energy demands. The solar technology is commonly used in solar thermal and photovoltaic cells.

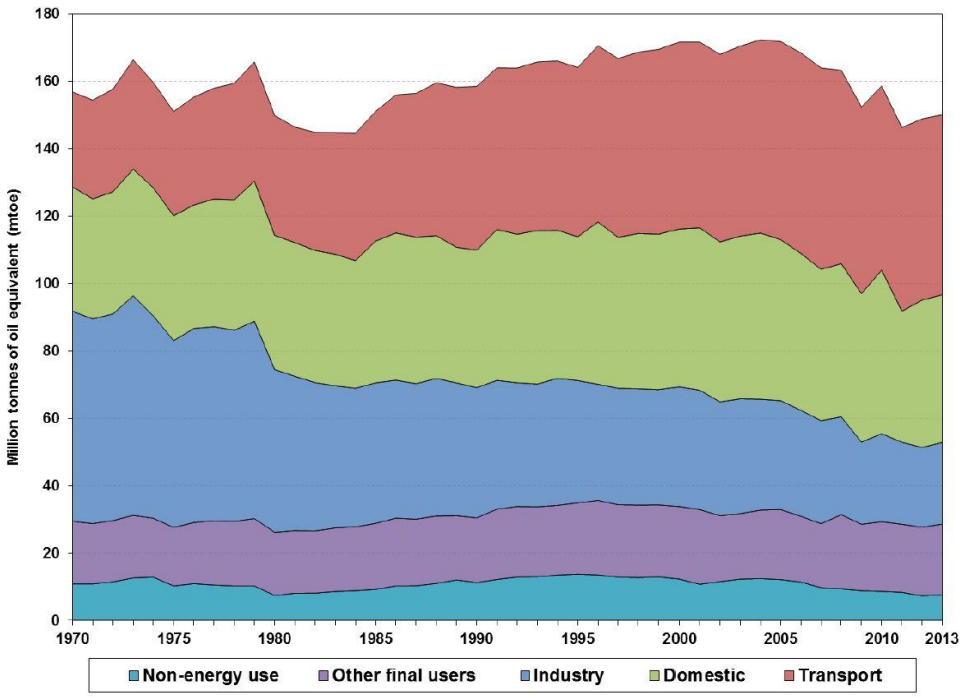


Figure 1.1 Final energy consumption by sector, UK, 1970 to 2013 (Source: DECC, ECUK Table 1.05)

Photovoltaic (PV) cells, as one of the solar technologies, convert solar radiation into electricity. Thus, PV cells are considered the key solution to the energy

crisis in the 21st century. However, PV modules or cells can only convert around 70% of solar irradiance to electricity. As most of the solar irradiance absorbed by PV cells is converted to heat, this increases the temperature of PV modules, leading to a further decrease in the electrical efficiency (Tripanagnostopoulos, 2012). For most common PV material such as monocrystalline (c-Si) and polycrystalline (pc-Si) silicon solar cells, each unit (1 ^{o}C) increase of PV unit in temperature above its optimisation point will lead to the efficiency decreases by about 0.45%(Kalogirou, 2006). They (Kalogirou, 2006) also reported that a decrease in about 0.25% per unit increase in temperature for amorphous silicon (a-Si) cells, depending on the module design. In order to increase the PV electrical efficiency while making use of the extra heat, a hybrid photovoltaic thermal system (PVT), referred to as PV thermal system, was introduced and developed over the last 30 years (Parida et al., 2011). Hybrid PVT systems can provide both electrical and thermal energy, achieving a higher solar radiation and electrical energy conversion rate relative to a single PV or solar thermal collector of the same surface area. The system consists of a photovoltaic module coupled to the heat extraction devices, in which the air or water is used to store excess heat from the PV cell to maintain its operating temperature. However, the total initial cost of combining the PV and solar thermal system is higher than that of the standard PV modules. Therefore, it is important to increase the total PVT system energy output in order to compensate for the greater expenditure.

Although the main objective of implementing a PVT system is to increase its electrical performance, the thermal energy still can be used to meet part of the heat demand for building the application. One of the most attractive PVT system applications is in building integrated photovoltaic thermal (BIPVT) modules,

which have been the subject of extensive research and development in recent years. The system is usually designed as a wall- or roof-mounted PV array with air gaps at the back side. Natural or forced air circulation is applied for removing heat from the PV and supplying heating.

By using PVT technology in the UK, the government can achieve the target of 15% of energy coming from renewable sources by 2020, as well as reduce the carbon emissions by 80% by 2050 (DECC, 2016). This potential increase in renewable energy utilisation will implicitly result in a decline in the reliance on fossil fuels, while providing buildings with clean electricity and thermal energy.

Providing thermal comfort is the one of main purposes of building designers within building codes. Maintaining comfortable indoor conditions is beneficial for work performance, while providing higher living standards at home. Thermal energy storage is an effective means of compensating for the time mismatches between energy supply and demand due to the natural sunlight/darkness cycles and changes in weather conditions, which is typically achieved via heat recovery and free cooling technologies.

Among all currently available thermal storage system types, phase change material (PCM) has emerged as a highly effective material for temperature regulators with many applications. It has been approved to be a novel approach to apply solid or liquid PCM with a phase change similar to the PV operating temperature for regulation the PV temperature (Susman, 2011; Gowreesunker, 2013; Biwole, 2013). At the same time, the energy stored in the PCM can be released to provide building heating and enhance natural ventilation effects at night.

However, incorporating PCM into a BIPVT system greatly augments its complexity in both performance investigation and system design. The aim of this study is to investigate the performance of a designed building integrated photovoltaic thermal system (BIPVT) with PCM as thermal storage for building applications.

1.2 Research aims and objectives

The purpose of this study is to investigate the performance of a designed building integrated photovoltaic thermal system (BIPVT) with PCM as thermal storage for building applications. The system utilises an integrated photovoltaic panel design and a phase change material (PCM) as latent heat storage, which also acts as a heat remover from the PV. The heat stored in the PCM unit can be utilised to enhance ventilation under control.

The hypothesis driving the research postulates that, the excess heat from PV temperature rising would be absorbed by PCM until it has completely melted. During the night time when the temperature of PV decrease, the solidification of the PCM can provide heat for the air in the air duct, which can supply heat to the applications, or act as an insulation material.

The main objective of this research was to investigate the thermal and electrical performance of the newly designed PVT air system with thermal storage and to improve its performance.

Thus, the specific study objectives were as follows:

1. Review of extant literature on PVT and thermal storage system applications.

2. Analytical analysis of a PVT system for primary designing experiment work.
3. Experimental investigation of the designed PV/PCM system.
4. Computational Fluid Dynamics (CFD) modelling of the designed PV/PCM system with an air duct, and the validation of the findings yielded via comparison with the experimental results.
5. Parametric studies on the PV/PCM air system using the validated model.
6. Performance simulation of the newly designed building integrated PV/PCM system to provide design guidelines for PV/PCM air systems.
7. Economic analysis of the PV/PCM air system.

As most of the investigations on PV/PCM that have been conducted to date focused on energy storage and release of PCM only, very few attempts to integrate the convection heat transfer into the model or experiment have been made. In practical applications, the heat transfer at the back side of the PV/PCM system varies depending on the ambient conditions; thus, enhancing this heat transfer would be highly beneficial. This was the goal of the present study, where the PV efficiency was increased by incorporating PCM while utilising the heat from the PCM through convection for controlling the indoor ambient temperature.

1.3 Research methods

1.3.1 Experimental method

The aim of this study is to investigate the performance of a designed building integrated photovoltaic thermal system (BIPVT) with PCM as thermal storage for building applications. Thus, a series of experiments have been carried out to investigate the thermal and electrical performance of the PVT system designed as a part of this research. An analytical model was developed first, as this assisted in experimental design.

1.3.2 Modelling method

A series of 2D and 3D Computational Fluid Dynamics (CFD) models were built and developed for use in simulations in ANASYS Fluent 13.0 in order to present a parametric study on the designed PVT system. The entire building energy performance and economic analysis of the aforementioned PVT system under weather conditions prevalent in several locations were also simulated employing ENERGY PLUS 8.3 software.

1.4 Thesis structure

Chapter 1 introduced the present study by providing the research background and specifying the research hypothesis and objectives, as well as the research method employed.

Chapter 2 is designated for a review of pertinent literature, focusing on the state-of-the-art technologies in the solar energy sector, as well as different solar application classifications, and design and performance evaluation techniques. In particular, the Building Integrated Photovoltaic (BIPV) thermal collector system design and performance is discussed and the pertinent literature sources reviewed. Prior research in the field of thermal energy storage systems, with the focus on phase change materials, is also presented through a literature review and case studies.

Chapter 3 presents the methodologies used in this research study. As the current research was performed in four stages, methodologies for each stage are presented in chronological order. In Stage 1, an analytical model for preliminary study of the PVT system was developed and the results were used for designing an experiment. In Stage 2, the experimental methodology was determined and experiments were conducted. Stage 3 was designated for developing the methodology for the CFD model and subsequent modelling activities. The study culminated with Stage 4, which comprised of developing the methodology and simulating the energy performance of the PV/PCM system within a building.

Chapter 4 presented the results yielded by the stage 1, which commences with the discussion of the analytical investigation of a PVT, the results of which were subsequently used to design the experiments on the PV/PCM configuration.

Chapter 5 presents the experimental investigation of the designed PV/PCM system. It illustrates the concepts of system design and outlines the research methods utilised in the present study. Experimental results are also presented and discussed.

Chapter 6 is designated for a numerical study of the designed PV/PCM system. As a part of the work discussed in this chapter, CFD was applied to predict airflow and temperature field of the model which was validated experimentally. Time step and grid dependent studies are also presented, along with the simulation work. Simulation results for three different cases are presented and discussed before ending this chapter.

Chapter 7 presents a parametric study of the system designed in this research endeavour, including solar irradiation, collector characteristics, PCM gap size and fins.

In Chapter 8, simulation of the PVT system with PCM as thermal storage for an entire domestic house is presented. The main purpose is to investigate the real influence of the PV/PCM system on the thermal and electrical performance. Economic and environmental analyses of the designed system are also presented.

The thesis ends with Chapter 9, where the main conclusions that can be inferred from the present study are presented, along with suggestions for future work in this field.

Chapter 2 Literature review

2.1 Introduction of review

In this chapter, a comprehensive review of pertinent literature is presented, focusing on published works of relevance for this research. The literature review starts with available publications discussing environmental concerns associated with the energy demand increase, which is posited as the main contributor to global warming. Sustainable energy technologies are presented next, as these are proposed as the most viable alternative capable of reducing the greenhouse gas emission levels. As the literature reviewed as a part of this study has shown, greater use of the existing renewable energy sources is urgently needed, which can only be achieved by improving the energy conversion efficiency. Researchers should also investigate viability of new technologies that have the potential to reduce the current energy demand.

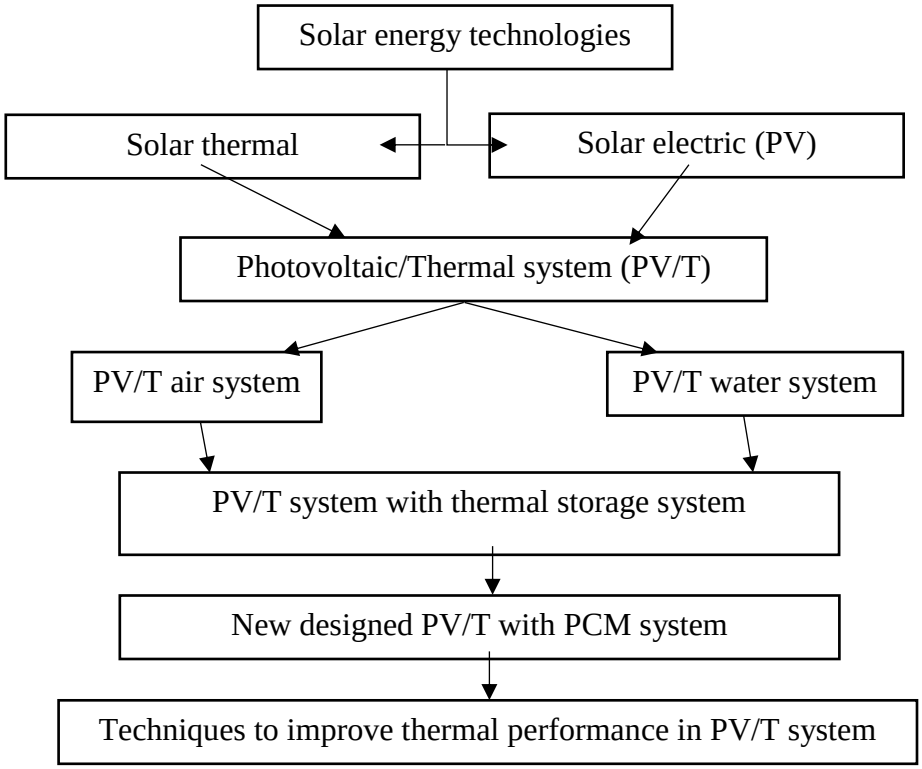
Solar energy is a sustainable energy that has great potential for many applications. Solar energy has been utilized by humans even before civilization occur, resulting in a wide range of technologies. Existing technologies based on solar energy include solar thermal and solar cell, which transform solar power into electricity. Due to the temperature dependent performance of solar cells, a hybrid of solar thermal and electric system, photovoltaic/thermal (PVT) was developed in the 1970s. As the main aim of PVT was to increase the total system efficiency, its main market comprised of domestic applications. The usage subsequently expanded, and both air-based and water-based PVT models were utilised, as will be discussed later in this chapter. Researches have been focus

on building integrated photovoltaic thermal (BIPVT) system in recent years which have undergone rapid developments. It has the potential to generate both electric and thermal energy due to its higher reliability and lower environmental impact (Fudholi et al., 2014).

In the next section, extant studies on thermal storage energy will be reviewed. The systems are designed to shift the time of energy supply and demand. Three storage type categories are reviewed and discussed here, namely sensible, latent and chemical reaction type. This is followed by the introduction of a special type of PVT system with latent heat storage. Finally, the literature pertaining to the techniques utilised to improve thermal performance of PVT systems is presented.

In sum, the aim of this chapter is to present the pertinent works in the field of solar energy utilisation and application, according to classification, design and performance evaluation. The findings yielded by this comprehensive literature review allowed establishing the theoretical framework for the PVT application in building service area. Moreover, it allowed identifying extant works, models, and case studies that may help in designing and developing a new PVT system. The diagram below shows the literature review outline.

LITERATURE REVIEW OUTLINE



2.2 Solar energy and technologies employed in the conversion of solar energy

The solar power technology, as a solar and photovoltaic thermal technology, has several benefits and downsides relative to alternative power sources (Mahajan, 2011). One of its main advantages is absence of noise and waste during the energy production process. Secondly, it is highly reliable, with a lifespan after installation and optimization. However, its key disadvantages include varying distribution of sunlight on the Earth's surface, necessitating highly flexible design, as well as a relatively long return on investment (ROI) period due to low efficiency, and the significant upfront cost associated with production and installation.

The use of solar energy is usually discussed in the context of passive and active systems. A passive system is based on designs that assist in easier solar energy utilisation in various applications. For example, buildings, windows, walls and floors all required the work of optimisation to maximize the use of solar power, in kind of heat in winter (Thomas, 2012). Active solar systems, on the other hand, may use solar energy with the assistance of mechanical equipment. Modern products, such as solar thermal collectors and water-based photovoltaic-thermal (PVT) hybrid systems are examples of such active systems. Different design features and performance characteristics of flat plate PVT solar collectors are compared and discussed next.

2.2.1 Solar thermal technology

Solar thermal technology aims to gather alternative solar power and to generate thermal/electrical power for industrial, residential and commercial use. Based on its operating temperature, it can be divided into low-temperature and high-temperature collectors. Systems for utilising low-temperature solar thermal energy includes heat collection. Heat storage can be either short-term or seasonal, and can be designated for distribution within a structure or via a district heating network. Most solar thermal technology in commercial and residential buildings relies on low-temperature models. High-temperature

collectors, such as parabolic trough designs, are employed in industrial applications and are beyond the scope of this work.

Solar thermal system can be also divided into two categories based on its working fluid, liquid or air. The most common liquid type of solar thermal system is solar water system which prove to be most effective solar thermal system and efficiency can reach up to 70% (Jaisankar, 2011).Figure 2.1 shows a schematic diagram of a simple solar hot water system. In this design, the solar collector absorbs solar heat, whereby the heated fluid moves to a storage tank either by passive thermal siphon or a pump. Once the heat from the liquid is transferred to water in the tank, the liquid returns to the collector and the aforementioned cycle is repeated. Thermal performance of such system mainly depends on the transmission, absorption and physical phenomenon of solar power and sensible conduction of the operating fluid (Jaisankar et al, 2011). Flat plate collectors glaze on the front of the panel with air duct or pipes boned to the back of the absorber, which accounts for 26.4% of the world installed solar thermal content and up to 84.9% of the EU has this installation (Weiss and Mauthner, 2014).

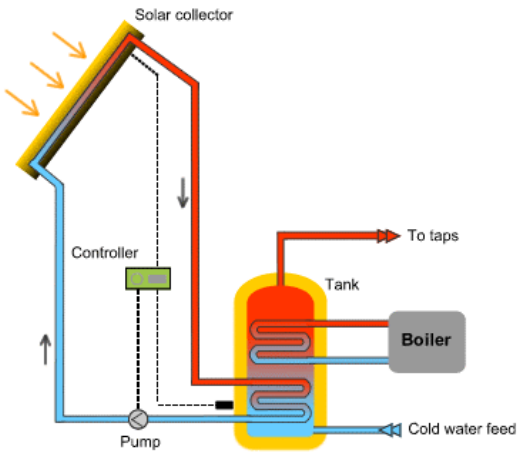


Figure 2.1 Simple solar hot water system (from internet)

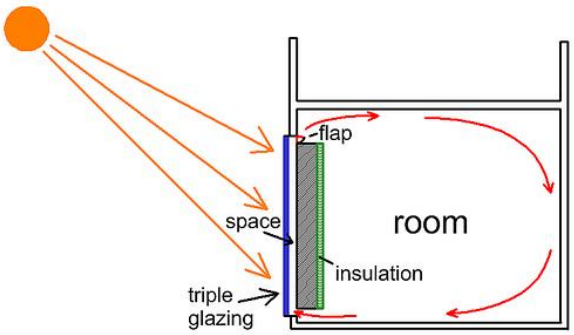


Figure 2.2 Schematic diagram of Trombe wall (solar energy house, 2003)

Facade integration of solar thermal system is another example of a solar thermal system. It comprises of a surface of large dimensions that is covered by an exterior glazing with an air gap in between. Figure 2.2 shows a schematic diagram of a classical Trombe wall. As can be seen in the diagram, the wall absorbs and stores the solar heat through the glazing. The efficiency of Trombe wall greatly depend on its design and location and it can contributing 20% -30% of the total heating to the building (Liu et al, 2012; Hordeski et al, 2011; Hami et al, 2012). Transpired solar collects that are supported by heat air between layers of the façade are more and more common (Shukla et al., 2012).

2.2.2 Solar cell

Solar cell uses photovoltaic conversion process to directly convert sunlight into electricity without of the need for a heat engine. A typical photovoltaic electricity formation system dwell of different elements, including solar cells, mechanical/electrical connections, and regulation of the electrical output. All solar cells need a light absorbing material to absorb photons and to achieve free heat via the photovoltaic impact.

Solar cells are typically classified depending on the light absorbing material used, such as silicon, cadmium telluride (CdTe), cadmium sulphide (CdS), organic and polymer cells, thin film and hybrid photovoltaic cell.

According to Bruton (2002), historically, silicon technology has dominated the power supply module for photovoltaic applications. However, recently, high efficiency polycrystalline and monocrystalline silicon solar cells have been developed, allowing thinner wafers and ribbon silicon technology to be introduced into the market. Goetzberger et al. (2000) briefly described the history of photovoltaic materials and discussed possible future silicon applications. Crystalline silicon solar cells constituted approximately 86% of the global market PV in 2012.

In this literature review, only crystalline silicon is discussed, due to its high efficiency relative to all other commercial solar cell materials and its commercial maturity. The electrical performance of any solar system is primarily influenced by the type of PV used. When silicon PV cell exposes to sun radiation, it tend to convert only short wavelength radiation to electricity, while the longer wavelengths are absorbed and converted into heat in the laminate leading to increase of PV temperature. One of the main important factor that influence the PV efficiency is its operating temperature. The operating temperature of PV in this research is defined as the mean temperature of PV panel under Standard Test Conditions (STC) when the designed maximum electrical efficiency is reached. The efficiency of crystalline PV will be reduced when the PV temperature over its operating temperature. Kalogirou (2006) indicated that high operating temperatures create a decline in the electrical conversion rate at about 0.5%/◦C for crystalline PV. In hot weather

conditions, PV temperature can reach up to 70 ºC, thereby introducing 25% reduction in the conversion rate from STC. Therefore, in recent years, significant research effort has been dedicated to the strategies for maintaining the PV cell operating temperature. Among the techniques proposed, active cooling and passive heat removal are particularly significant. Active systems usually use a pump to circulate water (Agarwal et al, 1994; Garg et al 1995) or air to cool (Kaiser et al, 2014), while passive methods rely on ducts at one or both sides of the PV for natural ventilation (Chow et al, 2006). Some systems employ high heat capacity materials, such as PCM at the back of the PV for direct heat absorption from the front side (Atkin et al, 2015; Ciulla et al, 2012).

Despite these measures, at present, only about 16% of the solar energy incident on crystalline PV is converted to electricity (Kalogirou, 2006). The remaining insolation is transformed into heat, which can be used to meet the part of the household heat requirements, such as air heaters and hot water. The hybrid PV thermal is then introduced and developed which combined both solar system together and will be discussed in next section.

2.3 PV Thermal system (PVT)

Solar panel using semiconductors that exhibit the photovoltaic effect to generate electrical power by converting solar radiation into direct electric current. As heat will also be generated during the process, the PV temperature will increase significantly, resulting in a reduction in the PV panel efficiency. Thus, the purpose of developing hybrid PVT system is to improve the electrical efficiency by reducing the PV collector temperature while making use of the thermal energy. This idea emerged in the 1970s and, over the following 40 years, extensive research on PVT collectors was carried out (Vokas, 2006). The main advantage of the PVT system is that it can produce more electrical and thermal energy than can be generated by the same area covered with conventional PV systems or conventional thermal collectors (Huang, 2011). In domestic building applications in particular, where the roof surface area is limited, this could be one of the important benefits of PVT usage. Such systems can also reduce the installation cost, as only one type of system will be installed instead of two. The majority of extant studies on PVT systems have focused on the thermal absorber, i.e., air, water or evaporative materials.

The simplest PVT systems rely entirely on the available technologies, and are therefore constructed by taking a standard photovoltaic panel and integrating it into a thermal collector without any modifications. In the sections that follow, sextant studies exploring different types of PVT systems are reviewed, and the models and numerical approaches underpinning these works are presented.

2.3.1 PVT water system

Zondag et al. (2003) investigated the efficiency of seven different PVT collectors utilising water as the thermal absorber and compared their annual yield performance. Nine designs of PVT water collectors were classified into four groups, shown in Figure 2.3. The results of this investigation indicate that the total efficiency for all PVT types of PVT exceeds 50%, while the channel-above-PV design has the highest efficiency of 65% (Zondag et al., 2002). These authors also investigated and simulated a series of steady state and dynamic models for PVT energy performance (Zondag et al., 2003). In keeping with their findings, channel-below-PV (transparent) configuration seems to be the foremost economical, whereas the additional economical single-cover sheet-and-tube style could be a different, the potency is 2% lower.

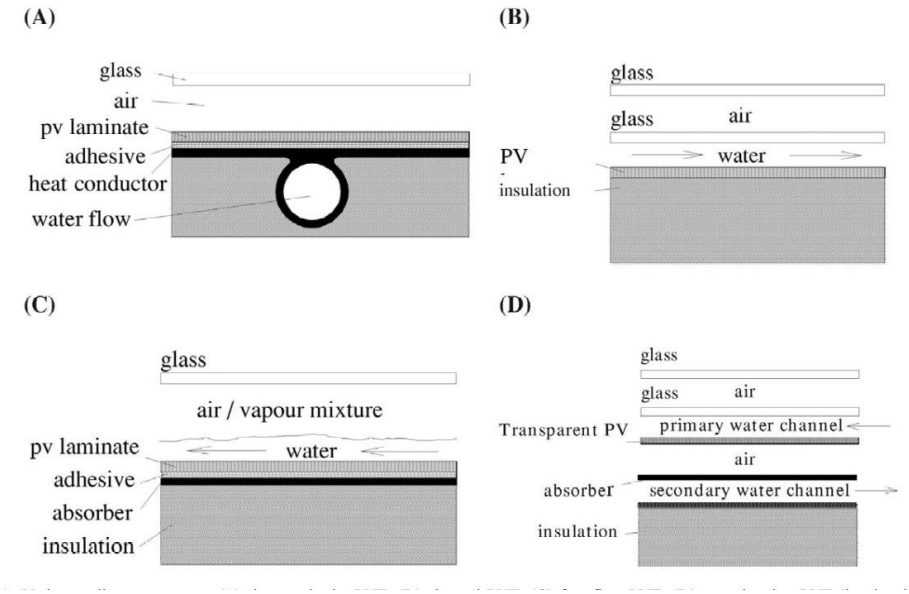


Figure 2.3 Various collector concepts: (A) sheet-and-tube PVT, (B) channel PVT, (C) free flow PVT, (D) two-absorber PVT (insulated type) (Zondag et al., 2003)

Sandnes et al. (2002) had the research on the energy performance of a PVT with crystalline silicon solar cells attached to the polymer to absorb heat. The black back side surface also acted as a solar collector when turned upside down. Square-shaped box-type absorber acting as the channel was also filler by ceramics granulates to improve transformation of heat to the flowing water. The research reported by the authors indicated that the presence of solar cells reduces the heat absorbed to 10% of the incident radiation, while the glass coated decreased the potency at about 5%. The authors then concluded that the system had a great potential for low-temperature hot water supply applications.

Kalogirou et al. (2006) presented TRNSYS simulation results for hybrid PVT solar systems for domestic hot water applications. In the investigation, each active and passive (thermosyphonic) systems designed for use at three locations - (named Madison (US), Athens (Greece) and Nicosia (Cyprus) at completely different latitudes were investigated. The authors incontestable that a substantial quantity of electrical and thermal energy is created by the aforementioned PVT systems, and also the economic viability of the systems is enhanced. Hence, the PVs significantly helpful in cases within which each hot water and electricity are needed, in domestic utilizations.

Chow et al. (2007) performed an experimental study of wall system by hot water collector and electrical phenomenon which will function as a water pre-heating system. Natural water circulation was found preferred to forced circulation during this hybrid reflector system. Thermal potency of 38.9% was measured at zero with decreased temperature, therefore the corresponding electricity conversion potency was 8.56%, throughout the late summer in urban centre, for example Hong Kong. The authors concluded that the utilization of the PVT wall

reduces the spacial thermal masses in each weather, winter and summer, this comes to the result of substantial energy savings. They additionally come with different ways on how to develop the system achievement in the future.

Boddaert and Caccavelli (2005) developed and designed hybrid solar panels consisting of polycrystalline silicon cells and a heat exchanger. Cheap roll-bond technology using aluminium was designed specifically for this study, incorporating a hollow tube (sheet-and-tube concept) in its middle, which acted as the heat exchanger system underneath the PV module.

Bakker et al. (2005) studied a system construct consisting of a 25 m2 surface coated by PVT panels and a ground coupled apparatus with simulation program. The authors purported that this method is in a position to fulfil 100% of the overall heat demand for a typical freshly designed Dutch one-family living accommodations. In addition, they indicated that the household would be ready to derive all of the electricity needed from the system, while maintaining the ordinary ground temperature unchanged in long-term. The price of a program in this mode was compared to the price of a coordinate system that was identical in every respect apart from replacing the PVT panels with separate PV panels (26 m2) and solar thermal collectors (7 m2). The thermal and electrical yield of this coordinate system was found to like that of the PVT system. The authors additionally noted that both systems needed an almost equivalent commencing investment.

2.3.2 PVT air system

The PVT air systems of two types are presently in use. They can be designed as a conventional solar collector, or to be moderated as a part/parts of the building

outer shell by creating an air gap between the PV panel and the wall; another type is called building integrated photovoltaic thermal collector (BIPVT) that works on the same principle as the conventional air-based PVT. Thus, the BIPVT performance also depends on the efficiency of heat transfer to the air and it varies from 14% to 60% (Zondag, 2008). The range is so wide because the heat transfer is highly dependent on the air velocity, which is a complex and essential parameter in the research on air PVT. The heated air can be used directly to meet part of the ambient heating demand, or to heat water through a heat exchanger, or in the BIPVT case, to assist the through exploiting nature convection for a better building ventilation.

More recently, a natural air circulation PV system is investigated by Tripanagnostopoulos (2012). It is conducting comparison of designs using water and air as resources of heat transfer fluid with and while not glazing (Figure 2.4). The result shows that water circulation for heat extraction is more potency compare with air. Electrical efficiency increased was achieved by the hybrid PVT in which water served because the transfer fluid attributable to more adequate heat removal. In addition, using glazing provided up to 30% increase in thermal efficiency compared to the basic PVT system due to the reduction in thermal losses.

The author further instructed that, once the collectors are placed in parallel, well separated rows to avoid shading, affordable booster diffuse reflectors may be placed between the adjacent rows to extend the radiation received at collector

surfaces.

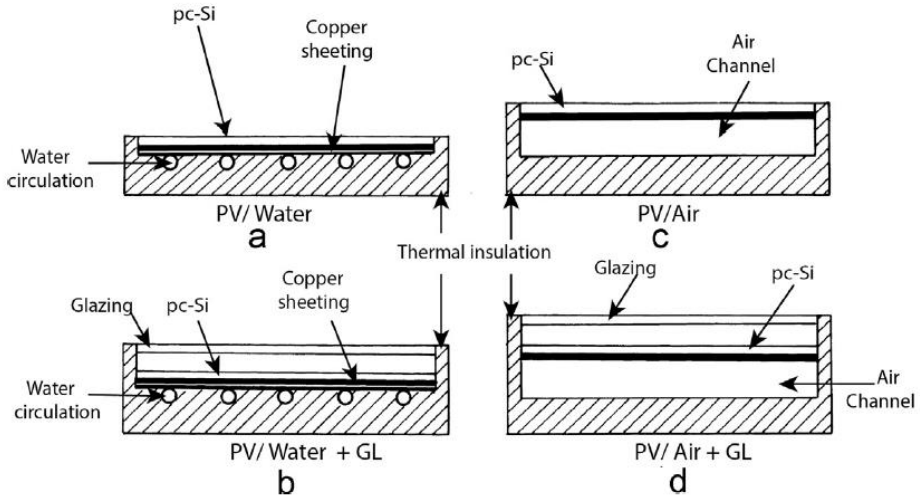


Figure 2.4 Cross-section of PVT experimental models: (a) PV/Water, (b) PV/Water + Glazing, (c) PV/Air, and (d) PV/ Air + Glazing

Tiwari et al. (2006) appraised the general potency achievement of an unglazed PVT representative in Republic of India. Among the reported outcomes were duct depth, duct length and the optimum airflow rate. Energy matrices were derived considering the embodied energy at various convert stages. In their subsequent process, Tiwari et al. (2008) appraised the general achievement of the photovoltaic module integrated with air duct and its suitability in relating to the weather in India. The authors have resulted compliance in both theoretical results and experimental observations, concluding that the overall thermal efficiency of the PVT scheme was increased considerably due to higher performance of thermal energy in the PV module.

Aste et al. (2008) introduced both the theoretical results and experimental of a development and research plan accomplished at the Politecnico di Milano, Spain, on the composition, evolution and achievement monitoring of a hybrid

PVT air collector. They also presented a case study of acknowledged economical appliance of the integrated solar roof in an experimentation centre department.

2.3.3 Building integrated photovoltaic (BIPV) thermal collector

The rate and capability of energy generation from solar power remain incredibly low compared to different various of sources and type of energy. To gain in advance of energy production from solar, adoption of localised model in alternative sectors for example workplace and household is compelling. Building integrated PVT (BIPV) systems are designed to not solely generate electricity however as well as providing heat. The heat has taken into account a waste by-product during this the system that weakened the potential of generation. Once BIPV is combined with illumination, daylighting and shading devices, it is able to decrease within the total energy gained in the building. Thus, BIPV transforms buildings from energy consumers into active power generators, this is necessary with the renewable energy development within the construction space. A typical schematic diagram of BIPVT air system on the wall and roof is shown in Figure 2.5.

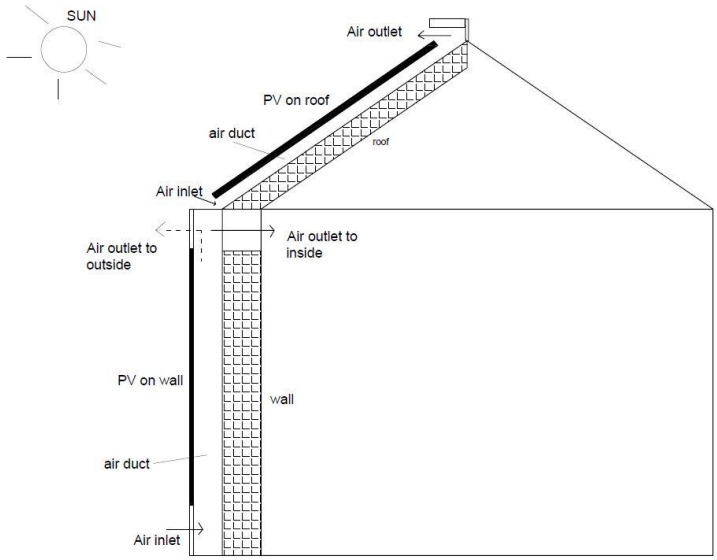


Figure 2.5 Schematic diagram of BIPVT system on wall and roof

In BIPV systems, passive heat removal also depends on buoyant circulation of air through an opening or air channel instead of a duct behind the PV. Yun et al. (2007) presented a theoretical analysis of with an opening behind the PV for three locations within a natural ventilated façade-integrated PV. They found that a maximum 5 ºC temperature decrease each month due to natural ventilation yielded an annual 2.5% increase in electrical output of the PV. The maximum heat removal has been shown to occur at a duct l/D of 20, resulting minimum temperature (34 C°) in a PV subjected to 50 W/m^2 heat flux with 5 m duct length (Brinkworth, 2006).

BIPV modules are available in several forms, including façade (Figure 2.6), roof (Figure 2.7) and glazing (Figure 2.8) type.



Figure 2.6 The CIS Tower in Manchester, England

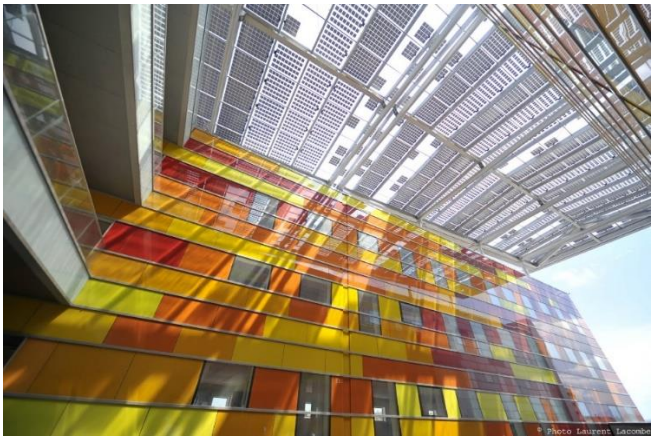


Figure 2.7 Projet BIPV, Gare de Perpignan, Southern France



Figure 2.8 BIPV solar façade on a municipal building located in Madrid (Spain)

A typical type of BIPVT comprises of double-skin façades that are manufactured from glass layers with a vented mid-pane shading device and are typically applied in business constructions. However, such construction could lead to a high temperature in the façade during the hot period and the possible overheating of the building. Fossa et al. (2008) investigated the physical mechanisms influencing the thermal behaviour of double-skin façades in an open channel. Different heating configurations were applied to two parallel walls, which were cooled by natural convection by airflow. The reported results indicate the outcome between the wall gap and the heat structure significantly changes the heat transfer conditions at the constant overall heat flux. The authors also provided a procedure for calculating the outer shell temperature, district heat transfer constant and district and moderate Nu figures.

Zogou and Stapountzis (2012) investigated a testing device specifically designed for their study, which formed the basic module of a PVT façade, combined with flow visualisation and hot wire anemometry measurements for enhancing the understanding of flow and turbulence inside the channel with

natural and forced convection modes. The outcome of this research demonstrated that the selection of flow rate and also the heat transfer characteristics of the rear sheet is critical to the performance of the PV façade.

Mei et al. (2003) introduced a dynamic thermal model supported TRNSYS for a construction with an integrated airy PV façade system. The construction model invested by the authors was subsequently validated against experimental information pertaining to a 6.5 m in height PV face in Barcelona. This finding revealed that the cooling loads are marginally higher with the PV façade for all areas taken into account, considering the impact of the façade on the heating load is primarily obsessed on area.

Kamthania et al. (2011) conducted an achievement analysis of a hybrid photovoltaic thermal (semi-transparent PVT) double-pass façade for energy supply within a specific area. A thermal model was developed by using the energy balance equations of the proposed hybrid photovoltaic thermal double-pass façade under quasi-steady state condition. In addition, the authors conducted numerical computations for the complex weather of New Delhi, India. Those engineers found that the semi-transparent PV module has higher electrical potency relative to that of an opaque PV module, while the area condition is increased by about 5 ºC.

Anderson et al. (2009) analysed the design of a novel building integrated photovoltaic thermal (BIPVT) solar collector. Their results show that both electrical and thermal efficiency of BIPVT are greatly affected by fin efficiency, thermal conductivity between PV cells and their supporting structures, and lamination methods. In addition, the authors point out that BIPVT can be made

of lower cost materials such as pre-coated coloured steel without significant reduction in efficiency.

Crawford et al. (2011) have connected PV modules with a heat recovery unit and analysed the system with two types of photovoltaic cell. The first system comprised of two c-Si 75 W with PV modules made of aluminium frames that were attached to the hardwood afters; whereas the other one was the same with the original system with the addition of a heat recovery unit. The authors estimated the energy payback (ROI) period in the 4 to 16.5 years range, this calculate on the BIPV system specifications.

Abdolzadeh and Ameri (2009) had the study on the consequence of spraying water over the photovoltaic cells on decreasing cell's temperature and reflection capacity. A 23% contraction in the PV temperature of the PV was observed when front surface of the PV was sprayed over by water, corresponding to a rise in the mean PV cell efficiency of 3.26%.

2.4 Thermal energy storage systems

Although the sun provides an ample, environmental and natural source of energy, the inventory is periodic due to the annual and diurnal cycles. Thus, insolation is intermittent, often unpredictable and diffused. Solar energy concentration is low when compared with the energy change densities found in ordinary fossil fuel devices, like oil-fired or coal furnaces. The demand for energy in both industrial and domestic sector, thus, is also highly uneven also follows yearly and constantly period (Ataer, 2006). Therefore, solar energy requires safe and reliable storage.

Thermal energy storage systems are designed to accumulate energy once production exceeds demand and to form it available at request. They will facilitate to meet power production and consumption, as well as exploit the variable production of renewable energy sources, such as solar energy. Thus, combining these two power resources increases the general potency of the power scheme and reduces CO2 emissions. Thermal energy storage system (TES) unit ensures a more efficient usage of the collected solar energy. This is particularly important for PVT domestic applications. In this section, storage system in both heat and thermal energy are briefly reviewed.

TES can be classified into three categories, depending on the stored energy type, namely sensible, latent heat storage, and thermo-chemical energy.

2.4.1 Sensible thermal energy storage

The sensible thermal energy storage systems have been in use for thousands of years. The use of large heat capacity materials as a wall for solar-heated building structures is extensive worldwide, and nearly any material will be used for thermal energy storage. Thermal energy is to be keep in rocks or pebbles packed in insulated vessels. This kind of ways for storage is applied frequently for temperatures up to 100 °C in conjunction with solar air heaters.

Another commonly used medium in sensible heat storage systems is water with water tank. Most domestic water heating and space heating systems use hot water storage tanks to achieve a high efficiency and energy savings. Thermal storage tank is essential for solar water heating systems, as it can hold hot water

for night-time usage. The disadvantages and advantages of water storage will be summarised as below (Abduljalil et al., 2012):

Advantages:

1. Water is usually low cost, easy to manage, non-combustible, non-toxic and widely available.
2. Large density and specific heat is for water.
3. Water can be used as the heat transfer fluid in heat exchangers.
4. Water have great mobility which is good for natural convection and siphon
5. Adjustment and control of a water system is variable and flexible.

Disadvantages:

1. Water could freeze or boil.
2. Working temperature is limited to 100 ºC and should be below this limit for most applications.

Design for sensible heat storage systems are simpler than other thermal storage systems and the initial and maintenance costs are relatively low. However, their large size and inability to store or deliver energy at a constant temperature are their key disadvantages.

2.4.2 Latent heat storage

In latent heat storage, the material changes its phase from one state to another by absorbing heat as latent heat. Such latent heat storage materials are thus commonly referred as phase change materials (PCMs).

When the stored heat in material is removed, it will revert to its original phase. The latent heat released from one solid phase to another is small, while solid to vapour and liquid to vapour transitions are accompanied by significant changes in volume, which make the system complex and expensive (IRENA, 2013). As the solid-liquid transformations involve comparatively insignificant difference in volume, such materials are available in a range of transition temperatures and might be used for both long and short term energy storage, applying range of materials and techniques.

One simple PCM application in building temperature control scheme involves the application of PCMs that react at a specific temperature. The PCM may be keep inside the building's air vent ducts and cold air will be able to deliver via large-area ceiling and floor ventilation systems.

According to Sharma et al. (2012), PCM defined into three main groups: eutectic, inorganic and organic mixtures, with a large number of PCMs under each category. However, not every PCM has the required target properties for sufficient thermal storage (Pasupathy et al., 2008b; Sharma et al., 2009). The comparison of inorganic and organic components for heat storage is given in Table 1.

Table 1 Comparison of organic and inorganic materials for heat storage

Organic		Inorganic	
Advantage	Disadvantage	Advantage	Disadvantage
Non corrosiveness	Lower latent heat capacity	Larger latent heat capacity	Possible corrosiveness

Lower or no undercooling	Lower thermal conductivity	Larger thermal conductivity	Sub cooling effect
Chemically stable	Flammable		Prone to phase segregation
Thermally stable			Lower thermal stability

PCMs can also be classified in relation to their phase transitions, such as gas-liquid, solid-liquid, solid-gas and solid-solid types. The liquid-gas and solid-gas transitions are characterised by a significant figure adjustment and hence require massive and complex pressure vessels or unique construction features. Solid-solid transformation is particularly interesting as a result of the power transfer involved in that conversion can be symbolic. It is noteworthy that several of materials display this characteristic at a certain melting point where around a specific temperature range. Solid-liquid transition is important because most of the material undergoes such transitions without significant volume changes, while releasing or absorbing large amounts of energy. The melting point of PCMs utilised in building applications usually ranges from 20 ºC to 30 ºC. In this research, 25 ºC was chosen in line with the typical UK climate changes. The size of the PCM unit depends on a combination of the system design requirements and the effective thermal conductivity of the phase change material.

2.4.3 Thermal energy storage through chemical reactions

Energy are often keep in systems composed of one or other chemical admixture that consume or release power. There are several different ways that thermal power is able to store by using chemical reactions. Chemical storage comprised a heat-absorbing reversible reaction, which can be reversed when it is necessary. Those products is to be keep in cold environments in most cases and able to therefore be transferred easily.

In ways of keeping thermal energy in chemical bond energy, reversible chemical reactions are preferable.

During the charge to provide heat, in order to consider the energy storage of the bond reaction, it should meet the conditions below (Abduljalil et al., 2012):

1. The reaction should occur near the equilibrium, i.e., it should be reversible.
2. The reactants with or without the addition of photosensitizers should be able to use as much sunlight as possible in the terrestrial atmosphere.
3. The energy keeps in the extra power considerably to be sufficiently large
4. The reactants need to be affordable

However, this form of thermal storage is not applicable for building utilizations due to inherently complex chemical reactions and will therefore not be discussed further.

In sum, for thermal energy storage, practical and inherent heat cache systems are preferable for building applications. Sensible types of energy have been in use for decades, but their large size and inability to store or supply energy at a

consistent temperature are their key disadvantages. Latent types, such as PCMs, can absorb large amounts of heat and can maintain a certain temperature for a long time due to phase change. Thus, applying PCM to thermal regulating PVs is a promising technology.

2.5 PV/ PCM systems

PCMs takes in thermal power as inherent heat at certain temperature. Hence, PCM with an appropriate process temperature can be used to regulate the temperature of PV cells therefore maintaining the potency for an extra period of time. By comparing with other ways of adjusting the temperature, the benefit of PCM is shift the time of heat transfer.

PCM heats up sensibly and, when it reaches the melting/solidification temperature, the material absorbs latent heat and starts to melt. Melted PCM maintain heat till a further stage. The continuation and temperature length over which the phase change takes place was calculated on the PCM mass and thermal physical phenomenon. Once PCM has fully modified phase, the material is going to start heat reasonably once more.

The main difference between PV/PCM and PVT systems depends on whether the thermal energy is used directly or indirectly. The heat in the PVT is collected and be used directly, while PV/PCM uses a PCM for that purpose. Another difference is that in PVT, the thermal distribution is timely because the preheating of the fluid is provided directly for end applications. However, PCM is different because heat may be maintained and used in the final application at a further stage.

Figure 2.9 illustrates a typical PV/PCM system with air duct at the back side (Huang, 2000). The PV cell is attached to the front of the PCM container and the rear plate is made from metal to ensure sufficient conduction. An air gap is maintained between containers and the building wall to allow heat to be removed by natural convection. This configuration not only protects the solar cells from overheating and increases electrical efficiency, but also enhances air ventilation.

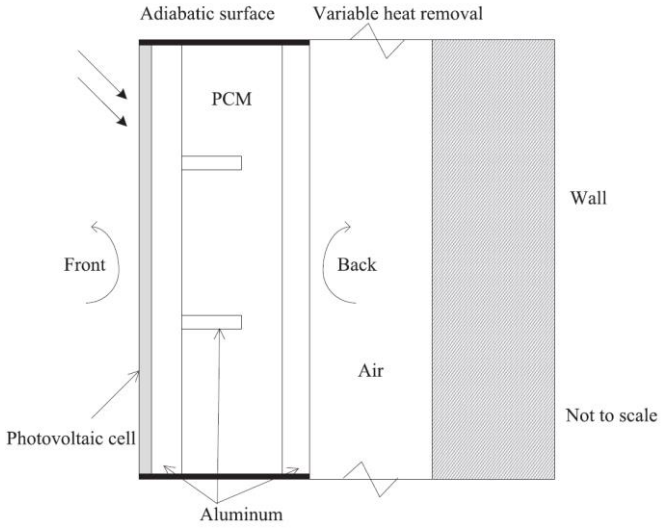


Figure 2.9 Diagram of the designed PV/PCM system (Huang, 2000)

Aelenei et al. (2013) conducted a simulation of BIPVT with vented and un-vented Trombe wall system, illustrated in Figure 2.10. Their results were validated experimentally using a BIPVT system. The calculated thermal and electric efficiencies indicated a thermal system efficiency of about 10% and an overall system efficiency (electrical and thermal) of about 20%.

Enibe (2002) presented a passive solar powered air heating system that consists of a single-glazed flat plate solar collector integrated with a PCM heat storage system. The authors suggested that this system would be appropriate for use as a solar cabinet crop dryer, as it does not require direct exposure to sunlight. In the subsequent work, Enibe (2003) provided a transient thermal analysis of a natural convection solar air heater with a PCM energy storage.

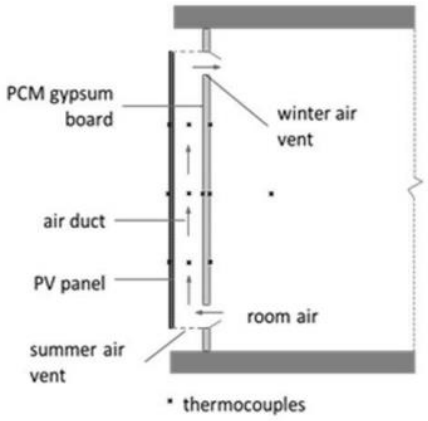


Figure 2.10 System configuration of PV/PCM

Huang et al. (2006) conducted a research on a PV/PCM system with a range of metal fin configurations incorporating into the PCM, employed to passively limit temperature increase in the BIPV. They compared this system with a conventional air-cooling system through experimental and simulations. They found that by applying metal fin, it had significantly effect on controlling the temperature increase in the PV incorporated into the BIPV system. Huang et al. (2011) continued their evaluation, by examining the effects on convection and crystalline segregation within the PV/PCM system. Their results indicated that optimisation of internal fins can greatly improve the temperature control of the PV in a PV/PCM system.

Malvi et al. (2011) performed a simulation model for a hybrid photovoltaic solar thermal system with PCM as thermal storage. The authors reported that, by including a selected PCM, the electrical efficiency can be typically increased by 9%. However, increasing PV performance was accompanied by a decrease in the solar thermal performance. Nonetheless, the authors concluded that a practical and worthwhile compromise can still be achieved.

Tanuwijava et al. (2012) studied a BIPV system with a microencapsulated phase change material (MEPCM). Parametric investigation of the electrical and thermal performances of the PV module were performed. The outcome indicates that incorporating the acceptable microencapsulated PCM layer is able to improve the thermal and electrical performance of the electrical phenomenon module. Additionally, consistent with the authors, the melting temperature and ratio considerably affected both electrical and thermal achievement of the PV module.

Biwole et al. (2013) investigated the use of PCMs to remain the panel temperature constant to the ambient temperature as possible. Their CFD modelling results indicate that adding a PCM on the back of a solar panel can remain the operating temperature for panel is under 40 °C for 80 minutes under a constant solar radiation of 1000 W/m^2.

Assis et al. (2009) performed an experimental and numerical analysis of the melting process of RT27 with a PCM in a spherical geometry filled with 98.5% solid PCM as the initial condition of the simulation. The remaining 1% accounted for the rise in the PCM volume throughout the phase process conversion. The authors found that the PCM melting process was affected by its

thermal parameters and geometry, including the Stefan number and the shell diameter.

Annabelle et al. (2011) had a research on comparison between their experimental and numerical results pertaining to a PCM conditioned in a parallelepipedic polyolefin envelope. Their numerical prediction was based on 1D Fortran code and a 2D model developed in Fluent commercial software tool. Both results were validated experimentally, and an agreed adjustment for the melting process was noted. However, both numerical code versions failed to predict the phase change process.

Ho et al. (2011) conducted a study aiming to investigate both the thermal and electrical PV performance utilising a microencapsulated PCM as a passive cooling device. The thermal and electrical properties of PV modules were simulated and the effects of external and internal environmental environments, daily solar radiation and thickness, and melting point of MEPCM were studied. The authors concluded that incorporating the suitable microencapsulated physical change material layer will enhance performance both in the way for electrical and thermal of the electrical phenomenon module, which was however affected by the melting temperature and aspect ratio.

Pascal et al. (2013) conducted computational fluid dynamics (CFD) modelling of heat and mass transfer in systems consisting of impure phase change materials located on the back of solar panels. In their work, the authors used a change in the enthalpy method to simulate the thermophysical changes in the properties of the material. Their results show that the addition of PCM on the

back of the solar panel maintains the operating temperature of the panel at 40ºC for 80 minutes at a constant solar radiation of 1,000 watts per square meter.

Hasan (2011) investigated melting temperatures for five PCMs within temperature at 25 ± 4 ºC range and heat of fusion in the 140−213 kJ/kg range for regulating the BIPV temperature using PCMs, which reduces the loss of temperature-dependent PV efficiency. They experimented with three daylight intensity to evaluate the performance of each PCM in four different PV / PCM systems. Their results show that the effect of thermal regulation on PV is determined by changing (i) the quality of the PCM and (ii) the thermal conductivity of the PCM and PV / PCM systems. The authors further noted that, for about 30 min, a maximum temperature decrease of 18 ºC could be reached, while 10 ºC temperature decrease was remained for five hours at 1000 W/m2 insolation.

Benli et al. (2009) experimentally investigated an inherent heat storage scheme with PCM for a newly designed solar collector in greenhouse heating to analyse the transient thermal behaviour of the storage unit during the charge and discharge periods. The reported results indicate that the proposed size of collectors with integrated PCM provided about 18–23% of general daily thermal energy requirements of the greenhouse for three to four hours, compare with the conventional heating device.

Hassan et al. (1994) proposed and analysed a simple solar air heater with built-in thermal energy storage system. They investigated the main thermal physical properties of one sensible heat (sand) and two latent heat (paraffin wax and hydrate salt) thermal energy storage materials.

In this section, an overview of previous studies of PV/PCM systems was presented. The findings reported in pertinent literature indicate that simple PV/PCM systems may not be economically feasible if used only to enhance PV conversion efficiency. Therefore, it is necessary to efficiently utilise the heat in order to achieve better performance.

2.6 Techniques employed to improve thermal performance

Based on the extant literature on the strategies that can be employed to enhance the heat transfer of a PVT system, the following techniques had typically utilized to boost the thermal achievement: through the composite high conductive material, fins and capsules to extend the heat transfer surface, the use of intermediate heat transfer medium or heat pipe, and the use of multiple PCM to increase the thermal conductivity..

Nallusamy et al. (2007) experimentally investigated the thermal performance of a packed bed of a combined sensible and inherent heat thermal energy storage (TES) unit. The authors designed, constructed and integrated the aforementioned TES unit with solar collector to study its performance. Their results show that mass flow has a significant effect on the heat extraction rate of solar collectors, which in turn affects the loading rate of TES tank.

Badescu (2003) modelled a sensible heat thermal energy storage device integrated into a space heating system. The reported outcome demonstrates that less TES units afford a better heat flux and discharge more rapidly, while the

larger TES units provide heat for longer periods. In addition, both the COP of heat pumps and exergy efficiency decrease when the TES unit length increases.

Wang et al. (2001) studied the melting procedures of the three PCMs filled in the cylindrical heat storage capsules with the lowest melting point PCM at the centre, the remaining two are arranged in order of increasing melting point from the centre to the outer surface. The results show that the melting time was 37−42% shorter in the three-PCM capsule relative to that measured for the single PCM capsule.

Hammou and Lacroix (2006) presented a hybrid heat energy storage system (HTESS) using a phase change material which is proposed for the simultaneous management of heat storage from solar and electrical energy (Figure 2.7.1). They developed a heat transfer model of the HTESS and validated it with experimental data. The results of the report show that space heating power consumption by nearly 32%, more than 90% of the electricity consumption in the off-peak hours.

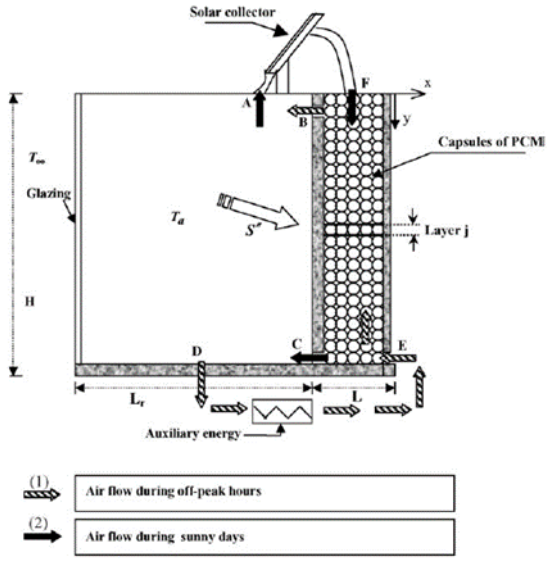


Figure 2.11 Hybrid thermal energy storage system (HTESS)

In order to improve the thermal conductivity of the thermal storage system, in many studies conducted to date, fins were applied either inside or outside of the storage unit. Two types of fins were typically utilised, i.e., plate type fins or pin type fins. Stritih (2004) assessed by compare an inherent energy storage unit alongside a finned surface with those ones in a plain surface energy storage unit from characteristic of heat transformation. This reported results indicate that the thermal release is able to energetically reinforce with fins. The natural convection effect that is effective and increases heat transfer during heat storage is reduced by the presence of fins. The authors further noted that heat transfer was higher during energy release and 40% reduction was achieved within unleash period when using fins.

Several studies on PCM systems with extended surfaces have been conducted for several calculations, particularly finned tubes (Ismail et al., 2001), where the numerical models were built, omitting consistency characteristic between both liquid and solid phases and presuming absence of convection in the melt.

Lamberg and Siren (2003) carried out a study in a semi-infinite PCM memory cell with infinite length of thin horizontal fins. In this model, In this model, continuous temperature end walls and fins are used as heat transfer plates during the melting process. The authors observed presence melting procedure into three parts: pure conductivity from the stable temperature end-wall and therefore the fin, conductivity from the fin with some natural conductivity from the end-wall, and at last solely natural convection from the fin. Thus, Lamberg and Siren (2003) proposed a coherent analytical model in a system with two parallel heating walls and a finite length of horizontal fins as a connector between them.

Hasan et al. (2007) introduced the use of conductive fins, grids or encapsulated in the PCM layer to improve the thermal conductivity of the PCM. In their laboratory tests, the authors found that PCM conductivity increased by 10% through laboratory testing to increase PV output by 3%.

The discussion discussed in this section shows that one of the major barriers to greater PCM utilization results from the need to improve low-PCM thermal conductivity to achieve fast thermal response and to provide longer thermal control periods for photovoltaic panels.

2.7 Opportunities for further work

Although significant works have been conducted on PVT and thermal storage systems, the inherent design complexity and economic issues still prevent its greater commercial application. This provides ample opportunities for further research and development in this field.

Current PVT system applications mainly focus on improving the electrical performance. Thus, authors of future studies should aim to develop new solar air systems employing PVT technology to replace conventional solar air heaters.

Most of the investigations on PV/PCM that were reviewed in this chapter focused on energy storage or release of PCM only. There is evident paucity of studies in which researchers combined the convection heat transfer into the model or experiment. As the heat transfer at the back side of the PV/PCM system depends on the ambient conditions, it would be highly beneficial if this heat transfer could be enhanced. To develop an economically feasible and

energy-efficient PV/PCM system, further validations through theoretical and experimental studies are still required.

Existing PVT systems are maturely operating for industrial and business use and there is not significant areas for performance enhancements. However, it is possible to make in advance for their achievement during research of the structural/geometrical framework, which should be pursued in the future.

The additional electricity output produced by incorporating PCM system is currently insufficient to cover the additional costs associated with the PCM use, resulting in the ROI period exceeding the typical limit of 20 years. Hence, it is essential maximise energy utilisation from the PV/PCM system. This can potentially be achieved by combining the system with interior building environment control to reduce heating load and provide ventilation.

2.8 Summary

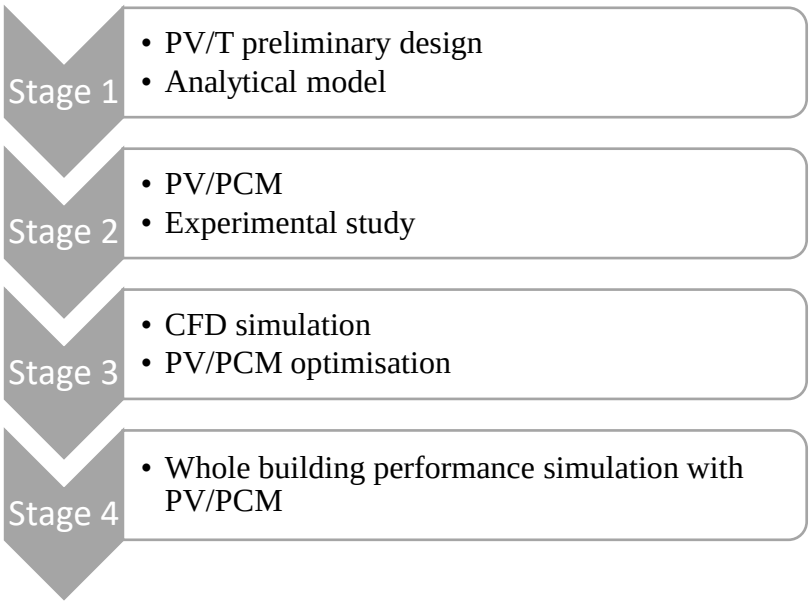
In this chapter, extant literature on solar energy and its applications in the building sector was reviewed. The review started with solar energy convection technologies, including solar thermal and solar photovoltaic cells. A hybrid technology, known as photovoltaic /thermal (PVT), was introduced and discussed. Prior research efforts on different types of PVT using water and air as thermal energy medium were also reviewed and discussed. The building integrated photovoltaic thermal system (BIPVT) was presented next, followed by commonly utilised thermal energy storage systems. The final section was designated for a review of a PVT system with PCM as thermal storage, and techniques for improving thermal performance concluded the review.

Although the PVT concept is considered as a promising sustainable technology, its design complexity and economic issues currently prevent its widespread commercial application. The aim of the present study was thus to design and develop a type of PVT for building applications, utilising the key findings yielded by this literature review.

Chapter 3 Methodology

3.1 Introduction

In this chapter, the methodology adopted for meeting the study objectives is presented. The work was conducted in four stages displayed below. Methodology pertinent to each stage will be presented in the next section.



In a PVT air system, once the PV module is heated by the incident solar radiation, detailed heat is transmitted to the air channel by deportation and emission. During the daytime, heat is received through the air in the rear surface of the PV module and the pipe in the rear wall of the air passage, resulting in a high outlet temperature, which generates heat by heat from the air. Consequently, the thermal and electrical properties depend on the airflow pattern, the channel depth, and the airflow rate. While natural air circulation constitutes a simple and low-cost way to dissipate heat from PV modules, this will reduce efficiency. Forced air circulation is comparatively capable; however,

the additional energy supply to the pump or fan reduces the net power gain of the system. Thus, in Stage 1 of the present study, the aim was to develop the primary design for an optimal PVT air system, which was achieved via an analytical model. In Stage 2, a series experimental investigations of a PVT system with PCM as thermal storage were conducted based on the results yielded by the analytical model. The experimental results were evaluated in Stage 3 and were subsequently used to validate the CFD model, which employs a more accurate simulation method to develop and optimise the PV/PCM system. Finally, the designed PV/PCM system was further simulated within different building envelopes in order to investigate the energy and economic achievement of the system in real building applications and provide simple guidelines for architects and engineers.

3.2 Stage 1 Analytical model

The purpose of stage 1 is to preliminary investigate the PVT system with a simple method to investigate the parameters for experiment design. In this stage, analytical method was employed to develop the experiment design of the PVT system for the present study. The results yielded were subsequently used for designing experiments aimed at a further investigation of the PVT system performance.

In order to analyse the thermal performance of the PVT, a simple PV façade thermal model was developed based on the famous Hottel–Whillier–Bliss

model (Duffie and Beckman, 2006). This model was widely employed and approved to be an appropriate methodology in PVT analysis. Figure 3.1 shows the diagram of one-dimensional heat transfer model.

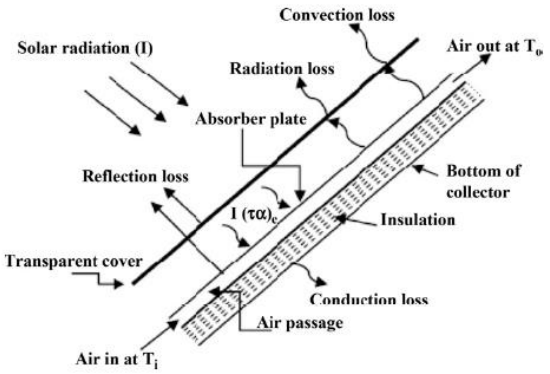


Figure 3.1 One dimensional heat transfer model (Duffie and Beckman, 2006).

In this model, it was assumed that the collector could be represented as a flat plate thermal collector. The thermal performance of a typical flat plate solar collector operating under steady state conditions can be described by (Florschuetz, 1979):

$$\eta = \frac{Q_u}{AG} = \frac{F_R\left[G\tau\alpha - U_L(T_p - T_a)\right]}{G} \qquad (1)$$

where η is the collector efficiency; Q_u denotes the useful energy gain; A is the effective collector surface area; G is the total radiation incident on the collector surface; F_R denotes the overall collector heat removal efficiency factor; $\tau\alpha$ is the transmittance-absorbance product of the photovoltaic collector; U_L is the overall collector heat loss coefficient; and T_i and T_a represent the temperature of air collector inlet and ambient, respectively.

The heat removal efficiency factor (F_R) can be calculated using Equation 2 (Florschuetz, 1979), where m is the mass flow rate in the collector and C_p is the specific heat of air.

$$F_R = \frac{mC_p}{AU_L}\left[1 - \exp(-\frac{AU_L F'}{mC_p})\right] \quad (2)$$

For a simple air channel, the collector factor F' can be calculated using Equation 3 (Duffie and Beckman, 2006), where h_c is convective heat transfer coefficient between the PV and the back wall, and h_r is the radiative heat transfer coefficient.

$$F' = \left[1 + \frac{U_L(h_c + h_r)}{h_c^2 + 2h_c h_r}\right]^{-1} \quad (3)$$

The overall collector heat loss coefficient U_L is calculated as the sum of the losses at the collector's edge, bottom and top. Typically, the edge losses are assumed to be negligible or are included in the back loss, resulting in:

$U_L = U_b + U_t$

While the bottom loss coefficient is given by the inverse of the insulation's U-value (i.e., K/L), the top loss calculation is more complex and depends on the glazing type.

For the unglazed type, i.e., the PV panel exposed to ambient environment, the top loss is given by Equation 4 (Duffie and Beckman, 2006):

$$U_t = h_w + h_{r,c-a} \quad (4)$$

where h_w is convective heat transfer coefficient of wind (if applicable) given by $h_w = 2.8 + 3V_w$ and $h_{r,c-a}$ is the radiative heat transfer coefficient from glass cover to the ambient expressed as:

$$h_{r,c-a} = \sigma \varepsilon_p \frac{(T_c^4 - T_s^4)}{T_c - T_a} \tag{5}$$

where the subscript *g* should be replaced by *PV* for the unglazed (UNGL) types and the equivalent sky temperature *Ts* is given by $T_s = 0.0552 T_a^{1.5}$, which is stand for the heat loss by radiation from the receiver involved heat exchange with the sky.

For glazed PV panels or more complex cases, Klein empirical equation is used (Equation 6), as given by Duffie and Beckman (2006).

$$U_t = \left(\frac{N}{\frac{C}{T_{pm}}\left[\frac{T_{pm} - T_a}{(N+f)}\right]^e} + \frac{1}{h_w}\right)^{-1} + \frac{\sigma(T_{pm} + T_a)(T_{pm}^2 + T_a^2)}{\frac{1}{\varepsilon_p + 0.00591 N h_w} + \frac{2N + f - 1 + 0.133\varepsilon_p}{\varepsilon_p} - N} \tag{6}$$

where *N* = number of glass covers

$f = (1 + 0.089 h_w - 0.1166 h_w \varepsilon_p)(1 + 0.07866 N)$;

$C = 520(1 - 0.000051\beta^2) for\ 0 < \beta < 70^\circ ; for\ 70^\circ < \beta < 90^\circ , use\ \beta = 70^\circ$

$e = 0.430\left(1 - {}^{100}/_{T_{pm}}\right)$;

β = collector tilt (deg)

σ =Stefan-Boltzmann constant，standard deviation

The U_L calculated by the equations above pertains to the flat plate collector. However, in practice, it is better approximated by the actual overall heat loss coefficient U'_L for PV thermal. Nonetheless, as shown in Equation 7, the difference between U_L and U'_L is usually negligible (Florschuetz, 1979).

$$U_L^{'} = U_L - \tau\alpha\eta_{ref}\beta_{ref}G \tag{7}$$

In the case of using natural convection, the expression for the induced airflow rate is calculated from Equation 8 (Tonui and Tripanagnostopoulos, 2007)

$$\dot{m} = \left(\frac{2g\beta(A_{ch}\rho)^2 A\eta GL\sin\theta}{C_p\left[K + \frac{fL}{D_H} + 2\beta T_o(A_{ch}/A_2)^2\right]}\right)^{\frac{1}{3}} \tag{8}$$

where A_{ch} and A_2 are channel and exit vent area, respectively (however, they are identical in the current model). The parameter D_H is the hydraulic diameter of the air duct that is equal to four times the cross-sectional area of the duct divided by the wetted perimeter. The constant K denotes the loss coefficients at the respective locations and is equal to 2.2 when the PV angle is 45^o. If the PV is perpendicular to the surface, the loss coefficients can be assumed to be zero (Equation 9). Equation 9 can be used to calculate the mass flow rate in the natural convection case after modification from Equation 8.

$$\dot{m} = \left(\frac{2g\beta(A_{ch}\rho)^2 A\eta GL}{C_p\left[\frac{fL}{D_H} + 2\beta T_o(A_{ch}/A_2)^2\right]}\right)^{\frac{1}{3}} \tag{9}$$

Brinkworth et al. (1998) developed a similar model to calculate the natural convection flow rate, as shown in Equation 10 below.

$$\dot{m} = \frac{2S(A_{ch}\rho)^2 gL\beta Q sin\theta}{C_p\left[\frac{fL}{D_H} + K_1 + K_2\right]} \quad (10)$$

Above, f denotes the friction factor that can be calculated from the equation given by John Finnemore (2006) for laminar and turbulent flow for forced ventilation (Equation 11). The parameters K_1, K_2 are loss coefficients at the respective location and are due to contraction and expansion associated to inlet and outlet vents, or change of direction of airflow.

On the other hand, f for natural convection is calculated by applying the equation given by Tsuji and Nagano (1988) for laminar and turbulent flow (Equation 12).

$$f = 64Re^{-1}(Re < 2300) \quad f = 0.316Re^{-0.25}\ (Re\ up\ to\ 20000) \quad (11)$$

$$f = 1.906(\frac{G_r}{P_r})^{1/12}\ (laminar) \quad f = 1.386\left(\frac{G_r}{P_r}\right)^{1/11.9}\ (Turbulent) \quad (12)$$

The Rayleigh number for the vertical surfaces is defined based on the height of the enclosure (H), while for the horizontal surfaces, the characteristic length (L) is defined as the ratio of surface area to its perimeter.

Randall et al. (1979) introduced Equation 13 for calculating average Nusselt number for the overall heat transfer coefficient of vertical enclosures.

$$Nu = 0.965Ra^{0.29} \quad (13)$$

where Ra is the Rayleigh number and is given by Equation 14:

$$Ra = \frac{g\beta' \Delta T D^3}{v\alpha} \tag{14}$$

Hollands et al. (1976) showed the relationship between the Nusselt number and Rayleigh number for tilt angles from 0 °to 75° (Equation 15).

$$Nu = 1 + 1.44\left[1 - \frac{1708(\sin 1.8\beta)^{1.6}}{Ra\cos\beta}\right]\left[1 - \frac{1708}{Ra\cos\beta}\right]^{+} + \left[\left(\frac{Ra\cos\beta}{5830}\right)^{\frac{1}{3}} - 1\right]^{+} \tag{15}$$

where the + exponent indicates that only positive values of the terms in the square brackets should be used.

For forced convection in reality, the heat transfer process involves a combination of forced and natural convection, laminar flow and turbulence. A useful expression of the Nusselt number for such mixed flow conditions is given in Equation 16 (Duffie and Beckman, 2006).

$$Nu = \sqrt{Nu_{lam}^2 + Nu_{turb}^2} \tag{16}$$

$$with \qquad Nu_{lam} = 0.644\sqrt{Re}\sqrt[3]{Pr}$$

$$Nu_{turb} = \frac{0.037Re^{0.8}Pr}{1 + 2.444Re^{-1}(Pr^{\frac{2}{3}} - 1)}$$

where $\mathrm{Re} = \sqrt{Re_{force}^2 + Re_{H,free}^2}$, and $Re_{force}^2 = \frac{vH}{v}$ $Re_{H,free}^2 = \sqrt{\frac{G_{rH}}{2.5}}$

Consequently, the convection heat transfer coefficient can be calculated by using the following expression:

$$h_c = \frac{K}{D_H} Nu \tag{17}$$

Radiative heat transfer in the air cavities is determined using the linearised coefficient from Stefan–Boltzmann equation (Duffie and Beckman, 2006):

$$h_{r,1-2} = \sigma(T_1 + T_2)(T_1^2 + T_2^2)\left(\frac{1}{\varepsilon_1} + \frac{1}{\varepsilon_2} - 1\right)^{-1} \tag{18}$$

When T_1 and T_2 are close in value, the numerator of Equation 15 can be expressed as $4\sigma T_f^3$, where T_f is the mean temperature.

$$T_f{}^3 = \frac{1}{4} * \left(T_p^2 + T_W^2\right)\left(T_p + T_w\right) \tag{19}$$

Radiative heat transfer from cover to ambient is given by:

$$h_{r,c-a} = \varepsilon_c \sigma(T_c + T_a)(T_c^2 + T_a^2) \tag{20}$$

Because the mean temperature of the PV plate (T_p), mean temperature of cover (T_c) and mean temperature of air (T_f) remain unknown, the equation is solved iteratively.

First, an estimate of the mean plate temperature is made, based on which the overall heat loss coefficient factor U_L, the collector efficiency factor F_R and useful heat gain Q_u are calculated. With the calculated values, a new mean temperature of the plate is obtained from Equation 21 (Duffie and Beckman, 2006). If the variation in the new mean temperature is smaller than a specified small value, the process is complete, otherwise the process should be repeated until this condition is met. By using Equation 22, the mean temperature of air could also be calculated.

$$T_p = T_i + \frac{Q_u/A}{F_R U_L}(1 - F_R) \tag{21}$$

$$T_f = T_i + \frac{Q_u/A}{F_R U_L}\left(1 - \frac{F_R}{F'}\right) \tag{22}$$

Heat transfer process is always accompanied by a more rapid decline in pressure. Since pressure decrement determines the fan power, it is important to evaluate its rate in order to design and optimise the pumping power for a forced convection system. Normally, the increase of electrical output power to generate larger airflow rate for pumps, leading to lower PV temperature, should be sufficient to compensate for the additional power expended by the f.

The calculation of hydraulic fan power is derived by applying Equation 23 below.

$$Power = \Delta P \cdot Q \tag{23}$$

The pressure decline $\Delta P = g\rho\Delta H$, where ΔH is total head loss, can be calculated from Equation 24 and Q is heat transfer. For the case of air, where the change in pressure is very small, it is considered as incompressible flow.

$$\Delta H = H_{kinetic} + H_f + K\frac{v^2}{2g} \tag{24}$$

where K is the loss coefficient in the duct entrance and exit. Using the values given by Finnemore (2002), the total value of K was estimated at 1.5. H_f is the friction head loss along the duct and is determined from the Darcy-Weisbach equation, given by:

$$H_f = \frac{v^2}{2g} f\left(\frac{L}{D}\right) \tag{25}$$

where f is the friction factor and was given in Equation 11.

Thus, fan power can be calculated by:

$$Fan\ power = Qg\rho\left[\frac{v^2}{2g} f\left(\frac{L}{D}\right) + K\frac{v^2}{2g} + \frac{\Delta v^2}{2g}\right]$$

$$= Q\rho\frac{v^2}{2}\left[f\left(\frac{L}{D}\right) + K + 1\right] \tag{26}$$

It should be noted that the electrical efficiency, η_{el}, of a PV cell varies inversely with the increase in its operating temperature. Thus, Equation 27 (Evans, 1981) is used to calculate the operating PV electrical efficiency.

$$\eta_{el} = \eta_{ref}\left(1 - \beta_{ref}\left(T_p - T_{ref}\right)\right) \tag{27}$$

where the β_{ref} is the temperature coefficient, in this case equal to 0.006 K^{-1}, according to manufacturer's specifications.

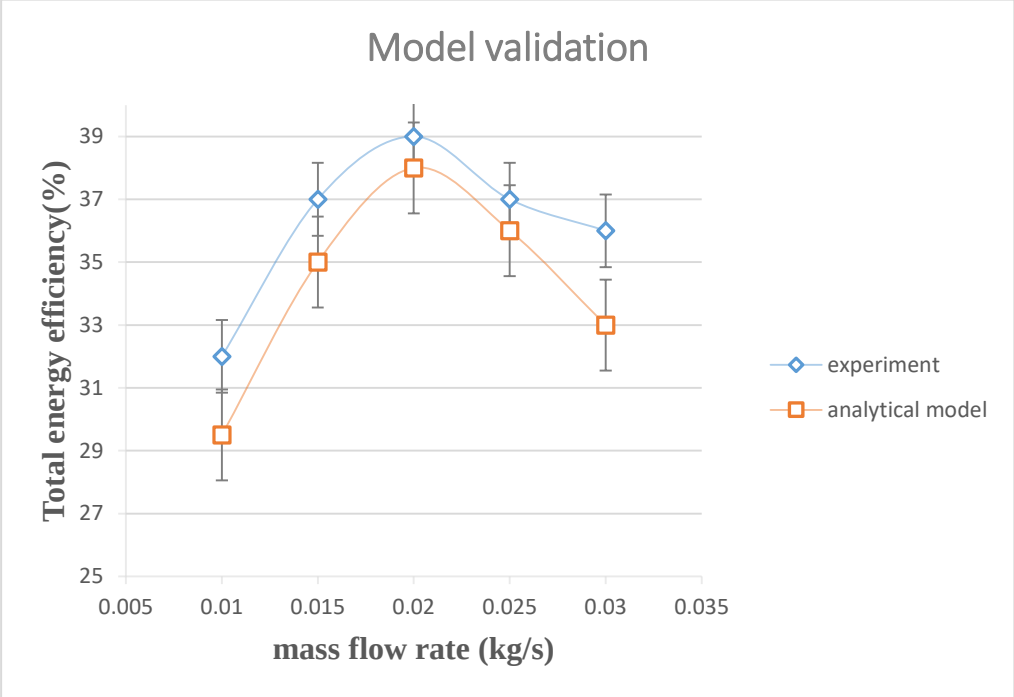


Figure 3.2 Validation with total energy efficiency

Figure 3.2 show the validation of analytical model with experiment result from Saygin et al(2017) with 5mm gap size. The graphs show that there is a good correlation between the predicted values and the measured data, with maximum. Similar results were observed when comparing the mean air outlet temperature from Tonui and Tripanagnostopoulos (2007). Based on the validation, it indicate that the model is satisfactorily validated considering its simplicity and can be used to preliminary investigate the PVT system.

System performance

The evaluation of the overall system performance of the PVT/PCM was based on the sum of thermal efficiency and electrical efficiency.

$$\eta_{total} = \eta_{themral} + \eta_{el} \tag{28}$$

Thermal performance was calculated as a function of the useful heat gain from the air outlet divided by the solar radiation multiplied by the area of PV. The

useful heat gain in PVT system is the difference between the heat through the air outlet and the air inlet, as the back wall of the air duct is assumed to be well insulated.

$$\eta_{themral} = \frac{Q_{outlet} - Q_{inlet}}{G \times A} \tag{29}$$

Electrical efficiency was calculated from the PV mean temperature using the temperature correction function below.

$$\eta_{el} = \eta_{ref}\left(1 - \beta_{ref}\left(T_p - T_{ref}\right)\right) \tag{30}$$

The heat exchange effectiveness of the PVT/PCM system was defined as the ratio of the actual air temperature increase to the maximum possible temperature increase (Kutscher, 1994):

$$\varepsilon_{EX} = (T_{outlet} - T_a)/(T_{PV} - T_a) \tag{31}$$

3.3 Stage 2 Experimental study

In this section, the methodology utilised in the experimental investigation is presented. A series of experiments were designed and conducted based on the analytical model results. Specific conduction and martial chosen will also be discussed in this section.

3.3.1 Solar cell selection

In PVT-air systems, the PV modules do not solely produce electricity, as well as producing heat. Hence, it is important to choose a suitable type of PV modules.

Most of the PV panels incorporated into the PVT system are produced from amorphous silicon (a-Si) and crystalline silicon (c-Si). Tripanagnostopoulos et al. (2002) presented experimental measurements on PVT-liquid and PVT-air collectors for both a-Si and c-Si. The authors found that for their PVT liquid collector, the efficiency of the c-Si and a-Si prototype was 55% and 60%, respectively. For the PVT air collector, the c-Si prototype and the a-Si prototype achieved 38% and 45% efficiency. However, the electrical performance for the c-Si modules, at 12%, was well above that of the a-Si at 6%. A higher thermal yield was also found for a-Si by Ji et al. (2003). In their study, c-Si was chosen because of its higher overall efficiency. Among the types of crystalline silicon utilised in solar cells, monocrystalline silicon was found the most beneficial, owing to its longevity and efficiency, along with lower installation costs.

For the present study, two pieces of monocrystalline photovoltaic panel (Biard 100W Solar Panel) were required, and were supplied by BIARD SOLAR and the manufacturers' specifications are listed in Table 2.

Table 2 Specifications of the photovoltaic panel

Specification	
Peak power (Pmax)	100 W
Cell type	Monocrystalline
Maximum power voltage (Vmp)	19.3 V
Maximum power current (Imp)	5.18A
Open circuit voltage (Voc)	22.9 V
Short circuit current (Isc)	5.56 A

Maximum system voltage	750 V
Temp. Coeff. of Isc (TK Isc) Temp.	0.06±0.01
Coeff. of Voc (TK Voc) Temp.	-(78±10)
Coeff. of Pmax (TK Pmax)	-(0.5±0.05)
Normal operating cell temperature	45 ℃±2 ℃
Power tolerance	-3%~+3%
Dimension (mm)	1200×540×30 mm
Weight (kg)	8 kg
Solar cells	36(4×9)

Glazing the solar cell commit a better thermal achievement and lower thermal deficiency encountered in common thermal plates. However, according to deficiency such as reflection and absorption, the electrical productivity of the PV module is diminished compared to the unglazed designs.

3.3.2 PCM selection

Phase change materials (PCMs) can absorb or release a large amount of phase transition latent heat under isothermal conditions. In recent years, scholars have conducted numerous investigations on PCMs. However, it is essential and critical for designers to choose a PCM in designing thermal energy storage system for different locations, especially if the PCM is also used to maintain the PV temperature, as is the case in the present study.

After careful consideration, salt hydrates PCM was chosen for this research due to its relatively high thermal conductivity and high phase change enthalpy. The

major disadvantage of using salt hydrates PCM arises from recrystallization and segregation of the salt during repeated cycles of charge and discharge.

The PCM used throughout this research was supplied by Phase Change Material Products Ltd, PLUSICE S25, which has been previously used in commercial applications. Its main component is calcium chloride hexahydrate ($CaCl_2 \cdot 6H_2O$) that solidifies and melts at 25 ºC. The key specifications of this PCM are given in Table 3.

It is worth noting that problems may occur in using salt hydrates as PCM in latent heat storage, such as incongruent melting that causes phase separation, and super cooling of salt hydrates because of their weak nucleation properties (Abhat, 1983; Bo He, 2004; Zalba et al., 2003; Farid et al., 2004; Ryu et al., 1992). The capacity of PCM used in experiment is estimated from the weather data of a peak sunny day in UK, by the method introduced by Jiang et al (2011) who developed a simple analytical method to estimate the optimal phase change characteristics. The results suggest the melting temperature can be 25C˚and the optimum capacity is range between 20mm to 50mm of thickness when attaching to the back of PV in the condition given above.

Table 3 Thermal and physical properties of the selected PCM

PCM type	Phase Change Temperature	Density(Solid/ liquid) kg/m^3	Latent Heat Capacity KJ/Kg	Volumetric Heat Capacity MJ/m^3	Specific Heat (Solid/liquid) kJ/kg.K	Thermal Conductivity (Solid/liquid) W/m.K
salt hydrate	25 ºC	1530	180	275 MJ/m^3	2.2	0.54
		1710			1.4	1.09

3.3.3 Experiment construction

The experimental tests were carried out on a prototype PVT air system using two commercial monocrystalline photovoltaic modules rated at 100 W each at standard test conditions and about 0.65 m^2 each as absorber plate. A schematic view of the physical experimental model is presented in Figure 3.3. The PV panel specifications were given in Table 1.

To construct the test unit and ensure high conductivity, an aluminium box (1200 mm ×1100 mm) was constructed and filled with phase change material (PLUSICE S25). Three aluminium boxes, with different depths (20 mm, 30 mm, and 50 mm) were made to test the effect of the PCM on the performance. A rectangular air duct box with adjustable channel depth ranging from 0 to 250 mm was designed and constructed to accommodate the PV module on the top and bottom using Celotex Insulation board of 100 mm thickness, which also served as the back and side insulation (Figure 3.3). The solar cell and aluminium

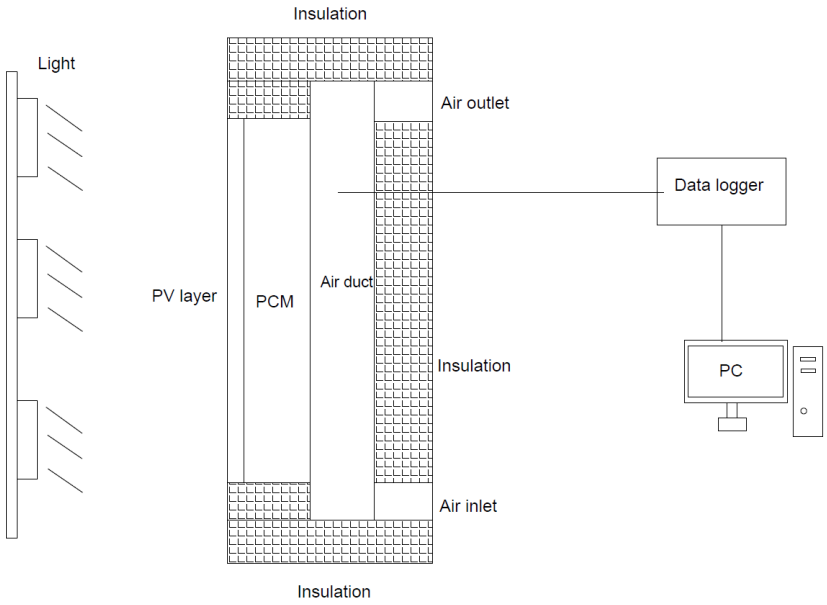


Figure 3.3 Schematic diagram of the experimental system

were physically bonded together with special thermal grease applied to both to provide good thermal conductivity and prevent short-circuiting the cells.

The unit was evaluated via two processes. First, the artificial light was applied to simulate the heat storage and the electrical performance of the PV panel was recorded. In the second test, the light was turned off to simulate the energy release process. Another unit was made with vertical fins inside the PCM unit. Simulated insolation was produced by nine 500 W lamps (Figure 3.4). In order to achieve a uniform level of radiation on the PV module, calibration of the solar simulator was required. The distance between the lamps and the test area was therefore varied by adjusting the distance between the lights and the PV frame.



Figure 3.4 Photograph of the test unit with the artificial light source



Figure 3.5 Photograph of the PCM container



Figure 3.6 Photograph of the test unit back side with the air duct inlet and outlet

Figure 3.6 shows the photograph of the PCM container with two openings on the top side. These openings were used to fill the container with a liquid state PCM. Figure 3.7 shows the back side of the final test unit with insulation, as well as air inlet and outlet.

Poor conductivity of the phase change materials is a common problem in latent heat thermal storage. The crystallising and thickening agents that prevent super cooling and phase separation in the PCM lower the thermal conductivity of the PCM and the inhibiting convection motion in the liquid PCM. This problem is particularly pronounced in the solidification process, where heat transfer is dominated by conduction. As natural convection has a limited effect on solidification, in some cases, heat transfer enhancement techniques may be required. The most common method for achieving this aim is based on using extended surfaces, such as fins and honeycombs. In this study, internal fins were implemented.

The same aluminium box of 30 mm thicknesses with vertical fins on its inside surface was created to improve the thermal performance. All fins had a 30 mm spacing, and the fin thickness, *t*, was very small (2 mm) compared to its length L, so that the effective surface area of one fin could be approximated by A = 2LH.



Figure 3.7 PCM container with vertical fins

3.3.4 Measurement equipment and uncertainty analysis

For capturing the relevant measurements, 23 T-type thermocouples with small wire diameter of 0.18 mm were distributed inside the test cell and on the walls, as shown in Figure 3.9. Twelve thermocouples were located at three identical depths within the PCM to measure spatial temperature variations. Six thermocouples were positioned equidistantly on the front and back surfaces to measure surface temperatures, while three thermocouples were placed along the air duct to measure air temperature. The operating temperature range for the T-type thermocouples is -100 ºC to 300 ºC. They were calibrated with a digital thermometer with the accuracy of ± 0.2 ºC, and the calibration range of 10 ºC to 80 ºC. Figure 3.8 shows the calibration curve of thermocouples obtained by using a digital thermometer as a reference.

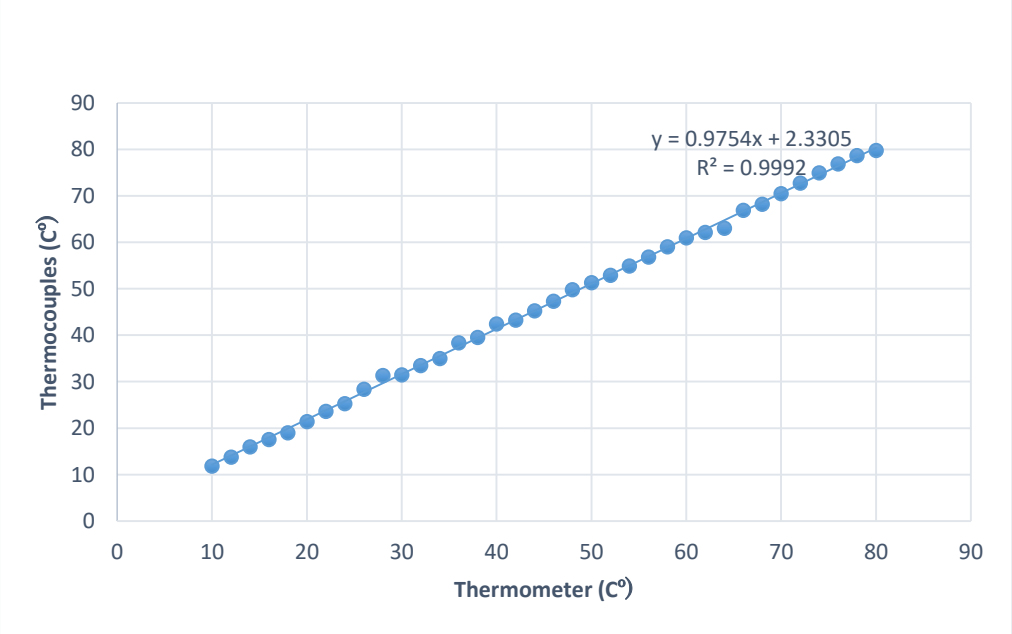


Figure 3.8 The calibration curve of thermocouples by using digital thermometer as a reference

The air velocity was measured using a hot wire anemometer (TESTO 425), with the accuracy of ± 0.03 m/s. The simulated solar energy from artificial light was measured by a solar power meter (ISM 400). A plate ammeter shunt (10 A, 75 mV) and two 100 W resistors were connected and used to investigate the electrical efficiency of the PV panel. All temperature and electrical data pertaining to the PV were recorded at 60 s intervals using a DT800 data logger (Figure 3.10).

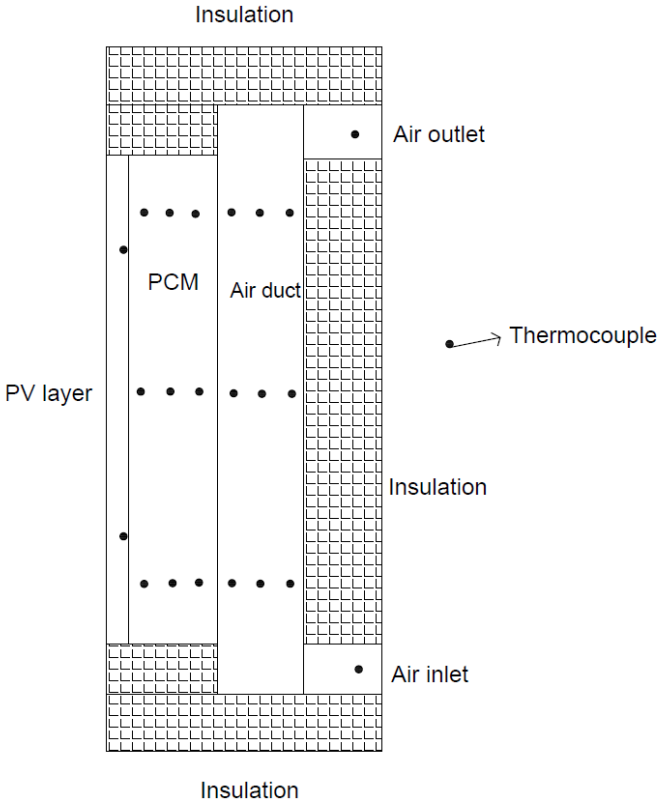


Figure 3.9 Possible observed point location

A list of locations of the observed points is shown in Table 4. The left bottom corner of the PV panel shown in Figure 3.9 was chosen as the point of origin (0, 0).

Table 4 Location of possible observed points

Point	Location
Three points for PV panel temperature Pa, Pb, Pc	Attach to back of PV layer (0,0.25); (0,0.5); (0,0.75)
Point 1 -3	Inside PCM, bottom (0.008,0.3); (0.016,0.3); (0.024,0.3);
Point 4-6	Inside PCM, mid (0.008,0.6); (0.016,0.6); (0.024,0.6);
Point 7-9	Inside PCM, top (0.008,0.9); (0.016,0.9); (0.024,0.9);
Point 10-12	Inside air duct, bottom (0.04,0.3); (0.08,0.3); (0.12,0.3);
Point 13-15	Inside air duct, mid (0.04,0.6); (0.08,0.6); (0.12,0.6);
Point 16-18	Inside air duct, top (0.04,0.9); (0.08,0.9); (0.12,0.9);
Point air outlet	air outlet (0.13, 1.175)
Point air inlet	air inlet (0.13, 0.175)



Figure 3.10 Data logger connection from the side of the test unit

In this research work, mean air velocity at air inlet and outlet are key factor for investigation into the system performance. A calibration has been performed to simplify the measurement of mean air velocity. A relative accuracy of mean air velocity was measured as benchmark by taking the average of air velocity at 20

points as displayed in Figure 3.11. The air outlet is was divided into 20 equal rectangular areas and the air velocity at the centre of each area was measured and the average of 20 velocities was then taken as the mean air velocity. The red square point as displayed in the Figure 3.11 gave the closest value with the benchmark mean air velocity with maximum of 5% error. So the red square point was used in this thesis to represent the air mean velocity.

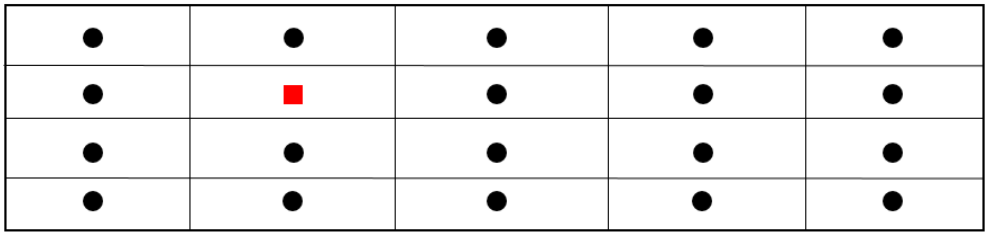


Figure 3.11 Measuring points for mean air velocity

Gauss propagation law was applied to determine the experimental uncertainties. The result is calculated as a function of the independent variables and is expressed by Buker et al (2014). The independent parameters measured in the experiments are: light radiation (±10W/m^2, 5%), PV panel temperature (± 0.2 ºC), PCM temperature (± 0.2 ºC), air temperature (± 0.2 ºC), and air flow velocity (± 0.03 m /s). The estimation implies that total uncertainty in calculation of the efficiency is found to be about 5%.

In the summary of this section, the general concepts, model and measurement instrument for the experimental phase of the study are discussed.

3.4 Stage 3 CFD simulation and system optimisation

Due to the increased interest in the use of natural ventilation to reduce photovoltaic efficiency and the use of excess heat, the CFT design computational fluid dynamics (CFD) model is commonly used. The advantage of CFD stems from its ability to calculate parameters that cannot be easily measured. The numerical program of the partial differential equation solution can be used to describe the physical parameters of the PVT unit, such as temperature, airflow velocity, liquid fraction, etc.. In the present study, the CFD model was validated against the experimental results obtained in Stage 2.

The developed model can be used to predict short cycle temperature cycling and fluid flow in two-dimensional regions of PV / PCM systems under different sunshine, ambient temperature and convective and radiant heat transfer boundary conditions.

The main difficulties associated with the simulation work for PV/PCM air system can be divided into two parts, the PCM simulation and air natural convection.

3.4.1 Phase change simulation

The mathematical formulation called phase transients called phase or moving boundaries is determined by the partial differential equation, which can be calculated by numerical analysis. The commercial CFD software Fluent by ANSYS was applied in the present investigation, as it was successfully utilised in the past to simulate many different engineering problems.

Two thermal characteristics are particularly relevant during the phase change, enthalpy temperature relationship and temperature hysteresis. The ANSYS Fluent code was used in the present study to solve the governing equations. The default model of phase change in the software is an enthalpy-porosity model that treats the solidified region as a porous medium. The porosity in each cell is set to be equal to the liquid fraction, whereby the cell and the appropriate momentum sink terms are added to the momentum equations to account for the pressure decline caused by the presence of solid material (Yu et al., 2010). In the fully solidified area, the porosity is equal to zero, which eliminates the speed of these areas. The paste area is a region in which the liquid fraction is 0 to 1. The characteristics are determined using a lever rule based on the difference between the melting and solidification temperatures. Using the lever rule allows calculating the density, viscosity and heat capacity of the mushy zone based on a proportionally weighted average of the liquid and solid properties (Fluent guide, 2012).

Susman et al. (2012) employed the enthalpy porosity method to simulate PCM sails and found that the method produced reasonable temperature prediction in global space temperature terms. Assis et al. (2011) carried out a numerical and experimental investigations of the melting process of RT27 with a PCM in a spherical geometry filled with 98.5% solid PCM as an initial condition of the simulation. They concluded that CFD is an effective way to study PCM.

The Fluent code utilised in the simulations performed in this research will be discussed in detail in Chapter 5.

3.4.2 Natural convection model

The complexity associated with simulating natural convection in buildings stems primarily from preferred of a turbulence model that is able to predict accurately the different types of flows encountered in the space.

Zhai et al. (2007) examined several primary turbulence models by simulating the inside surroundings in utilization purpose. The authors analysed turbulence models they believed exhibited a great potential in simulating airflow in an enclosed environment. Based on their findings, they suggested the difference in turbulence models is able to practice in different indoor counterfeit. As every single one has its advantages and disadvantages, a general turbulence model is not able to apply for limited inside environment airflow counterfeit. Zhang et al. (2007) appraised the achievement of eight turbulence models for four indoor airflows in easy understanding mathematical and compare with the arithmetical assumption with the data from experiment reported in pertinent literature. Their results indicate that the large eddy simulation (LES) provides more detailed flow information, but requires longer computing time compared to other Reynolds-averaged Navier–Stokes equations (RANS) models. Among the evaluated RANS models, the RNG k-ε exhibited better performance in all four cases.

Gebremedhin and Wu (2003) simulated a ventilated cattle facility using five RANS models, and concluded that the RNG k-ε provided the most suitable flow field modelling.

Rohidin et al. (2007) investigated three k-ε models, with a forced airing scheme and considering the effect of buoyancy to simulate a large packing facility. They found that the RNG k-ε outcomes are most decent according to validation outcomes.

Hussain et al. (2012) studied on six RANS models, reporting that, while all the turbulent models assessed and with approved assumption the fundamental subjective aspect of the progress and temperature disposal in the atria, insignificant result was achieved with the SST k-ε model.

Suarez et al. (2011) researched on the forced/buoyant airflow in a glazed gallery using the RNG k-ε, Standard k-ε and the k-w models. Result suggested that difference is insignificant amongst the models. However, on the basis of cohesion and reproduction time, the RNG k-ε model was found superior and was thus employed in their simulations.

As can be seen from the literature reviewed above, the RANS turbulence models have been extensively is applied for modelling compel inside airflows in easy understanding calculations in expected low cost involved. Authors of most of these comparative studies concluded that k-ε models were capable of simulating inside environment airflows. Nonetheless, the RNG k-ε model was found superior to the alternatives the general reproduction achievement. In the present study, Boussinesq approximation was used for natural airflow because the variations in temperature and density were small. Consequently, variations in volume expansion due to temperature gradients would be equally small.

3.4.3 Balance equations

Computational Fluid Dynamics (CFD) is assumed to be both PCM and airflow model output by numerically solving the Navier Stokes set of partial differential equations for mass, energy and momentum. Those formula were linearized, discretised, and applied in Fluent to obtain a detailed solution (Fluent User Guide, 2009).

Mass equation:

$$\frac{\partial \rho}{\partial t} + \frac{\partial}{\partial x_j} \cdot (\rho \mu_j) = S_M \tag{32}$$

where the source S_M is the mass added to the continuous phase from the dispersed second phase.

Momentum equation is given by:

$$\frac{\partial}{\partial t} \cdot (\rho u_j) + \frac{\partial}{\partial x_j} \cdot (\rho u_i u_j) = -\frac{\partial}{\partial x_j} \cdot p + \frac{\partial}{\partial x_j} \cdot \bar{\tau} + \rho g_j + F_j \tag{33}$$

where p is the static pressure, $\cdot\bar{\tau}$ is the stress tensor, and F_j are the external body force vector including porous media.

Energy equation is given by:

$$\frac{\partial}{\partial t}(\rho H) = -\frac{\partial}{\partial x_j} \cdot (\rho u_j C_p T) + \frac{\partial}{\partial x_j}\left[\lambda \frac{\partial T}{\partial x_j}\right] + S_E \tag{34}$$

where H is total enthalpy, the first term on right represents convective energy transfer, the second term represents conduction heat transfer, λ is conductivity and the third term denotes the volumetric heat source.

Energy equation for PCM is given by:

$$H = h + \Delta H \tag{35}$$

where hs is the sum of the sensible enthalpy (Equation 32 for incompressible flow) and ΔH is total latent heat.

$$h = h_{ref} + \int_{T_{ref}}^{T} C_p dT \tag{36}$$

h_{ref} = reference enthalpy

T_{ref} = reference temperature, 298.15 K

C_p = specific heat at constant pressure

Momentum equation for PCM is expressed as:

$$S = \frac{(1-\beta)^2}{(\beta^2 + \epsilon)} A_{mush}\left(\vec{v} - \overrightarrow{v_p}\right) \tag{37}$$

where β is the liquid volume fraction, ϵ is a small number (0.001) to prevent division by zero, A_{mush} is the mushy zone constant, and $\overrightarrow{v_p}$ is the solid velocity due to the pulling of the solidified material out of the domain (also referred to as the pull velocity).

The liquid fraction, β, indicates the fraction for the cell volume in liquid form, and can be defined as:

$$\beta = 0 \; if \; T < T_{solidus}$$

$$\beta = 1 \; if \; T > T_{solidus}$$

$$\beta = \frac{T - T_{solidus}}{T_{liquidus} - T_{solidus}} \; if T_{solidus} < T < T_{liquidus} \qquad (38)$$

The enthalpy porosity technique treats the cured region as a porous medium. The porosity in each cell is set equal to the liquid fraction in the cell. In the fully solidified area, the porosity is equal to zero, which eliminates the speed of these areas.

Radiation models (the P-1 model)

The P-1 radiation model is the simplest case of the general P-N model, developed by Siegel (1992). It was proven efficient in simulating the surface heat transfer problem in this research and is given by:

$$q_r = -\frac{1}{3(a + \sigma_s) - C\sigma_s} \nabla G \qquad (39)$$

where α is the absorption coefficient, α_s is the scattering coefficient, G is the incident radiation, and C is the linear-anisotropic phase function coefficient, described below. The C value ranges from -1 to 1. A positive value indicates that more radiant energy is scattered forward than backward, while a negative value indicates the opposite.

3.5 Stage 4 Building energy simulation with PVT/PCM system

During research and optimise period the performance of the PVT/PCM system for building applications in real conditions, it is required to replicate the scheme with a typical house subjected to realistic weather conditions.

However, the energy performance investigation of construction is always a complicated assignment as it needs to considering comprehensive cooperation within the construction, the HVAC system, and the outside issue (climate change), as well as obtaining mathematical/physical models that are effective in characterising every single elements.

Mateus et al. (2014) presented a thermal simulation validation of a double-skin naturally and mechanically ventilated test cell using Energy Plus. The reported results indicate approved concession between the simulation and the experimental values, with an average simulation error in air and radiant temperature of 1.4 ºC and an average daily maximum error of 2.5 ºC.

Velasco (2012) conducted authentication and acceptance of an Energy Plus phase change material model for opaque wall assemblies. The author reported findings confirming that Energy Plus is an effective way to simulate building energy performance with PCM. The reported results also indicated that detailed calculations and analysis is required when PCMs is designed in a home environment, as their thermal performance relate to varies of conditions, for example PCM properties and area in the construction environment.

The aim of this phase of the present study was to simulate a new design of PV on the surface of double-skin wall with PCM thermal storage at the back side.

The weather data was downloaded from the database maintained by World Meteorological Organization region and Country. Two different locations were chosen, namely Nottingham, UK, for temperate zone, and Shanghai, China, for subtropical climate.

Nottingham, UK, is characterised by warm summers and cold winters; thus, the design needed to focus on air heating. In Shanghai, China, where hot summers and cold winters prevail, both the cooling effect of PCM to PV and the heating effect of PCM to air should be in consideration. The modification of design in this study included changing the PCM characteristics, such as volume and melting temperature, changing air vent opening position and size, and changing the PV position from wall to roof mounted.

In this work, the PCM was simulated utilising the conduction finite difference algorithm solution provided by Energy Plus. CondFD discretises walls, floors, and ceilings into several nodes, and the implicit finite difference scheme is used to numerically solve the appropriate heat transfer equation (EnergyPlus guidebook). The CondFD algorithm in Energy Plus uses an implicit finite difference scheme, where the user can select Crank-Nicholson or fully implicit.

The validation of the PCM in Energy Plus was completed at the National Renewable Energy Laboratory (Judkoff and Neymark, 2006).

The following assumptions were made:

- Density of liquid and solid PCM is constant

- Melting temperature of PCM is fixed
- In each phase, thermal conductivity and specific heat of PCM are constant, only differ between the solid and liquid phases
- The PCM behaves ideally, i.e., phenomena such as property degradation and super cooling are not accounted for
- Thermal resistance across the wall of the container is neglected

3.5.1 Phase change model

Phase change materials are simulated by applying CFD solution algorithm, which permits simulating temperature dependent thermal conductivity and PCM in Energy Plus. The input temperature-enthalpy group specifies the temperature-enthalpy function of the two columns of the base material. The enthalpy temperature function for the PCM used in this study is shown in Figure 3.12. At low temperatures, the PCM performance should be similar to that of a sensible heat storage material. When temperature exceeds 25 ºC, the large heat capacity of the PCM provide certain advantage.

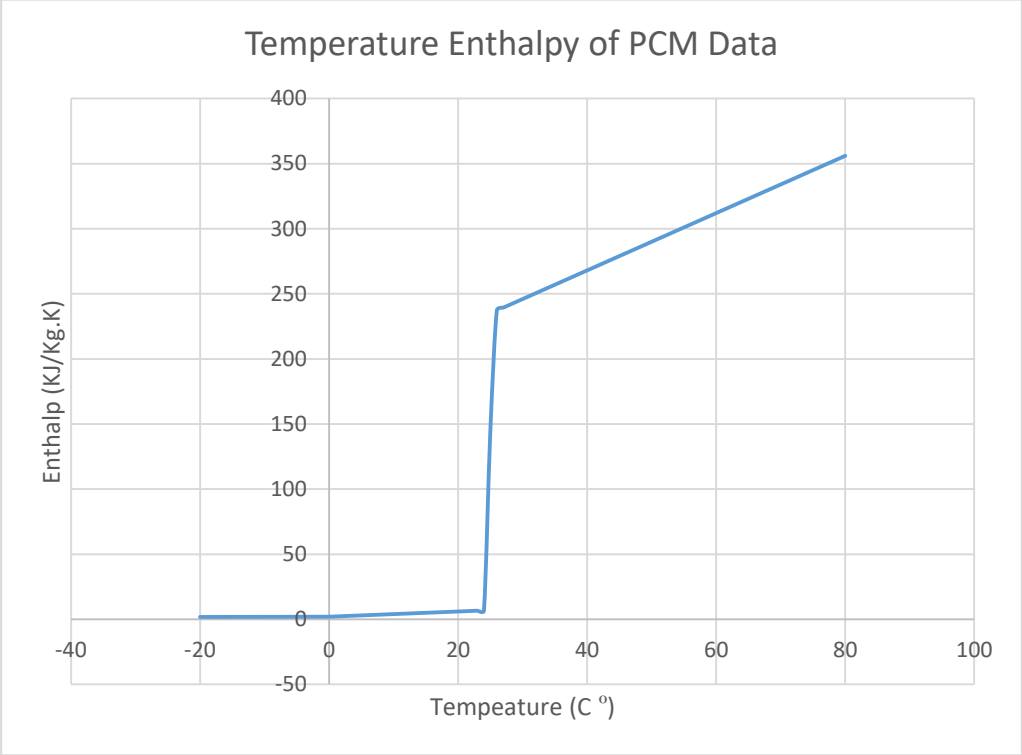


Figure 3.12 Temperature Enthalpy of PCM Data

3.5.2 PV performance model with electric storage system

There is a default simple PVT model in Energy Plus; however, its function is limited (thermal efficiency is fixed) and cannot integrate with other passive systems such as a PCM unit. Hence, in order to obtain relatively accurate results, PV and thermal air system were modelled separately.

PV performance was simulated by Equivalent One-Diode Model in Energy Plus, which is also known as the TRNSYS PV model, to simulate temperature dependent electrical efficiency. The PV model allows for different ways of integrating with other Energy Plus heat transfer surfaces and models, and permits cell temperature calculation. *Integrated Surface Outside Face* mode was

chosen in the present study to simulate the heat transfer between the PCM and the PV panel.

The input values of the PV array, comprising of 12 modules, are shown in Table 5.

Table 5 PV cell specifications

Cell type	Crystalline Silicon
Number of Cells in Series {dimensionless}	36
Active Area {m^2}	0.8
Transmittance absorptance product {dimensionless}	0.95
Semiconductor Bandgap {eV}	1.12
Shunt Resistance {ohms}	1000000
Short Circuit Current {A}	4.7
Open Circuit Voltage {V}	21.4
Reference Temperature {C°}	25
Reference Insolation {W/m^2}	1000
Module Current at Maximum Power {A}	4.25
Module Voltage at Maximum Power {V}	16.5
Temperature Coefficient of Short Circuit Current {A/K}	0.028
Temperature Coefficient of Open Circuit Voltage {V/K}	-0.076
Nominal Operating Cell Temperature Test Ambient Temperature {C°}	25
Nominal Operating Cell Temperature Test Cell Temperature {C°}	45
Nominal Operating Cell Temperature Test Insolation {W/m^2}	1000
Module Heat Loss Coefficient {W/m^2-K}	30 (not used in Integrated Surface Outside Face mode)
Total Heat Capacity {J/m^2-K}	50000 (not used)

Thermal conductivity of the PV panel was set to 0.2 W/m^2k, which is typically used for a silicon based sandwich construction framed PV panel.

3.5.3 HVAC model

HVAC (heating, ventilation and air conditioning) system is the technology that provides inside and conveyance surrounding convenience. It is aim to provide comfortable thermal and inside environment in an acceptable air situation. HVAC scheme design is a sub discipline of mechanical engineering, based on the principles of thermodynamics, fluid mechanics, and heat transfer. The main purpose of simulating PV/PCM system with the HVAC system is to investigate the possibility of energy reduction on cooling and heating capacity.

In this section, the designed PVT system with full HVAC system was simulated in Energy Plus 8.3. In wintertime, when heating is required, PVT system can work as a preheater to induce air, thereby reducing the total energy cost. In spring and autumn, when neither heating nor cooling is required, PVT system can be utilised to enhance night ventilation. During hot weather, when cooling is essential, the heated air exhausts directly back to the external environment.

Figure 3.13 shows the layout of a HVAC system with a PVT as a preheater.

The main purpose of simulating a simple HVAC system is to calculate the heating and cooling load of a typical house, as well as the performance improvement achieved by the PVT/PCM system.

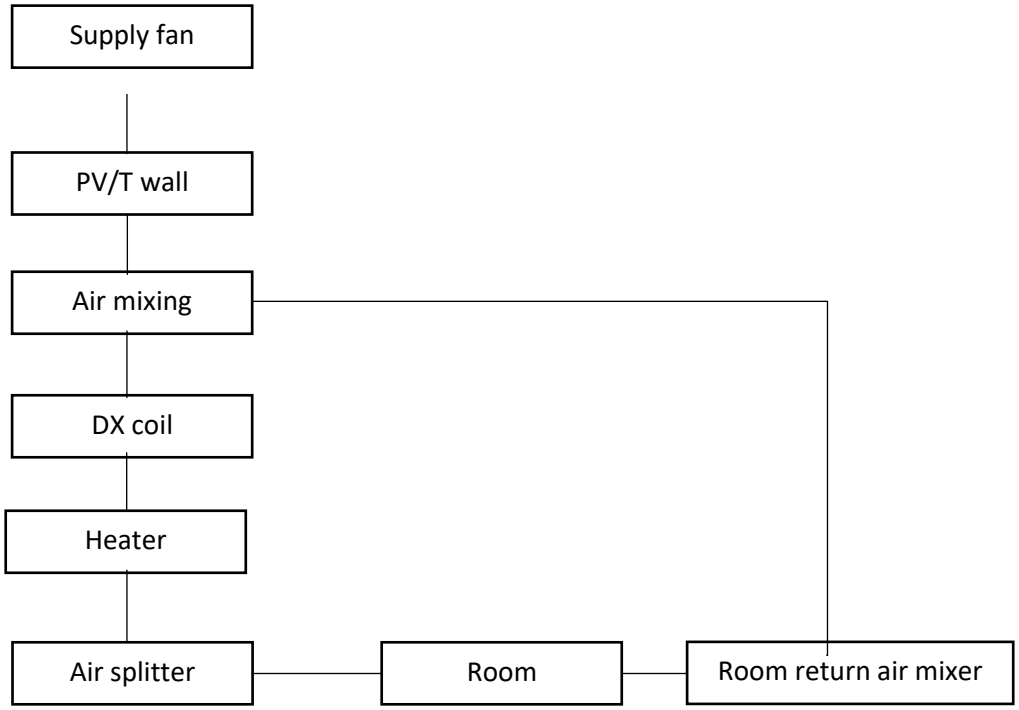


Figure 3.13 Layout of a HVAC system with a PV/T as preheater

3.5.4 Economic analysis

The use of PCM can provides thermal management to maintain the PV at a lower temperature, but requires more capital cost. Feasibility of the latter expenditure depends on the value of the additional electrical output. An economic evaluation is required for the PV/PCM system to determine whether the additional cost of introducing a PCM into the PVT system is justified. It is anticipated that these systems would have a relatively long Return On Investment (ROI) period, given the high initial cost of PV panels and the additional cost of the PCM.

Payback period in this study refers to the period of time required to recoup the funds expended in an investment. For domestic renewable energy application,

the payback period is determined by the balance of initial cost and the benefits from applying the technology. For economic analysis in this study, the comparison of normal PV system and PV/PCM will be conducted. The initial cost includes the capital cost for all the equipment, installation and maintenance fees. The benefit for normal PV system is reduction of electricity bill and the profit made from UK Government's Feed-in Tariffs scheme. The benefit for PV/PCM system includes the benefit for electricity production and it should be higher than that in normal PV system with same scale due to thermal regulation of PV by PCM. The extra benefit from applying PCM in house is reduction of energy bill by reducing the heat and cooling loads. So whether the PV/PCM system is economic efficient is depend on the comparison of payback period with normal PV system.

3.6 Summary

In this chapter, all the methodologies utilised in this research study were presented. The research process was divided into four stages, and the methodologies employed in each stage were discussed. The analytical model for the PVT system used in the preliminary investigation and designing the experiment in the first stage was presented. Methodology for all the experiments conducted in Stage 2 were also presented and discussed. Next, a CFD model for system optimisation performed in Stage 3 was built and described. Finally, the methodology for entire building performance simulation with PVT/PCM system was presented.

Chapter 4 Results of analytical investigations

The aim of the analytical phase of this study was to preliminary investigate the performance of PVT air system, while the results obtained could also be used in designing the experimental work on the final PV/PCM configuration. All the methodology involving in this chapter has been explained in section 3.2.

A PVT air system with the parameters presented in Table 6 was simulated and served as a reference for designing and optimising the PVT system. The parameter of PV panel is provided by manufacture. All calculations were thus based on the reference data, with the exception of the parameters that were the subject of the investigation.

Natural air circulation is a simple and low-cost strategy for removing heat from PV modules and maintaining the electrical efficiency at an acceptable level. While forced air circulation is more efficient, the additional energy supply to the pump required for this method reduces the net electricity gain of the system.

Table 6 Reference parameters used in the analytical method

A	Effective air collectors area (m^2)	1.25
β	Collector tilt angle (Degree)	90
C_p	Specific heat capacity of air (J/kg K)	1005
G	Incident radiation on the collector surface (W/m^2)	600
N	Number of glass covers	1
D	Spacing between the PV and the back wall (m)	0.3
D_h	Hydraulic diameter (m)	0.185

S	Spacing between the PV and the cover (m)	0.001
W	PV width (m)	1.1
L	PV length (m)	1.2
V_w	Wind speed (m/s)	0.01
T_a	Ambient air temperature (K)	293
T_i	Air gap inlet temperature (K)	293
$\tau\alpha$	Effective transmittance absorptance product	0.65
α	Cells absorptance	0.9
ε_c	Front cover emittance	0.84
ε_p	PV emittance	0.95
ε_w	Back wall emittance (insulation)	0.4
i	Back wall thickness (m)	0.05
K	Back wall conductivity (w/mK)	0.045
ρ	air density (kg/m^3)	1.2

4.1 Results for natural convection

4.1.1 Effects of incident radiation

The induced mass flow rate in natural convention depends on the heat flux gained from solar radiation. Hence, higher solar irradiance should result in a higher mass flow rate and flow speed due to a greater stack effect. The effect of incident radiation in the present study ranged from 100 W/m^2 to 1200 W/m^2. Figure 4.1 shows the variation of mass flow rate with irradiance at the ambient temperature of 293K for the PVT system. As can be seen from the graph, the mass flow rate increases with increasing solar radiation, as predicted, due to a greater percentage of irradiance being intercepted by the PVT collector. Consequently, more heat energy can be transferred to the air, creating higher stack effect. However, the mass flow rate increment gradually declines as the

solar radiation increases, possibly due to the heat transfer rate limitation on the heat exchange between air and the PV panel.

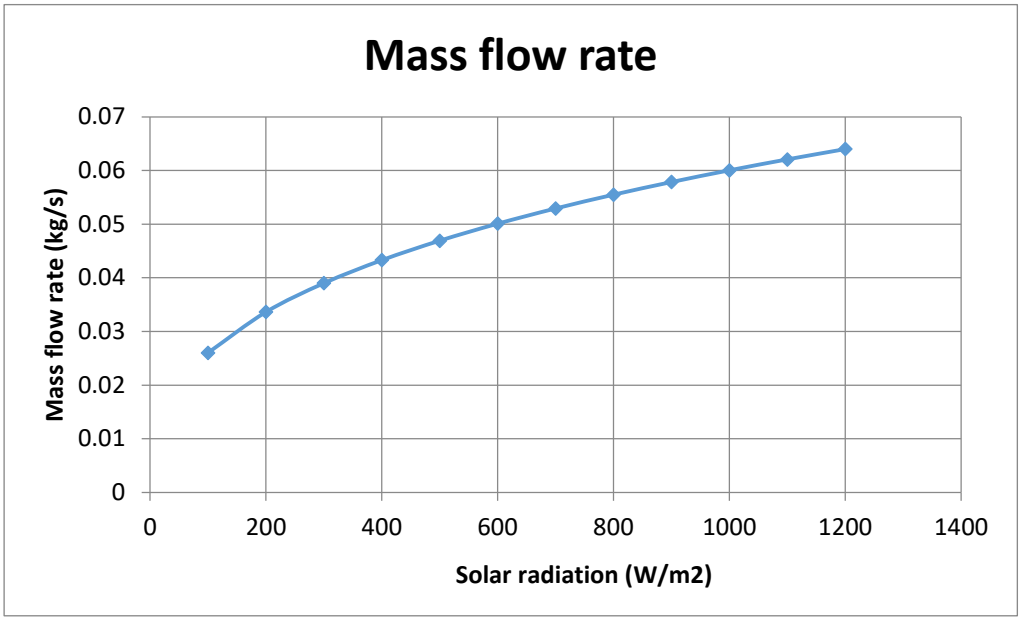


Figure 4.1 Variation of mass flow rate with irradiance

Figure 4.2 illustrates the variation in temperature measured at different system components as a function of irradiance. As can be seen from the curves, higher irradiation will also lead to a higher temperature of air and the PV panel, as more heat energy is transferred to the PV. However, as the mean temperature of the PV increases more rapidly than the outlet air temperature, this differential results in higher flow velocity. This may cause from the lower heat capacity of PV material and limited heat transfer between PV and air.

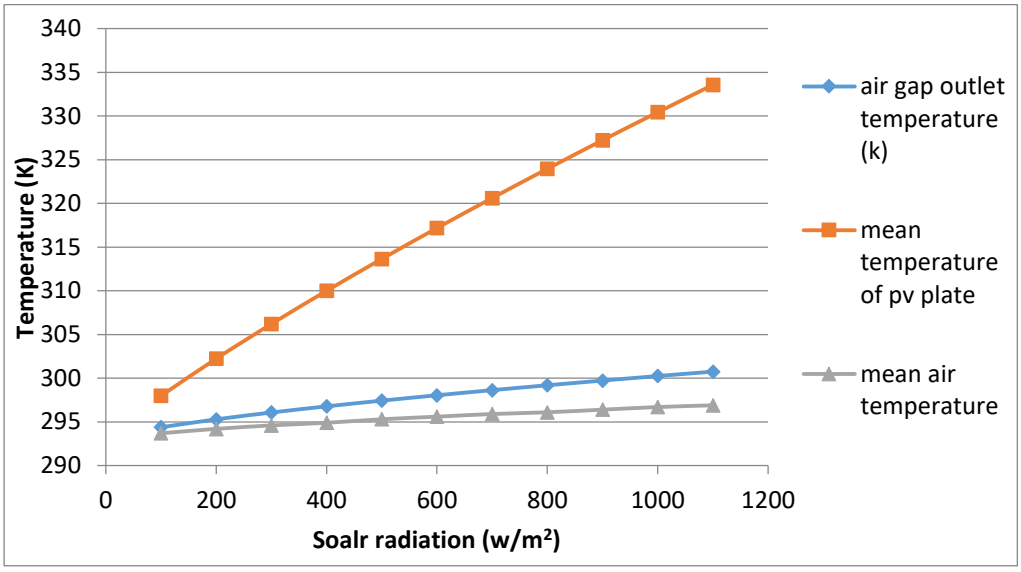


Figure 4.2 Temperature variation for different system components as a function of irradiance

Figure 4.3 illustrates the variation of thermal and electrical efficiency as a function of irradiance given by Equation 28, 29 and 30. The total efficiency of the PVT system in this study is compared by combining the values of the thermal and electrical efficiencies. As can be seen from the graph, the electrical efficiency remains at the maximum level at low irradiance and starts to decrease as the irradiance increases. This change is due to the PV panel overheating when irradiance exceeds 700 W/m^2. It can also indicate that, when irradiance increases beyond 700 W/m^2, the heat removed by natural convection of air in this configuration is not sufficient to maintain the PV temperature. Thermal efficiency also increases with irradiance due to the higher flow rate and higher thermal energy gain by the PV. However, thermal efficiency stabilises at high irradiance levels because of the slow growth of the mass flow rate and heat transfer rate at higher irradiance. Thus, the total efficiency of the PVT system initially increases, but starts to decline when solar radiation exceeds 700 W/m^2. These results indicate that there is an optimum solar irradiance at which a

specific PVT system would reach maximum energy efficiency, and in the case here, the optimum solar irradiance is around 600 W/m^2.

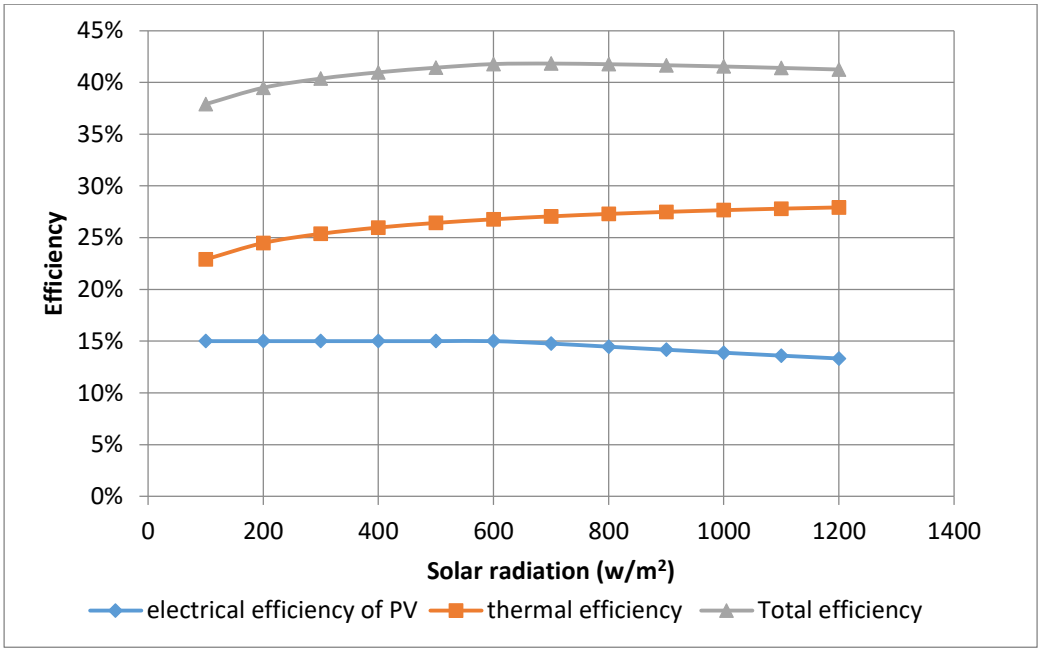


Figure 4.3 Variations in thermal and electrical efficiency with irradiance

4.1.2 Effects of air gap size

Figure 4.4 shows the plot of the temperature as a function of the channel depth, which was varied from 0.01 m to 0.4 m. As can be seen, the mean air temperature inside the air gap and at the outlet initially declines with increasing channel depth, gradually approaching the inlet temperature. The mean temperature of the PV panel also decreases as the gap size increases from 0.01 m to 0.1 m, after which it increases and finally stabilises at a certain temperature.

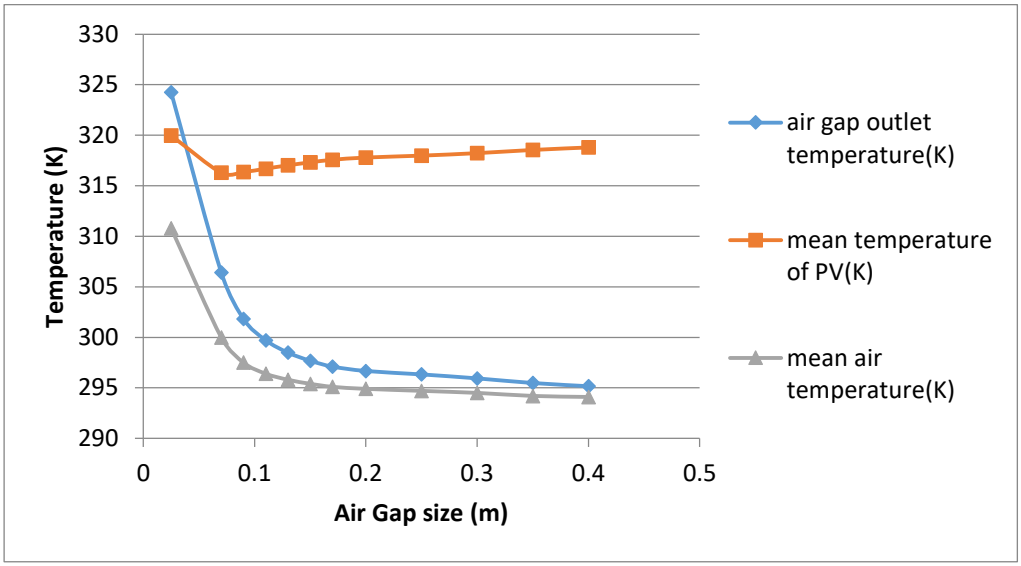


Figure 4.4 Temperature variation as a function of gap spacing

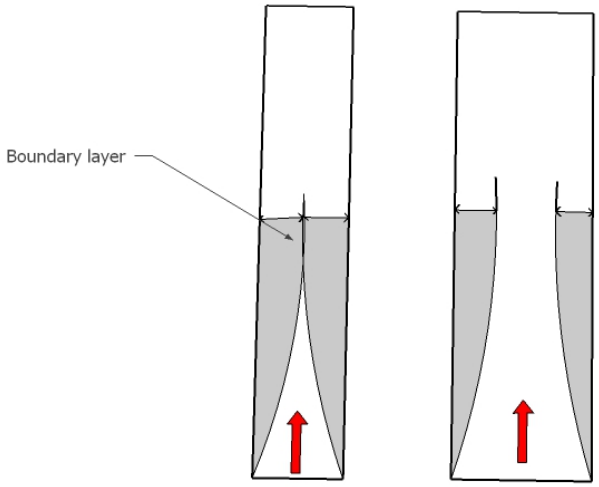


Figure 4.5 Boundary layer in the air duct

In this case, the buoyancy force is due to the presence of air density gradient caused by a temperature gradient. In the duct, the boundary layers from both sides merge near the top and flow is within the two boundary layers with small gap spacing (Figure 4.5). When the gap spacing increases, the boundary layer thickness at a given height remains the same, this may result in the two wall

boundary layers failing to merge at the top, leaving a free space between them where reverse flow may occur.

Beyond the optimum spacing, the outlet temperature is very high, and it decreases rapidly as the gap spacing increases. After the optimum point, it decreases slowly and tends toward ambient temperature. The mean temperature of the PV exhibits the same performance as the outlet air temperature beyond the optimum spacing, and thereafter increases gradually as the spacing increases further. These phenomena are attributed to the changes in the decline in pressure and convection heat transfer coefficient with gap spacing. The initial high temperature is due to the low heat transfer coefficient value. The optimum point occurs when the stack effect balances the frictional force.

Figure 4.6 presents the variation of thermal and electrical efficiency as a function of gap spacing. The graphs indicate that there exists an optimum gap spacing at which both electrical efficiency and collector thermal efficiency are at their respective maximum levels. The effect of gap spacing to the electrical efficiency is limited as the mean PV temperature is beyond its operating

temperature range. So the performance of total efficiency is determined by thermal efficiency and it reaches its maximum at the gap size of about 0.1 m.

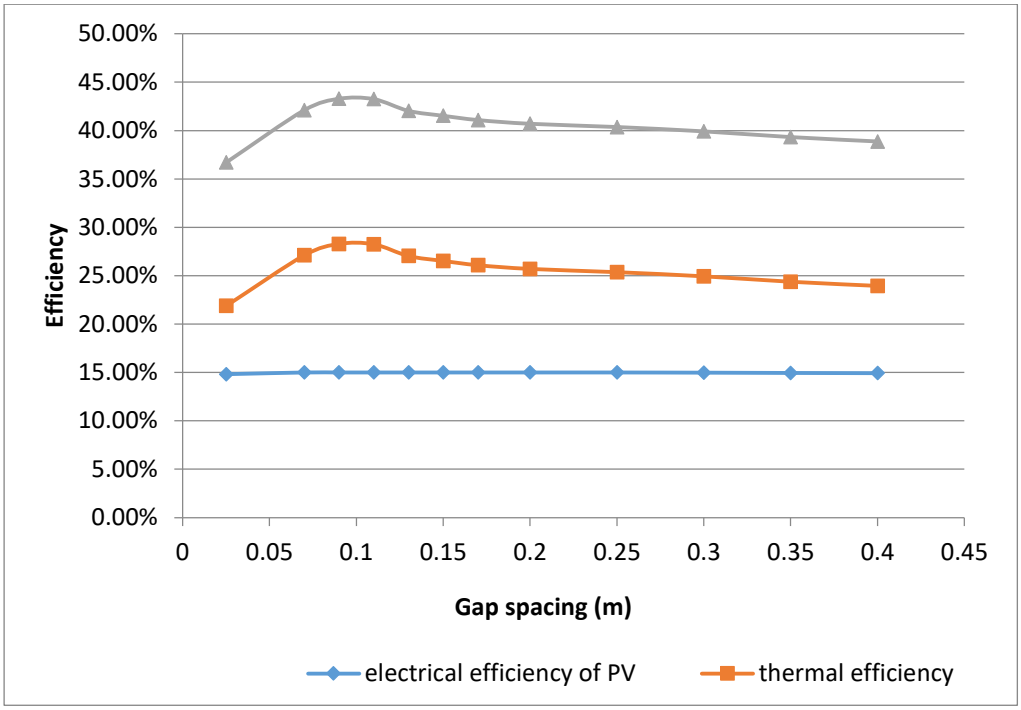


Figure 4.6 Variation in thermal and electrical efficiency with gap spacing

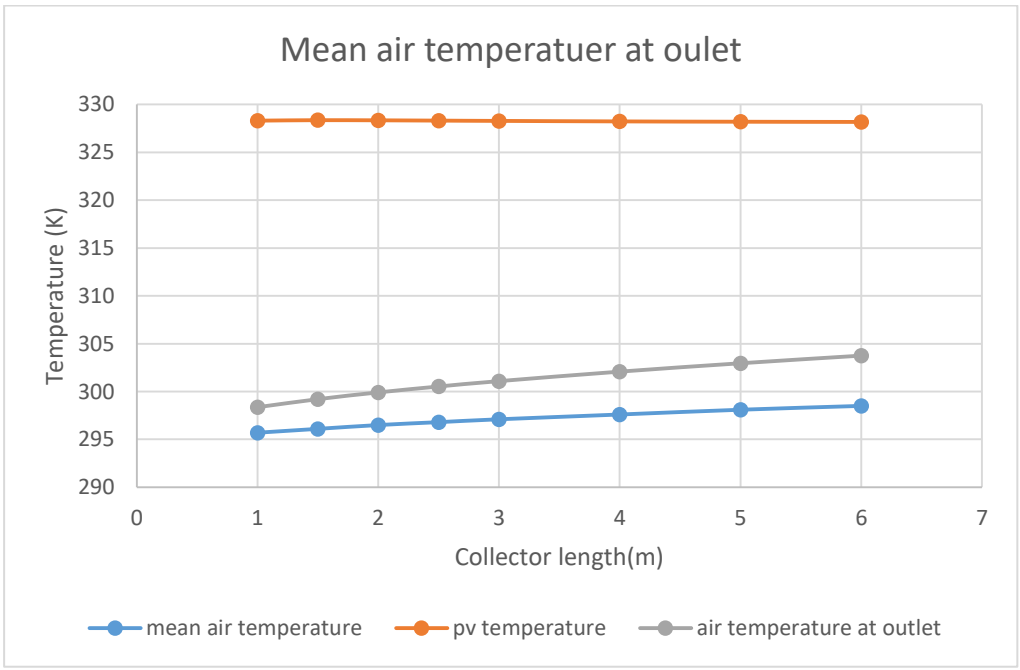


Figure 4.7 Variation in thermal and electrical efficiency as a function of PV panel length

4.1.3 Effect of PV panel length and total area

In this case, the PV panel length was increased from 0.5 m to 4 m, while the width remained constant at 1.1 m. Consequently, the total panel area also increased with the panel length.

Figure 4.7 shows the temperature variation as a function of the PV panel length, where it can be seen that all observed temperatures (except the PV temperature) increase with the panel length. In addition, the changes in the mean PV temperature are very small. As the increasing panel length increases the total heat absorbance area, more solar radiation is absorbed and more heat is generated.

Figure 4.8 presents the thermal and electrical efficiency as a function of PV panel length. As can be seen from the graph, the total electrical efficiency remains constant due to the stable mean PV temperature. The thermal efficiency decreases slightly (by about 1%) as the panel length increases from 0.5 m to 1 m, and remains stable at about 27% thereafter. Combined with the results depicted in Figure 4.7, these observations indicate that increasing the panel area does not have a significant effect on efficiency, even though it increases the air temperature in the air duct. As increased air temperature will lead to an increase in the air velocity in the duct, larger convective heat transfer rate is expected. This is also demonstrated in Figure 4.8, which depicts changes in the convective heat transfer coefficient between the PV panel and the back wall. Above 1 m, the convective heat transfer coefficient increases with PV panel length. When the PV panel length is less than 1 m, the aspect ratio is smaller than 2:1, as the frictional losses due to fluid viscosity and turbulence have a significant effect on airflow. Thus, unless the aspect ratio (the ratio of width to height of unit) is

low, increasing the PV panel length does not result in appreciable improvements in the PVT system efficiency.

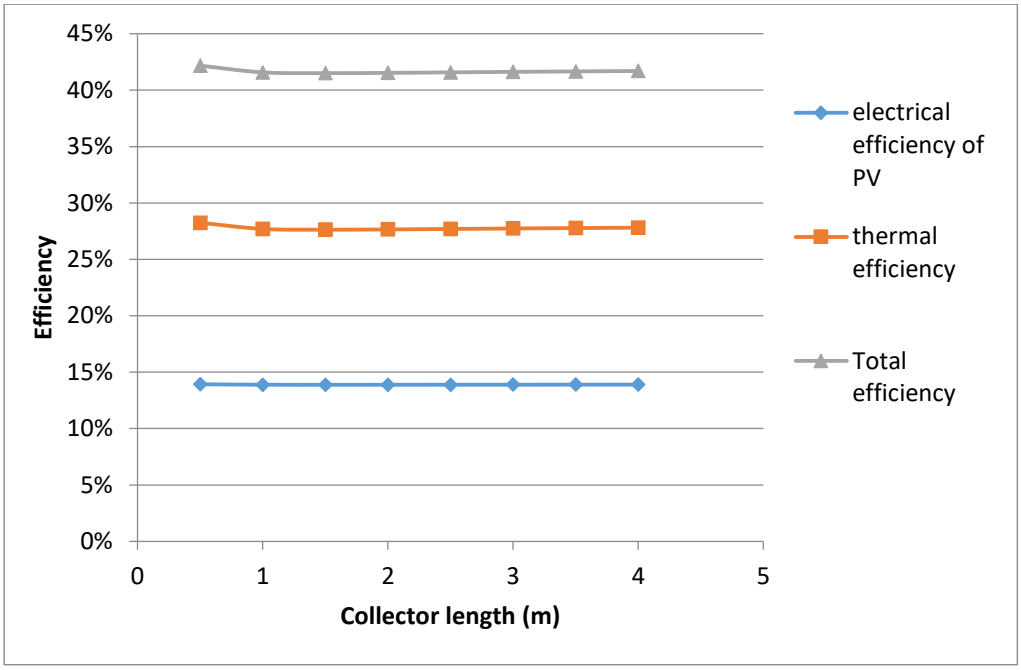


Figure 4.7 Variations in thermal and electrical efficiency as a function of PV panel length

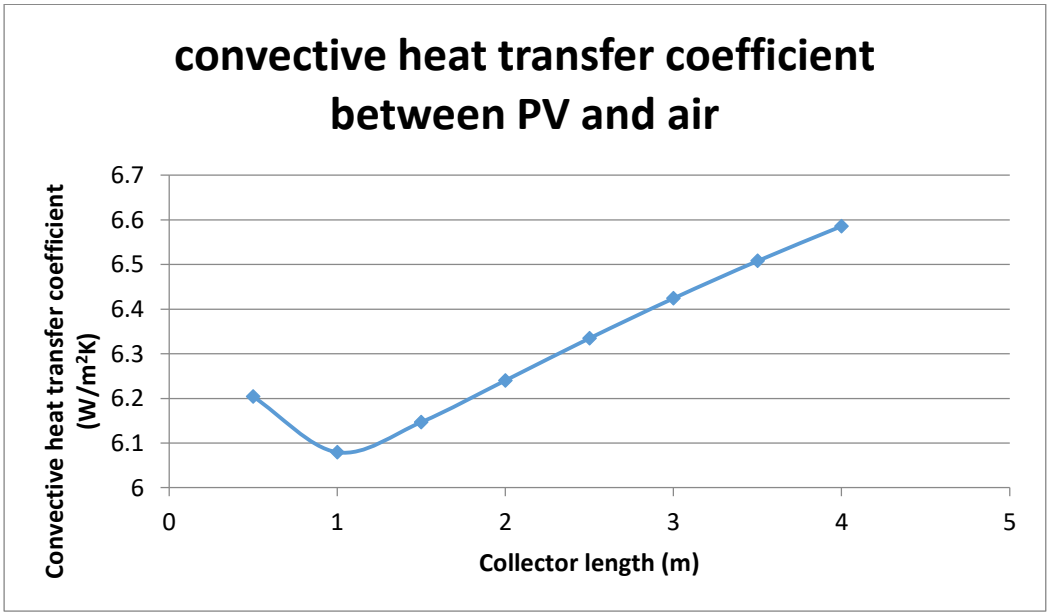


Figure 4.8 Convective heat transfer coefficient between the PV and the back wall

4.2 Results for forced convection

The purpose of forced convection is to improve the total PVT system efficiency and overcome some limitation observed in natural ventilation cases. However, the additional cost of the circulation fans reduces the net electricity gain of the system. Thus, in this section, the effect of varying the forced convection configuration on the total PVT system performance is investigated.

A typical sunny day in summer was chosen to evaluate the system performance, whereby the ambient temperature of 300 K was selected and solar irradiance was set to 600 W/m^2. The fan was a centrifugal fan where the air flows is in a radial direction relative to the shaft.

4.2.1 Effect of air velocity (Fan speed)

Figure 4.9 provides the plot of the temperature variation as a function of air velocity. It can be seen from the graphs that increasing the air velocity decreases the outlet air temperature, PV panel temperature and means to air temperature. Due to the decreasing PV temperature, both thermal and electrical efficiency increase, as illustrated in Figure 4.10. High air velocity enhances the convection; however, the system consumes more energy, due to the need to power the fan. Increasing the air velocity further is not energy efficient, as the resulting increase in energy collection could be very small, and would not compensate for the energy consumed by the fan. Therefore, there should exist an optimum airflow velocity, which is dependent on the system design and weather conditions. Figure 4.11 depicts the relationships between fan power and PVT electrical efficiency and the efficiency increase as the fan power increases (fan

efficiency is set 55%). When compared to the efficiency of the system using natural convection, the thermal efficiency is 26.6% and electrical efficiency is 9.19%, which is obviously less than that using forced convection. However, when using forced convection, part of electrical energy produced from PV is utilised to power the fan. Thus, the net fan power (equivalent to the difference between the total electrical power and the fan power) decreases after reaching its peak, suggesting existence of an optimum fan power. The optimum fan power occurs in this case is about 5.8m/s. This is very important when designing forced convection systems.

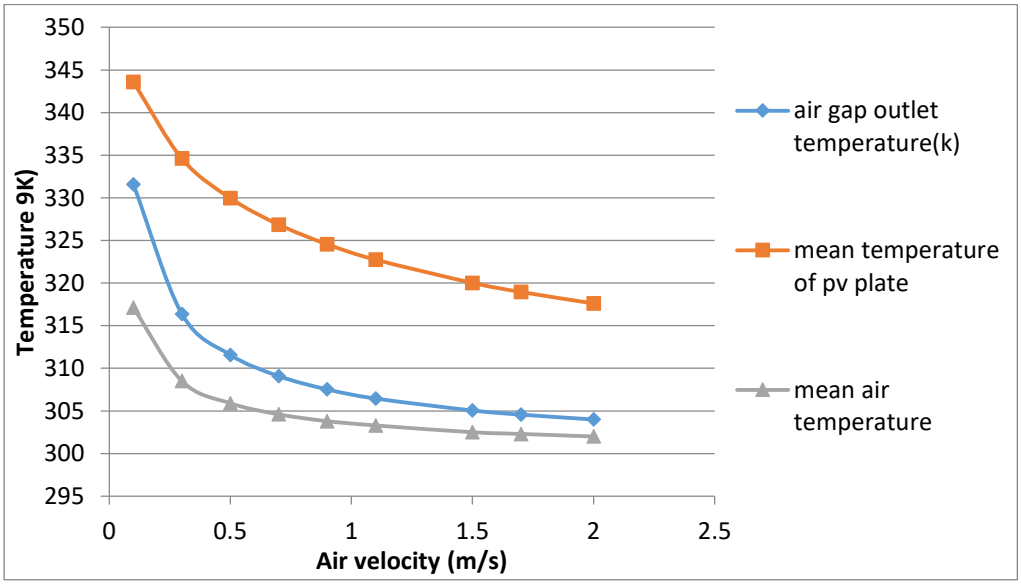


Figure 4.9 Variation in temperatures with air velocity

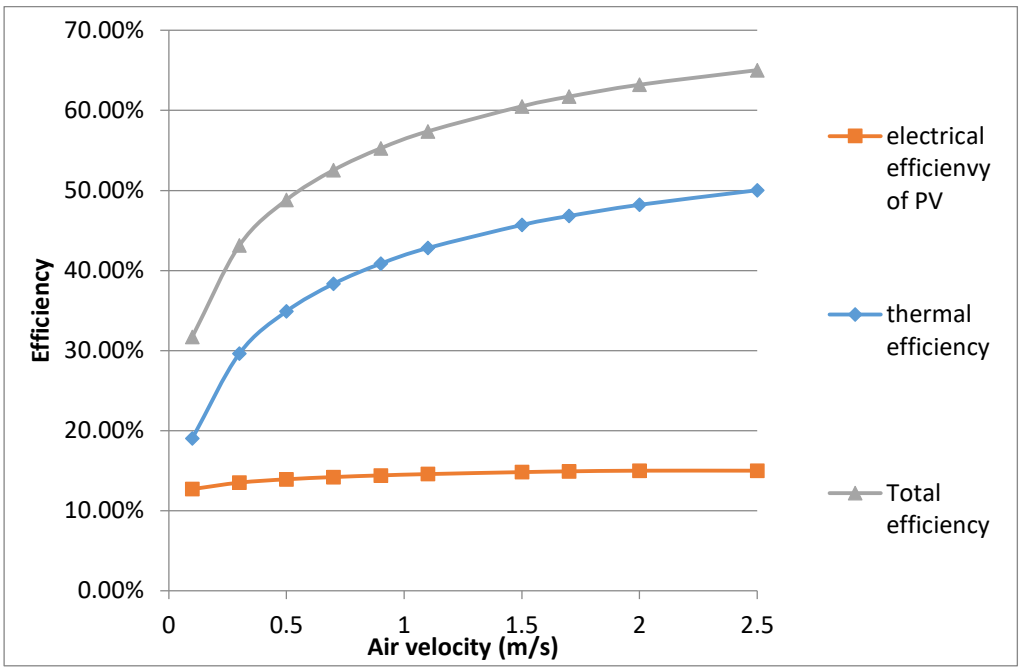


Figure 4.10 Variation in thermal and electrical efficiency with air velocity

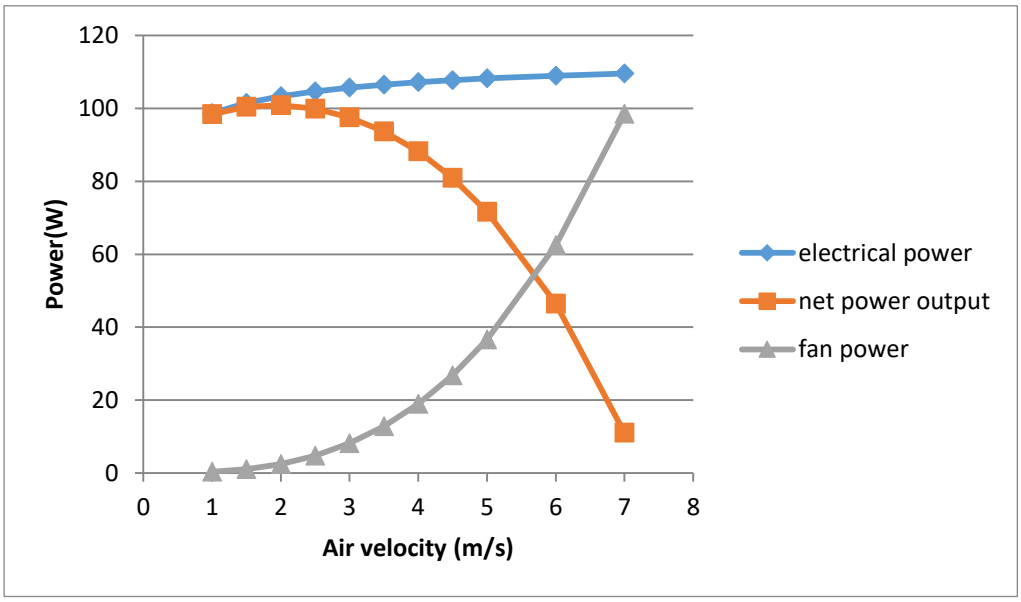


Figure 4.11 Variation in power with air velocity

4.2.2 Effects of gap spacing

Figure 4.12 and 4.13 show the variation in temperature, and thermal and electrical efficiency, respectively, as a function of gap spacing. The results are

comparable with those obtained in the natural convection case, indicating presence of an optimum gap spacing at which these temperatures are minimised and both thermal and electrical efficiency attain maximum value. Beyond the optimum spacing, the outlet temperature becomes excessively high, and it decreases rapidly as the gap spacing increases. After the optimum point, it decreases slowly and tends toward ambient temperature. The mean temperature of the PV plate exhibits the same performance as the outlet air temperature beyond the optimum spacing, and thereafter increases slowly with the increase in spacing. These observations are attributed to the variation in the rate of pressure decline and convection heat transfer coefficient with changes in gap spacing. The initial high temperature is due to the low heat transfer coefficient value. The optimum point occurs when the stack effect balances the frictional force. In this case, the optimum gap size is about 0.05m, which is smaller than it in natural convection case, 0.1m.

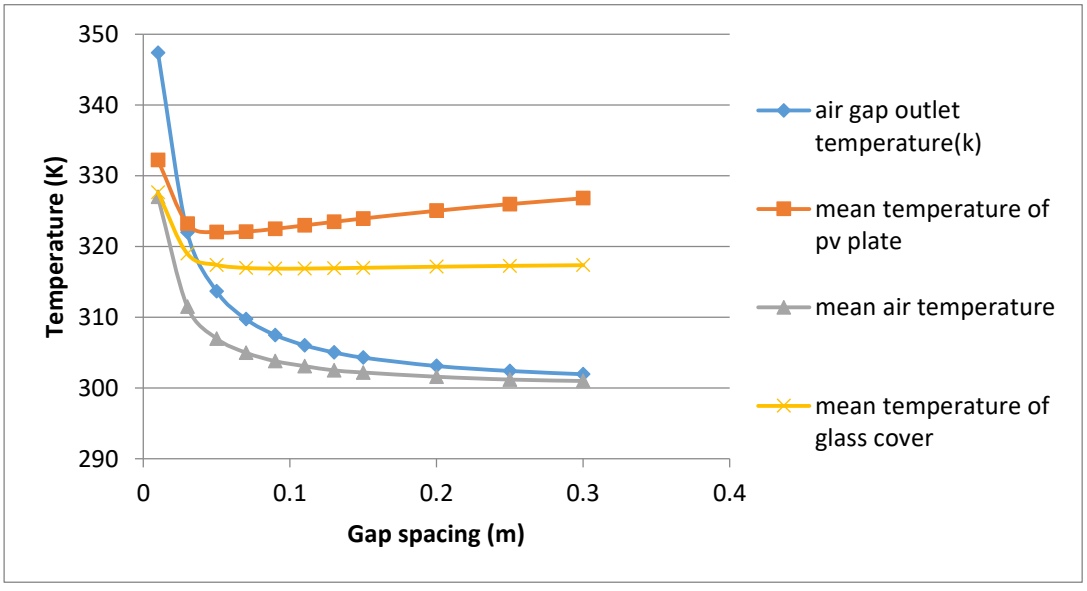


Figure 4.12 Variation in temperatures with gap spacing

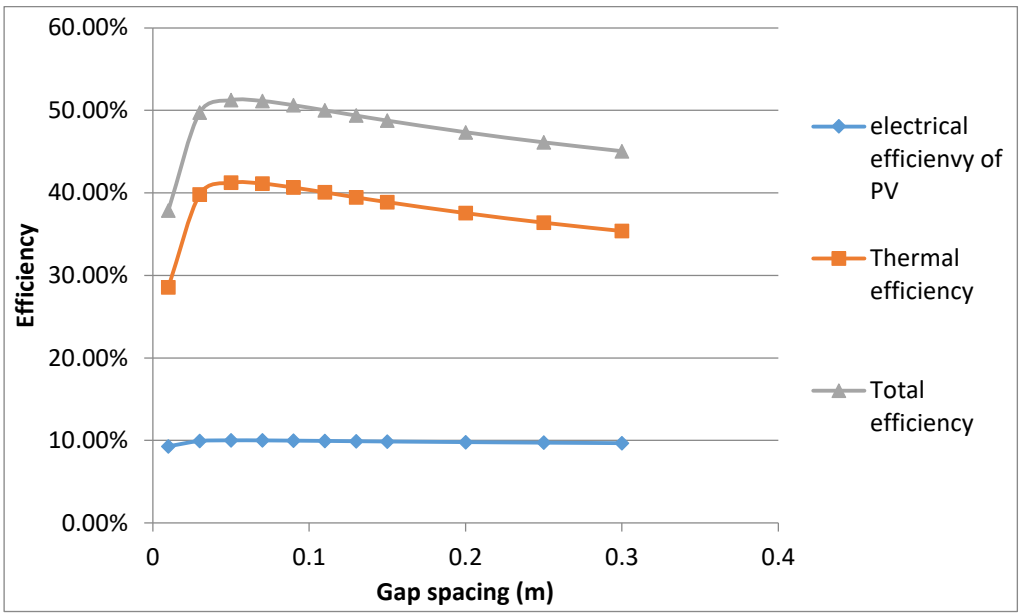


Figure 4.13 Variation in thermal and electrical efficiency with gap spacing

4.2.3 Effects of inlet air temperature

In this section, the work conducted in order to investigate if pre-cooling has a significant positive effect on the performance of the system is presented. The air velocity is 0.5 m/s in this section. Figure 4.14 shows the variation in the mass flow rate as a function of changes in the inlet air temperature, where it can be seen that the mass flow rate decreases slightly as the inlet air temperature increases. This may be due to the slightly lower air density at higher temperatures.

Figure 4.15 shows the plot of thermal and electrical efficiency against the inlet air temperature. Electrical efficiency remains stable, as it is almost at the maximum level. Even though it is decreasing, the decline is negligible (about 0.3%). Thermal efficiency is also decreasing, as shown in Figure 4.15. It can be

concluded from the graph that pre-cooling of the inlet air can increase the thermal performance. In sum, in summer conditions, where PV electrical efficiency is low due to high PV plate temperature, precooling the inlet air could be beneficial.

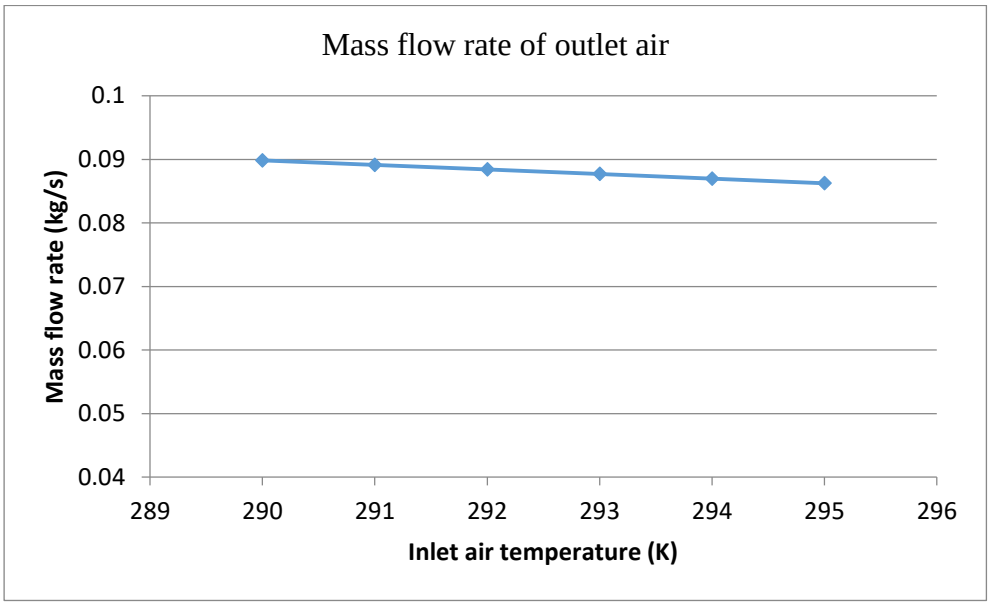


Figure 4.14 Variation in temperatures with the changes in inlet air temperature

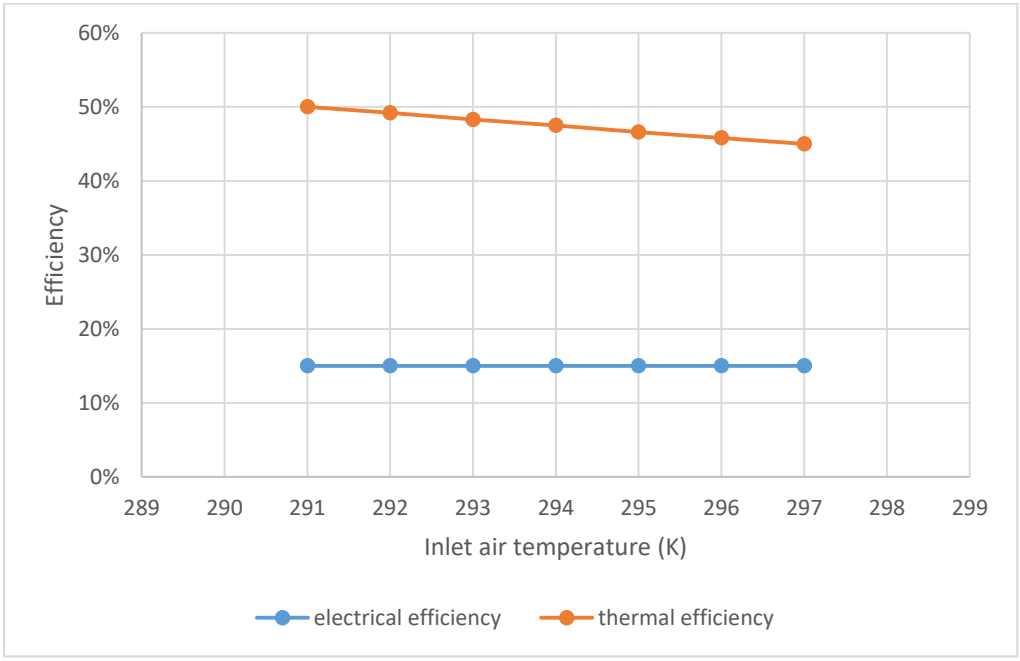


Figure 4.15 Variation in thermal and electrical efficiency as a function of inlet air temperature

4.3 Summary of analytical results

Summary of results pertaining to natural convection

High irradiance results in a higher flow rate and hence higher thermal efficiency. On the other hand, high irradiance also yields a higher PV plate temperature, which decreases the electrical efficiency. The optimum irradiance in the given parameter is this chapter is about 600w/m^2.

There exists an optimum gap spacing at which flow velocity attains a maximum value and all relevant temperatures attain a minimum value. The result suggest that 100mm air gaps size should be an efficiency value for a PVT system with the parameter in Table 6. The thermal and electrical efficiency are also maximised at this optimum gap spacing. Changing collector length has a limited effect on the mean PV temperature, air duct and air outlet, electrical and thermal efficiency, but it increases the total heat gain.

Summary of results pertaining to forced convection

High velocity yields a better performance in terms of both thermal and electrical efficiency, although the system consumes more energy due to the need to power the fan. The optimum gap spacing in forced ventilation case is 0.05m.There also exists an optimum fan power that would result in the maximum net fan power. The optimum fan power occurs in this case is about 5.8m/s. The energy required to power the fan can be attained by using part of the PV electricity. In cold conditions, when the temperatures are not high, forced convection is not necessary. On the other hand, in the hot summer months, the PV plate

temperature may become too hot and will affect the system performance greatly; thus, forced convection could be used to reduce this adverse effect.

Chapter 5 Experimental design and results of a PV/PCM system

5.1 Introduction

In this chapter, the study phase designated for the experimental investigation of the PV/PCM system is discussed. A PV/PCM system was designed, as described in the next section. A suitable phase change material was chosen and was placed in a metal box, which was attached to the back of the PV to improve its overall performance. An air duct was placed behind the PV/PCM system for ventilation purposes. The PV panel was positioned vertically to enhance natural ventilation. The PV, PCM, and air duct temperatures, as well as the air velocity in the air duct, were measured.

The results of the experimental investigation of the designed PVT/PCM system are also presented in this chapter, including thermal energy storage and energy release process. Results and discussion of the tests pertaining to six different experimental configurations for comparing different PCM thicknesses, air gap sizes and systems with fins are presented at the end of this chapter.

5.2 Experimental design and procedure

The main purpose of the experiments discussed here was to investigate the thermal and electrical performance of the designed PV/PCM air system. As the first step, a PV/PCM test unit was designed and built using proper material in certain condition. Next, experimental trials were performed on the test unit to establish its thermal and photovoltaic performance. Finally, the temperature and velocity data were recorded and were subsequently used to validate the simulation model for further study.

Six different configurations were tested and recorded, as noted in Table 7. All test conditions were identical, and the ambient temperature was maintained at about 20 ºC. Thermocouples were attached at similar locations for different cases and were connected to a data logger to measure the temperature and electrical power at 60s intervals.

In all configurations, 8 hours of light were employed for the melting process, with further 12 hours of darkness dedicated to the solidification process. Velocity was measured by the hot wire anemometer and was recorded manually.

Table 7 Configuration of six test units

Case	PCM thickness (mm)	Air duct spacing (mm)	Fins installed (y/n)
Case 1	30	100	no
Case 2	20	100	no
Case 3	30	50	no
Case 4	50	100	no
Case 5	30	75	no

Case 6	30	100	yes

Solar intensity from artificial lights was measured by solar power meter at nine positions (Figure 5.1) and the results are listed in Table 8. So the measured average intensity applied to the PV surface was about 600 W/m^2 which is the suggest value from analytical model.

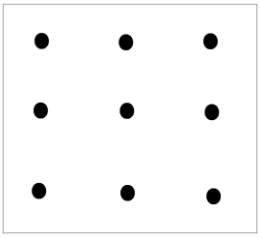


Figure 5.1 Intensity measurement positions

Table 8 Intensity on measured points

420 W/m^2	640 W/m^2	420 W/m^2
730 W/m^2	950 W/m^2	730 W/m^2
420 W/m^2	640 W/m^2	420 W/m^2

5.3 Experiment results for Case 1

5.3.1 Thermal energy storage

The PV temperature adjustment provided by the PV / PCM system depends on the thermal performance of the PCM in the PV / PCM system.

Figure 5.2 shows the temperature of three points inside the PCM for Case 1. Three points were chosen from the front, mid and back positions (20mm, 50mm, 80mm distance from rear of PV) in middle of the PCM unit. As the melting temperature of the PCM is 298 K, when the temperature at a point exceeds 299 K, it can be concluded that the PCM has melted at that particular point. Point 1, located at the front, takes 100 minutes to fully melt after the artificial light is turned on. Point 2, in the middle, takes 150 minutes to fully melt, while Point 3 takes 200 minutes. A rapid increase occurred between 270 and 330 minutes, due to the transition of PCM status, where melting started.

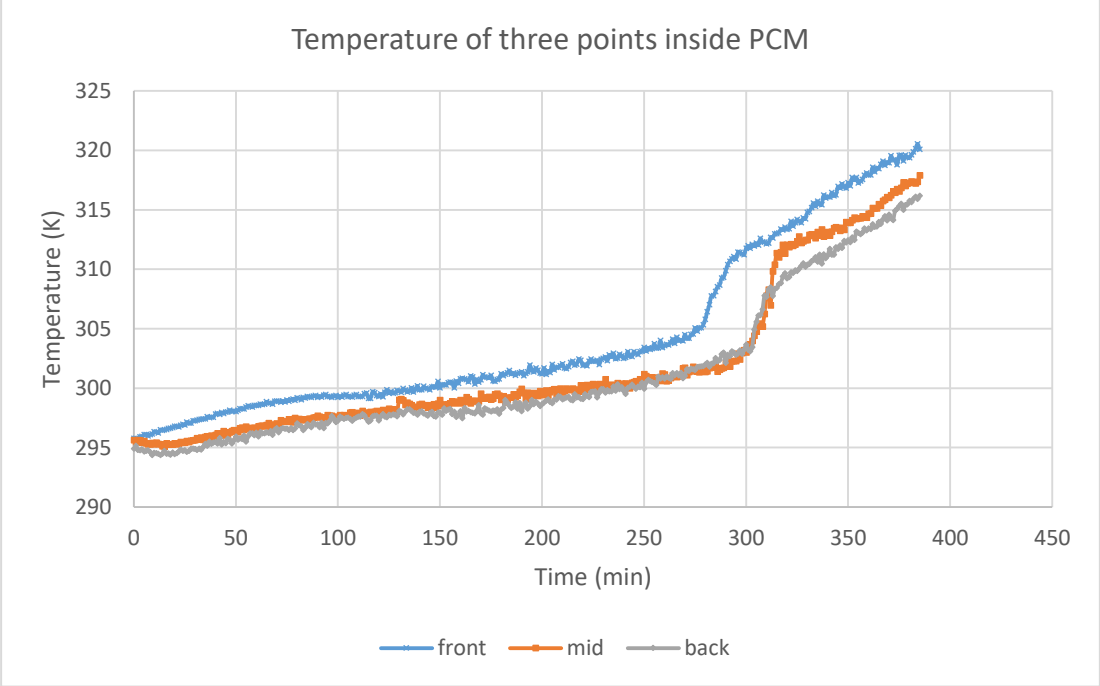


Figure 5.2 Temperature of the three points at the centre of PCM

Figure 5.3 shows the temperature of three points inside the PCM at different heights. P1 is located at the top, P2 is situated in the middle, and P3 is at the bottom (900mm, 600mm, 300mm distance from bottom of unit). All points

exhibit a linear relationship between temperature and time at the start, which indicates that, initially, the conduction is the dominant mode of heat transfer. After 300 minutes, a sharp increase in temperature at Point 1 was observed due to convective heat transfer at the point. The same sharp increase was also observed for the other two points.

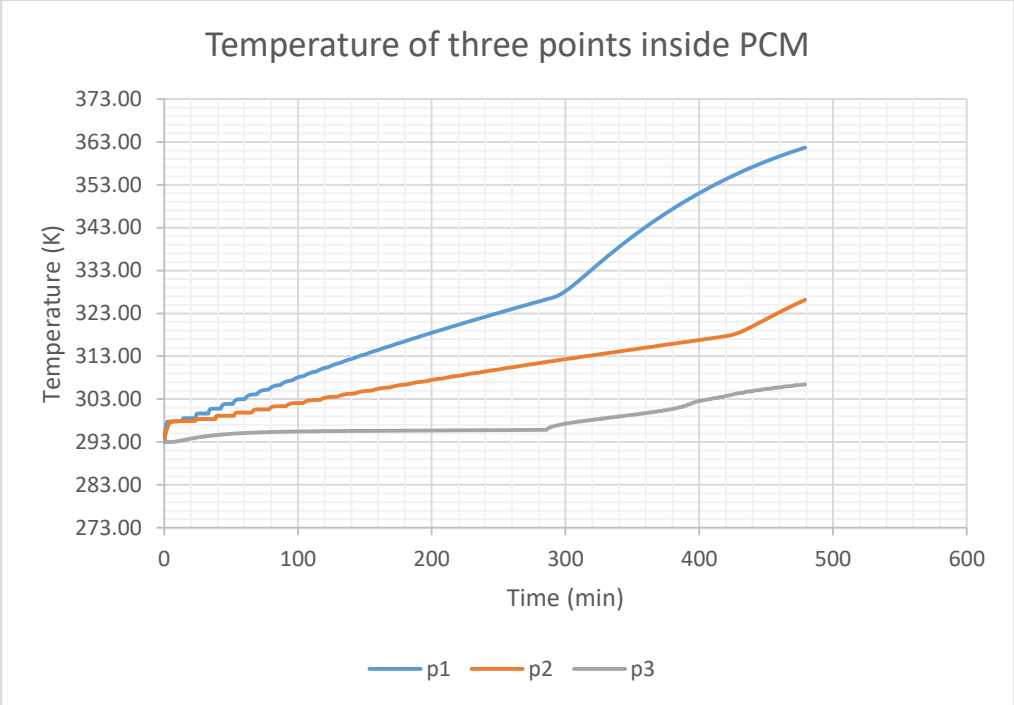


Figure 5.3 Temperature of three points located at different heights inside the PCM

As the volume of molten PCM increases, the phase change temperature control effect is reduced. The point 1 located on the upper part of the PV / PCM system has experienced a higher temperature rise rate than the points 2 and 3 in the solid phase. This difference is due to the high volume of heat in the centre of the PCM encountered at the top of the central area.

Initially, the heat was absorbed by the PCM as sensible heat until the PCM reached the melting point. Beyond this temperature, PCM began to melt and

absorb heat from PV as latent heat. The temperature gradient decreases and the PV temperature deviates from the reference curve. After the close layer of the PCM layer melts, it continues to melt and heat transfer is in convection and conduction combinations. Convective heat transfer in the melted PCM continues to increase as the melt fraction increases, resulting in an increase in the sensible heating. After the entire PCM volume melted, convective heat transfer became dominant, leading to a sharp rise in its temperature, until it equalised with the reference temperature.

The difference in the heat capacity of the solid and liquid PCM state also contributes to the increase in temperature. Higher heat capacity in solid PCM (2.2kJ/kg,K compare to 1.4 kJ/kg,K in liquid) results in a slower increase in temperature. However, as a greater proportion of PCM changes to liquid state, this reduces the total heat capacity, leading to a greater temperature increase gradient.

At the beginning of the solidification, a solid layer of PCM is formed on the plane in contact with the PV plate, which is a layer that separates the liquid PCM. Due to the low thermal conductivity of solid PCM, solidification continues to slow.

These results highlight the difficulty of estimating the amount of heat transfer and the rate in the material due to the presence of supercooling and thermal conductivity differences between the solid and liquid phases.

Figure 5.4 presents the comparison of the mean PV temperature with and without the PCM unit at the same insolation and ambient temperature for Case 1. The mean PV temperature is determined by using the average of six different

point at the back side of PV panel. As can be seen from the graph, the reference system without the PCM unit reached steady state at 334 K in about 70 minutes, while the system with the PCM reached its steady state at 318 K in 90 minutes. In both cases, initially, the temperature increased rapidly, until it reached a plateau. For the PV without PCM, this plateau was at 334 K, while it was 318 K for and the PV with PCM. Once the PCM transition was complete, the temperature increased rapidly again. The benefits of using PCM to thermally control the PV are clearly significant. The unit with PCM in this case can maintain the PV temperature below its operating temperature of 320 K for about 210 minutes.

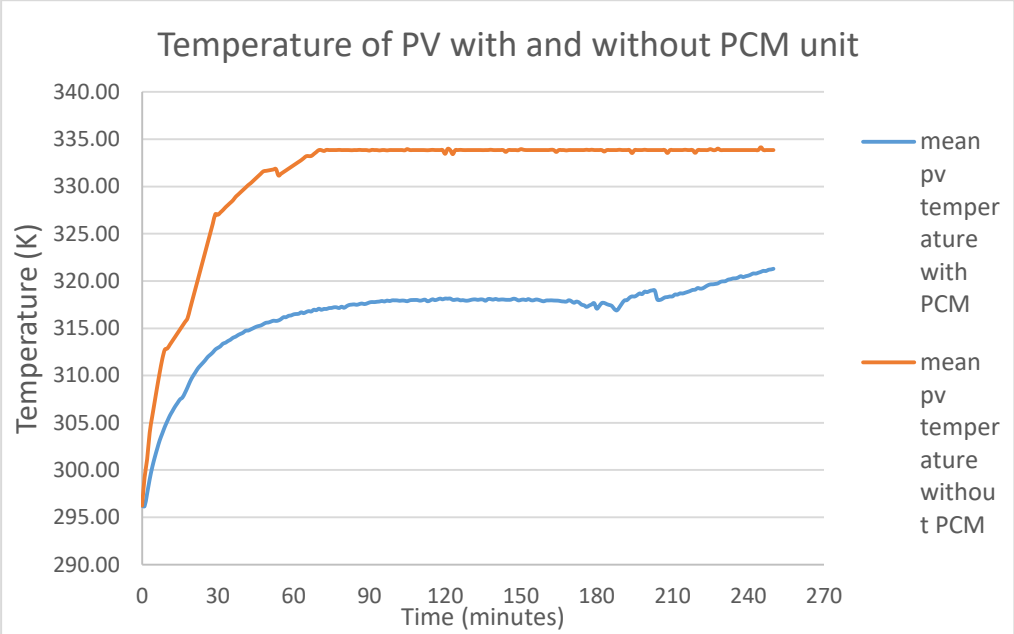


Figure 5.4 A comparison of the mean PV temperature with and without a PCM unit

Air velocity in the air duct is another important parameter and was examined in this study, as it controls the natural convection and heat redistribution effects.

Figure 5.5 shows the mean air velocity at the outlet which is measured by taking the average of the three velocity values from three different points. As can be seen from the graph, the velocity increased sharply during the first 60 minutes as the temperature increased, after which it remained stable at 0.14 m/s due to the PCM melting process. It rose sharply (to 0.27 m/s) again after the PCM fully melted, reaching its maximum temperature over the test period. The air velocity was within the range of values expected for a natural circulation system (Enibe, 2003). However, the accuracy of the anemometer used in the experiment was about ±0.03 m/s, resulting in about 12% relative error. Thus, the results may be erroneous when the velocity is small. Therefore, a more accurate instrument should be used in practical applications.

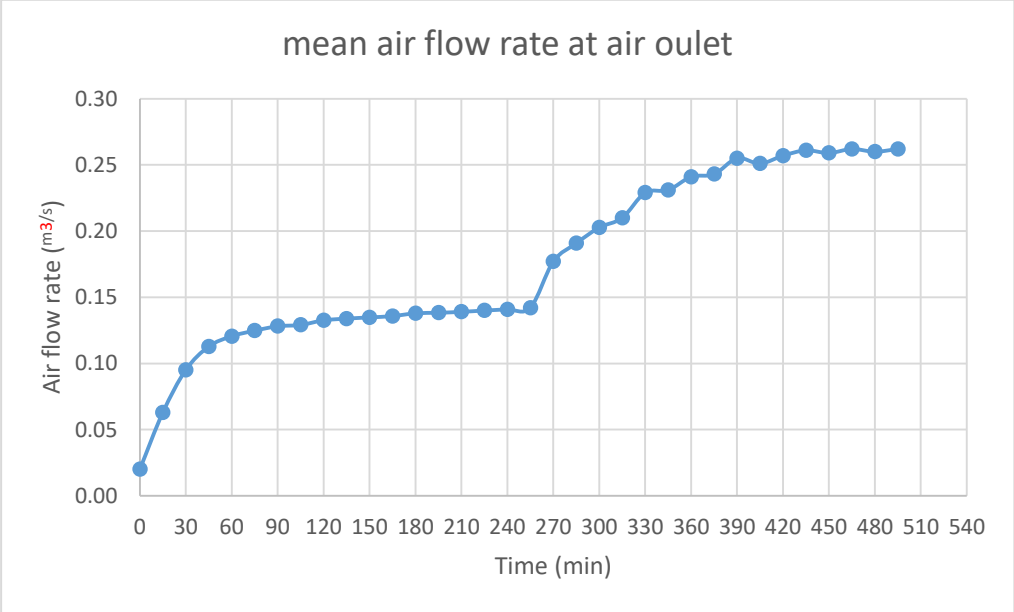


Figure 5.5 Mean airflow rate at the air outlet

Figure 5.6 presents the electrical performance improvement due to the PCM unit. Initially, no increase was observed due to the low temperature of the PCM unit. However, once the temperature exceeded the PV operating temperature, the

reference system electrical efficiency declined, while that of the system with the PCM unit declined more slowly owing to thermal regulation of the PCM. However, as its regulation is limited by its total heat capacity, the efficiency starts declining after 200 minutes, at which point the PCM is almost fully melted. Thus, the temperature increase is the main reason behind the decline in efficiency, as the PCM material has a relatively low thermal conductivity. Therefore, as it works as an insulator, its temperature increases quickly once it is completely melted. In summary, PCM volume is essential to the PCM unit design and depends primarily on the environmental conditions.

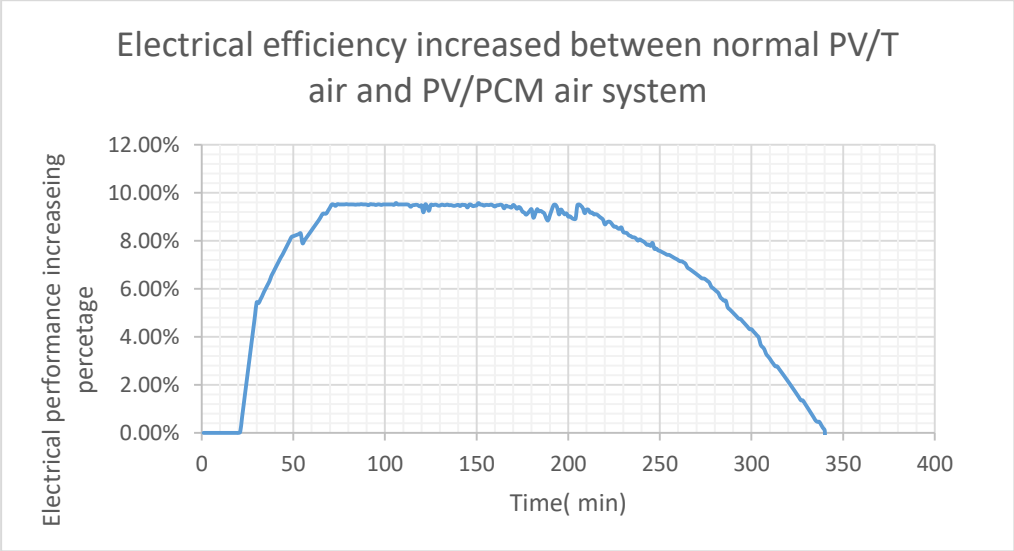


Figure 5.6 Electrical efficiency increase due to the PCM unit

Figure 5.7 presents the thermal efficiency of the PV/PCM system, which is calculated from the difference of heat transfer between air inlet and outlet, using Equation 40 below:

$$\eta_{themral} = \frac{Q_{outlet} - Q_{inlet}}{G \times A} \qquad (40)$$

In a standard PVT system, the PV is heated up to a stable temperature. As the heat transfer between the PV and air is also stable, it results in a constant thermal efficiency (about 53% in this case). For the PV/PCM system, the thermal efficiency is initially low (in the first 250 minutes), after which it increases rapidly, reaching 78% at 440 minutes. The low efficiency at the beginning is due to the PCM, which initially absorbs most of the heat from the PV and thus slows down the heat transfer to air. After 350 minutes, the thermal efficiency of the system with PCM exceeds that of the standard PVT system because the PCM releases the absorbed heat to air, resulting in greater heat transfer between the PCM and air relative to the direct transfer from PV to air due to the metal container, which increases the total thermal conductivity. The total heat transfer to air for two cases should be the same, as they are exposed to the same irradiance and the same ambient conditions. However, the heat output for normal PVT will cease once the light is switched off, while the PV/PCM will continue to produce heat output until the PCM solidifies. This is one of the main advantages of the PV/PCM system that is shift the heat release process to later time.

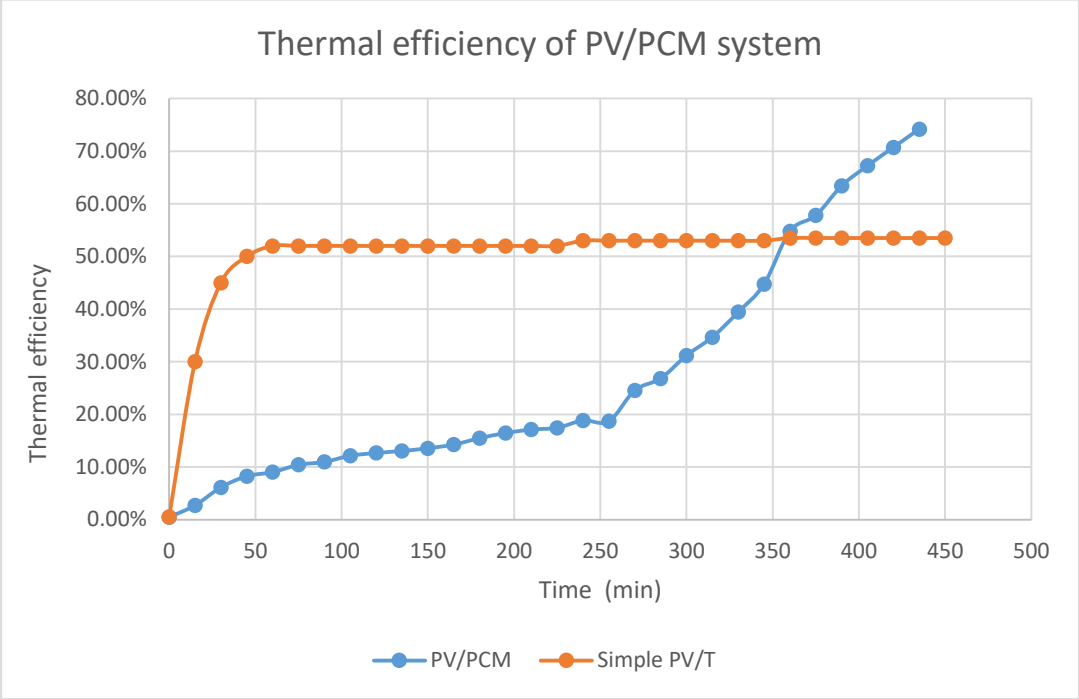


Figure 5.7 Thermal efficiency of the PVT and the PV/PCM system

5.3.2 Energy release process

When building a ventilation system, one of the important functions of a thermal storage system is that it absorbs excess heat during the day, and releases it at night to enhance ventilation. Figure 5.8 presents the temperature of three points inside the PCM(900mm, 600mm, 300mm distance from bottom of unit), which were utilised in the assessment of the heat release process. The thickness of PCM is 30mm and air gap size is 100mm. As can be seen, it took about 13 hours for the PCM to reach its solidifying point, and even at 17 hours, the temperature remained at about 298 K. Its poor performance is due to the high environment temperature in the test room (297 K), resulting in a small temperature difference between the ambient and the PCM unit. As the actual room temperature in the lab is about 295, K, the PCM unit increased the room by temperature 2 ºC.

The other reason is low thermal conductivity of the PCM. Consequently, it is recommended that PCM heat transfer be enhanced by applying extended

surfaces, such as fins or heat pipes, or using a composite PCM.

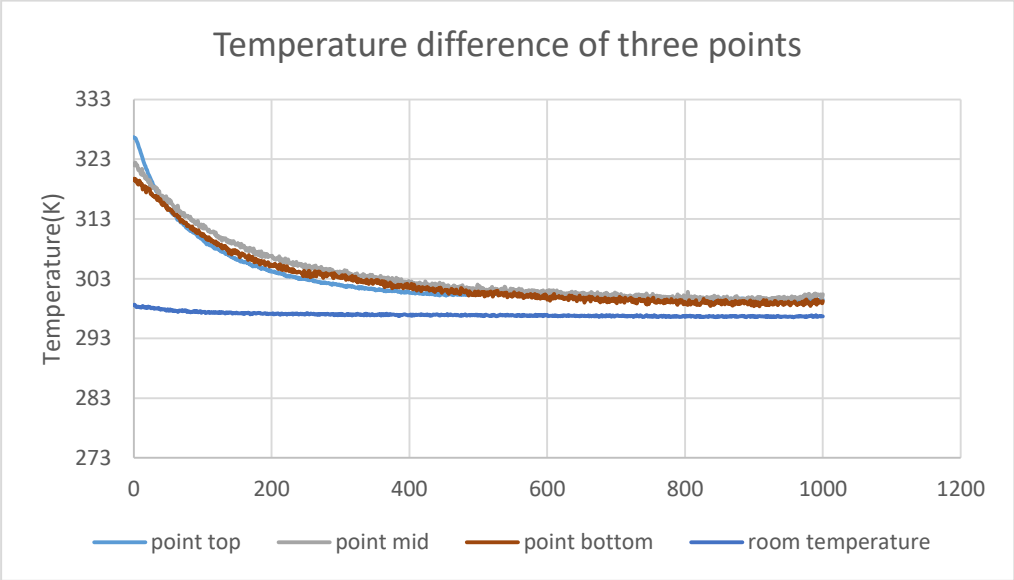


Figure 5.8 The temperature of the three points in the solidification phase

Figure 5.9 shows the airflow rate at the outlet during the solidification process. The heated PCM wall maintained the airflow rate about 20 L/s for 700 minutes, after which it decreased gradually to 15 L/s.

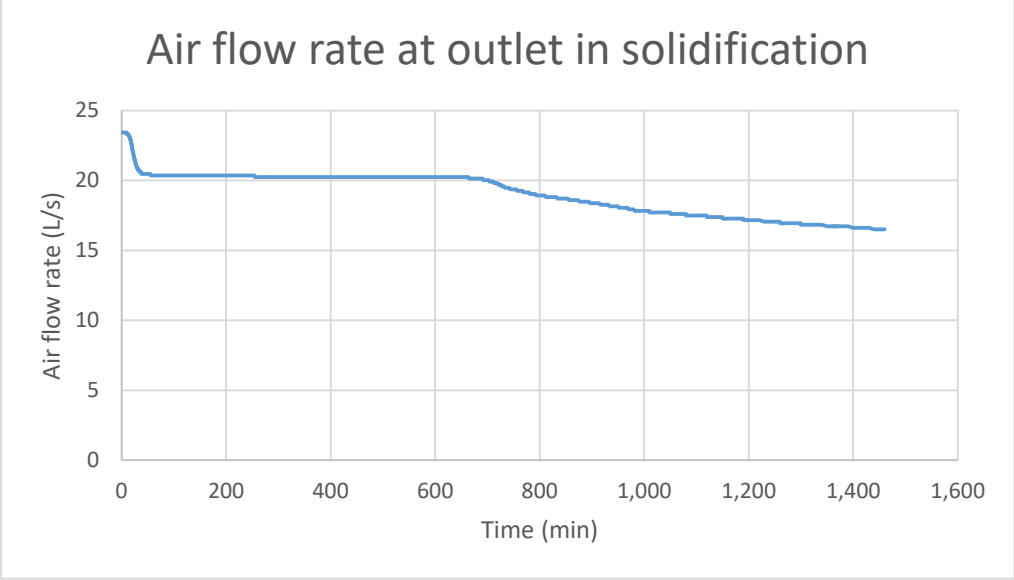


Figure 5.9 Airflow rate at the outlet in the solidification phase

Figure 5.10 shows the temperature difference between the air inlet and the outlet during an entire PCM transient period, including melting and solidification processes. The temperature difference increases rapidly from 0.4 K to 4.5 K when the lights are switched on for 250 minutes. However, it takes 600 minutes for the temperature difference to decline from 4.5 K to 0.4 K. The initial temperature difference between the air inlet and the outlet is due to the height of the openings, which are elevated at 1 metre when measured at centre of opening. This generated the natural convection in normal conditions, causing the pressure and temperature difference. When the lights are switched on, more heat is transferred to air; hence, the natural ventilation is enhanced and greater pressure and temperature difference between the air inlet and outlet are expected. When the lights are turned off, melted PCM (that has higher temperature than the ambient) releases the heat to the ambient air, thereby enhancing the natural ventilation in the duct. The enhancement by the PCM ceased until the PCM was fully solidified and the temperature decreased to that of the ambient air.

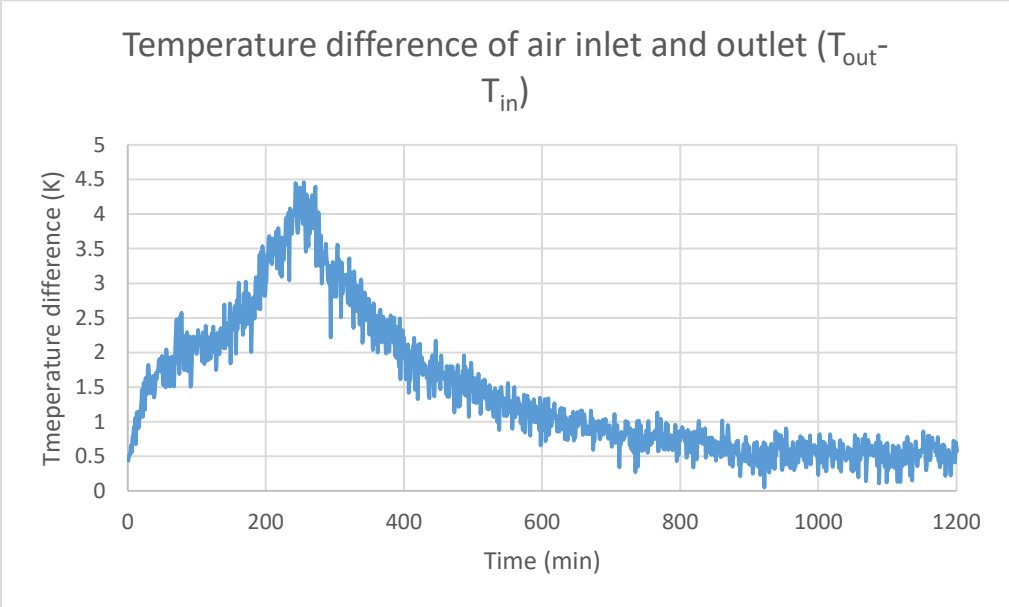


Figure 5.10 Temperature difference between the air inlet and the outlet

At night-time, the PV/PCM system acts as thermal mass in the building, providing delays in the temperature fluctuations. In the summer, during the day to absorb heat, released at night, cooling the breeze or clear night sky, keep the indoor temperature comfortable. In the winter, the same heat can store the heat of the sun or the heater, and release it in the building at night, helping to increase the indoor temperature.

The ventilation effect was important to examine in this study, as it helps remove the heat from PCM unit, allowing it to absorb excess heat gains from the PV in the daytime.

5.4 Experimental results for different cases and their comparison

In this section, the test results pertaining to six different configurations of experimental unit are presented and discussed. The different configurations are presented in Table 9 below. It should be noted that Case 6 is identical to Case 1, with the addition of internal fins.

Table 9 Configuration of six test units

Case	PCM thickness(mm)	Air duct spacing(mm)
Case 1	30	100
Case 2	20	100
Case 3	30	50
Case 4	50	100
Case 5	30	75

Case 6 (with fins)	30	100

5.4.1 Results of Case 1, 2, and 4, reflecting the variations in the PCM thickness

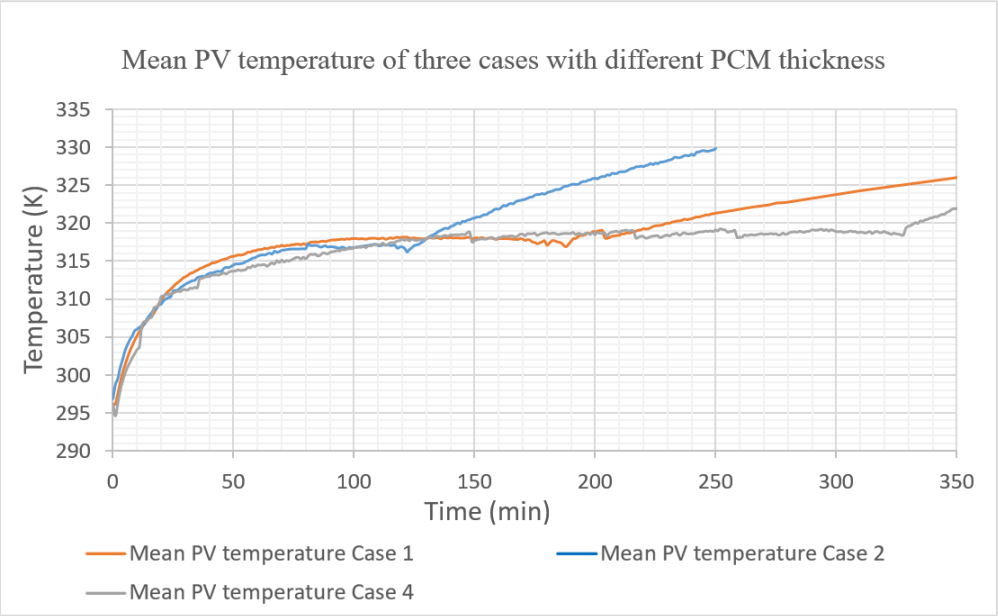


Figure 5.11 Mean PV temperature of three cases with different PCM thickness

The results obtained for the three cases with different PCM thicknesses are compared and discussed in this section. Case 1 has PCM of 30 mm thickness, Case 2 pertains to the system with 20 mm PCM, and Case 4 has a 50 mm thick PCM layer.

Figure 5.11 presents the mean PV temperature for Case 1, Case 2 and Case 4, each with the aforementioned PCM thicknesses. Case 2 (with 20 mm PCM) maintains the mean PV temperature below its operating temperature of 318 K for 140 minutes, Case 1 (with 30 mm PCM) maintains it for 200 minutes, while Case 4 (with 50 mm PCM) maintains its operating temperature for 330 minutes. It can also be noted that the mean PV temperature in all three cases increased rapidly once the PCM liquidised completely. This finding is expected, as is the observation that a thicker PCM can maintain the PV temperature below its

operating temperature for a longer time. The data indicate that each additional 10 mm of PCM adds 70 minutes to the maintenance time. The main problem associated with using a thicker PCM is that it increases the capital cost and adds extra weight to the system.

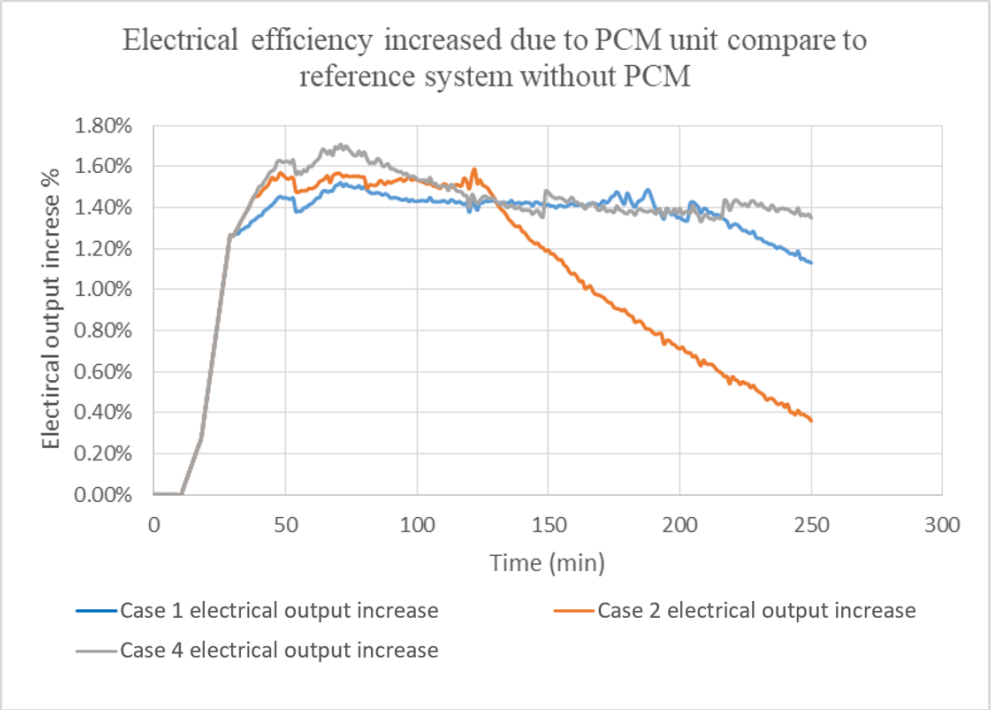


Figure 5.12 Electrical efficiency increase due to the PCM unit compared to the reference system without the PCM

Figure 5.12 shows the electrical efficiency improvement for the three systems using different PCM thicknesses and compares it to the reference system without PCM. As can be seen from the graph, in all three cases, the effect of the PCM unit on the electrical efficiency initially increases from 0 to about 1.5% compared to the reference system without the PCM. This phenomenon occurs because the PV temperature is below its operating temperature at the start, while the PV overheats once it generates too much heat. In Case 2, the 1.5% increase is maintained for 140 minutes, after which electrical efficiency starts to decrease due to the increase in the PV temperature. The same trend is observed for Case

2, where it persists for 200 minutes. No obvious decline in electrical efficiency were noted for Case 4 during the 250-minute experimental period. This result was anticipated, as thicker PCM holds the PV temperature for a longer time. The system in Case 4 produces a peak electrical output increase of 75 minutes because the front layer of the PCM absorbs the excess heat from the PV until it is fully melted and its thermal regulation ability is reduced. Once the front layer of the PCM is melted and the temperature increased, the mean PV temperature also increased, resulting in a decline in the electrical output. However, due to the heat transfer inside the PCM unit, the heat from the front to the back side continued to be transferred through conduction and convection, thus creating a balanced temperature on the front side. This may be the process by which the electrical output was kept stable after the peak period.

5.4.2 Results of Case 1, 3, and 5, reflecting the variations in the air gap size

The results obtained in three cases with different air duct spacing are compared and discussed in this section. The system denoted as Case 1 has 100 mm air duct spacing and Case 5 has 75 mm air duct, while it is only 50 mm in Case 3. Thus, the aspect ratio is 1:11, 1:14.7 and 1:22, respectively.

Figure 5.13 presents the temperature measured at the points at the centre of PCM container for the three air gap sizes noted above. The lights were turned down after 280 minutes. The results show that the system in Case 3, with smaller duct spacing, had a higher temperature during the entire experimental period,

achieving an overall increase of about 1 K. The heat removed from the PCM unit by air convection clearly has an effect on the PCM performance.

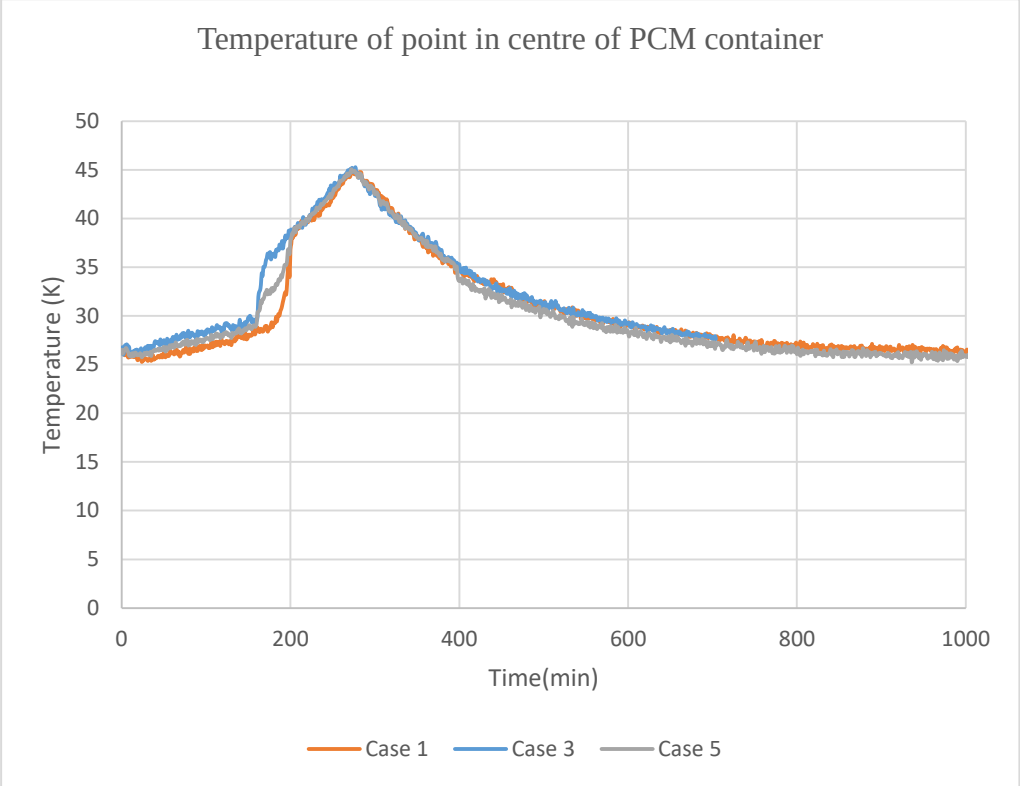


Figure 5.13 Temperature of the point at the centre of the PCM container for three different air gaps sizes

Figure 5.14 presents the mean air velocity at the outlet for the three cases. The displayed results show that the system in Case 3 with 50 mm air duct spacing has higher air velocity than the other two cases. In this case, the natural ventilation is affected by the friction and pressure difference between the air inlet and the outlet. As can be seen from Figure 5.12, as the system in Case 4 had a higher temperature, this was the main factor in its higher air velocity. A more detailed analysis of the effect of duct gap size on the flow patterns will be presented in Chapter 6, when the CFD model is discussed.

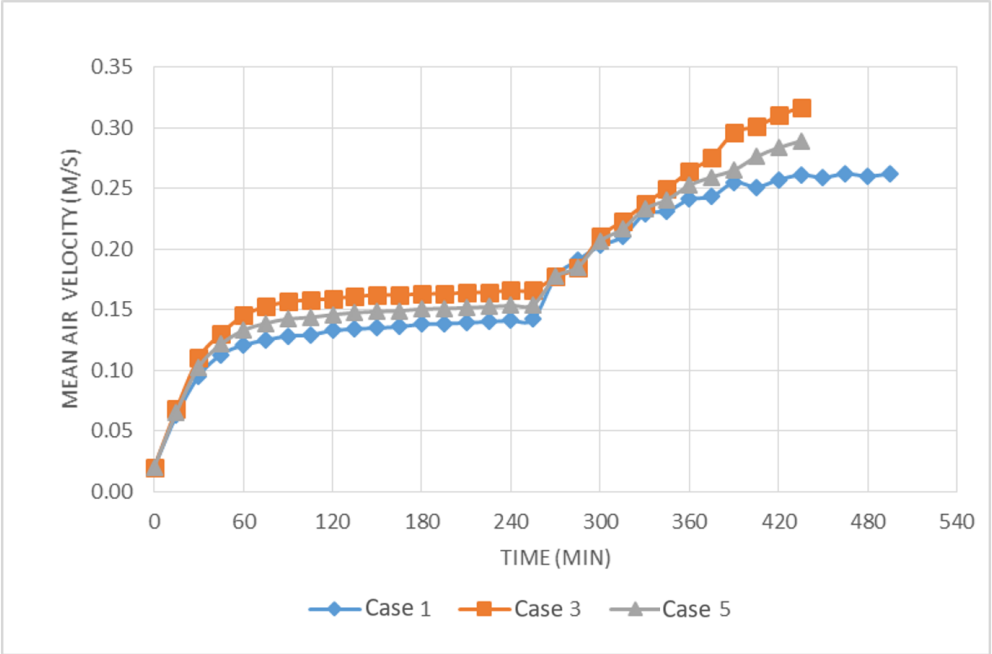


Figure 5.14 Mean airflow rate at the air outlet

5.4.3 Results of Case 1 and 6, comparing the system with vertical fins

The system denoted as Case 6 comprised of vertical fins inside the PCM. In its construction, the same aluminium box of 30 mm thicknesses was used, and the vertical fins were placed inside to improve the thermal performance. All fins had a spacing of 30 mm and a very small thickness (2 mm) compared to the length L(1100mm), so that the effective surface area of one fin could be approximated by A = 2LH.

Figure 5.15 shows the mean PV temperature with fins installed inside the PCM container in comparison with the results obtained in Case 1. It can be seen from the data that the fins were effective in moderating the PV temperature increase. Fins not only reduced the temperature rise on the front surface, but also the thermal stratification within the system. However, their presence reduced the

period over which temperature control was achieved due to the reduction in the PCM volume.

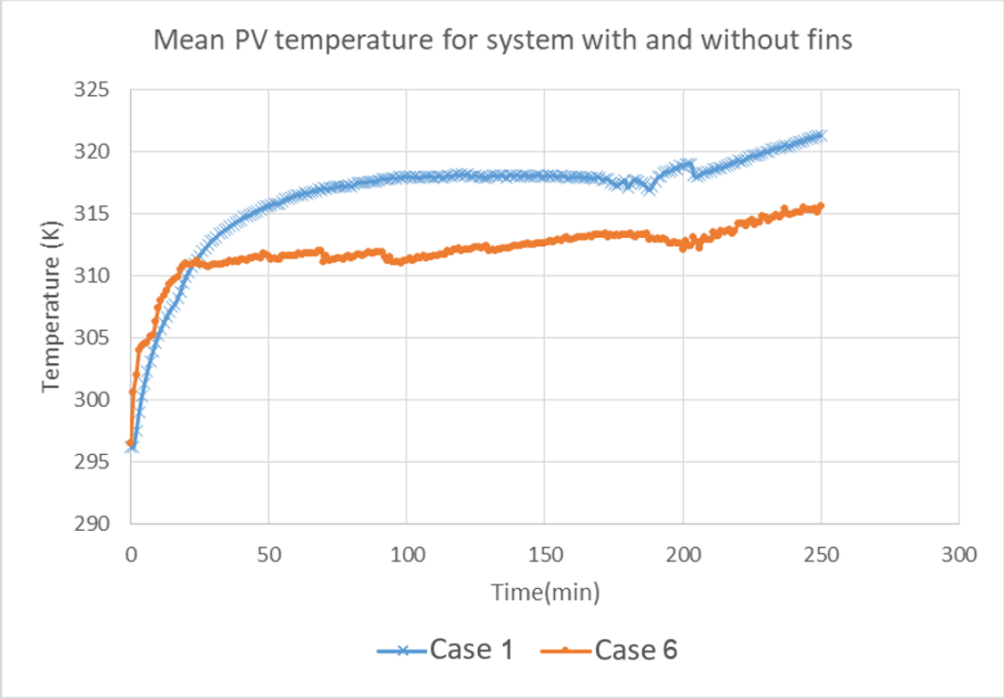


Figure 5.15 Mean PV temperature of the systems with and without fins

When vertical metal fins are installed into the PCM unit, their inclusion divides the PCM into several long rectangular units between each fin. This convection in the liquid PCM combined with phase change of the solid PCM stabilised the temperature in the liquid PCM.

Figure 5.16 shows temperature difference between the air inlet and the outlet for Case 1 and 6. It can be seen that, in the system with fins, the outlet air temperature was increased by about 4 K more than in the system without fins. Greater temperature difference will result in higher natural ventilation flow rate, leading to an improved thermal efficiency.

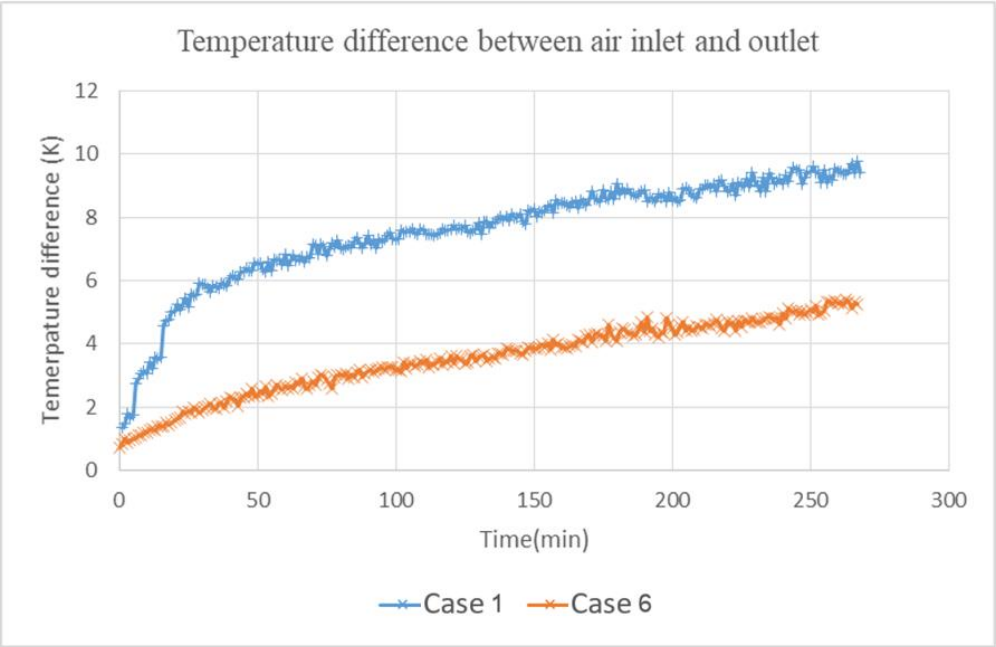


Figure 5.16 Temperature difference between the *air inlet and outlet for* Case 1 *and* Case 6

Figure 5.17 shows the air velocity at the air outlet for Case 1 and Case 6. The system with fins has larger velocity during the entire heating period, due to the higher temperature difference owing to the higher heat transfer rate. The system with vertical fins improves the velocity by about 30%. However, the advantage is smaller when the PCM is fully melted and the convection heat transfer inside the PCM starts to dominate, while the convection in the finned system is limited and reduced by the inclusion of fins.

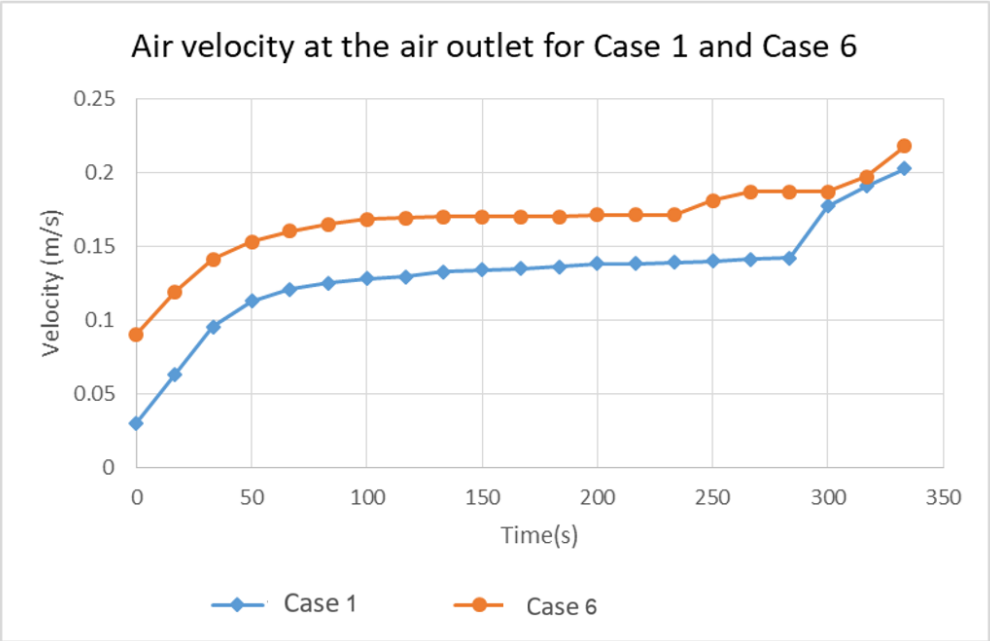


Figure 5.17 Air velocity at the air outlet for Case 1 and Case 6

5.5 Summary

In this chapter, the experimental investigation of the designed PV/PCM air system was presented and the findings were discussed. The experimental results show that PCM of a 30 mm thickness with the melting temperature of 25 ºC can maintain the PV cell temperature below its operating temperature for about 210 minutes under 600 W/m^2 insolation conditions. Thereby, it can increase the system's electrical efficiency by 10% during the PCM melting process compared with that measured for the system without the PCM. The system can also provide 15 L/s airflow rate for 240 minutes, after which point it starts to increase. However, the performance is poor during the solidification phase, as PCM may take more than 10 hours to solidify. Thus, thermal conductivity during the solidification process should be improved.

The results also indicate that thicker PCM can maintain the PV temperature below the operating temperature for a longer time and an increase of 10 mm in the PCM thickness extends the maintenance time by 70 minutes. The heat removed from PCM unit by air convection has a certain effect on the PCM thermal performance.

The system with vertical fins can increase the outlet air temperature by about 4 K and improve the velocity air outlet by about 30%, albeit at an increased cost and reduced PCM volume.

Chapter 6 CFD simulation work on the PV/PCM system

6.1 Introduction

The findings yielded by the literature review indicate that modelling of phase change processes presents a significant challenge, due to their inherent complexity and the sheer number of the involved physical phenomena. On the other hand, owing to its uncontrollable behaviour, natural airflow is always difficult to predict. The work discussed in this chapter is therefore dedicated to the numerical modelling of the designed PV/PCM system. Computational fluid dynamics (CFD) were chosen for this study phase, as this can be used to numerically solve the airflow and temperature by solving the partial differential equations of mass, energy and momentum. As most airflow is turbulent, the choice of a turbulence model is the most important aspect of simulating the airflow, as evident in the significant number of extant studies on this topic. This is mainly due to the very narrow temperature range in this case and at the same time developing technology of computer that gives more options for simulation.

The commercial CFD software Fluent is used to calculate the thermal behaviour of the unit. Comparisons with the experimental results and several simulations were performed to provide heat storage information during melting and solidification.

The aim of this study phase was to investigate the electrical performance of the PVT system and the convection heat from the back side. Thus, some assumptions had to be made to simplify the simulation process and reduce the computation time, namely: (1) Thermal expansion due to phase change was

neglected; (2) Motion of the solid in the melt due to density differences was ignored; and (3) The PCM material was treated as homogeneous and isotropic.

6.2 Fluent code

The continuity, momentum and energy equations are solved numerically by finite volume method. The PISO method in the commercial code FLUENT version 13.0 is used to solve the control equations. The power-law differential scheme is used to solve the momentum and energy equations, while the PRESTO scheme is used for the pressure correction equation.

The under-relaxation factors for the, thermal energy, pressure correction, liquid fraction and velocity components were, 1, 0.1, 0.9 and 0.3, respectively. In order to satisfy the convergence criteria (10^{-6}), the number of iterations per time step is 200-400.

6.2.1 Physical model description

A 2D model was built in Design Modeller that had the same dimensions as the experimental system, as shown in Figure 6.1. The element on the left side represents the PCM container of 1200 mm height and 30 mm width. The element on the right side is the air duct of the same height, and the gap size is set to 100 mm, with two 100 mm openings at the top right and the bottom, as shown on the right. The width of the PCM and the duct gap size can be varied, depending on the requirements. The parameter of the system is followed by the experiment unit.

Figure 6.2 shows a 3D rendering of the simulation model used to compare the results with the 2D model.

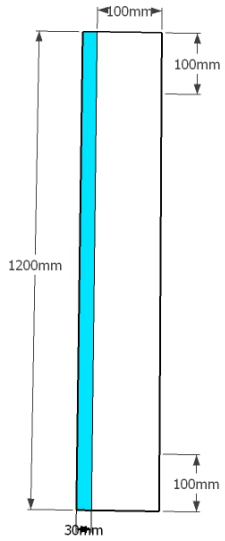


Figure 6.1 Schematic view of the 2D version of the simulation model

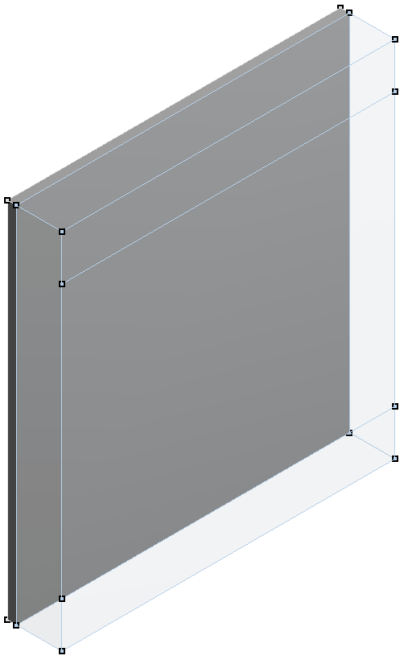


Figure 6.2 3D version of the simulation model

6.2.2 Boundary and initial conditions

The diagram of boundary conditions for a two-dimensional PV/PCM air system is shown in Figure 6.3. The coupled-wall boundary condition is specified to allow for conjugate heat transfer. A fixed heat flux condition is applied to the PV face, so the heat transfers from PV to PCM through conduction before being transferred to air through convection. The front face of the PV was divided into three zones, which were used to validate the experimental results where the heat flux distribution is not uniform. In all other cases, the three heating zones were in the same condition, if not specially indicated.

In all simulation cases, the PV cell was assumed to be attached perfectly to the aluminium front plate. The heat flux applied to the front of the PV was calculated using the analytical model presented in the preceding chapter, considering heat convection and radiation. The external surfaces of the test unit were assumed to be bounded by convective heat transfer condition. The radiation heat transfer for the PCM unit was not simulated, as it was negligible relative to the conduction heat transfer between the PCM and the PV panel.

Position E in Figure 6.3 denotes the air inlet for the duct, specified as pressure inlet in the natural ventilation case. Position D represents the pressure outlet in most cases. Inlet and outlet in the air duct were using pressure inlet and outlet in the natural ventilation case and were closed in the non-ventilated case. A lot of research (Gan. G.H, 2009.2010) indicated it is an acceptable treatment for natural convection to have pressure inlet/outlet condition and this is the method required by the software Fluent. They have shown that for narrow cavities used

in this investigation the difference between a domain of the same size as the cavity and a larger numerical domain is not significant. The inlet and outlet boundaries of the computational domain were defined as pressure inlet or outlet with air at the ambient temperature and same gauge pressure such that flow in the domain would result from thermal buoyancy only.

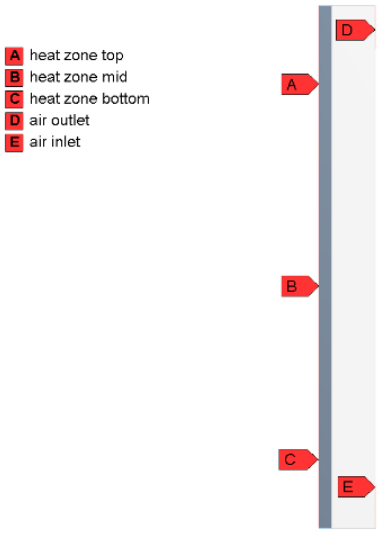


Figure 6.3 Boundary condition positions

In simulations, temperatures within the PV/PCM system and in the ambient environment were all initially set to 20 ºC. The coupled wall boundary condition was specified at the interface between PCM and air duct to allow heat transfer. The second-order upwind scheme was used for solving the pressure, momentum and energy equations and the transient formulation. Fixed heat fluxes were applied to the PV face (position A, B, and C in Figure 6.3), indicating that the heat transfers from PV to PCM through conduction, before being transferred to air through convection. The fixed heat fluxes were calculated based on the solar intensity, and the heat removal factor from convection and radiation at the front side. From measurements of artificial lights used in the experiments, an average

of 600W/m^2 heat fluxes were applied to three heat zones on the PV for validation purposes. Position E in Figure 6.3 denotes the air inlet for the duct. In the natural ventilation case, it is specified as the pressure inlet. Position D is the pressure outlet in most cases. All other walls are well insulated and no heat transfer takes place. The initial conditions were determined based on the measured data. Solidification process was simulated after 10 hours by turning off the lights and lowering the ambient temperature to 15 ºC.

6.2.3 Time step and grid independence study

The time step and grid size independence were carefully determined in the primary calculations. The numerical results can be regarded as time step and grid size independence, provided that the temperature, liquid fraction and air velocity do not change with the time.

A mesh independent test was carried out to examine the mesh independence of the numerical results. Three quadrilateral mesh sizes were studied at the 1000 W/m^2 heating condition. Mesh type 1 has large grid size with boundary layer inflation mesh and has about 620,000 element cells in total. Mesh type 2 uses face mapping methods and has 160,000 element cells. A fine mesh size of 0.25 mm was taken as the benchmark with about 2 million element cells as mesh type 3.

Three points were chosen to compare the temperature and air velocity in the unit, as shown in Figure 6.4. Only 200 s time step was simulated for comparison because the fine mesh type 3 takes extremely long time for the simulation to complete. As indicated by the results pertaining to these different grid sizes

shown in Figure 6.5, the differences in temperature at Point 1 inside the PCM are rather small for the simulation process time. The small difference only occurs after the PCM reaches its melting temperature.

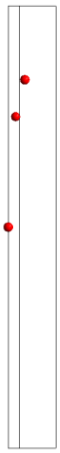


Figure 6.4 Point 1, Point 2, and Point 3 from left to right

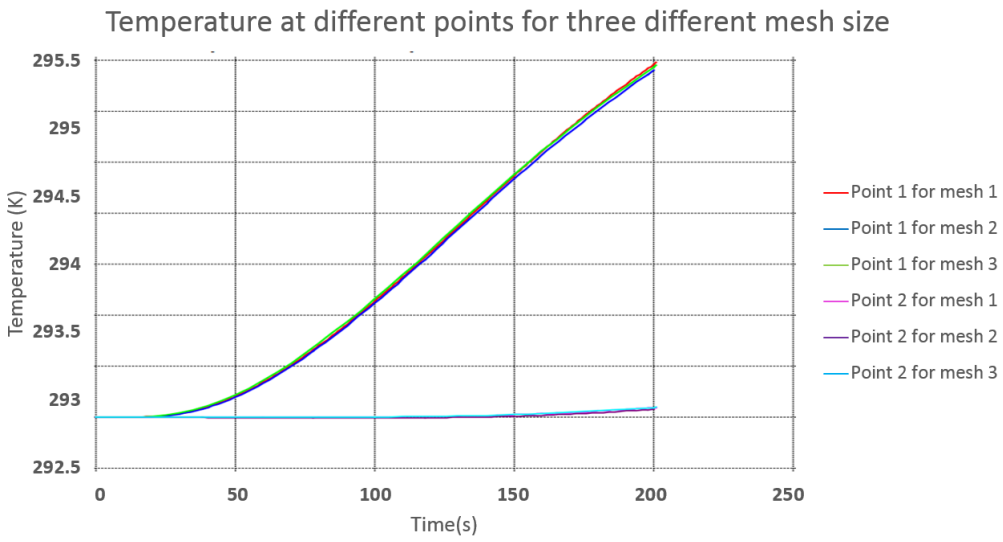


Figure 6.5 Temperature at different points for three different mesh sizes

Figure 6.6 shows the mean air velocity at the air outlet for three different mesh sizes. Small differences were observed for the three mesh sizes at the start, after which all mesh types tended to close at 0.35 m/s. However, mesh type 1 had a

difference of about 8% compared to fine mesh type 3 and mesh type 2, with about 4% difference. Thus, mesh type 2 was chosen for simulation.

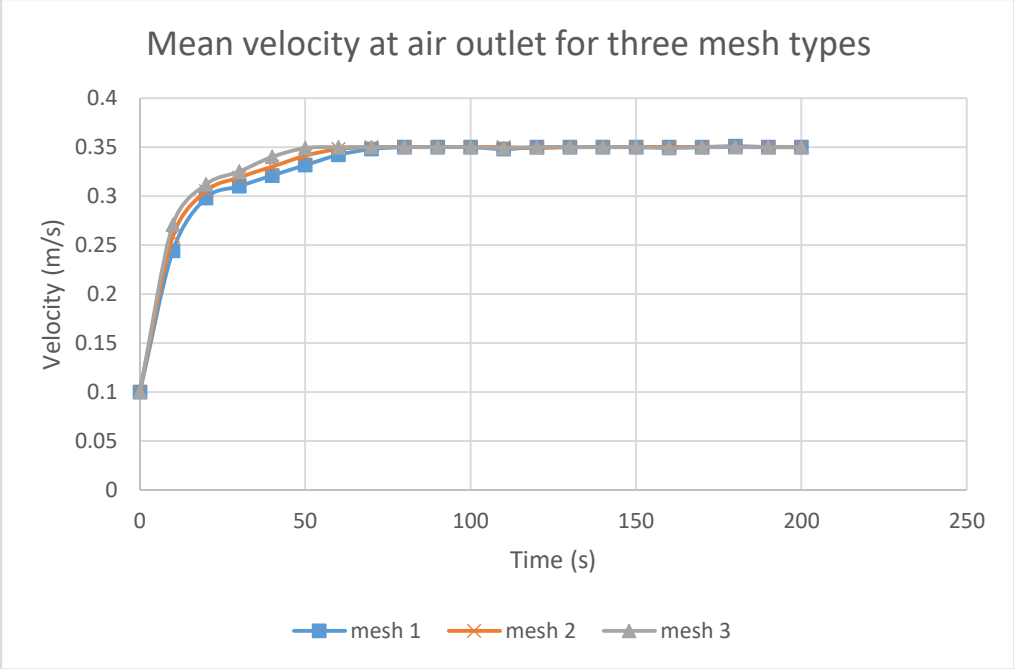


Figure 6.6 Mean velocity at the air outlet for three different mesh sizes

For the time dependency study, four time steps were chosen, namely 0.1 s, 0.5 s, 1 s, and 2 s. The results were compared through two observed points, as shown in Figure 6.7 and Figure 6.8. The temperature in the PCM for all cases shows a good agreement, while the velocity for the time step of 2 s shows large difference compared to the 0.1 s case. Time step of 0.1 s was thus used for the first 200 s, after which it was gradually increased to 30 s to reduce the total calculation time while ensuring accuracy.

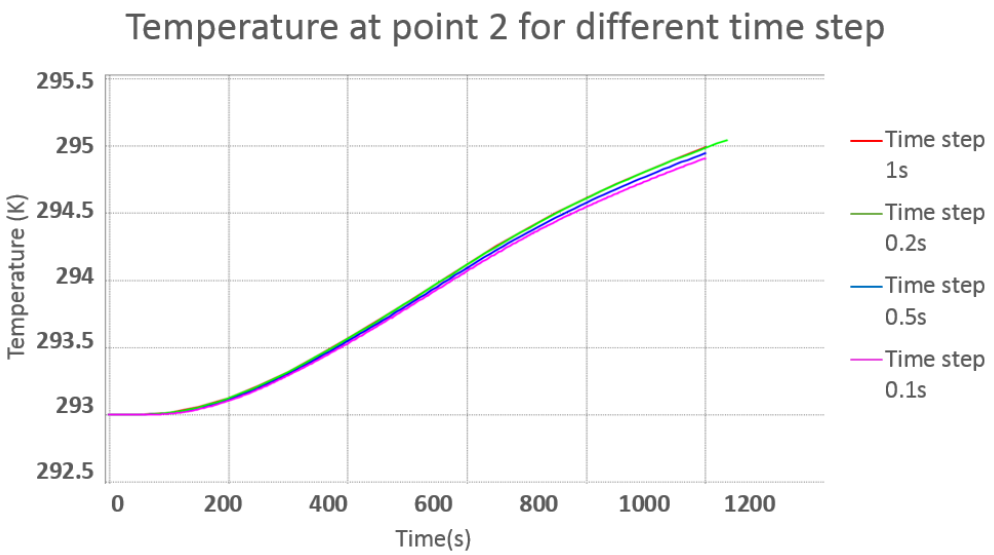


Figure 6.7 Temperature at Point 2 for different time steps

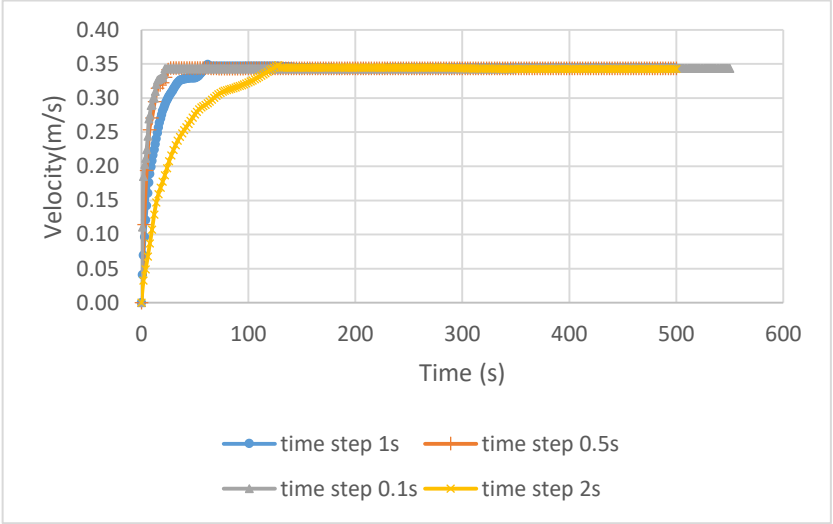


Figure 6.8 Velocity at Point 2 for different time steps

In sum, for the grid size and time dependency study, mesh type 2 and a variable time step with a minimum value of 0.1 s were used for all simulations.

6.3 Validation of the CFD model

The validation was based on the dynamic evolution of temperature and air velocity at various points in the test cell, which were compared with the experimental data. A list of observed points is presented in Table 4 in Chapter 3. Figure 6.9 shows the experimental and simulated temperatures of three thermocouples in the PCM unit. The temperature curves of experimental and simulation results are very similar to each other, with a maximum difference of about 8%. However, the predicted temperature is a little lower than the experimental result. The discrepancy could be attributed to several factors: (1) Air bubbles inside container at the start of the melting process inhibit heat transfer from the front surface to the PCM, and (2) The inlet air temperature increases as the ambient temperature increases due to the heat emanating from the lights, while the inlet temperature is treated as constant in the simulation.

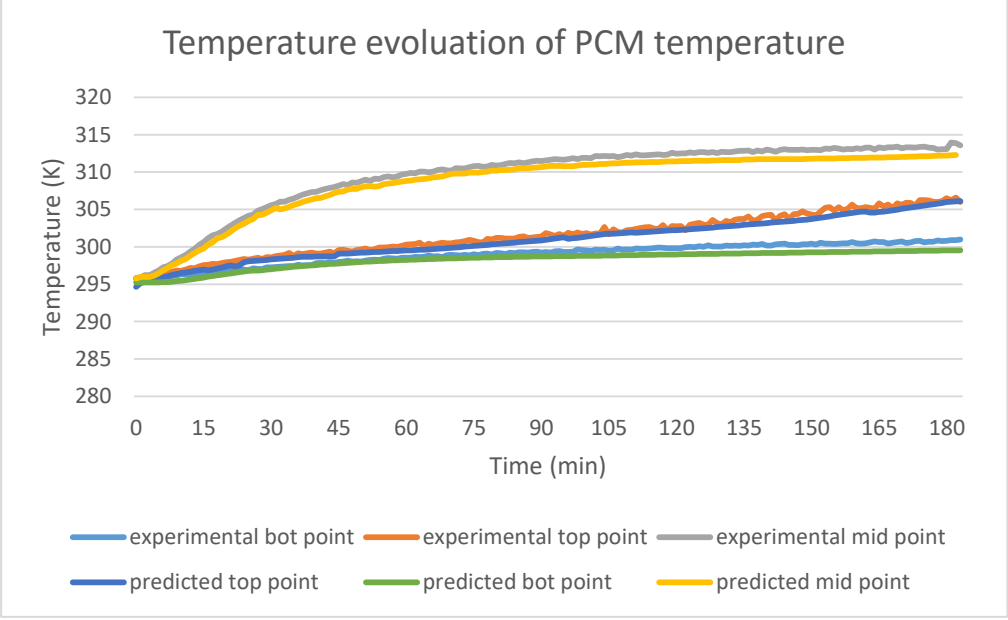


Figure 6.9 Predicted and experimental transient temperatures at three points inside the PCM

Figure 6.10 shows the predicted transient temperature of three points in the air duct. The agreement between the experimental results and the numerical simulation outputs is reasonable. However, the difference between the experimental and the predicted results is larger than the temperature in PCM. For lower temperatures, the difference was on average about 1 K, increasing to 2 K for higher temperatures. One major factor causing the larger difference is the temperature range is small for air temperature and the thermocouple accuracy error is relatively larger than it in PCM. This is also the reason for the fluctuation of measured air temperature. The insulation for system wall is not perfect, so the heat from light can directly enter into the air duct from the system wall and the air inlet. The possible sources of error in the simulation include neglecting the conduction resistance of the container box, the natural convection inside the PCM, the radiation heat transfer, and the uncertainty in the thermocouples (±0.2 K) and other instrumentation.

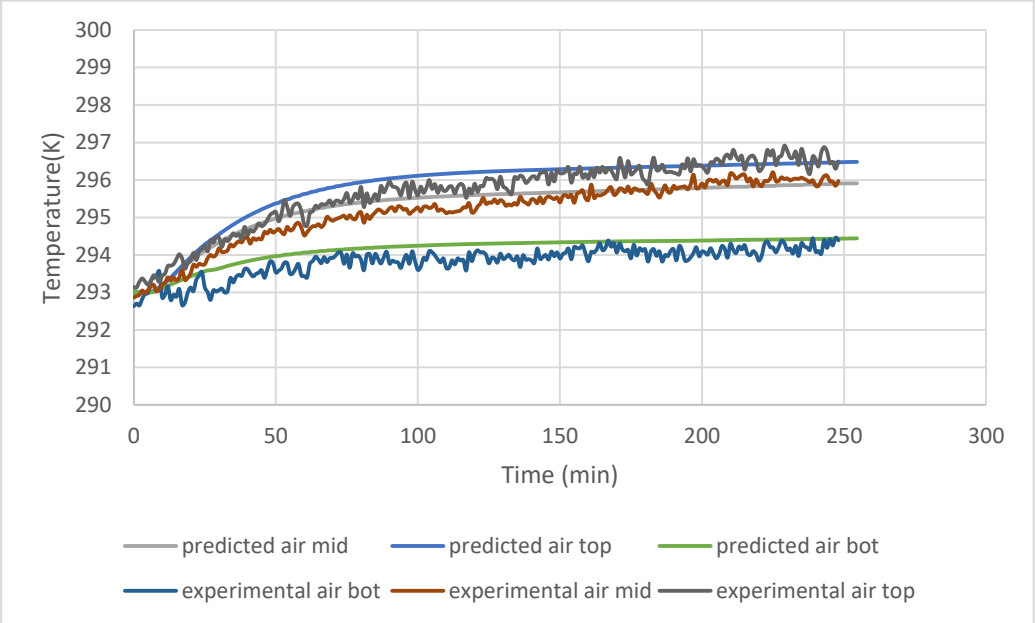


Figure 6.10 Predicted and experimental transient temperatures at three points inside the air duct

Air velocity was recorded at 15-minute intervals for three positions for validation purposes. Figure 6.11 shows the predicted and experimental transient velocity of the three points in the air duct. All curves obtained in the simulation align with those obtained experimentally. However, the air velocity has about 10% larger relative error than temperature validation. This may be due to the low magnitude of velocity in the natural ventilation and the limitation of hot wire anemometer with relatively large uncertainty. Laser Doppler velocimetry (LDV) with accuracy over ± 0.005 m/s is thus suggested for future use, as it provides more accurate measurements.

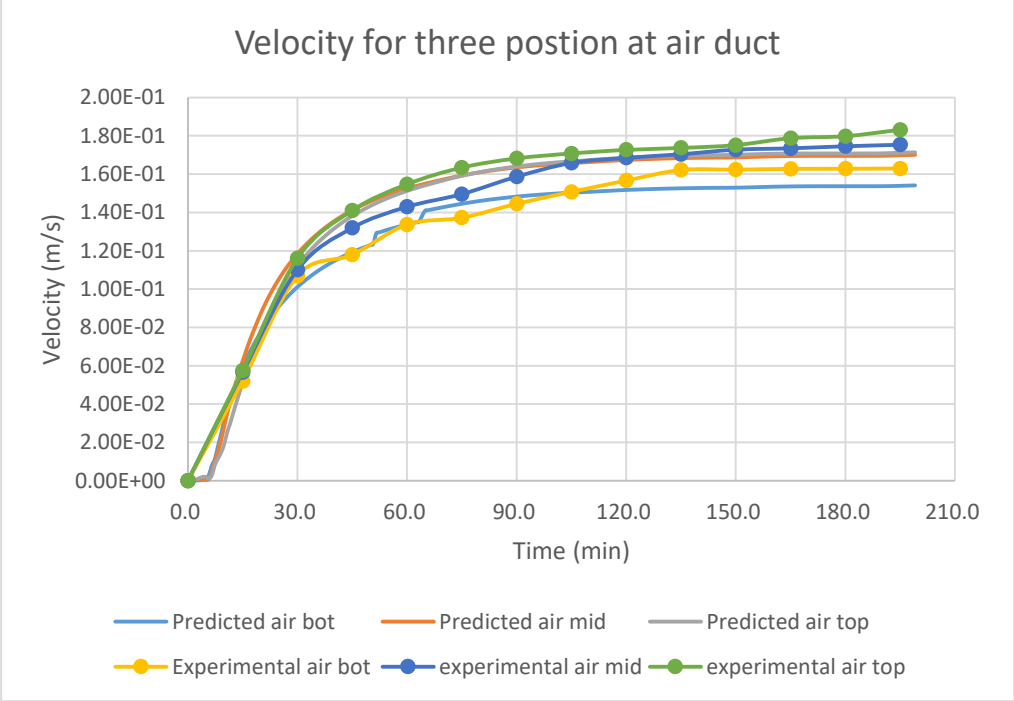


Figure 6.11 Transient velocity of three points in the air duct

In summary, the CFD model is reasonable and valid based on its agreement with the experimental results, within experimental uncertainties. The misalignment between the CFD model output and the experimental data may arise from

several sources, including: (1) It is impossible to position the thermocouples in the exactly same location in simulation inside the container; (2) Experimental data were obtained from charts, which may reduce accuracy; (3) The accuracy of measurement instrument is limited; (4) The assumptions made in the CFD model to simplify the simulation reduced the output accuracy.

The numerical model was used to predict the natural ventilation and heat transfer performance of the entire unit and the results are presented in the next section.

6.4 Simulation results

Several PV/PCM systems in different conditions and using different designs were investigated by using the validated 2D model. Predictions of temperature and velocities were compared and are presented below.

6.4.1 Case 1

The aim of Case 1 was to simulate the average solar intensity for a wall-mounted PV/PCM system on a typical sunny day in summer time in Nottingham, UK. Solar intensity was set to 300 W/m^2 to simulate daytime. To illustrate system operation, Figure 6.12 shows various temperatures over a 9 h period for the reference system. Three points inside PCM, PCM-1 (0.016,0.9), PCM-1 (0.016,0.6), PCM-3 (0.016,0.3) were chosen as observed point.

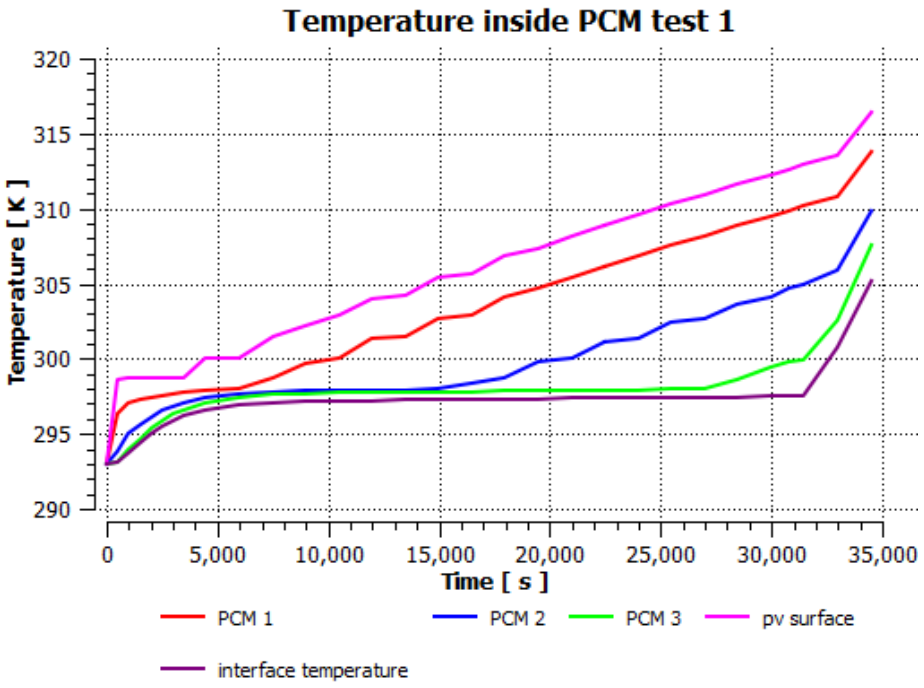


Figure 6.12 Temperature distribution in the PCM for Case 1

It is obvious that Point 1 starts melting first, and other points melt later depending on their position. After about 8.75 hours, the back side of the PCM was fully melted, as the line was sharply moving upward. Nonetheless, the PCM can maintain the PV temperature below its normal operating cell temperature of 325 K for about 9.7 hours, which is sufficient to prevent overheating of the PV on a typical sunny day in the UK.

Figure 6.13 shows the temperature in the air duct for Case 1, where Point 6 is located at the centre of air outlet (0.13,1.175), point 5 located at the centre of air duct (0.08,0.6) and point 4(0.13,0.175) located at the centre of air inlet. Thus, an increase of 1.8 ºC was achieved during the melting process. Point 5 exhibits a slight increase in temperature due to natural convection heat transfer from the back side of the metal box.

Figure 6.14 shows the velocity distribution in the air duct in Case 1 at time 3,000s and 10,000 s. The maximum velocity is about 0.186 m/s near the back of the metal box and its average of 0.086 m/s was noted at the outlet.

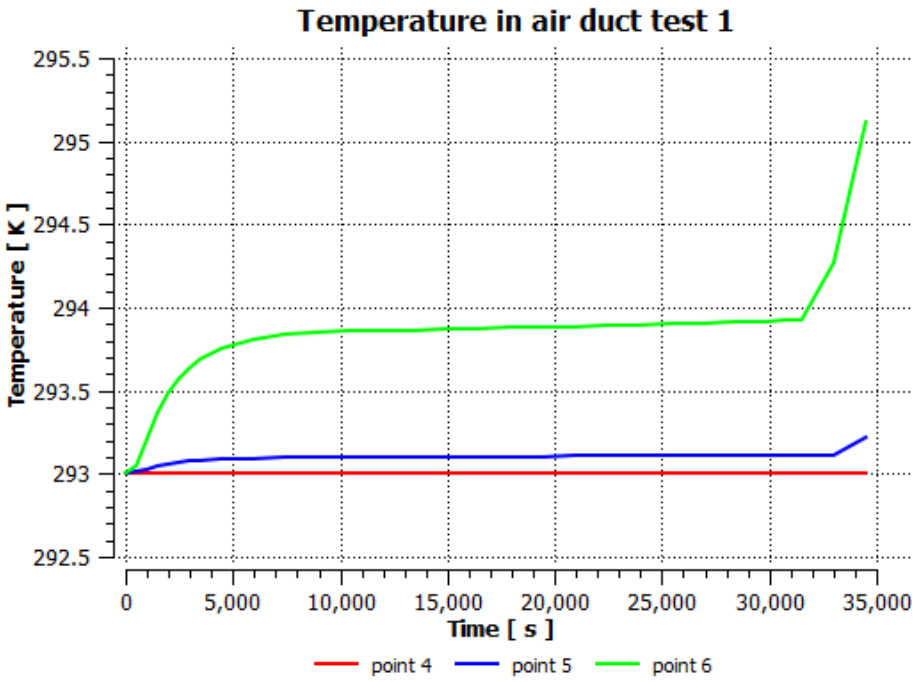


Figure 6.13 Temperature in the air duct for Case 1

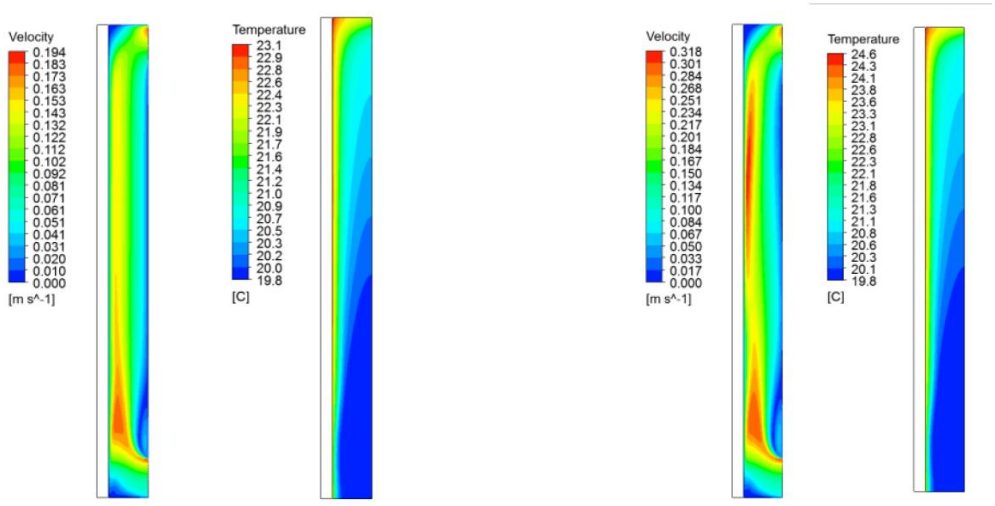


Figure 6.14 Velocity and temperature distribution contours in the air duct at time 3,000 s (left) and 10,000 s (right)

Simulation was also performed for the solidifying process with natural ventilation for night-time cooling. The air temperature was fixed at 15 °C.

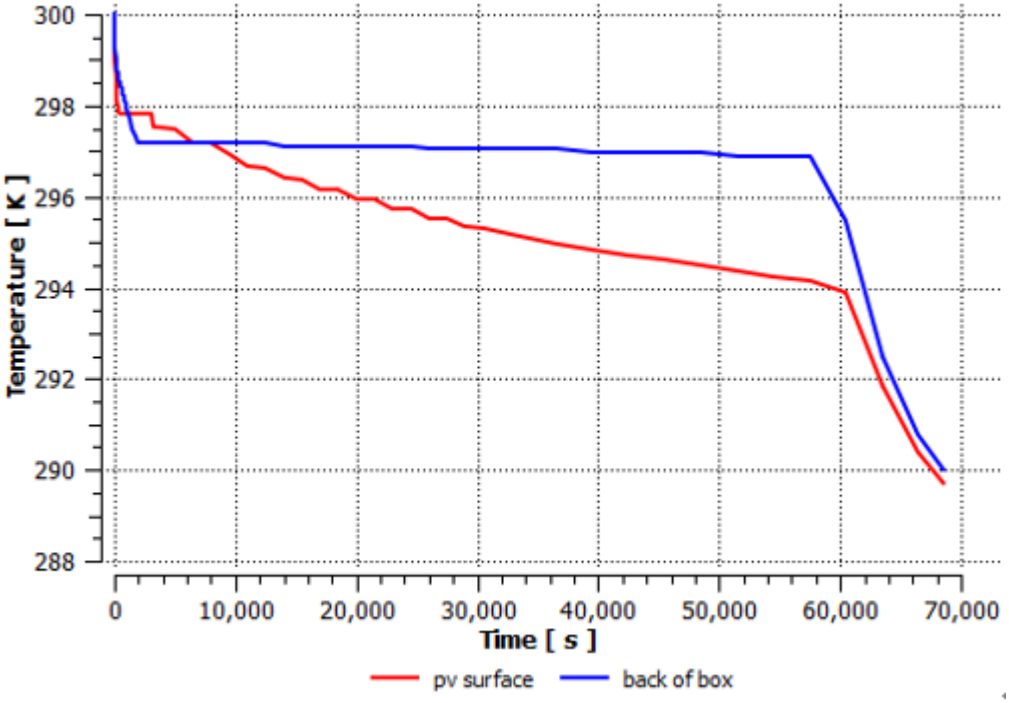


Figure 6.15 Temperature distribution in the PCM in the solidifying process

Figure 6.15 shows the temperature distribution in the PCM in the solidification process. As can be seen from the graph, the PV surface temperature declined rapidly due to high heat convection at the front side, which is exposed to the outside, while the temperature at the back of the PCM declined slowly due to the solidifying process and low heat convection factor characterising the indoor conditions. It takes almost 16.67 hours for full PCM solidification, which would occur only if the following day is cloudy or raining. Hence, either forced convection or use of fins is recommended to increase the heat removal.

6.4.2 Case 2

Solar intensity was set to 750 W/m^2 to simulate a hot day in a city at a low latitude. Figure 6.16 shows the temperature variations of the PV surface and rear temperature with time when the solar intensity rises to 750 W/m^2. PCM maintains the PV temperature below its normal operating cell temperature of 325 K for about 2.5 hours and fully melts in about 3.75 hours. However, increase in the ambient temperature does not result in a significant change in the PCM temperature, even though the time required for the PCM to fully melt declines. In this case, more PCM material or higher PCM melting temperature should be employed if better operating conditions and longer operation time are required.

Figure 6.17 presents the velocity at two points in the air duct. The system maintains the air velocity of about 0.17 m/s at the outlet.

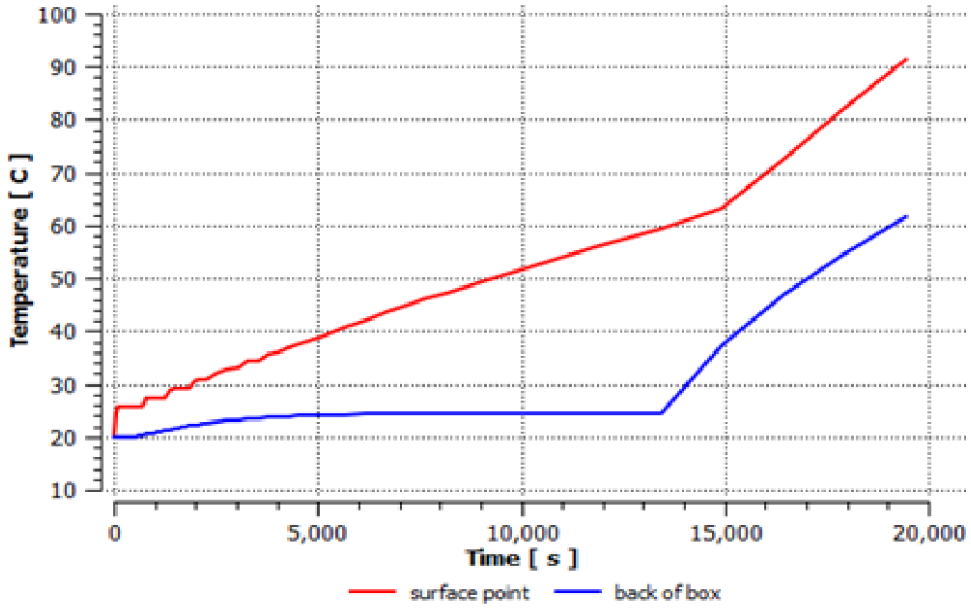


Figure 6.16 The temperature variations of the PV surface and rear temperature with time

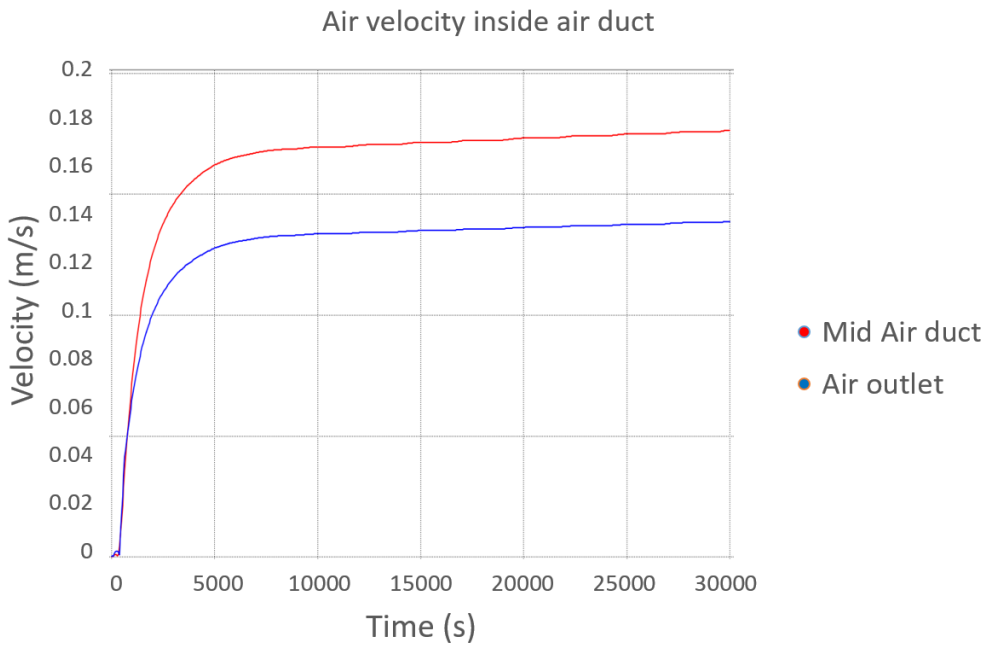


Figure 6.17 Velocity at two points in the air duct

6.4.3 Case 3

In order to improve the thermal conductivity in the solidification process, vertical fins were applied inside the PCM. Solar intensity in this case was set to 300 W/m^2 in order to compare with Case 1. Figure 6.18 shows the schematic diagram of the PV/PCM system with vertical fins inserted into the PCM.

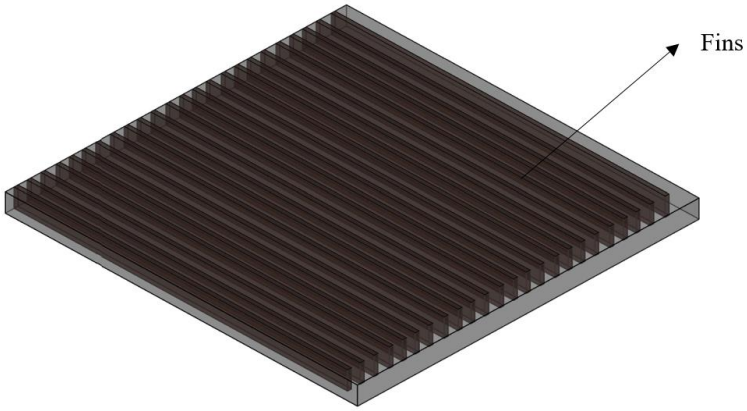


Figure 6.18 Schematic diagram of the PV/PCM system with fins inside the PCM

The system in Case 3 included vertical fins with 30mm spacing inserted inside the PCM, which is same with the result in experiment described in section 3.3.3. These fins were added in order to improve heat conduction inside the PCM. Figure 6.19 shows the temperature at three observed points in the PCM for Case 3. The point locations are displayed in Figure 6.4. The initial steep increase in the PV temperature is due to the large time step used. The performance in melting process is similar to the case without fins.

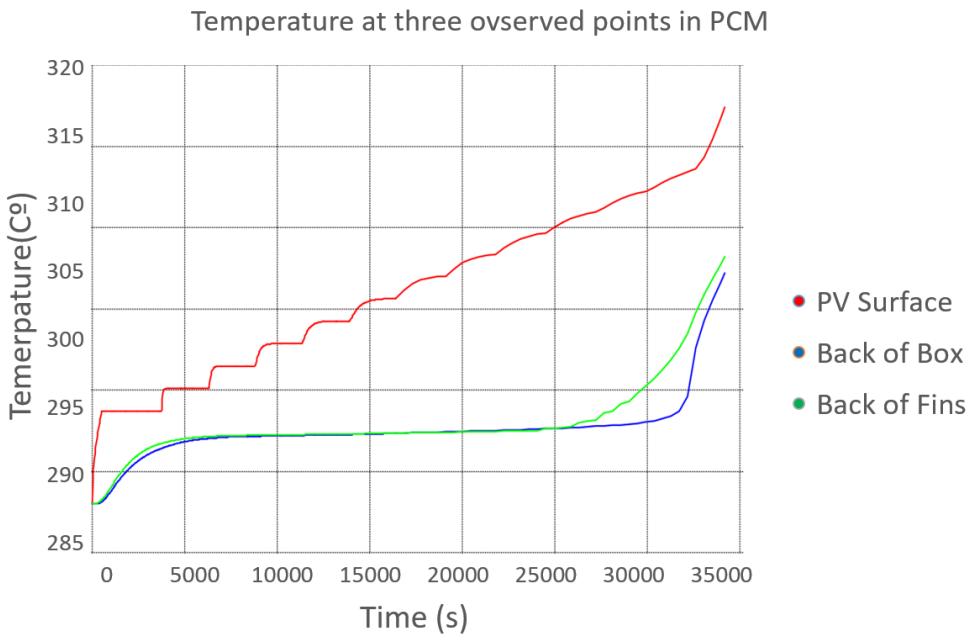


Figure 6.19 Temperature at three observed points in the PCM for Case 3

Figure 6.20 shows the temperature distribution at the top side of the model in Case 3 at time 10,000 s. Compared to the Case 1 without fins, the temperature at the back is slightly higher due to the inclusion of fins. Thus, the use of fins significantly improved the system's thermal control. It can be seen that the fins effectively alleviate the temperature rise of the front surface of the PV / PCM system. Fins can reduce the temperature rise on the front surface and the thermal stratification within the system. However, Fins reduced the time to achieve

temperature control due to the reduced PCM volume and the added weight of the metal fins, which could be a potential problem.

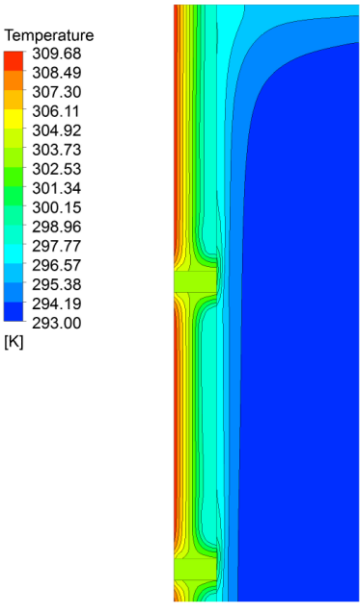


Figure 6.20 Temperature distribution at the top side of model in Case 3 at time 10,000 s

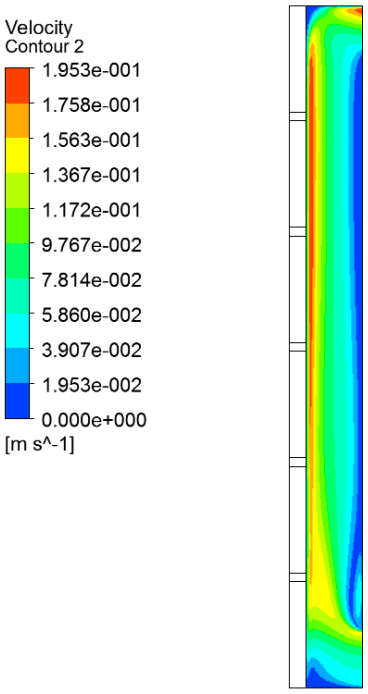


Figure 6.21 Velocity distribution in the air duct in Case 3 at time 10,000 s

Figure 6.21 shows velocity distribution in the air duct in Case 3 at time 10,000 s, indicating that, compared to Figure 6.14 for Case 1, an average 5% increase in the velocity is achieved when fins are incorporated into the PCM.

Figure 6.22 shows the temperature distribution in the PCM in the solidification process for Case 3. Compared to Figure 6.15 pertaining to Case 1, where 16.7 hours were required for solidification, the time is substantially reduced.

In summary, the simulation results for the case with fins inside the PCM indicate that a small number of fins has a limited effect on heat storage, but can reduce solidification time and increase the air velocity in the duct.

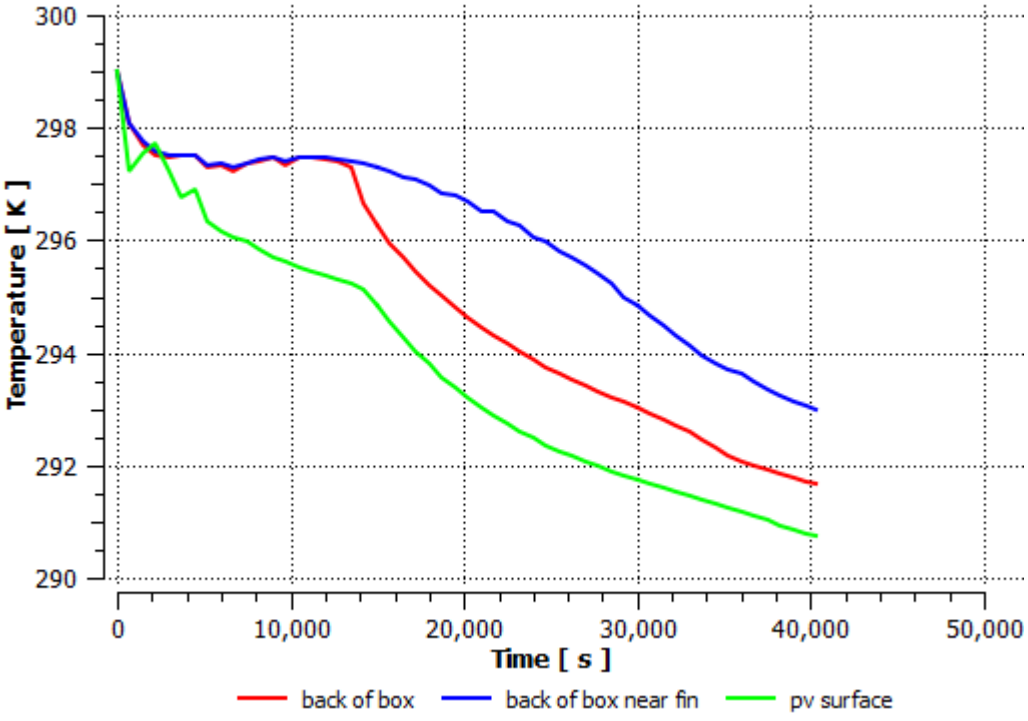


Figure 6.22 Temperature distribution in the PCM in the solidification process for Case 3

In conclusion, the simulations discussed in this chapter indicate that this process is useful in validating the experimental results. Specifically, a typical situation,

in which PCMs are used for overheating prevention for photovoltaic panel by absorbing excessive heat during the daytime and releasing it at night, was examined. The results revealed that increasing the solar intensity does not change the temperature of the PCM surface significantly; however, the time required for the PCM to fully melt is reduced. Thus, the required amount of PCM is greatly affected by the environmental conditions. The use of fins provides improved thermal control. However, the fin geometry, type and number should be optimised for improved outcomes.

6.5 Summary

In this chapter, a numerical study on designed PV/PCM system was presented. Computational fluid dynamics (CFD) were utilised to predict airflow and temperature by numerically solving the set of partial differential equations for mass, energy and momentum. Methodology and simulation model were discussed and a proper model was chosen to use in Fluent 13.0. The validation of the CFD model was based on the dynamic evolution of temperature and air velocity at various points in the test cell, which were compared with the experimental data. The results indicated that the model is both reasonable and valid. The numerical models were subsequently used to predict natural ventilation and heat transfer performance of the entire unit. Three case studies based on the validated model were presented and the results confirmed that the PCM can maintain the PV temperature efficiently during the heat gain period. However, problems may occur during the very long solidification process. Improvements, such as inclusion of fins inside the PCM unit were also

investigated, resulting in a better thermal performance during the solidification process.

Chapter 7 Investigation of the PVT/PCM system performance

7.1 Introduction

A validated CFD model of the PV/PCM system was described in Chapter 6. In this chapter, the results of the parametric study will be discussed and analysed. The simulation model was used to analyse the parametric behaviour of the PV with thermal storage systems to determine which improvements would produce the most benefit to the system and which research areas are the most beneficial. The study of such a model can help designers in evaluating thermal and electrical performance for a wide variety of potential applications. The parametric study was based on the change in the CFD model, including isolation, collector characteristics, channel depth, PCM gap size and fins. All the characteristics and ambient condition for this chapter is same as Case 1 in Chapter 6 if not specified in the section.

7.2 Effects of solar isolation

The induced mass flow rate in natural convection depends on the heat flux gained from solar radiation. Hence, higher solar irradiance should yield a higher mass flow rate and flow speed due to a greater stack effect.

The effect of solar insolation on the system refers to the heat flux absorbed by the PV panel. Three different heat fluxes were applied to the PV—200 W/m^2, 600 W/m^2 and 1000 W/m^2—to simulate different solar irradiance cases. The PCM thickness in this section is 30mm. Figure 7.1 shows the plot of the

temperature at the point (0.015, 0.6) against time for three solar isolation cases. The results were as expected, as the temperature in the 1000 W/m^2 case increased faster than in other cases and an even more rapid increase occurred at time 12,000 s due to the PCM fully melting. In the 600 W/m^2 case, the rapid increase took place at about 17,000 s. No obvious steep increase was observed in the 200 W/m^2 case.

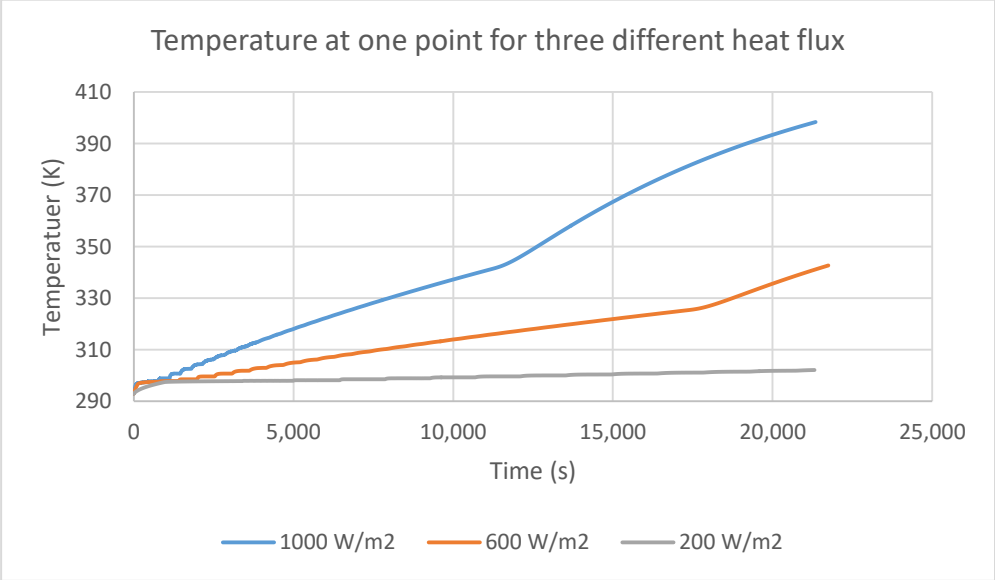


Figure 7.1 Temperature at Point 1 for three different heat fluxes

The mean velocities of the three cases are compared in Figure 7.2. The velocities are initially similar, as the heat transfer from front to back occurs slowly. After that, the air velocity at the outlet increases rapidly for higher solar radiation, which was expected, since more heat is transferred to the airflow in the PV channel. For the 1000 W/m^2 intensity, the increase occurred at about 12,000 s, and for the 600 W/m^2 intensity, the increase started at 17,000 s. No obvious increase in velocity was noted for the 200 W/m^2 intensity case in the simulation period. The rapid increase occurs once the PCM is fully melted and the back plate temperature increases rapidly (above the PCM melting temperature),

which increases the buoyancy effect in the air duct. Another reason for the sharp increase in mean velocity is that the heat capacity of the liquid PCM is smaller than that of the solid PCM. As a result, the temperature of liquid PCM will rise faster than in the solid state; hence, the heat transfer between the PCM and air is sharply increased, leading to higher air velocity.

In sum, larger solar intensity reduces the melting time and can transfer more heat to the ambient air. In addition, higher temperature in the air duct produces greater stack effect.

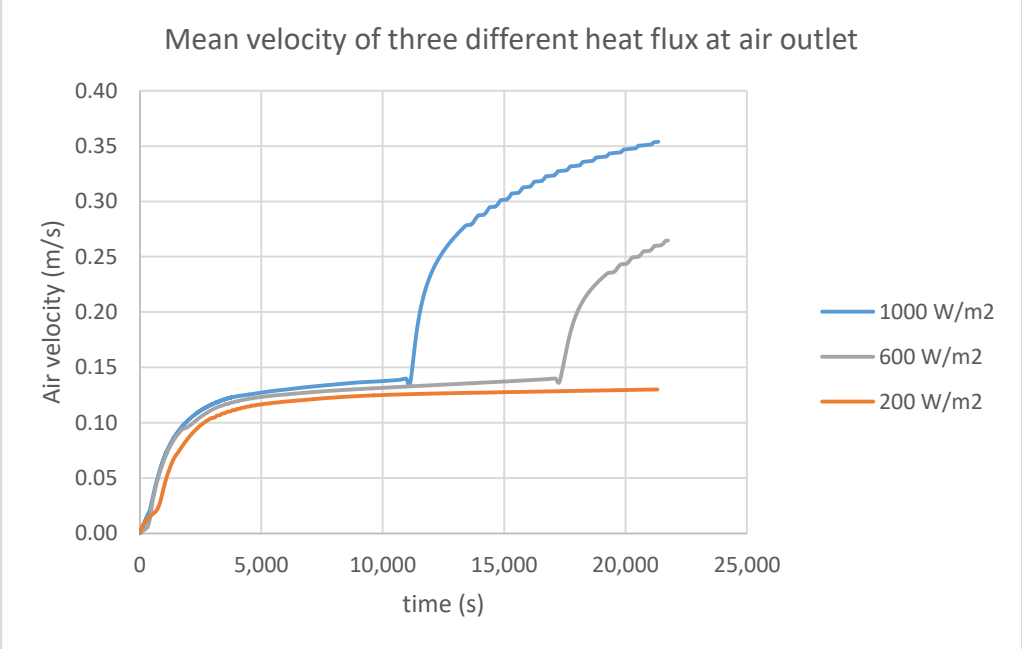


Figure 7.2 Mean velocity of three different heat fluxes at the air outlet

These results are particularly useful for the Building Integrated Photovoltaic (BIPV), where PV modules are incorporated as either mounted ventilation façades or sloping roofs of buildings. In winter, when the sun is low in the sky,

vertical BIPV has better performance because it receives more radiation than roof-mounted BIPV. On the other hand, in the summer, when the sun is high in the sky, the roof-mounted BIPV exhibits higher performance than the façade-installed BIPV. However, these two building-integrated photovoltaic systems (façade and roof) can be coupled to each other.

7.3 PCM thickness

A parametric investigation of the effect of geometric parameters on the PV/PCM unit was carried out. Two points inside the PCM, denoted as P1 (0.001, 0.6) and P2 (0.02, 0.6), were chosen for comparison under 600 W/m^2.

The thickness of the PCM layer not only determines the heat capacity, but also affects the heat transfer across the PVT unit. Three PV/PCM units were simulated with different PCM thicknesses, namely 30 mm, 40 mm, and 50 mm. Figure 7.3 and 7.4 show the temperature at Point 1 and Point 2 located inside the PCM. The results indicate thicker PCMs would take more time to melt as expected and the thickness has little effect on

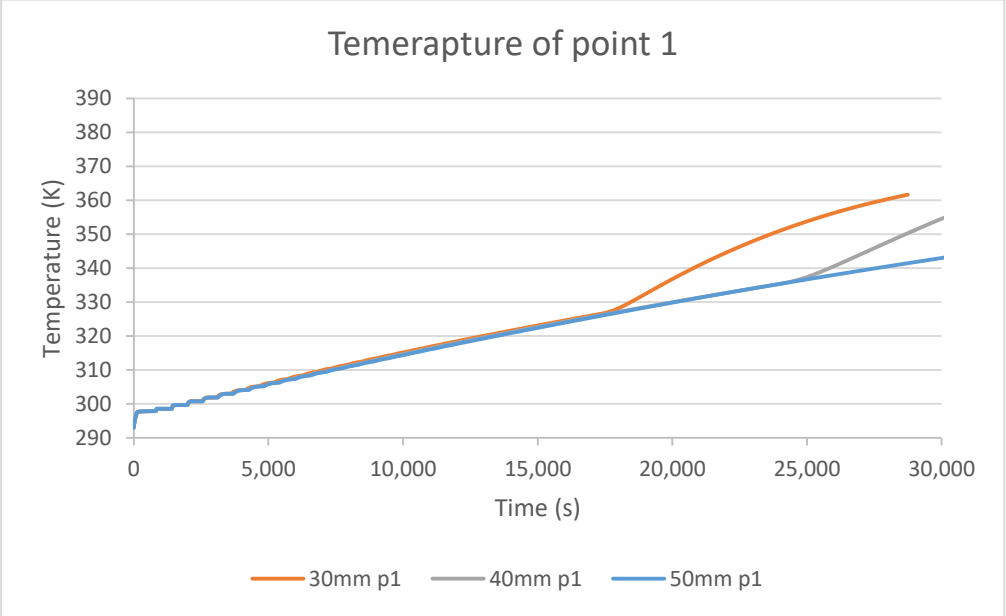


Figure 7.3 Temperature of Point 1 in the PCMs of different thickness

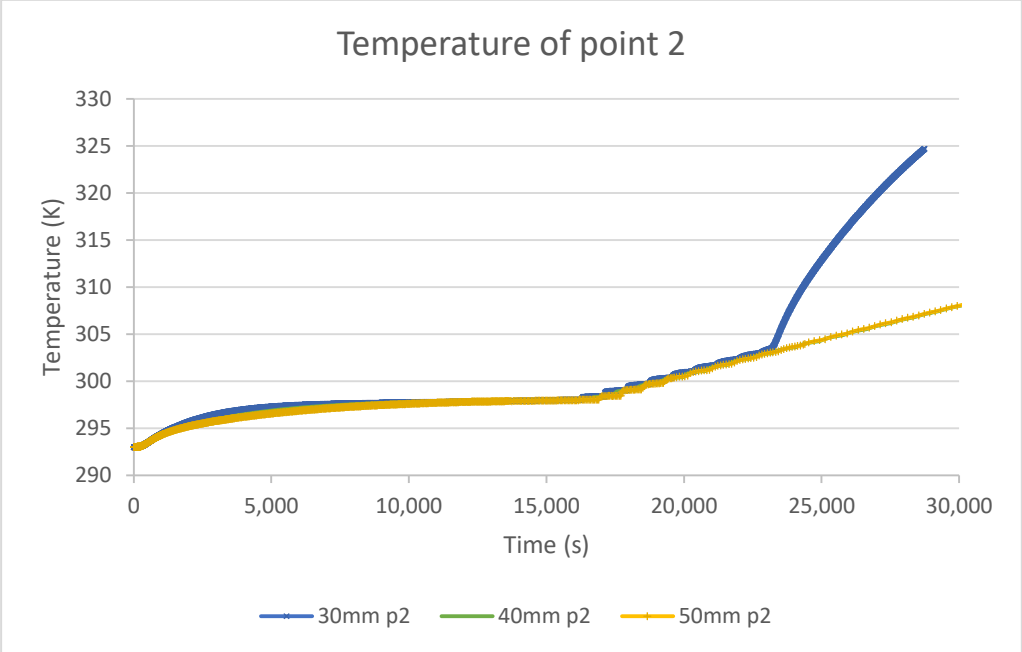


Figure 7.4 Temperature of Point 1 in the PCMs of different thickness

Figure 7.5 shows the liquid fraction of PCM in the container, where non-melting to complete melting is expressed from 0 to 1. Thicker PCM melted slower, as expected, as 30 mm thick PCM only takes 16,000s to fully melt, while those with 40 mm and 50 mm thickness take 22,000 s and 28,000 s, respectively.

These results suggest that the melting time is prolonged by 6,000 s for every additional 10 mm of PCM thickness.

Figure 7.6 shows the surface Rayleigh number (Ra) for the back of the PCM container wall. The Rayleigh number describes the importance of buoyancy forces that drive convection compared to the diffusive processes (heat and momentum), which act to stabilise convection. For free convection near a vertical wall, Ra is defined by Equation 14, where β stands for thermal expansion coefficient, α denotes thermal diffusivity, ν represents kinematic viscosity and d is collector length. In the first 16,000 s, the Rayleigh number for all three cases remained at about 8×10^7, after which it increased for the thin PCM case when the heat transfer inside the PCM is increased due to larger thermal conductivity of liquid phase PCM. The results also indicate that thicker PCM has a lower Rayleigh number at the start, and the disadvantage is reduced after 10,000 s, as Rayleigh numbers for all three thicknesses tend toward a similar value before the PCM is fully melted.

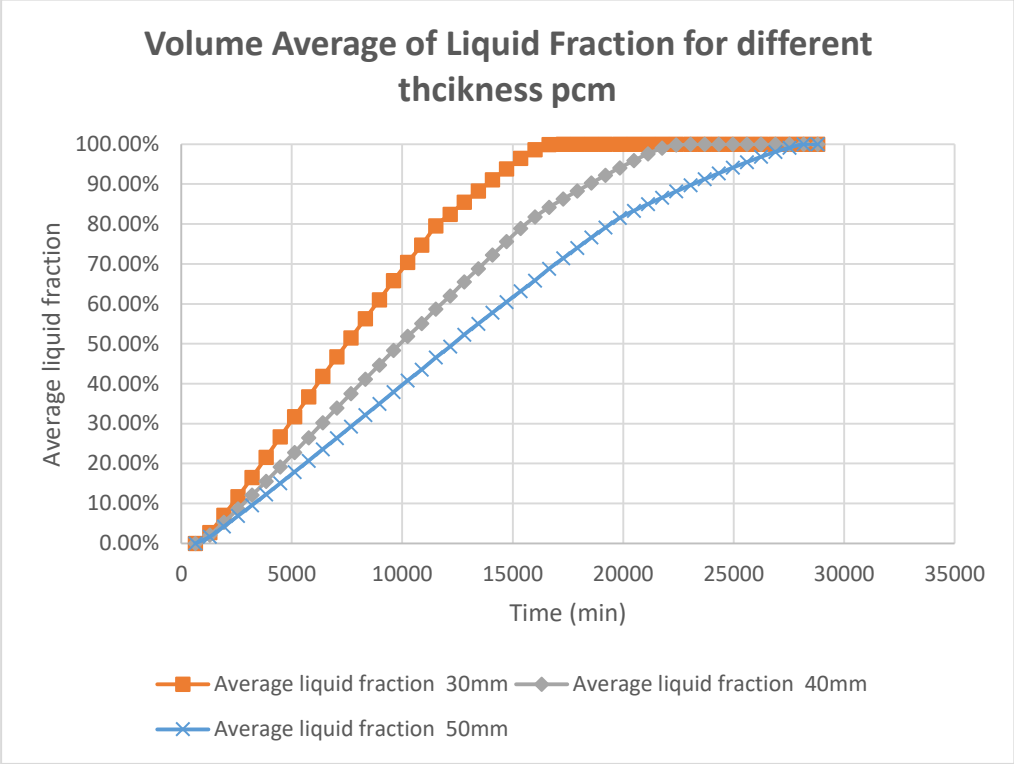


Figure 7.5 Liquid fraction 1 for PCMs of different thickness

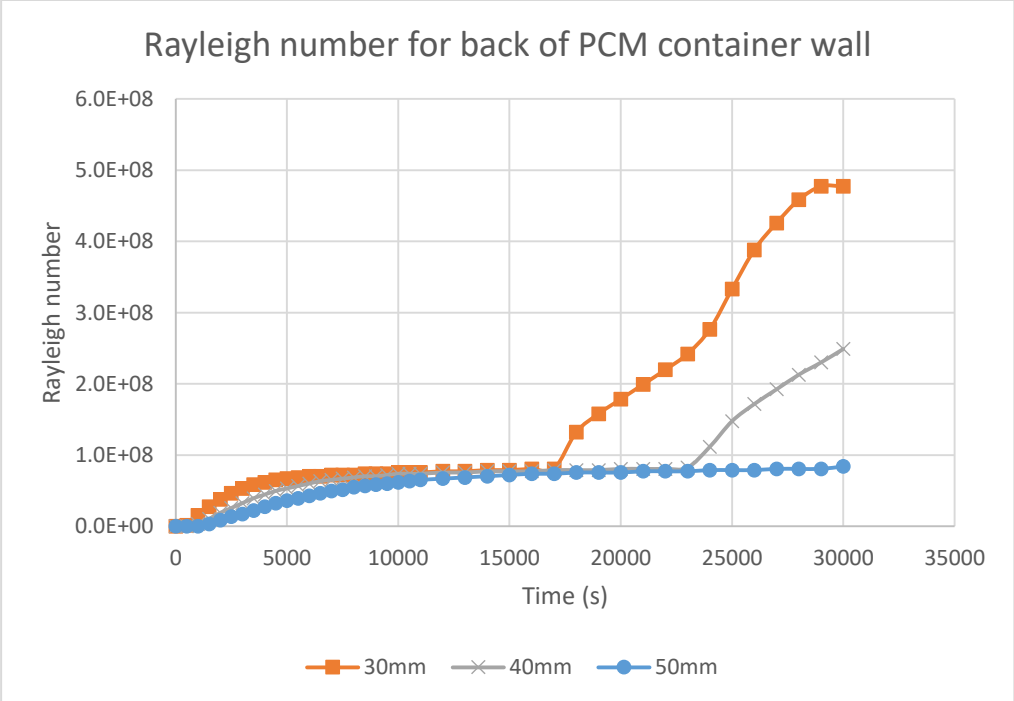


Figure 7.6 Rayleigh number for the back of the PCM container wall

7.4 Air duct depth

Three different air channel depths (50 mm, 100 mm, and 150 mm) were chosen to determine the effects of natural ventilation on the PVT/PCM system performance. Figure 7.7 shows the temperature of two points P1 (0.015, 0.3) P2 (0.015, 0.6) inside the PCM at 40,000 s.

The results indicate that air duct size has a limited effect on the required melting time for the PCM unit, as the temperature remains stable for the same period of time at both points. However, the sharp temperature increase at both points indicates that the air duct depth has a certain effect when convection heat transfer predominates inside the PCM unit. High temperature inside the PCM suggests a low heat transfer coefficient between the PCM container and the air in the duct. Hence, low air velocity is generated by natural convection. The air duct of 100 mm depth has the lowest temperature increase gradient among the three duct sizes, suggesting that there may be an optimum duct size for lowering the temperature inside the PCM. With a small air duct, viscosity between the duct walls is significant and airflow is low, while reverse flow may exist in larger ducts. At steady state, the buoyancy force and the opposing forces balance

and control the induced airflow rate in the channel under the operating conditions.

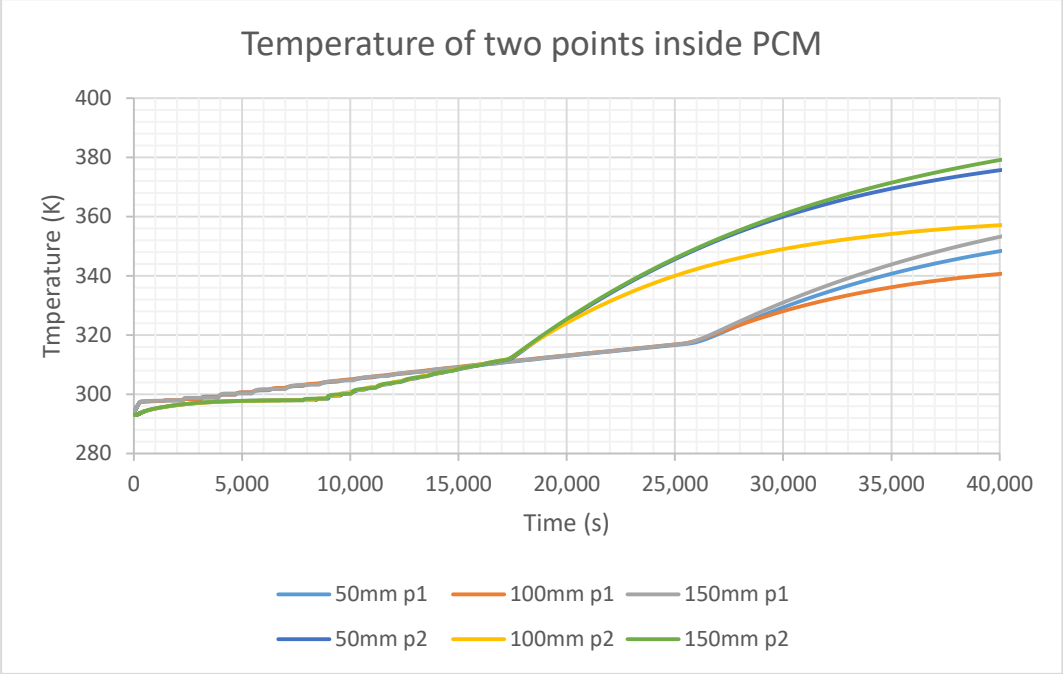


Figure 7.7 Temperature of two points inside the PCM

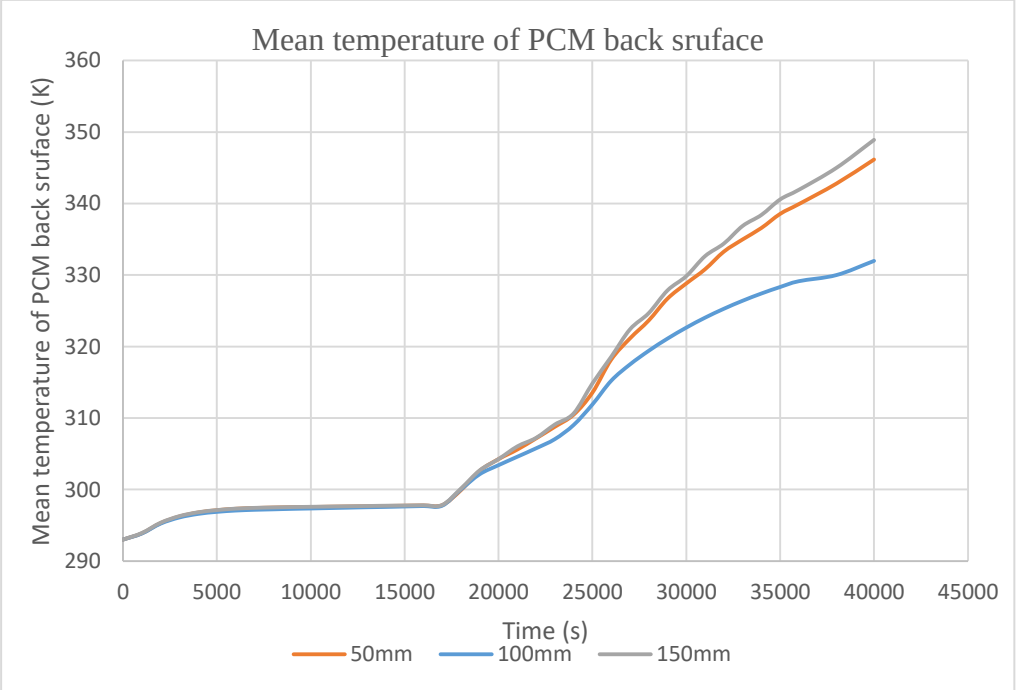


Figure 7.8 Mean temperature of the PCM back surface for different duct sizes

Figure 7.8 shows the mean temperature of the PCM back surface for different duct sizes. As can be seen, in all three cases, the temperature of the PCM back wall initially remained at 298 K, after which it increased rapidly for 50 mm and 100 mm duct sizes, while in the 100 mm case, the increase was slower. Before 18,000 s, the heat transfer inside the PCM was dominated by conduction and after that point, the convection heat transfer started to predominate, which led to a higher heat transfer though the PCM unit to air, increasing its temperature. The 100 mm case has the lowest temperature in the convection dominated period, resulting in the greatest heat transfer coefficient.

Figure 7.9 presents the mean velocity at the air outlet for three different duct sizes. The results show that the 100 mm case has the greatest air velocity (approximately 0.04 m/s higher than the other two cases, which have similar velocity). Figure 7.10 presents the mass flow rate at the air outlet for three different duct sizes. The 100 mm case also has the largest mass flow rate and the 50 mm case exhibits similar performance before 18,000 s, after which it increases at a slower rate. The 150 mm case has small mass flow rate over the entire period. Results presented in Figure 7.8 indicate that the 100 mm case has the lowest Rayleigh number, which means that it has the lowest heat transfer between the back surfaces of the PCM unit and air. Figure 7.9 and 7.10 also indicate that the 100 mm case has both the largest air velocity and the largest mass flow rate. It can thus be concluded that 100 mm duct size exhibits better thermal performance in the melting process. In a small duct, the boundary layers from both sides merge while air flow within the two boundary layers and the viscosity becomes significant. At a larger gap size, the boundary layer thickness for the same height remains the same, which may lead to the failure of the two

wall boundary layers to merge at the top, leaving a free space between them where reverse flow may occur. Figure 7.11 shows the velocity vector distribution in the air duct for the 150 mm case at 20,000 s. The graph confirms that the reverse flow exists inside the air duct of a 150 mm size. Therefore, the optimum gap size should balance the viscosity and reverse flow.

This result also confirms the findings yielded by the PVT analytical model presented in Chapter 4, which indicated that there may exist an optimum gaps size for the best thermal performance of the system. The results from three cases indicate that the optimum gap size should range from 50 mm to 150 mm.

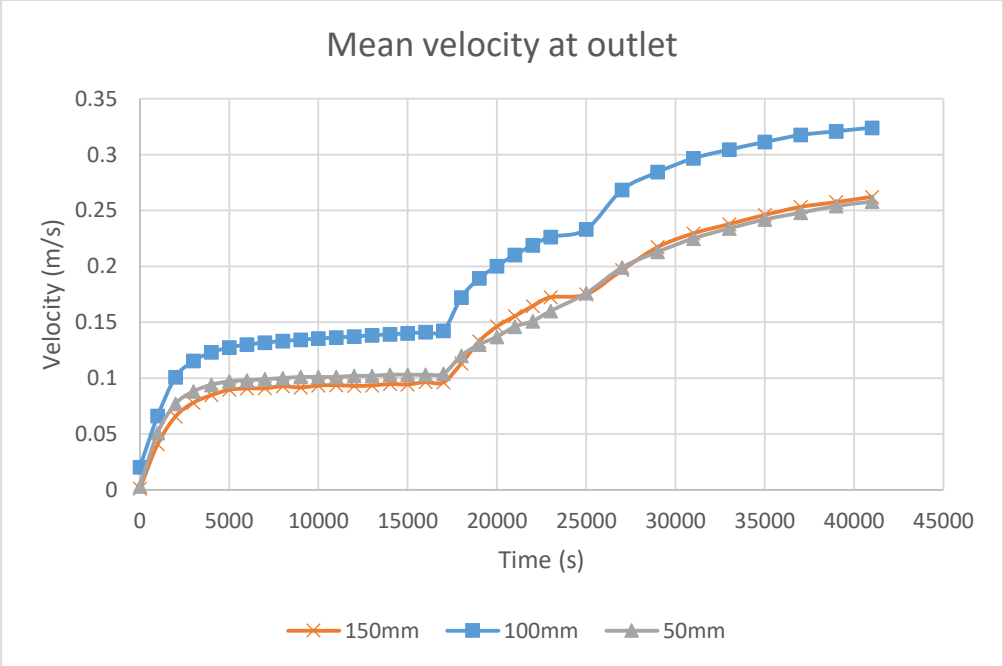


Figure 7.9 Mean velocity at the air outlet for three different duct sizes

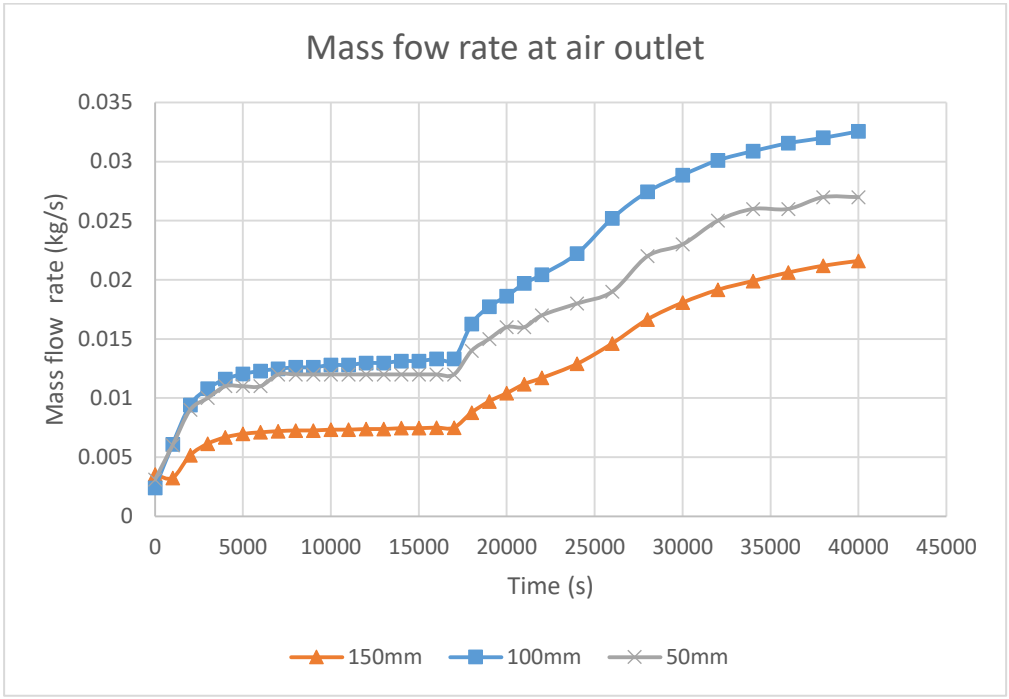


Figure 7.10 Mass flow rate at the air outlet for three different duct sizes

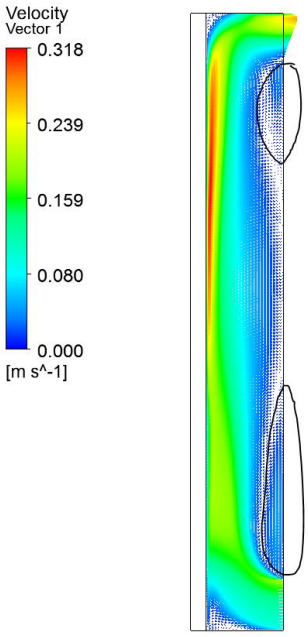


Figure 7.11 Velocity vector distribution in the air duct for the 150 mm case at 20,000 s

7.5 Effects of the PV angle

In general, the PV angle is the key element in the PV system design, as an optimum angle can maximise electrical output. However, optimum solar angle usually ranges from 30 degree to 60 degree for maximum PV power output in UK, while the natural convection is small compared to 90^{o}. The work presented in this section aimed to investigate the thermal and electrical performance for the units with three PV angles, 30 degree, 60 degree and 90 degree, under the same conditions.

Figure 7.12 shows the mean PV temperature of for three cases for the same solar intensity of 600 W/m^2. The temperature in the vertical case increased linearly at the beginning, and rose sharply after 270mins, while the temperature in the 30 degree and 60 degree case remained same before 180min and then 60 degree started to rise. The result shows 30 degree case has the best performance of controlling the PV temperature.

Figure 7.13 and Figure 7.14 show the liquid distribution for 60 degree and vertical cases at 90min and 180min. The melting process for the 60 degree unit starts from the bottom and rises up with time, while in the vertical case, the interface between the liquid and solid moves from the outside to the inside. The difference in the interface position leads to a higher mean PV temperature for the vertical case than for the 60 degree case, as shown in Figure 7.12. This phenomenon could be attributed to the convection inside the PCM, while the different convective heat transfer rate between the PCM and air is due to the differences in the stack effects.

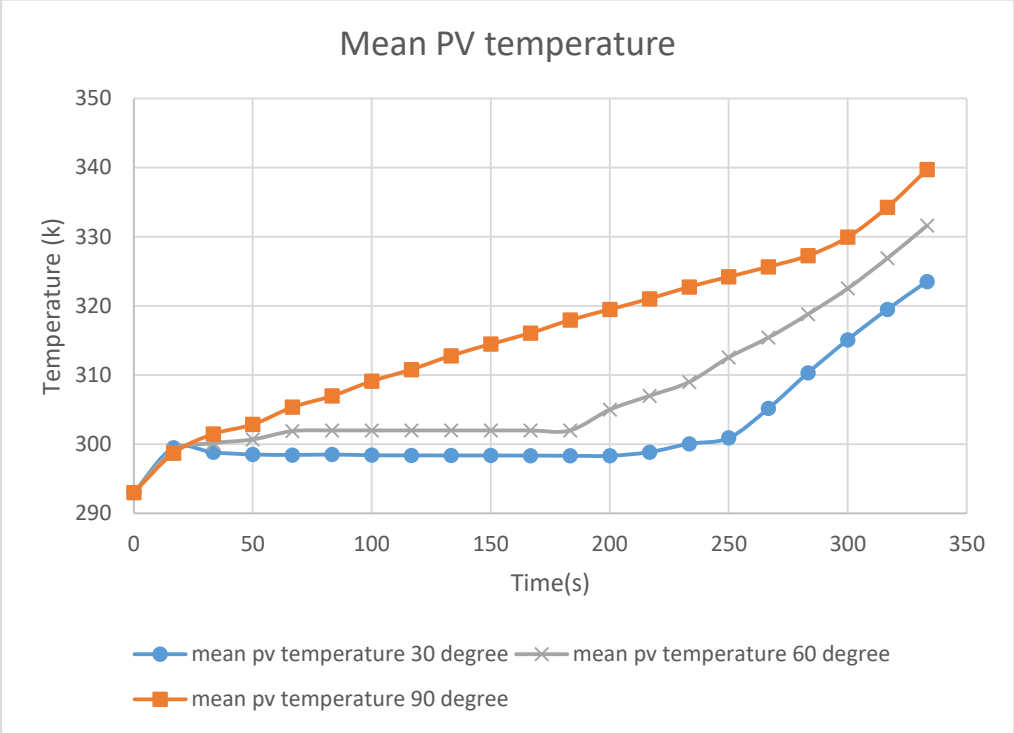


Figure 7.12 Mean PV temperature for two PV angle cases

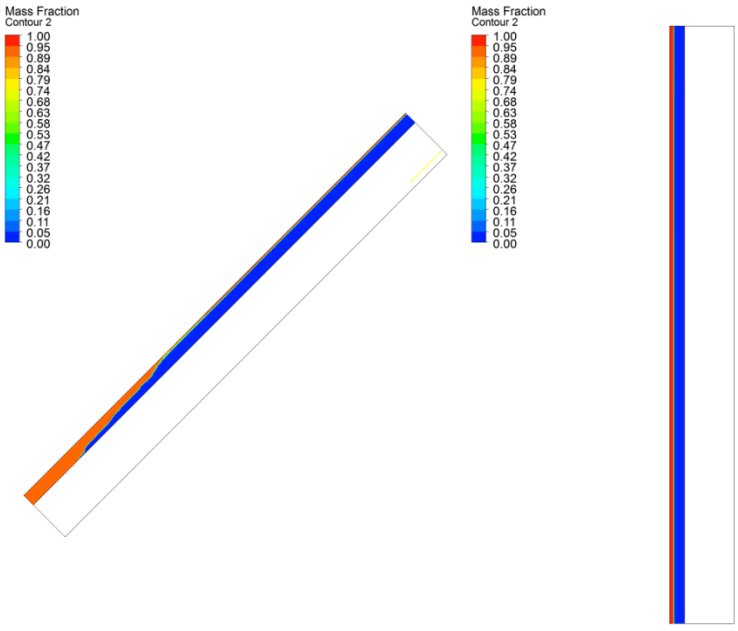


Figure 7.13 Liquid distribution for two cases at time 90min

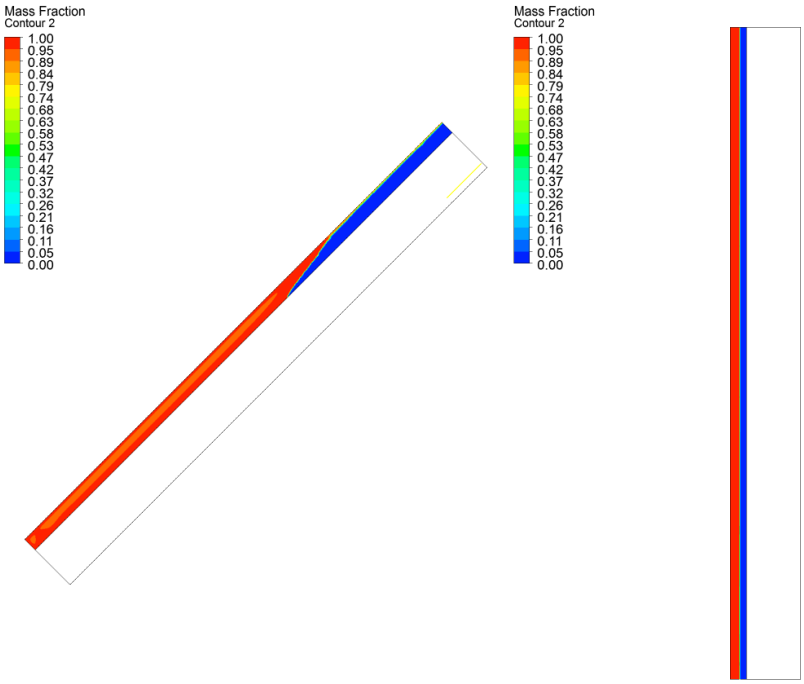


Figure 7.14 Liquid distribution for two cases at time 180min

Figure 7.15 illustrates the liquid fractions as a function of time for three different angle cases. The PCMs in the two cases are melting in similar speed at the start and then 30 degree and 60 degree case rise faster until fully melted. The difference in the melting time in the three cases is approximately 20 minutes each. These results indicate that the PV unit positioned at 30 degree and 60 degree melts faster than the vertical unit, and can therefore regulate temperature for a shorter period of time.

Figure 7.16 illustrates the Rayleigh number of the air in the air gap for the three cases. Vertical case has a larger Rayleigh number at the beginning. When the unit at 30 degree and 60 degree are almost fully melted, the Rayleigh number increases sharply and its value exceeds that of the vertical case at about 230min. However, after the vertical PCM is fully melted, the Rayleigh numbers become very similar after 320min. Larger Rayleigh number means higher buoyancy

driven flow, and the higher Rayleigh number is mainly due to the higher stack effect for the vertical case.

In summary, analyses of PV performance positioned at different angles at the same intensity indicates that the 30 degree have a smaller mean PV temperature throughout the heating process, while the vertical case has higher Rayleigh number during the melting process to conduct larger buoyancy driven flow.

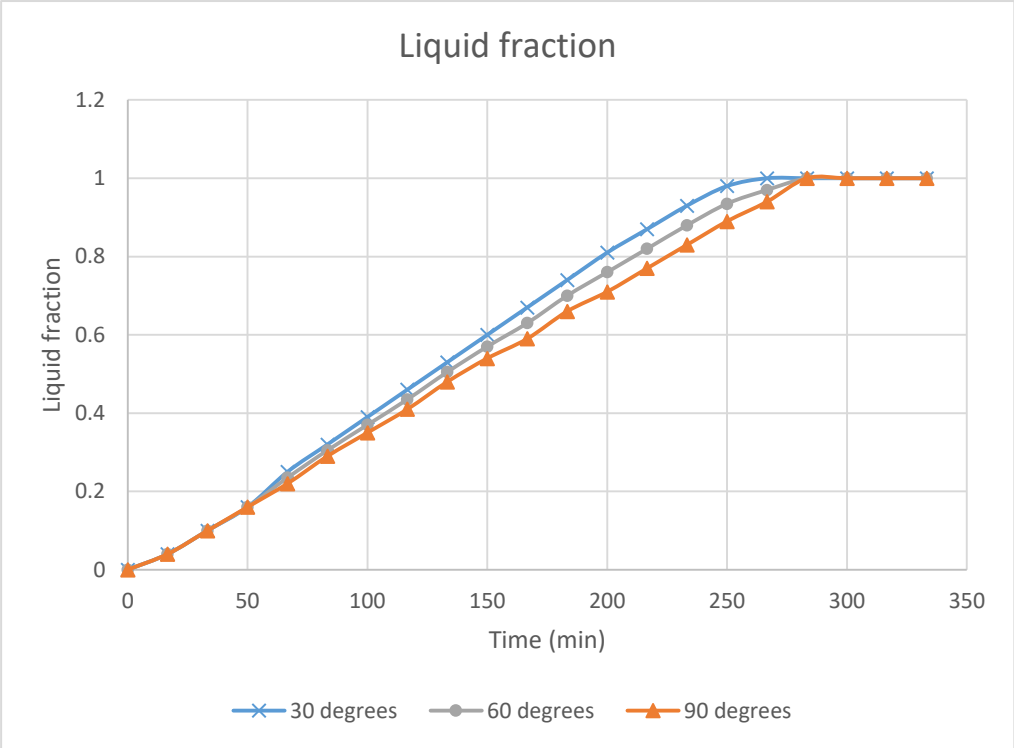


Figure 7.15 Liquid faction of three PVs positioned at different solar angles

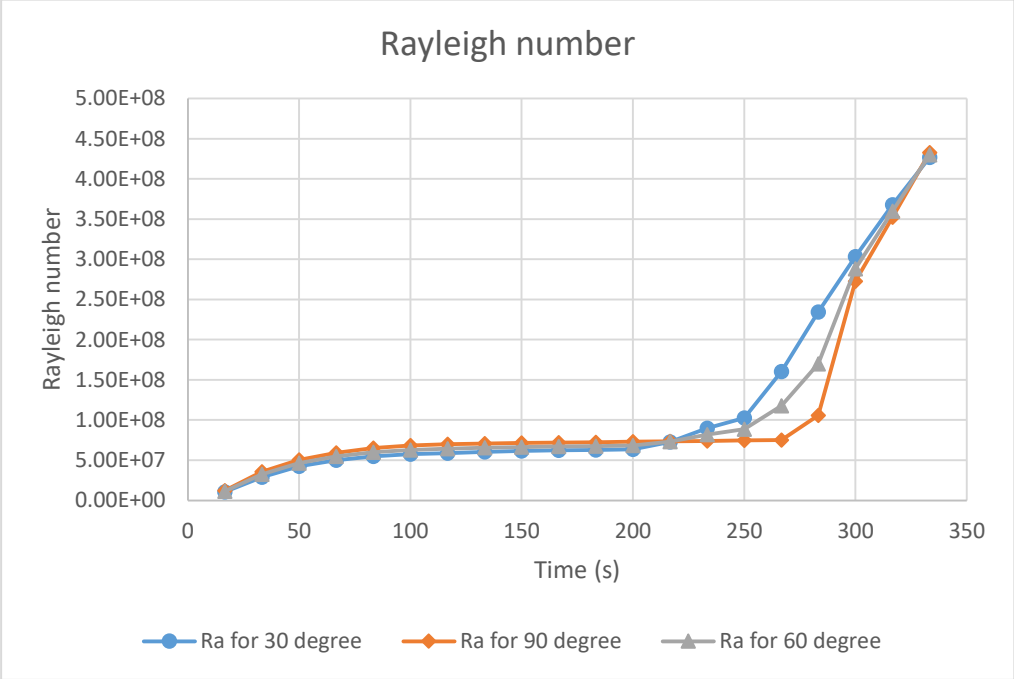


Figure 7.16 Rayleigh number for two different solar angles at the same intensity

However, in reality, the solar intensity differs for vertical, 30 or 60 degree PVs. During the morning and afternoon, when the sun's elevation angle is small, the vertical PV receives more solar intensity compared to the periods when the sun is directly overhead, when the PV at the certain angle receives more.

In summary, when the PV performance under three different PV angles was examined, the PVs have certain angle were found to have better electrical performance due to better temperature control, while the vertical case exhibits better thermal performance in this study.

7.6 Effects of forced ventilation

The simulation results reported in Chapter 6 indicated that the thermal performance of the PV/PCM system during the solidification process should be improved. Thus, in this section, to the aim is to investigate the thermal and electrical performance of a forced ventilation PV/PCM system by comparing the results with the natural ventilation case. For this purpose, a velocity inlet boundary condition was applied to the air inlet in the CFD model to simulate the forced convection system. The natural convection generates about 0.2 m/s to 0.5 m/s flow velocity in the air duct depending on the air temperature. For forced convection, two velocities were simulated, 0.7 m/s and 1 m/s, based on the results yielded by the analytical model.

7.6.1 Melting process

Figure 7.17 shows the temperature of Point 1 and Point 2 located inside the PCM for two forced ventilation cases and free convection. The performance of natural convection and 0.7 m/s forced convection is similar in the melting process. The 1 m/s forced convection, however, maintains a lower temperature at both points. After the melting process is completed, the temperature under free convection rises much faster relative to the 1 m/s case. These results indicate that forced convection exhibits limited ability to mitigate the temperature at low velocity during the melting process. At a larger velocity, improvements are relatively obvious. Figure 7.18 shows the liquid fraction for two forced ventilation cases and free convection. In the greater velocity case, the PCM takes additional 70 minutes to be fully melted, while no obvious differences are observed between

the 0.7 m/s case and the free convection case. This phenomenon is explained by the greater ventilation enhancing the heat transfer between PCM and air, thereby removing more heat from the PCM. The net heat gain (the difference between the heat gained and the heat removed) for the PCM is the smallest for the largest velocity. This is also evident in Figure 7.17, where the temperature in the PCM in the 1 m/s case is the lowest.

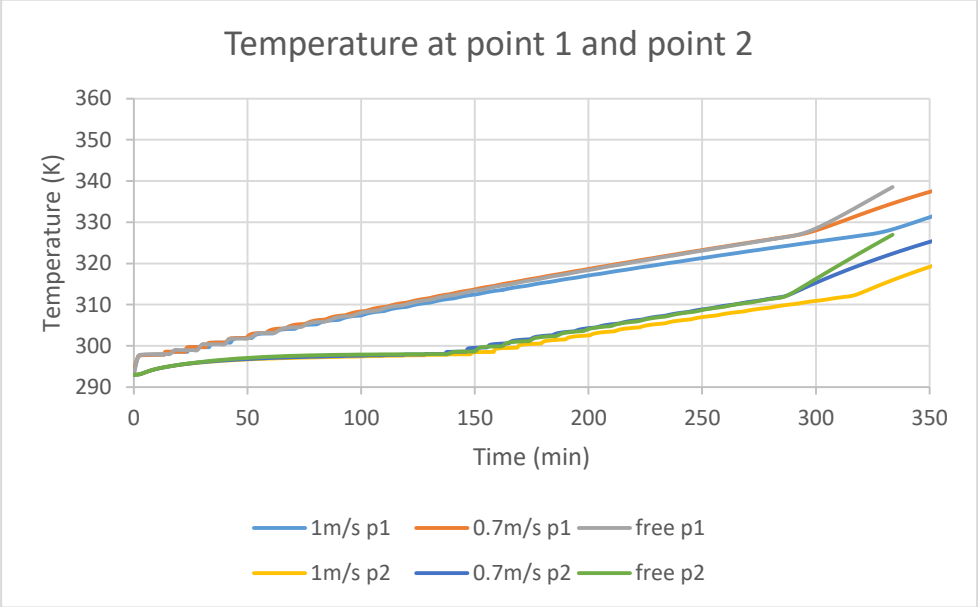


Figure 7.17 Temperature at Point 1 and Point 2 for two forced ventilation cases and free convection

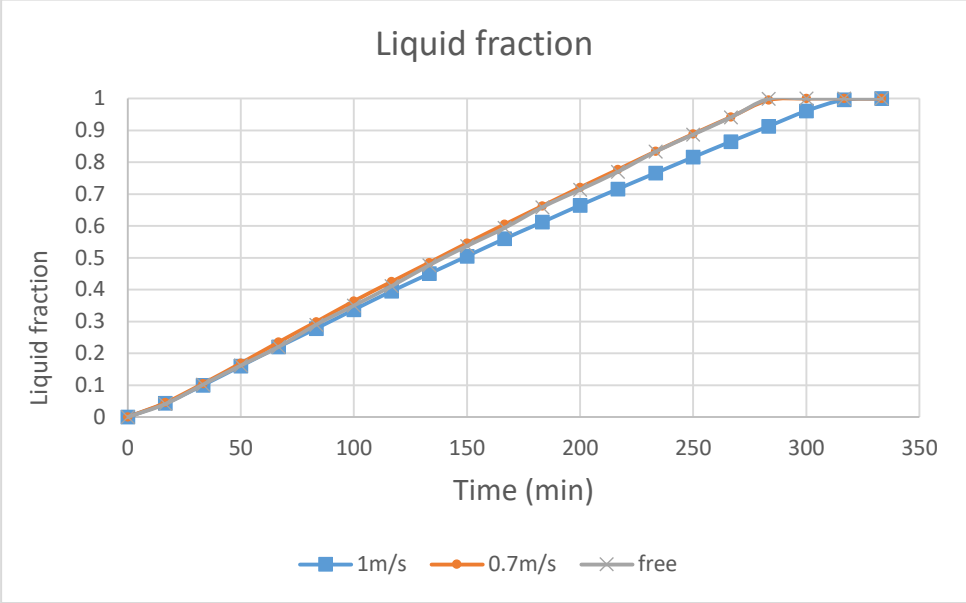


Figure 7.18 Liquid fraction for two forced ventilation cases and free convection

Figure 7.19 shows the thermal efficiency for two forced ventilation cases and free convection. The thermal efficiency is calculated from the temperature difference of the air inlet and outlet. The 1 m/s case has the largest mass flow rate, as well as thermal efficiency for the first 280 minutes, as expected, at about 10%. On the other hand, the 0.7 m/s case has 2% lower thermal efficiency during the same period, while the thermal efficiency is only 1.5% for the natural convection case. Thermal efficiency in the initial 280 minutes is affected by the PCM's ability to absorb heat from the PV and release to the air. After 280 minutes, once the PCM has fully melted, the thermal efficiency for all three cases increases rapidly because the PCM temperature rises rapidly once it has melted and heat transfer between the PCM and air is greatly increased. Thermal efficiency for the 0.7 m/s case is greater than that of the 1 m/s case after 270 minutes, because the PCM in the 0.7 m/s case melted earlier.

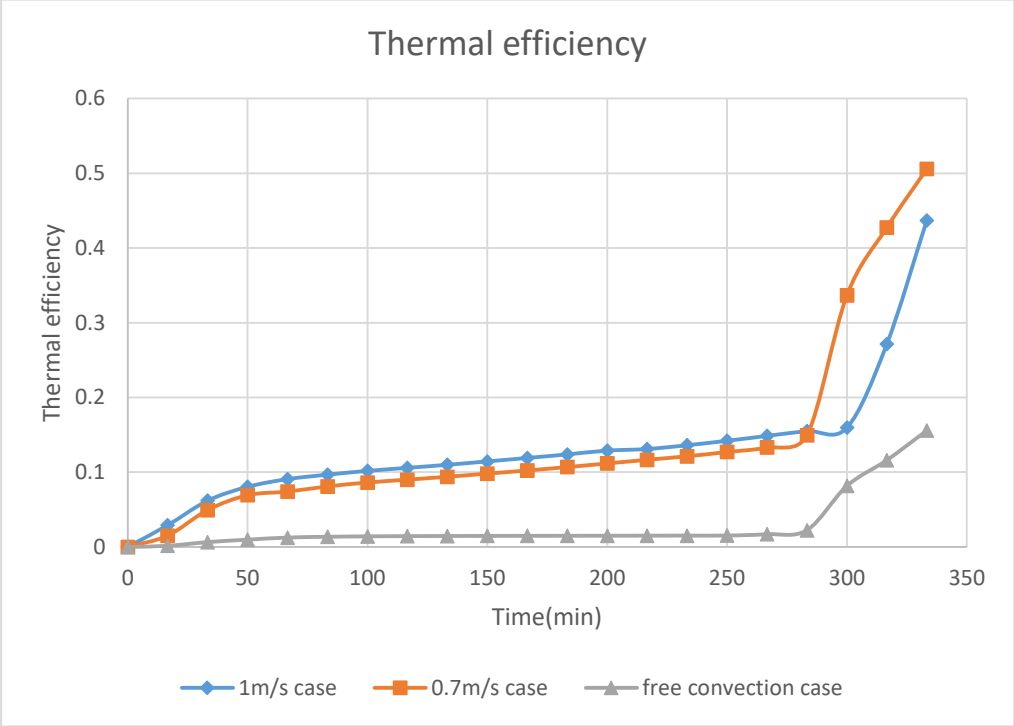


Figure 7.19 Thermal efficiency for two forced ventilation cases and free convection

The electrical performance is affected by the PV temperature. Figure 7.20 shows the mean PV temperature for two forced ventilation cases and free convection. The performance improvement is small even at larger velocity during the melting process, for about 20 minutes more for maintaining the PV below its operating temperature. However, significant improvement is observed after the PCM has fully melted, at about 300 minutes, which indicates that forced ventilation can significantly reduce the PV temperature after this phase change. These results can be helpful in some extreme weather conditions where PCM capacity is not efficient for thermal regulation. The findings suggest that forced ventilation has limited effect on the PV cooling, while greater air velocity increases the thermal performance.

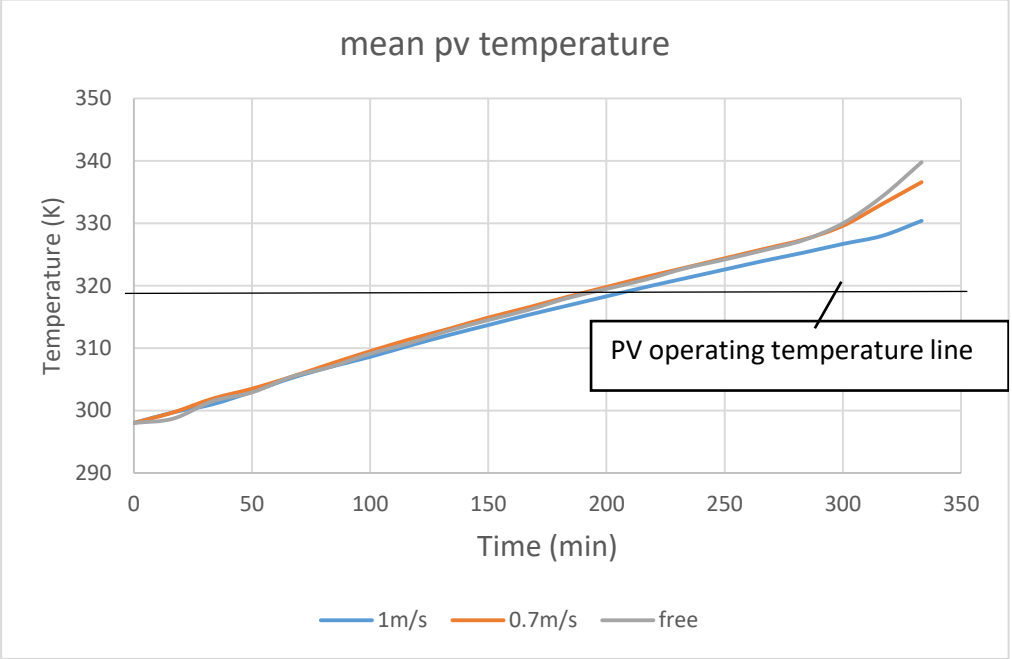


Figure 7.20 Mean PV temperature for two forced ventilation cases and free convection

7.6.2 Solidification

Solidification in all three cases was the same initially, with 300 K for PCM and 288 K for the ambient condition. Figure 7.21 illustrates the liquid fraction of two forced ventilation cases and natural convection in the solidification process. The results show that forced convection provides significant improvement in the energy release process. Both low and high velocity cases can reduce the solidification time by more than 4 hours and 5.5 hours, respectively. Therefore, forced ventilation can reduce about 40% of the total solidification time.

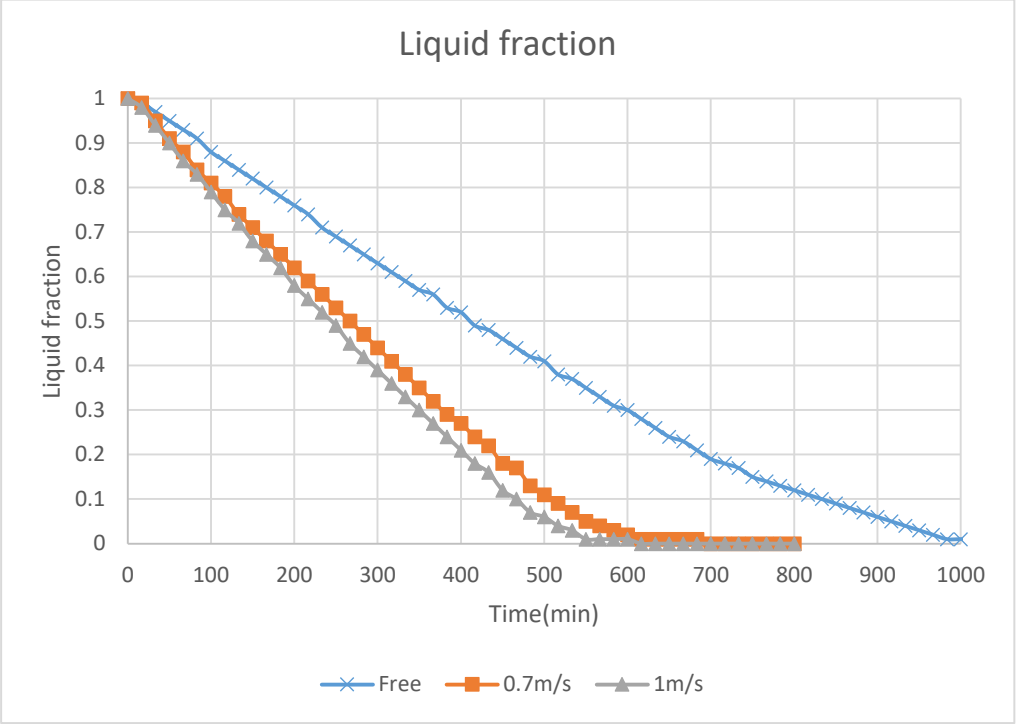


Figure 7.21 Liquid fraction for two forced ventilation cases and natural convection

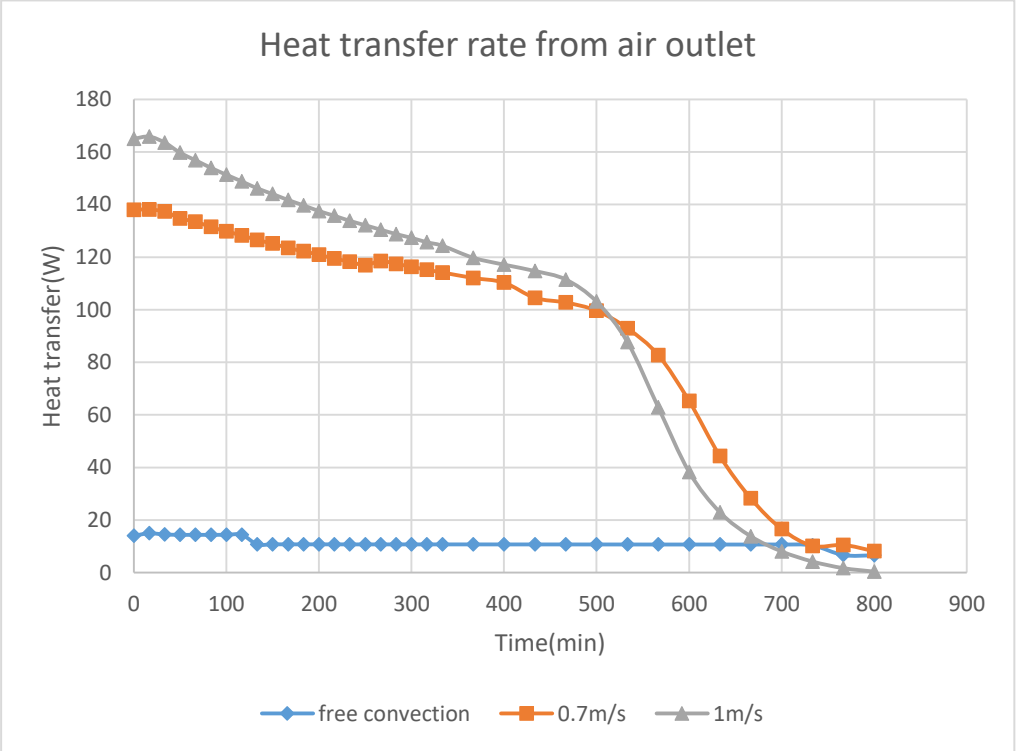


Figure 7.22 Heat transfer rate from the air outlet for two forced ventilation cases and natural convection in the solidification process

Figure 7.22 illustrates useful heat transfer rate for two forced ventilation cases and natural convection in the solidification process. Total heat stored in the PCM unit is same, but forced convection helps release the heat at a much faster rate compared to the free convection case. Free convection maintains the heat transfer rate into room from 14 W during entire solidification process. Forced convection reaches its maximum heat flux output at the start and its performance declines for 550 minutes, at which point a steep decrease is observed. At 800 minutes, forced convection finishes its cycle, while free convection needs more time for solidification.

In summary, the results of forced convection show that limited temperature regulating ability is observed in the melting process, while a significant improvement was achieved in the solidification process. Forced ventilation achieves a better heat transfer rate for both melting and solidification. High velocity gives a better performance for both thermal and electrical efficiency although it consumes more energy for the fan. In cold conditions, when the temperatures are not high, forced convection is not necessary. On the other hand, during hot summer months, the PV plate temperature may become too hot and will affect the system performance greatly; thus, forced convection could be used to reduce this effect.

7.7 Effect of fins

The fins applied in this research were internal fins, the goal of which was to improve thermal conductivity of the PCM during the energy storage and release phases. Vertical fins of 2 mm thickness and 30 mm spacing were applied inside

the PCM. A pair of fins with a metal container for a rectangular small unit is shown in Figure 7.23. However, the model must be converted into a 3D model for simulating a case with vertical fins, which will lead to a super large mesh size, comprising of more than 35 elements for accuracy. In order to simplify the CFD model and reduce the computation time, a small unit is simulated and the two side fins are set to symmetry boundary condition. The simplified simulated 3D model with 1 million elements is shown in Figure 7.24. Vertical fins are placed on both sides of the PCM unit of 34 mm width (2 mm fin each plus 30 mm PCM width), and an air gap of the same size is placed behind the unit.

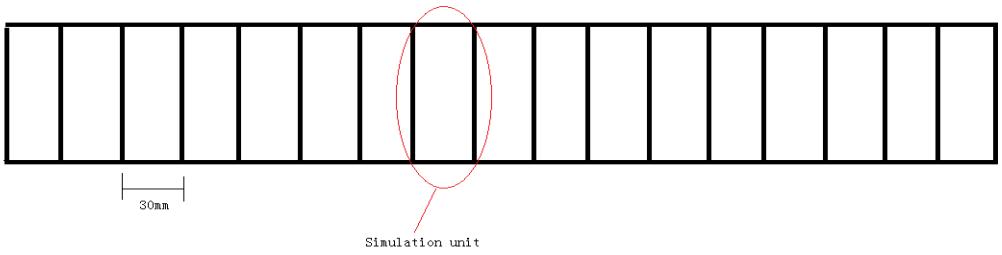


Figure 7.23 Top view of a PCM container with vertical fins

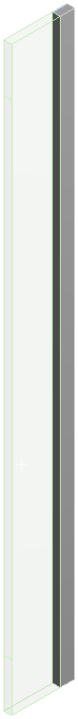


Figure 7.24 Simulated 3D model with vertical fins at both sides

Figure 7.25 shows the temperature at different locations within the PCM with and without fins. As can be seen, the PCM unit without fins fully melted at about 18,000 s, while the PCM with fins fully melted at about 28,000 s. Moreover, the case without fins can maintain the PV temperature below its operating temperature of 318 K for 12,000 s, compared to over 30,000 s for the case with fins. The PV/PCM system with fins can thus prevent the PV from overheating for over 8 hours due to the thermal regulating capacity of fins. The fins in this case not only improve the heat transfer inside the PCM, but also remove the heat from the PV by conduction directly to the air. This is also confirmed by the temperature of the back side of the PCM shown in Figure 7.25. The mean temperature of the air outlet is similar for the two cases. Starting at 1 K increase from the ambient temperature, once the PCM unit without fins fully melted, the heat transfer greatly increased, leading to a sharp increase in air temperature.

Figure 7.26 shows the liquid fraction for the PCM with and without vertical fins. The case with fins takes 30% more time to be fully melted. This is due to the thermal conduction enhancement by fins during the heating period. The net heat gain is smaller compared to the reference system.

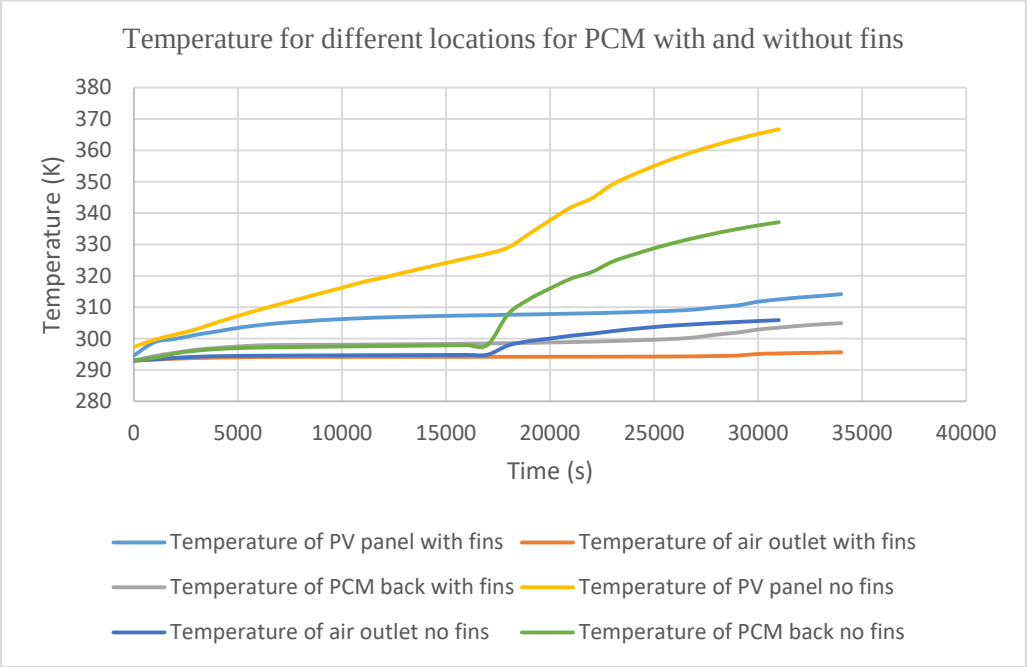


Figure 7.25 Temperature for PCM with and without fins

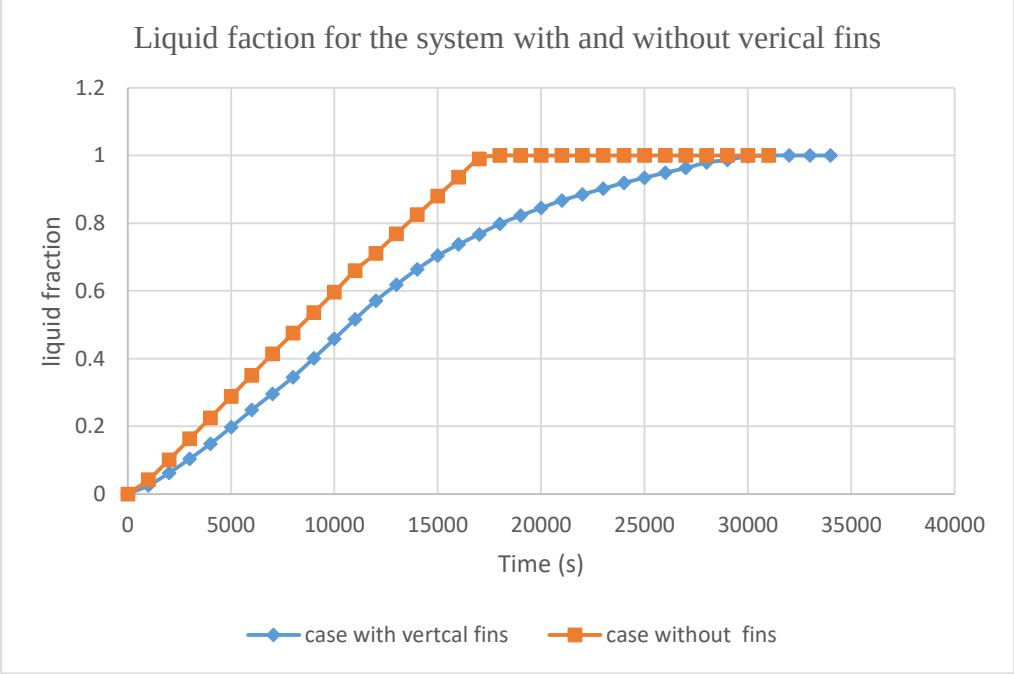


Figure 7.26 Liquid fraction for the system with and without vertical fins

Figure 7.27 shows the liquid fraction for three cases in the solidification process. The liquid fraction in the forced ventilation case decreases the fastest, followed by the case with fins, and finally the free convection case. These results indicate that the active system is characterised by the largest heat removal factor, while free convection case has the lowest. The passive heat removal by vertical fins is thus reasonable.

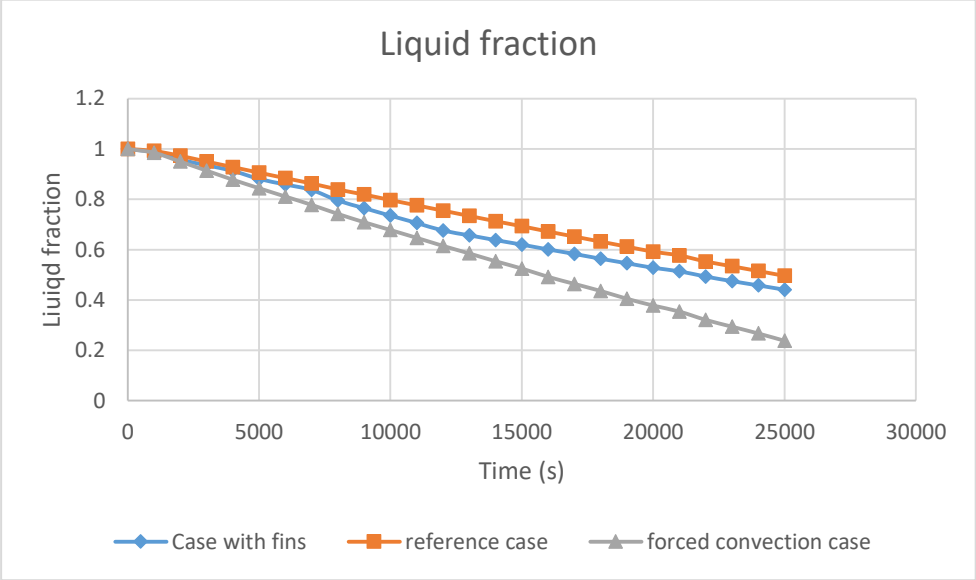


Figure 7.27 Liquid fraction for three cases

Figure 7.28 shows the heat transfer rate for three cases in the solidification process. The fin system maintains a 50 W heat output during the 25,000 s period due to larger thermal conductivity of the installed fins. The reference system has a 30 W output, which reduces gradually. The decline is due to the PCM melting from the side to the middle, causing a temperature difference, while the temperature difference is small in the system with fins. Output reduction is also observed in the forced ventilation case, which has a much higher heat output due to large mass flow rate compared to the other two systems. On the other hand, the heat output for the forced ventilation system decreases rapidly due to its significant heat removal capacity.

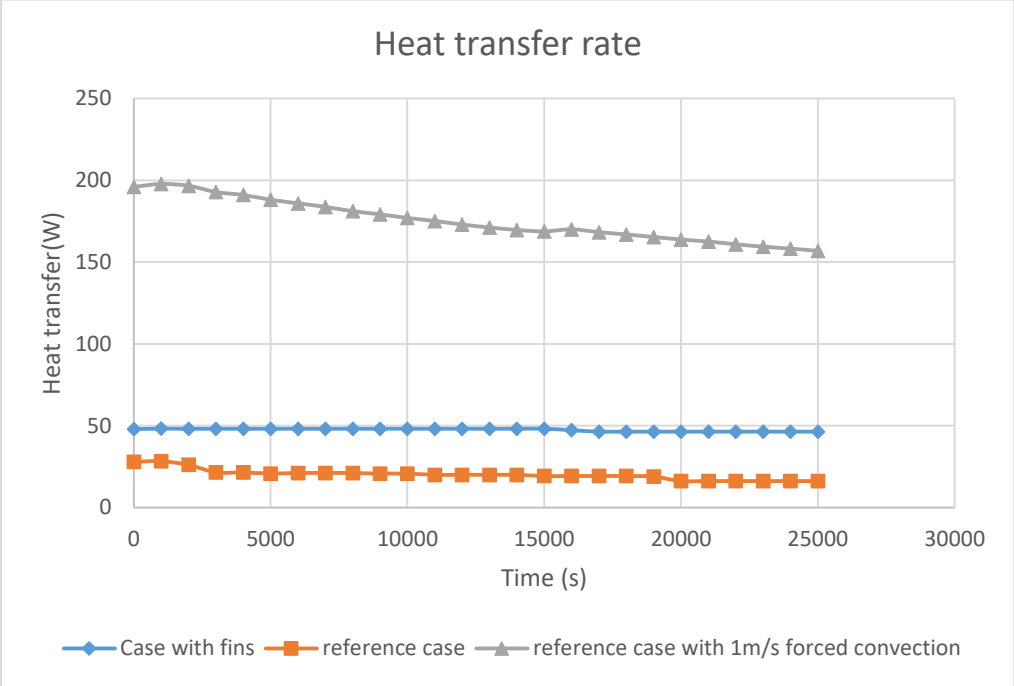


Figure 7.28 Heat transfer rate for three cases in the solidification process

7.8 Summary

This chapter presented a parametric study based on the validated model. Several parameters were compared and discussed. The result shows higher solar irradiance gives a higher mass flow rate and flow speed due to higher stack effect. PCM volume and melting temperature are very important in high insolation cases. Thicker PCM melted faster as expected, as 30mm PCM which only takes 16,000s for fully melted, where 40mm and 50mm PCM takes 22,000s and 28,000s. There does exist an optimum air duct size which has the best overall performance. Vertical sitting PVT system has better thermal performance during melting period, and has similar performance after fully melted. Forced ventilation system can improve the thermal performance for both melting process and solidification process. The system with fins significantly increases the thermal performance of the PV/PCM system. It takes

30% more time for fully melted and it have more ability for maintaining temperature. During solidification process, it have 50W heat output over 25000s while normal system have less than 30W output.

Chapter 8 Building simulation for a typical house equipped with the PVT/PCM system

8.1 Introduction

This chapter presents the simulation work of a PVT system using PCM as thermal storage in a domestic house. The main purpose is to investigate the more realistic influence of the PV/PCM system on the thermal and electrical performance. The construction system that was used in the simulation was modelled in real climatic conditions prevalent at two different locations.

Very few building energy simulation programs have the capability to simulate the PV/PCM simultaneously with building performance. In the work reported in this chapter, Energy Plus was utilised to simulate the model with conduction finite difference (CondFD) algorithm. Energy Plus is developed by the US Department of Energy's entire building energy analysis software program. Based on the thermal balance model, the program has been fully simulated for building envelope, window, HVAC system and lighting (Crawley et al., 2001).

This study includes a primary assessment of a residential building envelope technology containing PV/PCM air system. The aim of the simulation was to determine the effect of applying the designed PV/PCM system on indoor conditions and PV electrical efficiency.

8.2 Model configuration

A single zone house with the door facing south was built, as shown in Figure 8.1 and Figure 8.2. Two 2 m × 1.5 m windows are located at centre of east- and west-facing walls. The entire exterior wall is double wall with air gaps. The results for this base case were used as a reference for comparison with the other cases to study the performance of the newly designed system with PV.

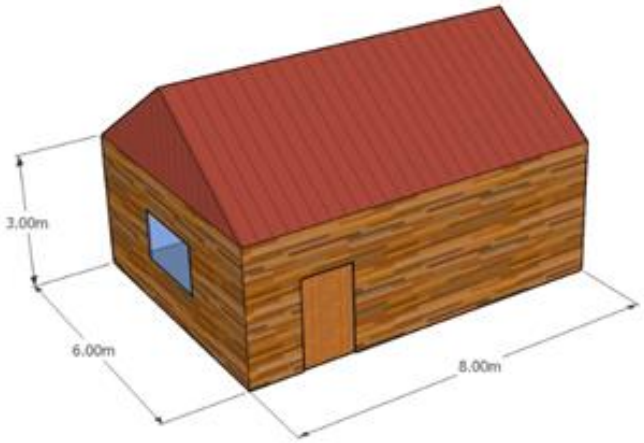


Figure 8.1 Base case, 3D view of the building model with a door facing south

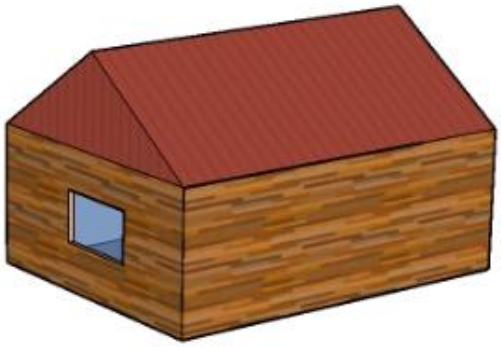


Figure 8.2 Base case, 3D view of the building model, the north wall view

Figure 8.3 shows the modified house, in which a part of the south wall is a PVT wall. The PV wall is 6 metres long and 3 metres high and contains 27 PV panels (3 layers) in total, with 2.7 kW output. The PV array is attached to the exterior wall and an air gap is maintained between the two layers, forming a double wall system. If phase change martial is applied, it can be either put directly behind the PV array, or inserted into the inside wall. The door and windows are in the same position as in the reference model.

Figure 8.4 shows the designed PVT wall with different openings. Two air inlets and two air outlets can be adjusted depending on the weather conditions of the location. On extremely hot days, when the cooling effect is important to the PV panel, cooler indoor air is supplied to PVT wall and the heated air is exhausted to the outside. On cold days, when the cooling effect to the PV panel is unnecessary, fresh outside air is supplied and heated air transferred to the house interior. The management of vent opening in PVT wall can be controlled by either simple on/off seasonal schedule or a complex zone thermostat system. More detailed information on the control system will be provided later in this chapter.

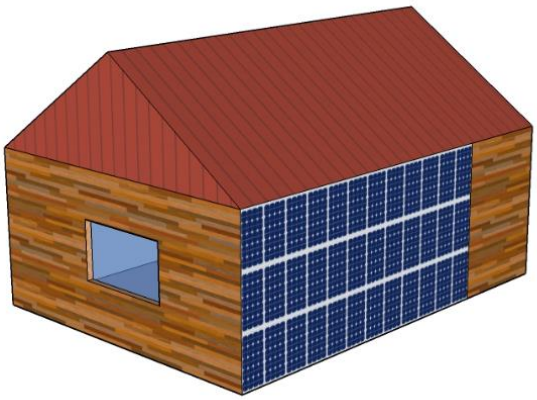


Figure 8.3 Model 1 PVT wall as a part of the south wall

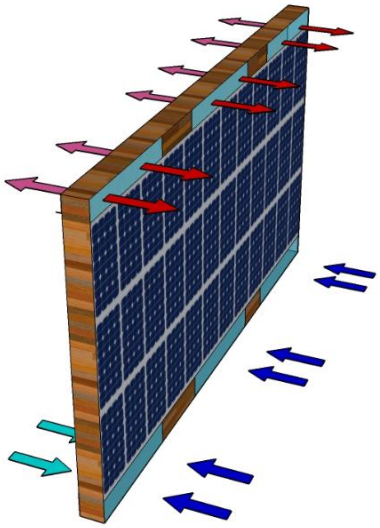


Figure 8.4 Designed PVT wall with different openings

Figure 8.5 presents the structure of the designed PVT wall. Its outside layer is a 15 mm thick PV panel, and the second layer is a PCM board that is directly attached to the PV for temperature control. The PCM used in this simulation is same as the one in experiment and CFD simulation.

The third layer is a 100 mm thick air duct for ventilation and heat removal purposes, based on the optimisation results presented in Chapter 6. The fourth layer is made of brick and concrete to support the structure, while 15 mm particle board is the final layer providing insulation.

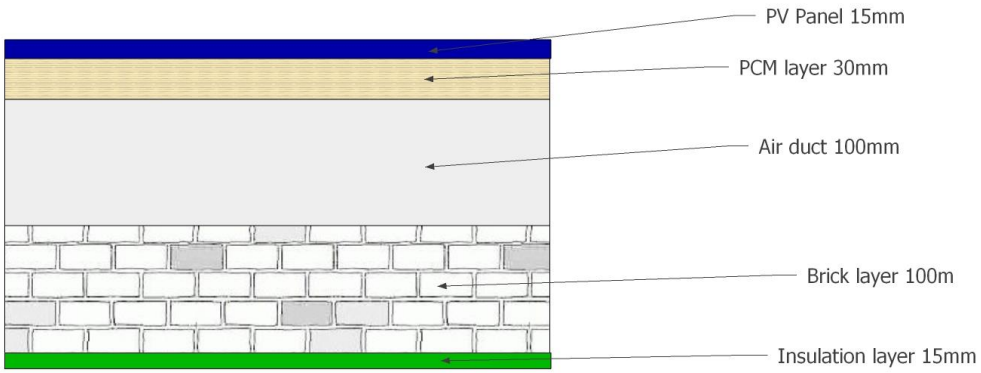


Figure 8.5 A special wall designed to simulate the PV façade



Figure 8.6 Model 2 PVT roof mounted as part of south roof

Figure 8.6 shows the modified house with PVT roof mounted as a part of the south facing roof pane. This model was compared with the PVT wall case.

8.3 Three cases and their descriptions

The house in Model 1 without PVT or PCM served as a reference case. All the weather condition imported into the program is based on data from Chartered Institution of Building Services Engineers (CIBSE, 2015).

Case 1a comprised of Model 1 with the PVT wall as a part of the south wall with the PCM layer behind, and a melting temperature of 25 ºC. The structure is displayed in Figure 8.5 and the whole PV wall is 6 metres long and 3 metres high and contains 27 PV panels (3 layers) in total, with 2.7 kW output in total. Case 1b comprised of Model 1 with the PVT wall as a part of the south wall, same as Case 1a but without the PCM layer. Instead, thermal mass material concrete with the same volume as the PCM was applied. Case 1c used the same configuration as that in Case 1a, with the addition of the forced air ventilation system to the PVT wall. The forced ventilation system utilised a simple central air system terminal unit with a single duct, constant volume and no controls other than an on/off schedule. Fan speeds were set to provide two constant ventilation rates, 0.1 m^3/s and 0.3 m^3/s, for comparison. Fan schedule 1 is simple seasonal based schedule. The fan is turned on from 9:00 to 19:00 from September 30 to March 31, and is turned off at all other times. Air inlet and outlet are on the inside wall of the PVT. Fan schedule 2 is a complex temperature controlled schedule used in HVAC systems.

8.4 Building energy performance simulation results

Three different cases were compared and are discussed below. January and July were selected to represent the winter and summer days, respectively. Two main parameters were investigated, mean room air temperature and PV electricity output.

8.4.1 Comparison of Case 1a and 1b for two different locations without an active thermal control system

Case 1a and Case 1b, location: Nottingham, United Kingdom

Figure 8.7 shows the hourly room temperature during three days in January for Nottingham weather conditions. Both PCM and thermal mass material have the ability to reduce temperature fluctuations. The results also indicate that, for external temperatures in the 0 ºC to 10 ºC range, both materials have similar performance, and no major improvement from PCM was observed. Higher room temperature is desirable in winter and the PCM reduced the peak room temperature at daytime, decreasing it at a later time. The total heat gain is the same for all cases because the absorbing area is the same. The shift in the temperature may be useful for domestic houses, which are typically occupied at a later time in the day.

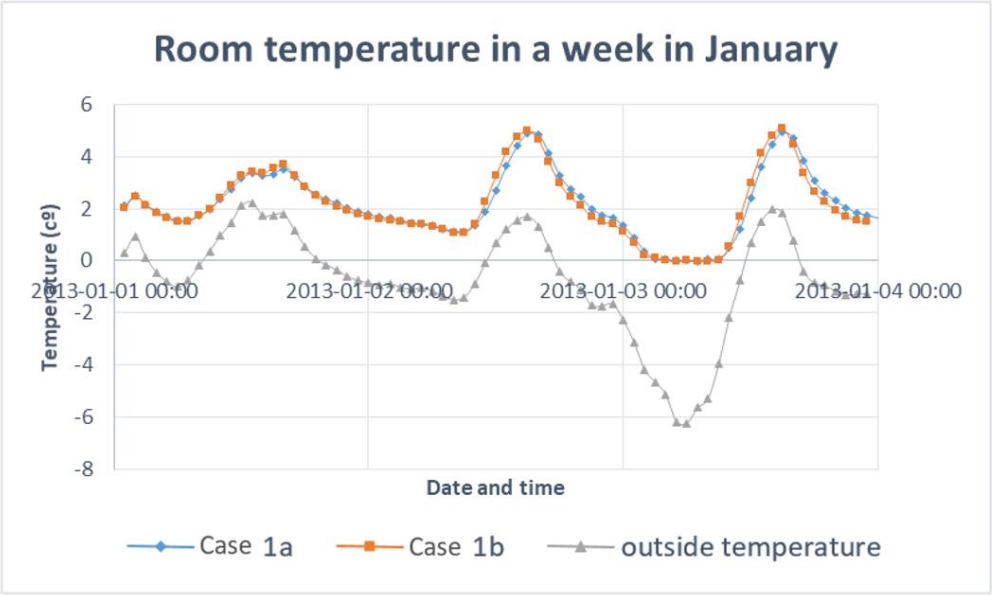


Figure 8.7 Room temperature during a week in January for location Nottingham, UK

Figure 8.9 shows the hourly room temperature in a week in July. The results show that the PCM can reduce the peak temperature by about 2 ºC, which increases at night by about 1 ºC. In summer time, PCM exhibits better performance than the normal concrete in shifting the room temperature. However, the improvement is still limited in this case, as the summer in UK is short and temperature is not high compared to the PV nominal operating temperature.

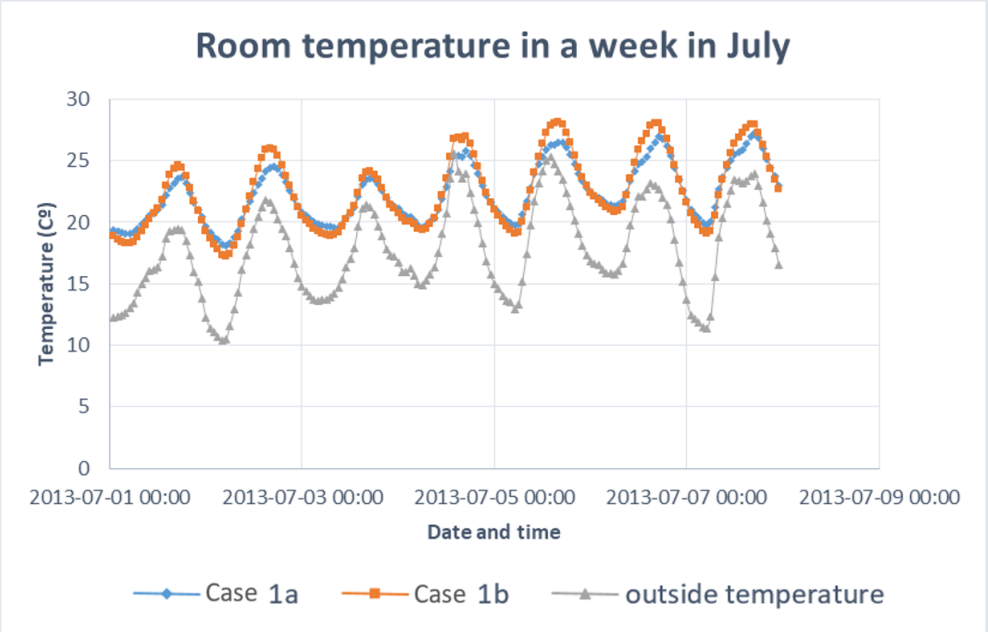


Figure 8.8 Room temperature during a week in July

Figure 8.10 shows hourly PV cell temperature in January. Even in winter, the PV temperature could exceed its operating temperature, as Nottingham is in a high latitude area, with the PV angle of 90 degrees in winter, and solar incident angle is large at the peak time. The improvement in the electrical efficiency is thus limited due to low ambient temperature.

One drawback of placing the PVT wall on the south face is that it may increase the heat loss by replacing the original insulation wall with the PVT material. The possible solution is to close the air opening between the PVT wall cavity and the inside room space at night time in winter.

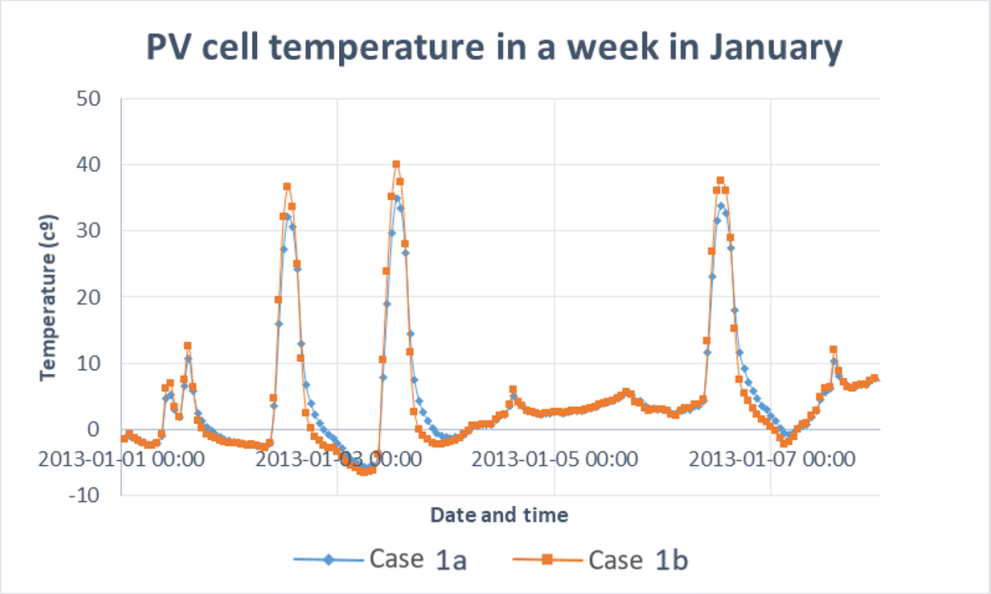


Figure 8.9 PV cell temperature in a week in January for Nottingham, UK

Figure 8.11 shows hourly PV cell temperature in July. The improvement due to the PCM is significant, as PV cell temperature exceeds its operating temperature almost every day. Thus, 2.1% more overall electric power could be produced from the PV due to PCM thermal regulation.

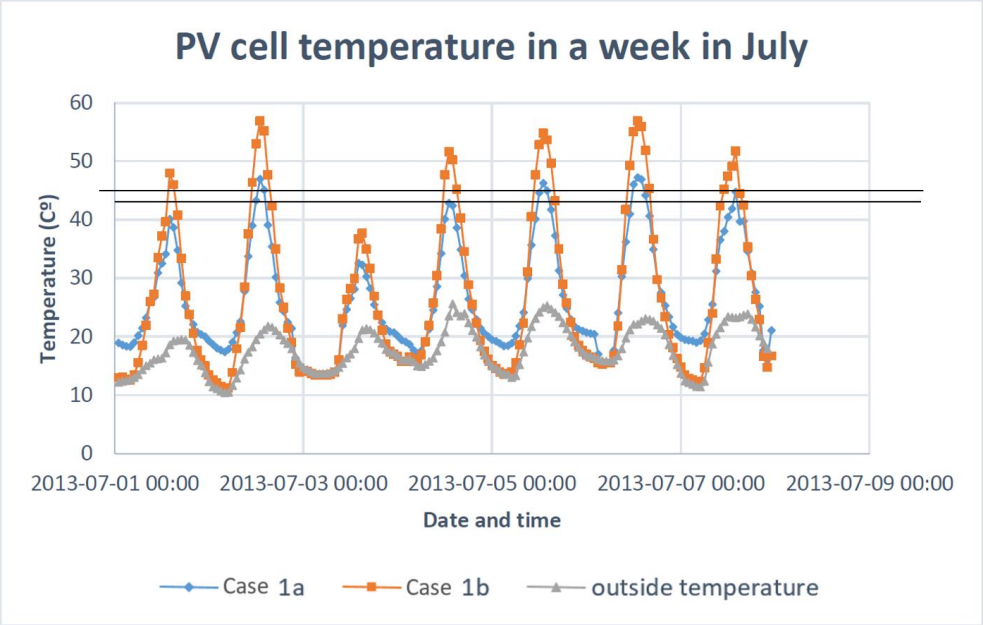


Figure 8.10 PV cell temperature in a week in January

Case 1a and Case 1b, location: Shanghai, China

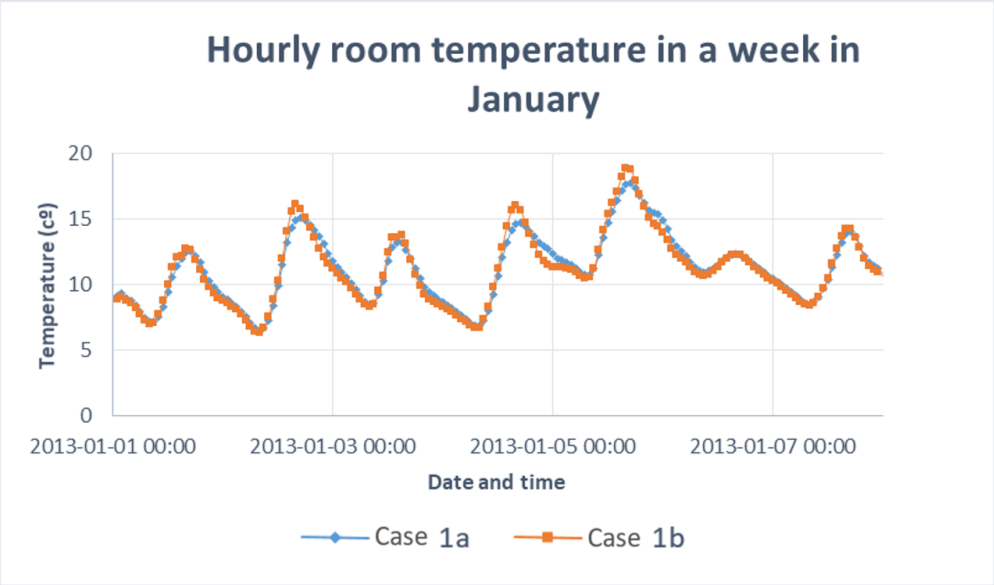


Figure 8.11 Hourly room temperature in a week in January for Shanghai, China, weather conditions

Figure 8.12 shows the hourly room temperature in a week in January for Shanghai, China, weather conditions. Case 1b without the PCM has the highest

room temperature during the peak period. However, Case 1a with the PCM layer experiences a delay in the peak time and achieves better performance at night due to the large heat capacity of the PCM. This is desirable for domestic use because residential buildings are usually occupied at night for most of the time and the temperature shift from the PCM can reduce the heating load.

Figure 8.13 shows the hourly room temperature in a week in July. No major differences were observed because outside air temperature exceeded the PCM melting temperature. In this situation, PCMs with higher melting temperature should be applied.

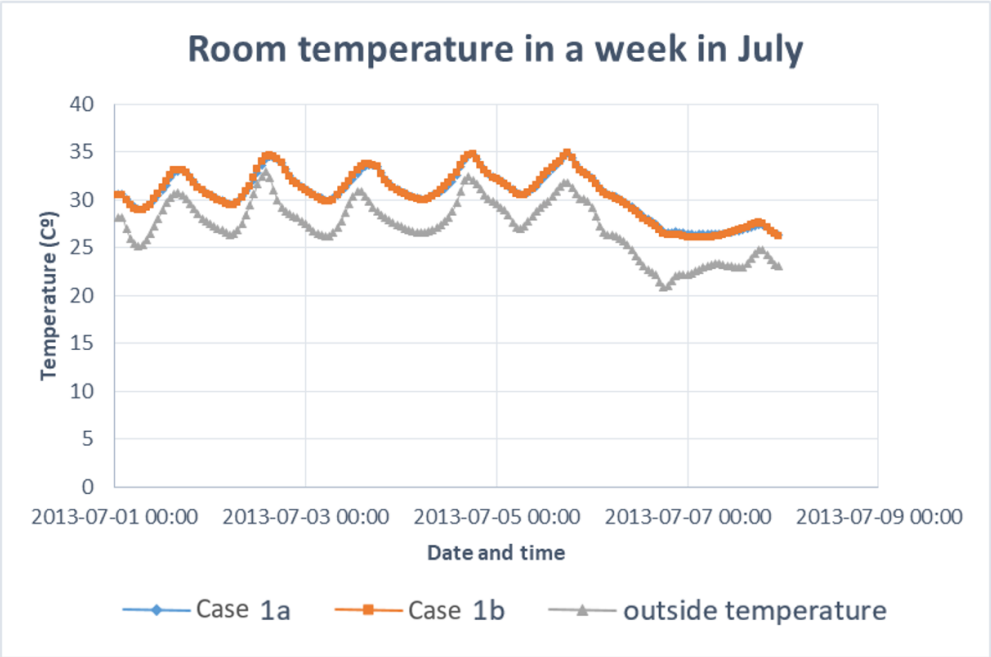


Figure 8.12 Hourly room temperature in a week in July

Figure 8.14 shows hourly PV cell temperature in January, indicating that Case 1a with PCM significantly reduces the overheating of the solar cell during the peak period in the day.

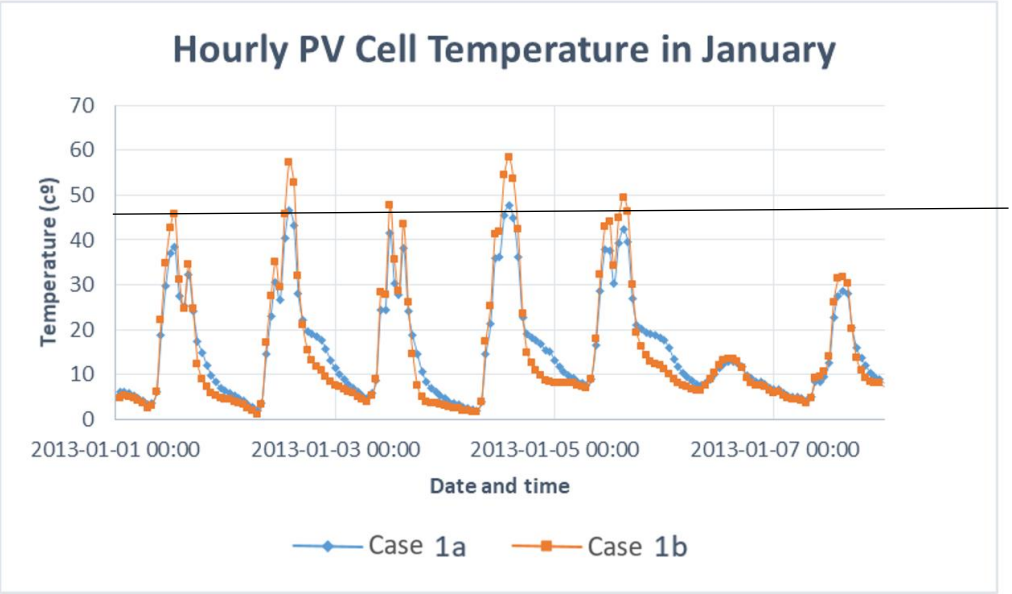


Figure 8.13 Hourly PV cell temperature in a week in January for Shanghai weather conditions

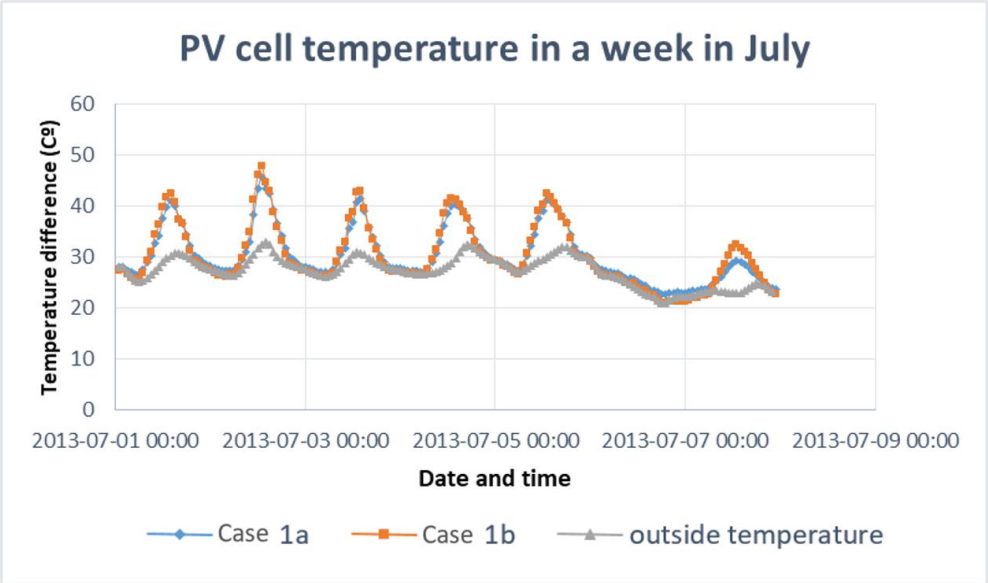


Figure 8.14 Hourly PV cell temperature in a week in July for Shanghai

Figure 8.15 shows hourly PV cell temperature in July. The system can produce 2.5% more overall electric power in July. However, the improvement due to the PCM is still small on hot days due to the high ambient temperature during the

entire day. High ambient temperature prevents the PCM from fully solidifying, resulting in no cooling effect in the PV. The recommendation for this situation could be either using PCM with a higher melting point, or employing an active method for solidifying the PCM, such as inducing cool air from a ground source and integrating it with the HVAC system for cooling.

Figure 8.16 shows temperatures of the PV cell with two different PCMs, with the melting temperature of 25 ºC and 30 ºC, respectively, as measured over a seven-day period in July in Shanghai. Better performance was observed for the PCM with the 30 ºC melting temperature, as it reduces the peak cell temperature compared to the 25 ºC case by about 3 ºC. In addition, 7% more electric power could be produced using the PCM with 30 ºC melting temperature, while 4.5% was measured for the PCM with 25 ºC melting temperature.

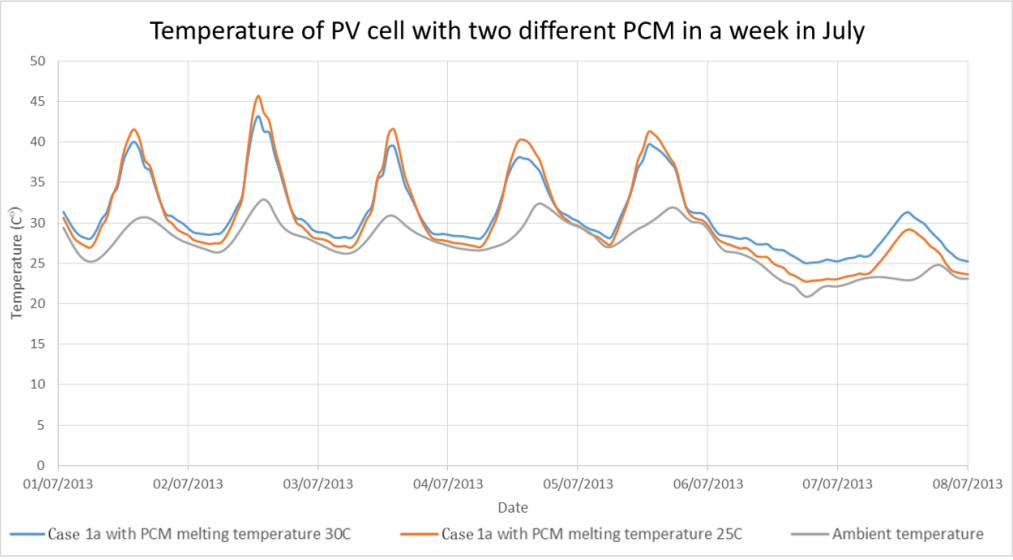


Figure 8.15 Temperature of the PV cell with two different PCMs in seven days in July

Figure 8.17 shows room temperature difference in two days in June as a result of applying two kinds of PCM. The performance varies over the year, but the room with the PCM with the melting temperature of 30 ºC is hotter than that in the 25 ºC melting temperature case. This is desirable in winter, but not in summer. The 30 ºC melting temperature PCM case increases the temperature at night time, as it takes longer time to melt. This may increase the cooling load when the nights are hot, unless the heated air is exhausted back to the outside.

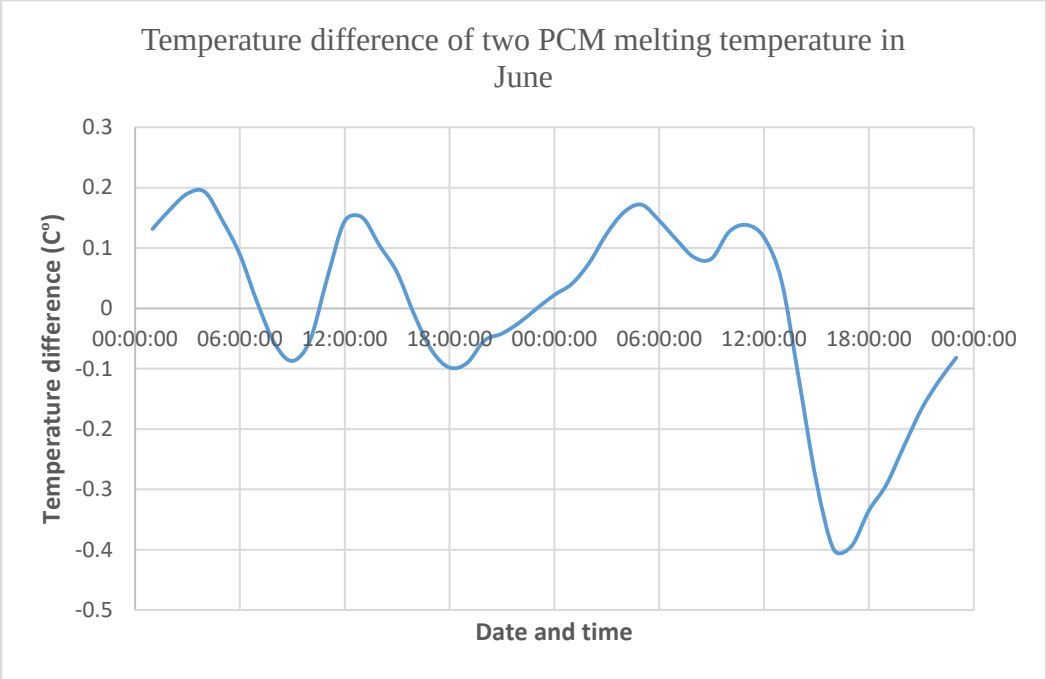


Figure 8.16 Room temperature difference with two different PCMs on two days in June

In winter, when the temperature is far below the melting temperature of either PCM, the thermal performance is the same. Yearly electrical output for the two PCM cases is 1551 kWh and 1502 kWh, resulting in about 3% increase when the 30 ºC melting temperature PCM is applied.

In summary, PCM has a certain effect on cooling the PV throughout the year, but the performance is more significant in hot climate locations. The heated air from the PVT system can reduce the heating loads in winter for both locations examined in this chapter. However, the heated air in summer seems useful in domestic situations but has to be exhausted back to the outside. In winter, the effect of PV cooling by PCM is small in UK due to low ambient temperature. The stored heat in PCM is more preferred in Shanghai for both summer and winter as it can utilize both the heat and cooling effect efficiently.

8.4.2 Case 1a and Case 1c, Model 1 for two different locations, with forced ventilation

Case 1a and Case 1c were utilised to investigate the performance difference when a simple forced ventilation system was employed.

Figure 8.18 and Figure 8.19 show yearly room temperature differences when applying a fan system with 0.1 m^3/s throughput under Fan Schedule 1 for two locations, which was compared with Case 1a in natural ventilation. An overall 0.7 ºC temperature increase as observed during the fan operating time. Fan power consumption is about 85 W. The thermal performance improvement due to fan application is similar for two different locations when the same PVT system is used, confirming that the fan system has a great influence on thermal performance.

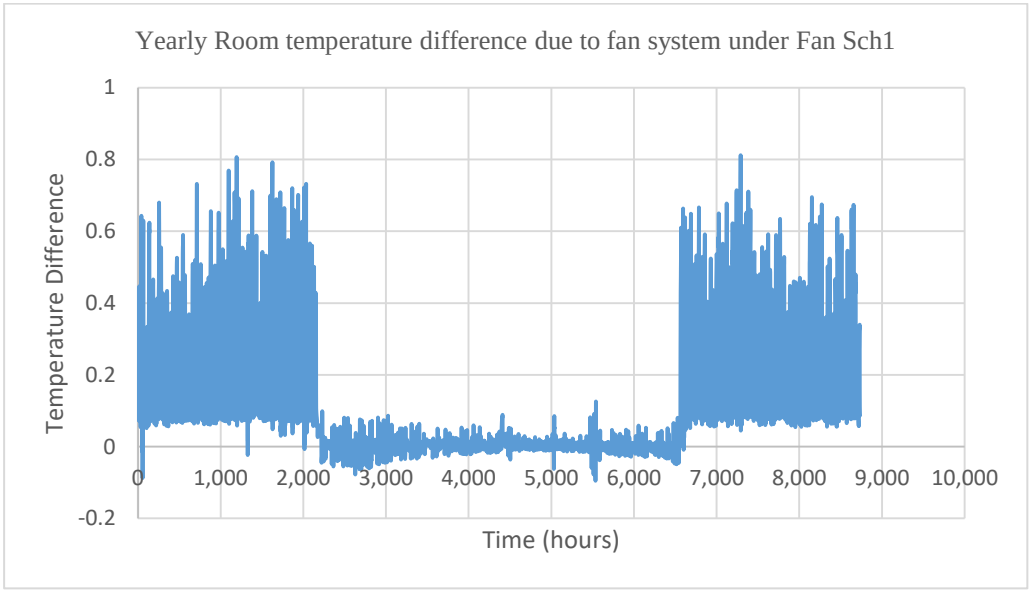


Figure 8.17 Yearly room temperature difference due to fan system in Fan Sch1 in Nottingham

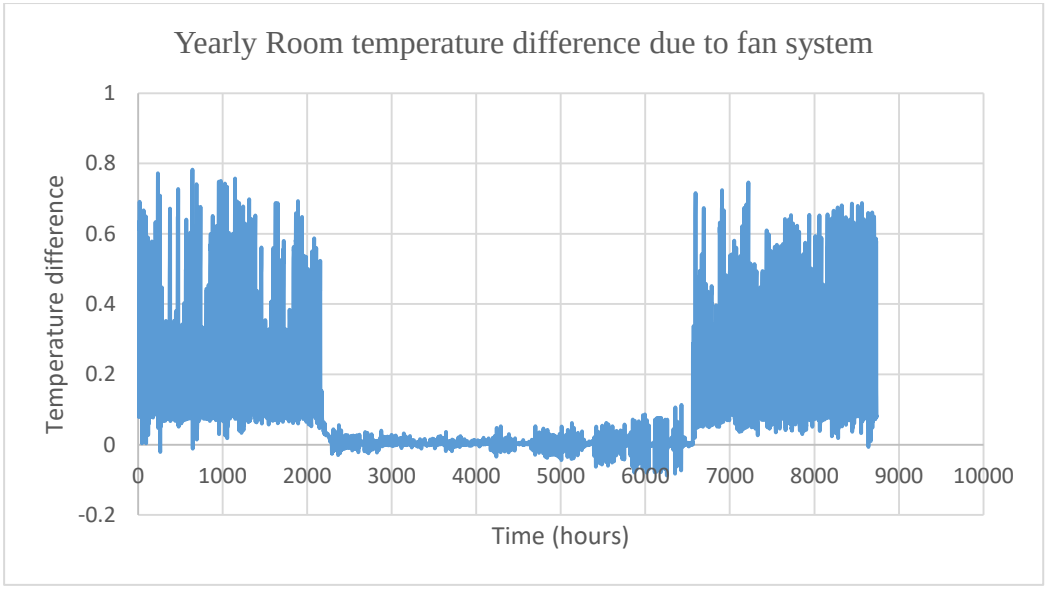


Figure 8.18 Yearly room temperature difference due to fan system in Fan Sch1 in Shanghai

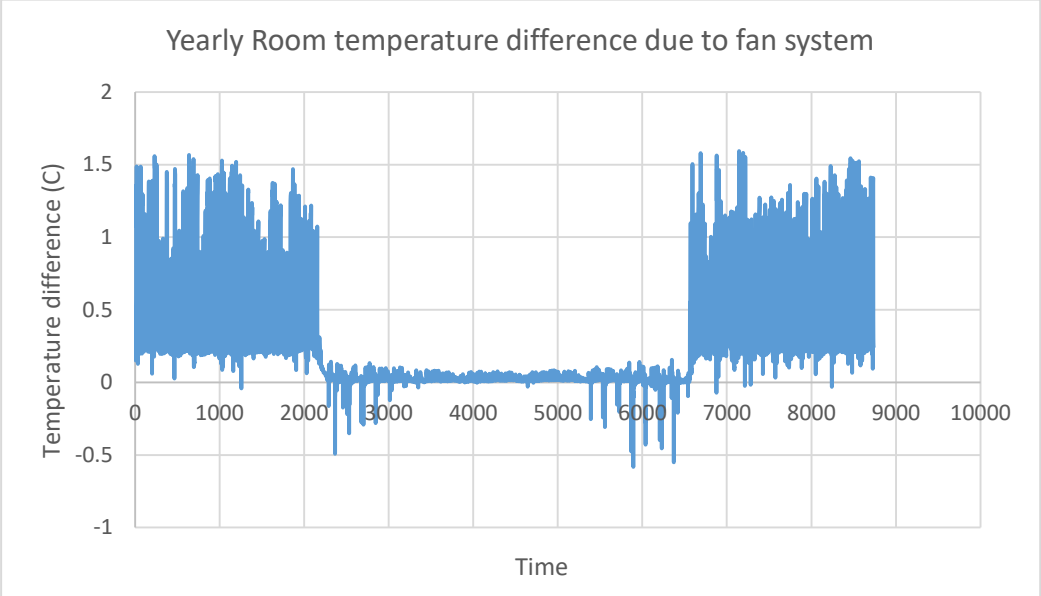


Figure 8.19 Yearly Room temperature difference due to fan system in Fan Sch1 in Shanghai at 0.3 m^3/s flow rate

Figure 8.20 shows the yearly room temperature difference due to fan system in Fan Sch1 in Shanghai at 0.3 m^3/s flow rate. As a greater flow rate would result in higher temperature difference, higher heat output is achieved. The system increases the temperature by 0.5 ºC compared to the 0.1 m^3/s flow rate.

However, the larger flow rate also requires greater fan power, and the extra heat output should exceed the fan input to make it viable. The fan power for the 0.3 m^3/s flow rate in this case is 260 W, compared to 85 W for the 0.1 m^3/s case; thus, an increase of 175 W consumption is required. The heat output to increase 0.5 ºC is about 150 W, which is less than the extra consumption of fan power at 175 W. Therefore, it is not economical to use 0.3 m^3/s flow rate in this condition. The optimum flow rate should be further investigated based on the weather conditions.

8.5 Economic considerations of the designed PVT with the PCM system

At low solar radiation climatic conditions, high PV temperature is not frequent and natural convection cooling of the front and adjacent surfaces may be sufficient. For a high solar radiation weather conditions, the use of PCM provides thermal management more effectively to maintain the PV at a lower temperature, but requires greater capital. Feasibility of the latter expenditure depends on the value of the additional electrical output. Under a very high solar radiation, it may also be possible to extract the heat stored in the PCM to cover part of the heat requirement. However, further additional costs that are incurred need to offset the PCM unit cost and the value of the extracted heat from electricity production by the larger cooler. At very high solar radiation climatic conditions, the extracted heat can be utilised for night-time cooling, and in some instances dehumidification.

Price in the UK for gas and electricity is about **4.7p** and **15p** per kWh, respectively. The number is calculated from the UK Annual Domestic Energy Bills 2016. (Department for Business, Energy & Industrial Strategy, 2016).

In the UK, the new Government's Feed-in Tariffs scheme was introduced on 8 February 2016, which replaced UK government grants as the main financial incentive to encourage uptake of renewable electricity-generating technologies, including solar PV. The extra electricity generated from the PV/PCM system could be sold to a supplier and thus reduce the capital cost of the system. Assuming the property has an Energy Performance Certificate (EPC) rating of level D so the generation tariff for electricity self-usage is about 4.39 p/kWh

and the export tariff to the national grid is about 4.91 p/kWh (The UK Government's Department for Energy and Climate Change, 2016).

The economy of the PV / PCM system is highly dependent on the amount of photovoltaic power generated at a location; high solar radiation increases the energy generation means higher PV temperature and heat regulation needs.

The initial cost of the system, including the BIPVT / PCM system, charge controller, battery pack, frequency converter, utility interconnection costs and the cost of building permits, maintenance and repair costs associated with the cost of the cost, should be defined as the operational phase.

8.5.1 Cost of the BIPVT/PCM wall

Cost for PVT panel

- Biard 100 W 12 V Black Monocrystalline Solar PV Panel at £80 Each
- 26 Solar PV Panel with 2.6 kW power output costs £2080
- Installation fee about £2400, including air duct behind the PV, charge controller, battery bank, inverter, and utility interconnection costs

In sum, the initial cost of a PV panel is around £4480

Cost for PCM

- PlusICE filled with S25 solution from PCM Products Ltd cost £2.5/ kg, £4/Litre
- Total PCM volume is 3 m × 6 m × 0.03 m = 540 L

- Package price (container of PCM) equal 20% of total prices
- Thus, total PCM price with package is 540 L × 4 £/L × 1.2 = £2592

Cost for PV/PCM

- Cost for PV equal to £2080
- Cost for PCM layer equal to £2160
- Estimated cost for PV/PCM system installation equal to £2400
- Thus, total PV/PCM price =£6640

Maintenance fee cost is estimated at 1% of the initial cost for PV and 0.5% for the PCM.

8.5.2 Three cases for economic analysis

Energy consumption, including heating in winter and all electrical devices in the house, is discussed below.

Base case is a normal house, all electricity supply is from National Grid and heating is supplied by gas heater.

Case I Normal house with a PVT system on the roof with an optimum angle (45º) to maximise electricity output. This arrangement requires the owner to pay for all heating bills and a part of the electrically bill, but the extra electricity can be sold through the UK Feed-in Tariffs scheme.

Case II Normal house with a PCM in the south facing wall construction only. This arrangement requires the owner to pay for the reduced heating bill and all electrically bills.

Case III Normal house with the PVT/PCM wall with a fan system, whereby the owner pays for a part of the heating bill and a part of electrically bill, and sells the extra electricity through the UK Feed-in Tariffs scheme.

Heating load calculation is based on the inside thermal comfort schedule below: heating up to 21 ºC during the occupied hours, 18 ºC otherwise. Cooling to 24 ºC while occupied, 30 ºC otherwise. Fans and coils are scheduled to be unavailable during the unoccupied hours.

Electrical consumption for the houses of all cases is assumed to be 2000 kWh per year and heating is by gas. The houses model used is same as the model in Figure 8.2. The heating and cooling load of the house is shown in Figure 8.21. The total heating load is about 4100 kWh and cooling is 300 kWh.

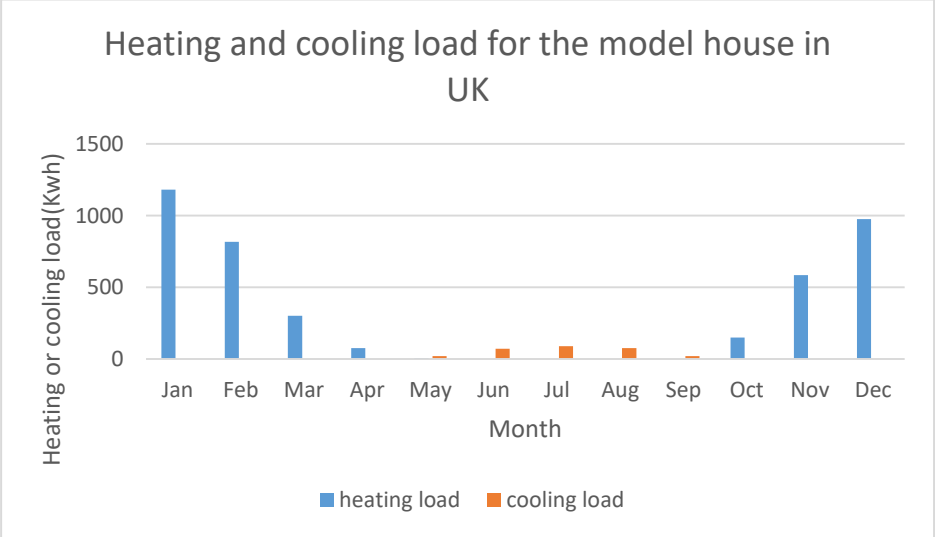


Figure 8.20 Heating and cooling load for the model houses in the UK

8.5.3 Economic analysis results

The competitive specific price for the PVT system has been derived from the balance of investment costs and operation costs for a 20-year lifetime period for conventional PV system and the PCM system.

The specific system price is determined when the total lifetime costs of hybrid PVT system and conventional PV system are equal. Interest rate in the UK in 2016 is at 0.5% (data from World Bank website) and the energy price increase is estimated at 2% per annum (BEIS, 2016).

Table 11 shows the yearly energy savings for three cases and Table 12 shows the calculation of annual costs and profits in these three cases. Case I with optimum PVT system has a payback period of 11 years if use electrical heating and 12 year if using gas heating. Case II with PCM thermal regulation has a payback period of 13 years, if the property owner uses electricity heating, and over 20 years if uses gas heating. However, the price for PCM will be lower for commercial usage and the payback period will be reduced. Case III with PVT/PCM system has a payback period of 14 years, if the property owner uses gas heating, and 11 years if electricity heating is used. The detailed calculation tables for the payback periods are presented in Appendix. These results indicate that, by applying PCM to the PV system, it has same payback period under prevailing UK weather conditions, as the benefit from thermal regulation by PCM. Furthermore, if the PV/PCM system is applied in low latitude areas, where the efficiency of the PV is greatly affected by temperature, it will have a shorter payback period and reduce the cooling loads.

Table 100 Yearly heating savings and electricity output for all cases

Case	System installed	Yearly heating and cooling savings (kWh)	Yearly electricity production (kWh)
Case I	PVT	250	1890
Case II	PCM	1273	-
Case III	PVT/PCM	1097	2020

Table 11 Initial costs and payback for all cases

Case	Initial cost at year (£)	Payback period (year)
Case I	4580	11 if use electricity heating, 12 if use gas heating
Case II	2592	13 if use electricity heating，not economic efficient if use gas heating
Case III	6740	11 if use electricity heating, 14 if use gas heating

8.6 Summary

In this chapter, the simulation of the PVT system using PCM as thermal storage in a domestic house with Energy Plus 8.3 was presented. The main purpose was to investigate the real influence of a PV/PCM system on the thermal and electrical performance. The construction system that was used in the simulation was modelled in real climatic conditions at two different locations.

Results show that the designed PV/PCM can reduce the peak temperature by about 2 ºC, and increase night time room temperature by about 1 ºC for a typical

small house in Nottingham, UK. It can also produce 2.1% more overall electric power. However, the improvement is still limited in this case, as summer in the UK is short and temperature is not high compared to the PV nominal operating temperature.

The results for the climatic conditions in Shanghai are more favourable, as the system can produce 2.5% electricity in winter and 4.5% in summer. The performance can be further improved by using PCM with 30 ºC melting temperature, which can produce 7% more electricity compared to a system without the PCM. The thermal performance is also significantly improved by PCM, as it shifts the peak temperature to a later time period when the house is occupied, thus reducing the heating load. The performance varies in summer time for PCMs with different melting temperature.

The BIPVT system, which circulates the indoor air and runs the heat source in the room, is advantageous in terms of heating and cooling of the building and overall energy, since the effect of heating energy reduction is greater than that of power generation. Greater airflow rate will result in higher thermal efficiency, but also higher fan consumption. Therefore, an optimised fan speed should be determined to maximise the output.

The PVT system and PV/PCM system has same payback time of 11 years c in the UK conditions if heating is provided with electricity. If the property use gas heating, PVT system has better economic performance. The result indicate that applying PCM to thermal regulate the PV in UK, may not reduce the total payback period as high initial cost of PCM is covered by its benefit from

reducing the heating cooling demands. Suggestion is to further optimize the system and lowering the total cost.

If the PV/PCM system is applied in low latitude areas, where the efficiency of the PV is greatly affected by temperature, it will have a shorter payback period and reduce the cooling loads significantly.

Chapter 9 Conclusion and Further work

9.1 Summary of the thesis

The aim of the present study was to develop and optimise building integrated PV thermal (BIPVT) air system combined with a thermal storage system. The system utilises integrated PV design and a phase change material (PCM) as latent heat storage. The main objective was to investigate the thermal and electrical performance of the newly designed PVT air system with thermal storage.

This thesis started with discussions of the issue of global warming due to increased CO_2 emissions. Applying renewable energy is widely agreed to be the most effective and promising way to solve the problem, whereby improvements in the solar energy and photovoltaic technology have been particularly pronounced in the recent decades.

In Chapter 2, the solar energy applications in buildings were briefly reviewed. The review started with solar energy convection technologies, including solar thermal and solar photovoltaic. Then a combined technology named photovoltaic/thermal (PVT) was introduced and discussed. Research work on different types of PVT using water and air as thermal energy medium was further reviewed and discussed. Then the review moved to the building integrated photovoltaic thermal system (BIPVT). Common thermal energy storage system was discussed in this chapter. Finally PVT system with a PCM as thermal storage and techniques for improving thermal performance were reviewed.

Chapter 3 presented all the methodologies that were used in this research study. The research process was divided into four stages and methodologies for each stage were presented. An analytical model for the PVT system was presented for primary investigation and designing the experiments in the first stage. Methodology for all the experiments in Stage 2 were presented and discussed. Then a CFD model for Stage 3 was built and described. The model was subsequently used for system optimisation. Finally, the methodology for entire building performance simulation with PVT/PCM system was presented.

Chapter 4 was designated for the discussion of the analytical investigation results pertaining to the PVT, which were also used to design the experiments aimed at investigating the PV/PCM configuration. The effects of incident radiation, air gap size and PV panel length were investigated for natural convection type PVT. The effects of fan speed, air gap size and inlet air temperature were also investigated for forced convection type PVT.

Chapter 5 presented the experimental investigation of the newly designed PV/PCM air system. Phase change material (PLUSICE S25) with melting temperature of 25C° was chosen and was placed into a metal box, which was attached to the back of the PV to improve its overall performance. A designed air duct was placed behind the PV/PCM system for ventilation purposes. The PV angle was vertical to achieve better natural ventilation. The temperature of certain observed points within the PV, PCM, and air duct and air velocity in air duct were measured and compared with the simulation results.

Chapter 6 presented a numerical study on the newly designed PV/PCM system. Computational fluid dynamics (CFD) were used to predict airflow and

temperature by numerically solving the set of partial differential equations for mass, energy and momentum. Methodology and simulation model were discussed and a proper model was chosen to use in Fluent 13.0. The validation of the CFD model was based on the dynamic evolution of temperature and air velocity at various points in the test cell, which were compared with the experimental data. The results indicated that the model is reasonable and valid. The numerical models were subsequently used to predict natural ventilation and heat transfer performance of the entire unit and the results were presented. Three case studies based on the validated model were presented and the results confirmed that the PCM can maintain the PV temperature efficiently during the heat gain period. However, problems may occur during the solidification process due to its extremely long duration.

A parametric study based on the validated model was the topic of Chapter 7, where several parameters were compared and discussed. The effects of solar isolation, PCM thickness, air duct depth, PV angle, forced convection and inclusion of fins were investigated. Simulation results for these parameters were illustrated and discussed and suggestions for PV/PCM were presented.

In Chapter 8, the simulation with Energy Plus 8.3 of a PVT system using PCM as thermal storage in a domestic house was presented. The main purpose was to investigate the real influence of the PV/PCM system on the thermal and electrical performance. The construction system that was used in the simulation was modelled in real climatic conditions at two different locations. An economic analysis was also presented at the end indicate that by applying PCM to thermal regulate the PV in UK. The result shows that the system in this study cannot reduce the total payback period due to high initial cost of PCM. At the same

time, benefit from PCM for reducing the heating cooling demands, and for gas heating, it c

9.2 Conclusions and contributions of this research

The contributions of the present research are summarised below.

The aim of the study was to investigate the newly designed PV/PCM air system, which was expected to exhibit the potential to overcome the difficulties associated with the existing PV overheating problems.

This investigation commenced by conducting a comprehensive review of pertinent literature, including solar technologies and thermal storage technologies. The review revealed the current research status as well as problems existing in the solar technology. It also assisted in the analysis of the new concept of a PVT system that combined the two solar technologies with its working principle and classifications. In building the application, a special type of PVT, which was integrated into the building, was discussed and current research status was reviewed. The review also included the basic concepts behind the thermal storage system in building applications, focusing on the phase change materials. As PCMs can act as thermal regulation units in the PV system, the review of the PVT systems with PCM was carried out. The literature review revealed that the aim of most current applications of the PVT system is improving the electrical performance only. Thus, there is an opportunity to develop new solar air systems employing PVT technology to replace conventional solar air heaters.

As a part of this research, a simple analytical model for designing the PVT system was developed and implemented in the primary design of the PVT

system. Its results indicated that high irradiance produces higher flow rate and thus higher thermal efficiency. On the other hand, high irradiance also results in a higher PV plate temperature, which decreases the electrical efficiency. Therefore, there exists an optimum gap spacing at which the flow velocity is maximised, while the temperatures is minimised. Such optimal gap spacing would also result in maximum thermal and electrical efficiency. Changing collector length had a limited effect on the mean PV temperature, air duct and air outlet, electrical and thermal efficiency, but it increased the total heat gain. Electrical efficiency was optimised when the collector length was in the 6−8 m range.

The present study also included a series of experimental arrangements for investigating the PV/PCM system. The experimental results revealed that a PCM of 30 mm thickness with the melting temperature of 25 ºC can maintain the PV cell temperature below its operating temperature for about 210 minutes under 600 W/m^2 insolation conditions. This arrangement can increase the electrical efficiency during the PCM melting process by 10% compared with that of a system without PCM. The system can also provide 15 L/s airflow rate for 240 minutes, which increases once the PCM is fully melted. However, the performance is poor in the solidification phase, as the PCM may take more than 10 hours to solidify. The results also indicate that a thicker PCM can maintain the PV temperature below its operating temperature for a longer time and every additional 10 mm of PCM thickness extends this period by further 70 minutes. The heat removed from the PCM unit by air convection has a certain effect on the PCM thermal performance. The system with vertical fins can increase the

outlet air temperature by about 4 K and improve the velocity air outlet by about 30%, albeit at the additional cost and reduced PCM volume.

Dynamic performance of the PV/PCM system was also investigated by developing a CFD model. The results revealed that higher solar irradiance results in a higher mass flow rate and flow speed due to the enhanced stack effect. PCM volume and melting temperature are very important in high insolation cases. Thicker PCM melted faster as expected, as 30 mm PCM only takes 16,000s to be fully melted, whereas 40 mm and 50 mm PCM took 22,000 and 28,000 minutes, respectively. There does exist an optimum air duct size that yields the best overall performance. Vertical PVT system has better thermal performance during the melting period, and retains similar performance level after the PCM is fully melted. Forced ventilation system can improve the thermal performance for both melting and solidification processes. Addition of fins significantly increases the thermal performance of the PV/PCM system. The PCM takes 30% more time to be fully melted and maintains temperature for a longer time. During the solidification process, the system produces 50 W heat output over 420 minutes, compared to less than 30 W measured for the standard system.

The energy performance of the PV/PCM system within a typical house under UK weather conditions was investigated in the final phase of this study. The results indicate that the PV/PCM system can reduce the peak temperature and increase the night-time room temperature. The effect is greatly affected by the weather conditions, as well as the design and material of the PV/PCM system. The designed PV/PCM was also shown to reduce the peak temperature by about 2 ºC, while increasing the night-time room temperature by about 1 ºC for a

typical small house in Nottingham, UK. It can also produce 2.1% more overall electric power. However, the improvement is still limited in this case, as the summer in the UK is short and temperature is not high compared to the PV nominal operating temperature. The results for the conditions in Shanghai, China, are better, as the system can produce 2.5% electricity in winter and 4.5% in summer. The performance can be further improved by using PCM with 30 ºC melting temperature, which can produce 7% more electricity compared to the system without the PCM. The thermal performance is also significantly improved by the PCM, as it shifts the peak temperature to a later time when the house is occupied, thus reducing the heating load. The performance varies in summer time for PCMs with different melting temperatures.

The BIPVT system, which circulates the indoor air and runs the heat source in the room, is advantageous in terms of heating and cooling of the building and overall energy, since the effect of heating energy reduction is greater than that of power generation. Therefore, an optimised fan speed must be found to maximise the output.

9.3 Recommendations for Future work

As a part of this research work, a laboratory scale investigation of a PV/PCM air system was carried out. There are still many opportunities to develop this research further, in order to enhance the performance of this system. Some of these are noted below:

1. Although some essential geometric parameters of the system components were examined and optimised and the enhanced system performance was achieved, other characteristic parameters should also be analysed, such as the

connection between the PV and the PCM and the use of PCMs with different melting temperatures.

2. Tests under real weather conditions and long-term schemes should also be conducted. Laboratory based testing could not reflect the actual system operation owing to the limitations of the laboratory conditions. Outdoor testing of PV/PCM system which integrated into a real buildings is important to provide more realistic results.

3. Heat transfer enhancement between the PCM and air duct should be attempted, via for example, optimisation of fins and by utilising composite of PCM products.

4. Further development of the energy building model and system control scheme should be pursued to optimise the system performance for real applications.

Reference

Abdolzadeh, M., & Ameri, M. (2009). Improving the effectiveness of a photovoltaic water pumping system by spraying water over the front of photovoltaic cells. Renewable Energy, 34(1), 91-96.

Abhat, A. (1983) Low Temperature Latent Heat Thermal Energy Storage: Heat Storage Materials. Solar Energy, 30, 313-332.

Al-abidi, A. A., Bin Mat, S., Sopian, K., Sulaiman, M. Y., & Mohammed, A. T. (2013). CFD applications for latent heat thermal energy storage: a review. Renewable and Sustainable Energy Reviews, 20, 353-363.

Anderson, T. N., Duke, M., Morrison, G. L., & Carson, J. K. (2009). Performance of a building integrated photovoltaic/thermal (BIPVT) solar collector. Solar Energy, 83(4), 445-455.

Aste, N., Chiesa, G., & Verri, F. (2008). Design, development and performance monitoring of a photovoltaic-thermal (PVT) air collector. Renewable Energy, 33(5), 914-927.

ASHRAE (2009). Handbook of Fundamentals. Atlanta, GA: American Society of Heating, Refrigerating, and Air-Conditioning Engineers.

Assis E, Ziskind G, Letan R. (2009) Numerical and experimental study of solidification in a spherical shell. J Heat Transfer 2009;131:024502

Baetens. R, Petter Jelle B, Gustavsen A (2010) Phase change materials for building applications: a state-of-the-art review. Review Article, Energy and Buildings 42 (9) 1361–1368.

Badescu V. (2003) Model of a thermal energy storage device integrated into a solar assisted heat pump system for space heating, Energy Conversion and Management, Volume 44, Issue 10, June 2003, Pages 1589-1604, ISSN 0196-8904

Bakker, M., Zondag, H. A., Elswijk, M. J., Strootman, K. J., & Jong, M. J. M. (2005). Performance and costs of a roof-sized PV Thermal array combined with a ground coupled heat pump. Solar Energy, 78(2), 331-339.

BEIS (2016) Annual domestic energy bills. Quarterly Energy Prices, available at : https://www.gov.uk/government/statistical-data-sets/annual-domestic-energy-price-statistics

Biwole, P. H., Eclache, P., & Kuznik, F. (2013). Phase-change materials to improve solar panel's performance. Energy and Buildings, 62, 59-67.

Browne, M. C., Norton, B., & McCormack, S. J. (2015). Phase change materials for photovoltaic thermal management. Renewable and Sustainable Energy Reviews, 47, 762-782.

Brinkworth, B.J., (2000b). Estimation of flow and heat transfer for the design of PV cooling ducts. Solar Energy 69, 413–420.

Brinkworth, B.J., (2006). Optimum depth for PV cooling ducts. Solar Energy 80, 1131–1134.

Buker, M.S; Mempouo, B; RIFFAT, Saffa B. Performance evaluation and techno-economic analysis of a novel building integrated PVT roof collector: An experimental validation. Energy and Buildings, 2014, 76: 164-175.

Burek, S. A. M., & Habeb, A. (2007). Air flow and thermal efficiency characteristics in solar chimneys and Trombe Walls. Energy and Buildings, 39(2), 128-135.

Chan, H.-Y., Riffat, S. B., & Zhu, J. (2010). Review of passive solar heating and cooling technologies. Renewable and Sustainable Energy Reviews, 14(2), 781-789.

Chen, C., Guo, H., Liu, Y., Yue, H., & Wang, C. (2008). A new kind of phase change material (PCM) for energy-storing wallboard. Energy and Buildings, 40(5), 882-890.

Cellura MC, Branco GL, Marvaglia V, Orioli A. (2012). A photovoltaic panel coupled with a phase changing material heat storage system in hot climates. In: Presented at 25th Conference on Passive and Low Energy Architecture. Dublin; 2008.

Chow, T. T. (2010). A review on photovoltaic/thermal hybrid solar technology. Applied Energy, 87(2), 365-379.

Chow, T. T., He, W., & Ji, J. (2006). Hybrid photovoltaic-thermosyphon water heating system for residential application. Solar Energy, 80(3), 298-306.

Chow, T. T., He, W., & Ji, J. (2007). An experimental study of façade-integrated photovoltaic/water-heating system. Applied Thermal Engineering, 27(1), 37-45.

CIBSE (2015) CIBSE Weather Data SetsWeather Data - Released [2015] available at http://www.cibse.org/knowledge/cibse-weather-data-sets

Daghigh, R., Ruslan, M. H., & Sopian, K. (2011). Advances in liquid based photovoltaic/thermal (PVT) collectors. Renewable and Sustainable Energy Reviews, 15(8), 4156-4170.

DECC (2016) Energy Consumption in the UK 2016, available: https://www.gov.uk/government/uploads/system/uploads/attachment_data/file/586245/ECUK_Tables_2016.xlsx

Duffie, John A. and Beckman, William A., 2006, Solar Engineering Of Thermal Processes, 3rd ed., John Wiley & Sons, Inc., New York, NY.

Drury B. Crawley, Linda K. Lawrie, Frederick C. Winkelmann, W.F. Buhl, Y.Joe Huang, Curtis O. Pedersen, Richard K. Strand, Richard J. Liesen, Daniel E. Fisher, Michael J. Witte, Jason Glazer, (2001) EnergyPlus: creating a new-generation building energy simulation program, Energy and Buildings, Volume 33, Issue 4, April 2001, Pages 319-331, ISSN 0378-7788

Evans D.L .(1981), Simplified method for predicting photovoltaic array output, Solar Energy, Volume 27, Issue 6, 1981, Pages 555-560, ISSN 0038-092X

Enibe S.O,(2002) Performance of a natural circulation solar air heating system with phase change material energy storage, Renewable Energy, Volume 27, Issue 1, September 2002, Pages 69-86, ISSN 0960-1481

Enibe S.O.(2003), Thermal analysis of a natural circulation solar air heater with phase change material energy storage, Renewable Energy, Volume 28, Issue 14, November 2003, Pages 2269-2299, ISSN 0960-1481

Farid M.M, Khudhair A.M., Siddique Ali K Razack, Said Al-Hallaj,(2004) A review on phase change energy storage: materials and applications, Energy Conversion and Management, Volume 45, Issues 9–10, June 2004, Pages 1597-1615, ISSN 0196-8904

Finnemore J.E. and Franzini J (2002) Fluid Mechanics With Engineering Applications 10th edition, WCB/McGraw-Hill.

Florschuetz L.W. (1979) Extention of the Hottel–Whillier model to the analysis of combined photovoltaic/thermal flat plate collectors. Solar Energy 22: 361–366.

Fleischer, A.S., Chintakrinda, K., Weinstein, R.D., Bessel, C.A., (2008). Transient thermal management using phase change materials with embeded graphite nanofibers for systems with high power. IEEE 561, 566.

Fossa, M., Ménézo, C., & Leonardi, E. (2008). Experimental natural convection on vertical surfaces for building integrated photovoltaic (BIPV) applications. Experimental Thermal and Fluid Science, 32(4), 980-990.

Gan, G.H., (2009) Numerical determination of adequate air gaps for building-integrated photovoltaics. Sol. Energy 83, 1253–1273.

Gan G.H, (2010) Impact of computational domain on the prediction of buoyancy-driven ventilation cooling, Building and Environment, Volume 45, Issue 5, May 2010, Pages 1173-1183, ISSN 0360-1323

Gebremedhin K.G., Wu B.X. (2003), Characterization of flow field in a ventilated space and simulation of heat exchange between cows and their environment, Journal of Thermal Biology, Volume 28, Issue 4, May 2003, Pages 301-319, ISSN 0306-4565

Gowreesunker, B. L., & Tassou, S. A. (2013). Effectiveness of CFD simulation for the performance prediction of phase change building boards in the thermal environment control of indoor spaces. Building and Environment, 59, 612-625.

Gowreesunker, B. L., Tassou, S. A., & Kolokotroni, M. (2012). Improved simulation of phase change processes in applications where conduction is the dominant heat transfer mode. Energy and Buildings, 47, 353-359.

Grag H P, Agarwal PK. (1995) Some aspects of a PVT collector/forced circulation flat-plat solar water heater with solar cells. Energy Convers Manage 1995;36:87–99.

Hammou Z.A., Lacroix M (2006), A new PCM storage system for managing simultaneously solar and electric energy, Energy and Buildings, Volume 38, Issue 3, March 2006, Pages 258-265, ISSN 0378-7788

Hasan, A., McCormack, S. J., Huang, M. J., & Norton, B. (2010). Evaluation of phase change materials for thermal regulation enhancement of building integrated photovoltaics. Solar Energy, 84(9), 1601-1612.

Ho, C. J., Tanuwijava, A. O., & Lai, C.-M. (2012). Thermal and electrical performance of a BIPV integrated with a microencapsulated phase change material layer. Energy and Buildings, 50, 331-338.

Hollands K. G. T., Konicek L., Unny T. E., and Raithby G. D (1976), Free convection heat transfer across inclined air layers. J. Heat Transfer 98, 189- 193

Huang, M. J., Eames, P. C., & Norton, B. (2004). Thermal regulation of building-integrated photovoltaics using phase change materials. International Journal of Heat and Mass Transfer, 47(12-13), 2715-2733.

Huang, M. J., Eames, P. C., & Norton, B. (2006). Phase change materials for limiting temperature rise in building integrated photovoltaics. Solar Energy, 80(9), 1121-1130.

Huang, M. J., Eames, P. C., Norton, B., & Hewitt, N. J. (2011). Natural convection in an internally finned phase change material heat sink for the thermal management of photovoltaics. Solar Energy Materials and Solar Cells, 95(7), 1598-1603.

Hussain S, Oosthuizen P.H., Kalendar A (2012), Evaluation of various turbulence models for the prediction of the airflow and temperature distributions in atria, Energy and Buildings, Volume 48, May 2012, Pages 18-28, ISSN 0378-7788

IEA, 2012. Technology Roadmap: Solar Heating and Cooling. Available at: https://www.iea.org/publications/freepublications/publication/Solar_Heating_Cooling_Roadmap_2012_WEB.pdf

IEA, 2013. Transition to Sustainable Buildings – Strategies and Opportunities to 2050. Available at: https://www.iea.org/publications/freepublications/publication/Building2013_free.pdf

Jay A, Clerc S, Boillot B, Bontemps. (2010), Jay F. Use of phase change material in order to maintain the temperature of integrated PV modules at a reasonable level. In: Presented at 25th European photovoltaic solar energy conference and exhibition and 5th world conference on photovoltaic energy conversion. Valencia, Spain; 2010.

Jiang F, Wang X, Zhang YP, A new method to estimate optimal phase change material characteristics in a passive solar room, Energy Conversion and Management, Volume 52, Issue 6, June 2011, Pages 2437-2441, ISSN 0196-8904

Ibrahim, A., Othman, M. Y., Ruslan, M. H., Mat, S., & Sopian, K. (2011). Recent advances in flat plate photovoltaic/thermal (PVT) solar collectors. Renewable and Sustainable Energy Reviews, 15(1), 352-365.

Incropera F.P, DeWitt D.P, (2007) Fundamentals of Heat and Mass Transfer, 6th Edn., John Wiley and Sons, New York, USA, 2007, pp. 569-593. ISBN-9780 471457282714.

Joulin, A., Younsi, Z., Zalewski, L., Lassue, S., Rousse, D. R., & Cavrot, J.-P. (2011). Experimental and numerical investigation of a phase change material: Thermal-energy storage and release. Applied Energy, 88(7), 2454-2462.

Kalogirou, S. A., Tripanagnostopoulos, Y. (2006). Hybrid PVT solar systems for domestic hot water and electricity production. Energy Conversion and Management, 47(18-19), 3368-3382.

Kamthania, D., Nayak, S., Tiwari, G. N. (2011). Performance evaluation of a hybrid photovoltaic thermal double pass façade for space heating. Energy and Buildings, 43(9), 2274-2281.

Malvi, C. S., Dixon-Hardy, D. W., & Crook, R. (2011). Energy balance model of combined photovoltaic solar-thermal system incorporating phase change material. Solar Energy, 85(7), 1440-1446.

Mateus N.M., Pinto A, Graça G.C, (2014) Validation of EnergyPlus thermal simulation of a double skin naturally and mechanically ventilated test cell, Energy and Buildings, Volume 75, June 2014, Pages 511-522, ISSN 0378-7788

Mei, L., Infield, D., Eicker, U., & Fux, V. (2003). Thermal modelling of a building with an integrated ventilated PV façade. Energy and Buildings, 35(6), 605-617.

Maiti S, Banerjee S, Vyas K, Patel P, Ghosh PK .(2011) Self regulation of photovoltaic module temperature in V-trough using a metal-wax composite phase change matrix. Sol Energy 2011;85:1805–16.

Nallusamy N., Sampath S., Velraj R.(2007), Experimental investigation on a combined sensible and latent heat storage system integrated with constant/varying (solar) heat sources, Renewable Energy, Volume 32, Issue 7, June 2007, Pages 1206-1227, ISSN 0960-1481

Omer, S. A., Wilson, R., & Riffat, S. B. (2003). Monitoring results of two examples of building integrated PV (BIPV) systems in the UK. Renewable Energy, 28(9), 1387-1399.

Osterman, E., Tyagi, V. V., Butala, V., Rahim, N. A., & Stritih, U. (2012). Review of PCM based cooling technologies for buildings. Energy and Buildings, 49, 37-49.

Parida, B., Iniyan, S., & Goic, R. (2011). A review of solar photovoltaic technologies. Renewable and Sustainable Energy Reviews, 15(3), 1625-1636.

Pascal H.B, Pierre E, Frederic E, Phase-change materials to improve solar panel's performance, Energy and Buildings, Volume 62, July 2013, Pages 59-67, ISSN 0378-7788

Pasupathy, A., Velraj, R., Seeniraj, R.V., (2006). Phase change material- based building architecture for thermal management in residential and commercial establishments. Renewable and Sustainable Energy Reviews 12, 30–64.

Pasupathy, A.,Athanasius, L.,Velraj,R., Seeniraj, R.V., (2008). Experimental investigation and numerical simulation analysis on the thermal performance of a building roof incorporating phase change material (PCM) for thermal management. Applied Thermal Engineering 28, 556–565.

Radziemska, E., Klugman, E., (2002). Thermally affected parameters of the current-voltage characteristics of silicon photocell. Energy Conversion and Management 43, 1889–1900.

Randall, K. R., Mitchell, J. W., and El-Wakil, M. M., 1979, ‘‘Natural Convection Heat Transfer Characteristics of Flat Plate Enclosures,” J. Heat Transfer, Vol. 101, pp. 120-125.

Rohdin P, Moshfegh B.(2007) Numerical predictions of indoor climate in large industrial premises. A comparison between different k-ε models supported by field measurements, Building and Environment 42(2007), pp. 3872-3882

Ryu H.W, Woo S.W., Shi B.C, Kim S.D (1992)., Prevention of supercooling and stabilization of inorganic salt hydrates as latent heat storage materials, Solar Energy Materials and Solar Cells, Volume 27, Issue 2, July 1992, Pages 161-172, ISSN 0927-0248

Saber, E. M., Lee, S. E., Manthapuri, S., Yi, W., & Deb, C. (2014). PV (photovoltaics) performance evaluation and simulation-based energy yield prediction for tropical buildings. Energy, 71, 588-595.

Saygin H, Nowzari R, Mirzaei N, Aldabbagh L.B.Y., Performance evaluation of a modified PVT solar collector: A case study in design and analysis of experiment, Solar Energy, Volume 141, 1 January 2017, Pages 210-221, ISSN 0038-092X

Shukla A., Nkwetta D.N., Cho Y.J., Stevenson V., Jones P.（2012）A state of art review on the performance of transpired solar collector Renew. Sustain. Energy Rev., 16 (2012), pp. 3975–3985

Silva, T., Vicente, R., Soares, N., & Ferreira, V. (2012). Experimental testing and numerical modelling of masonry wall solution with PCM incorporation: A passive construction solution. Energy and Buildings, 49, 235-245.

Stritih U., (2004) An experimental study of enhanced heat transfer in rectangular PCM thermal storage, Fuel and Energy Abstracts, Volume 45, Issue 6, 2004, Page 434, ISSN 0140-6701

Singh, G., Kumar, S., & Tiwari, G. N. (2011). Design, fabrication and performance evaluation of a hybrid photovoltaic thermal (PVT) double slope active solar still. Desalination, 277(1-3), 399-406.

Sopian K, Ibrahim MZ, Daud WRW, Othman MY, Yatim B, Amin N. (2009) Performance of a PV-wind hybrid system for hydrogen production. Renewable Energy;34:1973–8.

Suárez, M. J., Gutiérrez, A. J., Pistono, J., & Blanco, E. (2011). CFD analysis of heat collection in a glazed gallery. Energy and Buildings, 43(1), 108-116.

Susman, G., Dehouche, Z., Cheechern, T., & Craig, S. (2012). Tests of prototype PCM 'sails' for office cooling. Applied Thermal Engineering, 31(5), 717-726.

Tiwari, A., Sodha, M. S., Chandra, A., & Joshi, J. C. (2006). Performance evaluation of photovoltaic thermal solar air collector for composite climate of India. Solar Energy Materials and Solar Cells, 90(2), 175-189.

Tonui, J. K., & Tripanagnostopoulos, Y. (2008). Performance improvement of PVT solar collectors with natural air flow operation. Solar Energy, 82(1), 1-12.

Toppi T, Mazzarella L. (2013) Gypsum based composite materials with microencapsulated PCM: experimental correlations for thermal properties estimation on the basis of the composition. Energy Build 2013;57:227–36.

Tripanagnostopoulos, Y. (2012). Photovoltaic/Thermal Solar Collectors. 255-300.

Tyagi VV ,Panwar NL,Rahim NA, Kothari R. (2012) Review on solar air heating system with and without thermal energy storage system. Renew Sustain Energy Rev 2012;16:2289–303.

Vokas, G., Christandonis, N., & Skittides, F. (2006). Hybrid photovoltaic–thermal systems for domestic heating and cooling—A theoretical approach. Solar Energy, 80(5), 607-615.

Velasco P.C.T, Christensen C, Bianchi M (2012), Verification and validation of EnergyPlus phase change material model for opaque wall assemblies, Building and Environment, Volume 54, August 2012, Pages 186-196, ISSN 0360-1323

Wang Y.Q, Zhang X.S (2001), A dynamic modeling approach to simulating socioeconomic effects on landscape changes, Ecological Modelling, Volume 140, Issues 1–2, 30 May 2001, Pages 141-162, ISSN 0304-3800

Werner .W and Mauthner .F (2012), Solar Heat Worldwide – Markets and Contributions to the Energy Supply 2010, Solar Heating and Cooling Programme

Wu Y, Eames P. (2011) Experimental characterisation of an asymmetric compound parabolic PV concentrator complied with a phase change material. Presented at 7th photovoltaic science, applications and technology conference. Edin- burgh, Scotland: Heriot-Watt University;.

Yang, H., Marshal, R.H., Brinkworth, B.J., (1994). An experimental study of the thermal regulation of a PV-clad roof. In: Proceedings of the 12th European PV Solar Energy Conference, Amsterdam, 1115–1118.

Ye, W.B., Zhu, D.S., & Wang, N. (2011). Numerical simulation on phase-change thermal storage/release in a plate-fin unit. Applied Thermal Engineering, 31(17-18), 3871-3884.

Yun, G.Y., McEvoy, M., Steemers, K., (2007). Design and overall energy performance of a ventilated photovoltaic facade. Solar Energy 81, 383–394.

Zalba B, Marín J.M., Cabeza L.F., Mehling H,(2003) Review on thermal energy storage with phase change: materials, heat transfer analysis and applications, Applied Thermal Engineering, Volume 23, Issue 3, February 2003, Pages 251-283, ISSN 1359-4311

Zhai X.Q., Dai Y.J., Wang R.Z. ,(2005) , Experimental investigation on air heating and natural ventilation of a solar air collector, Energy and Buildings, Volume 37, Issue 4, April 2005, Pages 373-381, ISSN 0378-7788,

Zhao, X., Zhang, X., Riffat, S. B., & Su, Y. (2011). Theoretical study of the performance of a novel PV/e roof module for heat pump operation. Energy Conversion and Management, 52(1), 603-614.

Zhang Z, Zhang W., Zhai Z., Chen Q (2007). Evaluation of various turbulence models in predicting airflow and turbulence in enclosed environments by CFD. Part-2: comparison with experimental data from literature. HVAC and R Research, 13 (6) (2007), pp. 871–886

Zogou, O., & Stapountzis, H. (2012). Flow and heat transfer inside a PVT collector for building application. Applied Energy, 91(1), 103-115.

Zondag, H. (2008). Flat-plate PV-Thermal collectors and systems: A review. Renewable and Sustainable Energy Reviews, 12(4), 891-959.

Zondag, H. A., de Vries, D. W., van Helden, W. G. J., van Zolingen, R. J. C., & van Steenhoven, A. A. (2003). The yield of different combined PV-thermal collector designs. Solar Energy, 74(3), 253-269.

Appendix

Payback period calculation for three cases

Case 1

case I	Investment value	electricity savings	electricity profits from GOV	Heating and cooling saving using electricity	Heating and cooling saving using gas	total profit 1	Accumulated profits 1	total profit 2	Accumulated profits 2
2017	£4,580.00	-£268.50	-£78.58	-£37.50	-£11.75	-£384.58	£4,195.42	-£358.83	£4,221.17
2018	£4,602.90	-£273.87	-£78.58	-£38.25	-£11.99	-£390.70	£3,804.72	-£364.44	£3,856.73
2019	£4,625.91	-£279.35	-£78.58	-£39.02	-£12.22	-£396.94	£3,407.77	-£370.15	£3,486.58
2020	£4,649.04	-£284.93	-£78.58	-£39.80	-£12.47	-£403.31	£3,004.46	-£375.98	£3,110.60
2021	£4,672.29	-£290.63	-£78.58	-£40.59	-£12.72	-£409.81	£2,594.66	-£381.93	£2,728.66
2022	£4,695.65	-£296.45	-£78.58	-£41.40	-£12.97	-£416.43	£2,178.23	-£388.00	£2,340.66
2023	£4,719.13	-£302.37	-£78.58	-£42.23	-£13.23	-£423.19	£1,755.04	-£394.19	£1,946.48
2024	£4,742.72	-£308.42	-£78.58	-£43.08	-£13.50	-£430.08	£1,324.96	-£400.50	£1,545.97
2025	£4,766.44	-£314.59	-£78.58	-£43.94	-£13.77	-£437.11	£887.85	-£406.94	£1,139.04
2026	£4,790.27	-£320.88	-£78.58	-£44.82	-£14.04	-£444.28	£443.58	-£413.51	£725.53
2027	£4,814.22	-£327.30	-£78.58	-£45.71	-£14.32	-£451.59	-£8.02	-£420.20	£305.33
2028	£4,838.29	-£333.85	-£78.58	-£46.63	-£14.61	-£459.05	-£467.07	-£427.04	-£121.71
2029	£4,862.48	-£340.52	-£78.58	-£47.56	-£14.90	-£466.66	-£933.73	-£434.01	-£555.72
2030	£4,886.80	-£347.33	-£78.58	-£48.51	-£15.20	-£474.42	-£1,408.16	-£441.11	-£996.83
2031	£4,911.23	-£354.28	-£78.58	-£49.48	-£15.50	-£482.34	-£1,890.50	-£448.36	-£1,445.20
2032	£4,935.79	-£361.37	-£78.58	-£50.47	-£15.81	-£490.42	-£2,380.92	-£455.76	-£1,900.96
2033	£4,960.47	-£368.59	-£78.58	-£51.48	-£16.13	-£498.65	-£2,879.57	-£463.30	-£2,364.26
2034	£4,985.27	-£375.96	-£78.58	-£52.51	-£16.45	-£507.05	-£3,386.63	-£471.00	-£2,835.26
2035	£5,010.19	-£383.48	-£78.58	-£53.56	-£16.78	-£515.62	-£3,902.25	-£478.85	-£3,314.11
2036	£5,035.25	-£391.15	-£78.58	-£54.63	-£17.12	-£524.37	-£4,426.62	-£486.85	-£3,800.96

Case 2

case II	Investment value	year profits if use gas heating	Year profits if use electricity heating	Accumulated profits G	Accumulated profits E
2017	2592.00	-59.83	-190.95	2532.17	2401.05
2018	2604.96	-61.03	-194.77	2471.14	2206.28
2019	2617.98	-62.25	-198.66	2408.89	2007.62
2020	2631.07	-63.49	-202.64	2345.40	1804.98
2021	2644.23	-64.76	-206.69	2280.64	1598.29
2022	2657.45	-66.06	-210.82	2214.58	1387.46
2023	2670.74	-67.38	-215.04	2147.20	1172.42
2024	2684.09	-68.73	-219.34	2078.47	953.08
2025	2697.51	-70.10	-223.73	2008.37	729.35
2026	2711.00	-71.50	-228.20	1936.87	501.15
2027	2724.56	-72.93	-232.77	1863.93	268.38
2028	2738.18	-74.39	-237.42	1789.54	30.96
2029	2751.87	-75.88	-242.17	1713.66	-211.21
2030	2765.63	-77.40	-247.01	1636.26	-458.22
2031	2779.46	-78.95	-251.95	1557.32	-710.18
2032	2793.35	-80.52	-256.99	1476.79	-967.17
2033	2807.32	-82.14	-262.13	1394.66	-1229.30
2034	2821.36	-83.78	-267.38	1310.88	-1496.68
2035	2835.46	-85.45	-272.72	1225.43	-1769.40
2036	2849.64	-87.16	-278.18	1138.26	-2047.58

Case 3

case III	Investment value	electricity savings	electricity profits from GOV	Heating and cooling saving using electricity	Heating and cooling saving using gas	total profit 1	Accumulated profits 1	total profit 2	Accumulated profits 2
2017	£6,640.00	-£303.00	-£88.68	-£164.55	-£51.56	-£556.23	£6,083.77	-£443.24	£6,196.76
2018	£6,673.20	-£309.06	-£88.68	-£167.84	-£52.59	-£565.58	£5,518.19	-£450.33	£5,746.43
2019	£6,706.57	-£315.24	-£88.68	-£171.20	-£53.64	-£575.12	£4,943.08	-£457.56	£5,288.87
2020	£6,740.10	-£321.55	-£88.68	-£174.62	-£54.71	-£584.85	£4,358.23	-£464.94	£4,823.93
2021	£6,773.80	-£327.98	-£88.68	-£178.11	-£55.81	-£594.77	£3,763.46	-£472.46	£4,351.47
2022	£6,807.67	-£334.54	-£88.68	-£181.68	-£56.93	-£604.89	£3,158.57	-£480.14	£3,871.33
2023	£6,841.71	-£341.23	-£88.68	-£185.31	-£58.06	-£615.22	£2,543.35	-£487.97	£3,383.36
2024	£6,875.92	-£348.05	-£88.68	-£189.02	-£59.23	-£625.75	£1,917.61	-£495.95	£2,887.41
2025	£6,910.29	-£355.01	-£88.68	-£192.80	-£60.41	-£636.49	£1,281.12	-£504.10	£2,383.31
2026	£6,944.85	-£362.11	-£88.68	-£196.65	-£61.62	-£647.44	£633.68	-£512.41	£1,870.90
2027	£6,979.57	-£369.36	-£88.68	-£200.59	-£62.85	-£658.62	-£24.94	-£520.88	£1,350.01
2028	£7,014.47	-£376.74	-£88.68	-£204.60	-£64.11	-£670.02	-£694.96	-£529.53	£820.49
2029	£7,049.54	-£384.28	-£88.68	-£208.69	-£65.39	-£681.64	-£1,376.60	-£538.34	£282.14
2030	£7,084.79	-£391.96	-£88.68	-£212.86	-£66.70	-£693.50	-£2,070.11	-£547.34	-£265.20
2031	£7,120.21	-£399.80	-£88.68	-£217.12	-£68.03	-£705.60	-£2,775.71	-£556.51	-£821.71
2032	£7,155.81	-£407.80	-£88.68	-£221.46	-£69.39	-£717.94	-£3,493.65	-£565.87	-£1,387.57
2033	£7,191.59	-£415.95	-£88.68	-£225.89	-£70.78	-£730.52	-£4,224.17	-£575.41	-£1,962.99
2034	£7,227.55	-£424.27	-£88.68	-£230.41	-£72.20	-£743.36	-£4,967.53	-£585.15	-£2,548.13
2035	£7,263.69	-£432.76	-£88.68	-£235.02	-£73.64	-£756.45	-£5,723.99	-£595.08	-£3,143.21
2036	£7,300.01	-£441.41	-£88.68	-£239.72	-£75.11	-£769.81	-£6,493.80	-£605.20	-£3,748.41